Abstract

Title of Document: TRANSIENT PERFORMANCE EVALUATION OF AUTOMOTIVE SECONDARY LOOP SYSTEMS

Magnus Eisele, Ph.D., 2012

Directed by: Professor Reinhard Radermacher
Center for Environmental Energy Engineering
Department of Mechanical Engineering
University of Maryland, College Park

Automotive air-conditioning is a high impact technology where improvements in energy consumption and environmental performance can make a significant difference in fuel efficiency and comfort. The mandatory phase out of R134a as refrigerant in the European Union has set the stage for new systems and alternative refrigerants. While some of these refrigerants, such as R152a or R290, have a low Global Warming Potential, their flammability requires secondary loop systems to be used. The added thermal mass of such systems may increase power consumption and delay cool down while benefitting thermal comfort during start/stop operation. The recent revival of electric vehicles, as well as the associated focus on air-conditioning energy consumption, provides new challenges and opportunities.

This research focuses on the performance evaluation of refrigerants R152a and R290 during transient operation in secondary loop systems, quantification of thermal storage benefits for start/stop operation, and investigation of energy saving potentials in electric vehicles through the use of advanced air-conditioning system controls and cabin preconditioning.

A test facility was built to dynamically test secondary loop systems over a wide range of pull down conditions and drive cycles using a passenger cabin model and associated controls. It was shown that R290 is a viable alternative in secondary loop systems and system performance may be on par or better compared to R134a direct expansion systems. The preservation of cooling capacity and thermal comfort during off-cycle periods were quantified for a secondary loop system, as well as a combined ice storage system. System efficiency increases with longer off-cycle periods compared to direct expansion systems. Advanced compressor control strategies and the use of cabin preconditioning can make use of this characteristic and improve energy efficiency by more than 50%. Ice storage may be used in combination with cabin preconditioning to preserve comfort for an extended driving time with reduced use of the vapor compression cycle. A Modelica model of the secondary loop system was developed and validated with experimental data. The model enables dynamic simulation of pull-down and drive cycle scenarios and was used to study the effects of coolant volume and coolant concentration on transient performance.

TRANSIENT PERFORMANCE EVALUATION OF AUTOMOTIVE SECONDARY LOOP SYSTEMS

By

Magnus Eisele

Dissertation submitted to the Faculty of the Graduate School of the
University of Maryland, College Park, in partial fulfillment
of the requirements for the degree of
Doctor of Philosophy
2012

Advisory Committee:
Professor Reinhard Radermacher, Chair
Professor Gregory Jackson
Professor Kenneth Kiger
Associate Professor Bao Yang
Associate Professor Peter Sunderland

Dedicated to my wife Kyungha and our son Simon
with my deepest love and gratitude

Acknowledgments

It is often said that a dissertation is not written alone. I would like to take the opportunity to thank some of the people who have helped make this research succeed and who have shaped me throughout the last years.

With my sincerest gratitude I would like to thank my advisor Dr. Reinhard Radermacher for giving me the opportunity to work and study at the Center for Environmental Energy Engineering. His experience and advise throughout the last years were invaluable and his guidance inside and outside the framework of research was much appreciated. I am no less grateful to Dr. Yunho Hwang, who directed my research in the heat pump laboratory. His organization of the ACTA consortium, his knowledge and guidance of the day to day research, and his valuable support in the revision of publications, theses, and reports will not be forgotten. I also wish to express my appreciation to my committee members who helped guide this research: Dr. Gregory Jackson, Dr. Kenneth Kiger, Dr. Bao Yang, and Dr. Peter Sunderland.

I want to direct my gratitude to the CEEE staff and students, especially the heat pump lab group, whom I worked with in the past years. The spirit and team work in the group were deciding factors for me to embark on the PhD journey in this lab. Many thanks to the "old" group I started in: Cara Martin, Jan Muehlbauer, Ahmet Oers, Xudong Wang and Dae-Hyun Jin, as well as the "new" group: Daniel Leighton, Kyle Gluesenkamp, Hoseong Lee, Xu Xing, Jiazhen Ling, Ali

Alalili, Sahil Popli, Daniel Spencer and Bracha Mandel, as well as all the others I worked with over the years. It was a pleasure to work with you.

Special thanks go to Hongtao Qiao for his support and discussions about component and system modeling. I would also like to thank Gang Li for helping to build and install the ice storage box for the secondary loop system. A special thank you also goes to Toru Okuma for the fruitful discussions in the lab and the supply of compressors for my test facility.

I want to extend my deepest gratitude to my family, my parents Brigitte Eisele and Hans-Werner Eisele, as well as my wife Kyungha Park and our son Simon Eisele. You were a constant source of support, motivation and joy.

Table of Contents

List of Figures

List of Tables

Nomenclature

Symbols	Explanations	Units
(A)	Ambient Cabin Preconditioning	
(C)	Comfort Cabin Preconditioning	
(S)	Soak Cabin Preconditioning	
2LP	Secondary Loop System	
A	Area	[m^2]
A/C	Air-Conditioning	
AHU	Air Handling Unit	
air	Air-side	
AR	Actual Reading	
ATL	Atmospheric Life Time	
C+P	Compressor + Pump Power	
C+P+H	Compressor + Pump + Heater Power	
col	Coolant-side	
COP	Coefficient Of Performance	[-]
c_p	Specific Heat Capacity	[J/kg K]
D	Diameter	[m]
DAQ	Data Acquisition	
dP	Pressure Drop	[kPa]
DX	Direxpansion System	
E in	Energy Consumed by the System	[Wh]
EB	Energy Balance	[-]
EXV	Electronic Expansion Valve	
F cyc	Frost Cyclic Operation	
FS	Full Scale	
FTP	Federal Test Procedure	
GWP	Global Warming Potential	
h	enthalpy	[J/kg]
HC	Hydrocarbon	
HFC	Hydrofluorocarbon	
ht	height	[m]
htc	Heat Transfer Coefficient	[W/m^2 K]
HVAC	Heating, Ventilating, and Air-Conditioning	
hwy	Highway Operation	
HX	Heat Exchanger	
idle	Idling Operation	
IS	Ice Storage Facility	
k	Thermal Conductivity	[W/m K]
L	Latent Heat	[J/kg]
LEL	Lower Explosion Limit	[vol%]
LFL	Lower Flammability Limit	[vol%]
m/M	Mass	[kg]
MAC	Mobile Air-Conditioning	
MFR/mdot	Mass Flow Rate	[kg/s]
n	Number of ..	
NBP	Normal Boiling Point	[°C]
NEDC	New European Drive Cycle	
ODP	Ozone Depletion Potential	

Symbols	Explanations	Units
P	Power	[W]
p/P	Pressure	[kPa]
PID	Proportional Integral Deriviative	
Q	Capacity	[W]
Q (air)	Energy used in Form of Cooling Capacity	[Wh]
ref	Refrigerant-side	
RH	Relative Humidity	[%]
RH ctn	Relative Humidity Continuous Operation	
RH cyc	Relative Humidity Cyclic Operation	
rpm	Revolutions Per Minute	
s	Entropy	[J/kg K]
S/S	Start/Stop Cycle	
SHF	Sensible Heat Factor	[-]
SL	Secondary Loop	
SS3xI	Start/Stop Three Times Idling Cycle	
STD	Standard Deviation	
t/T	Temperature	[°C]
TPF	Transient Performance Factor	[-]
V	Volume	[m^3]
v	Velocity	[m/s]
VCC	Vapor Compression Cycle	
VFR	Volume Flow Rate	[m^3/s]
w	Humidity Ratio	[kg/kg]
wt%	Percent by Weight	
η	Efficiency	[%]
μ	Dynamic Viscosity	[mPa s]
ρ	Density	[kg/m^3]
ϕ	Relative Humidity	[%]
ω	Uncertainty	

1 Literature Review

Chapter 1 reviews the pertinent literature in the fields of dynamic testing of automotive air-conditioning systems, the use of alternative refrigerants in air-conditioning systems, and the use of secondary loop systems in air-conditioning and refrigeration.

1.1 Dynamic Testing of Automotive Air-Conditioning Systems

Early studies on transient testing of automotive air-conditioning systems were performed by J. E. Rubio-Quero et al. [1] who used a Ford 1994 Crown Victoria R134a system for transient testing of mobile air-conditioning systems. Rubio-Quero et al. stated that while steady state tests are common in the automotive industry, they often do not accurately reflect the operating conditions of mobile air-conditioning systems (MACs). Since typical control schemes involve thermostatic expansion valves, and/or compressor clutch cycling, MACs most often operate in transient conditions.

C. D. Collins and N. R. Miller [2] studied transient behavior of MACs. Their focus was on the development of a refrigerant charge loss diagnostic tool using measures of the transient behavior of the system to reduce premature clutch failure, and the experimental characterization of transient and steady-state performance of MACs. A narrow range of operating conditions was simulated, corresponding to a vehicle cruising at highway speeds with the MAC operating in full recirculation mode in a low humidity, high ambient temperature environment.

The test facility lacked the means of controlling humidity, since air loops were used, which controlled temperature by the power input to electric heaters and no air handling unit was present. The influence of humidity was neglected during this study.

P. G. Weston et al. [3] studied the design and construction of a MAC test facility for transient studies. The major operating transients that should be addressed by a test facility were found to include: changes in compressor speed due to variations in vehicle engine speed; changes in condenser air flow rate due to ram-air effects at the front of the vehicle; changes in the passenger compartment air temperature during pulldown; and cycling of the compressor clutch to prevent evaporator frosting. Drive cycle tests were performed by using a square wave generator for the input to a compressor motor inverter and condenser fan inverter. The setting of the duration of square wave plateaus controlled compressor behavior during the drive cycle. The concepts of an "environment controller" and a "system controller" were briefly introduced, but details on the development of both were stated to be future research.

P. Hrnjak ([4], [5], [6]), B. Hill ([7], [5]), J. Wertenbach [8], and Ward Atkinson ([9], [10]) presented work on the Society of Automotive Engineers (SAE) Alternate Refrigerant Cooperative Research Project. Steady-state tests to evaluate the coefficient of performance (COP) and cooling capacity, as well as transient tests to investigate soak and cool down performance were performed on an R134a system, as well as an enhanced R134a system and an R744 system. Transient experimental analysis on secondary loop systems using

hydrocarbons as refrigerant was planned but has not been published at the present time. Three environmental chambers were used (indoor, outdoor, and compressor chamber) which enabled the initial temperature conditioning of all components. The indoor, as well as the outdoor chamber initially housed open wind tunnels. The automotive passenger cabin was simulated by adding a closed loop to the evaporator chamber. A water to air heat exchanger with controllable water flow rate was used to simulate the cooling rate of vehicle thermal mass. The water could be heated according to changes in temperature of the thermal mass of the vehicle. Coefficient of performance (COP), as well as evaporator capacity of the different systems were compared in steady-state performance tests, as well as transient New European Drive Cycle (NEDC) tests. Tests were conducted only up to 2,500 rpm. A model, which was validated with experimental results, extrapolated capacity and COP data at higher compressor speeds. However, the NEDC cycle and the USA equivalent, Federal Test Procedure (FTP) include significant portions of compressor speeds higher than 2,500 rpm.

J. A. Baker et al. [11] presented research on building, testing and demonstrating a commercially viable, energy efficient secondary loop R152a MAC system. A test vehicle was equipped with a secondary loop system, and climatic wind tunnel tests, as well as road tests for cooling performance, were conducted. The wind tunnel tests included soak, cool down, as well as steady state performance tests and extended idle tests at an ambient temperature of 40°C and 40% relative humidity. Results were presented in the form of average cabin air temperature and average air-conditioning (A/C) vent outlet temperature.

A. Gado ([12], [13]) built a dynamic simulator to simulate a passenger cabin while testing actual air-conditioning components under laboratory conditions on a test bench. Inputs to the dynamic simulator included: supply temperature, supply air humidity ratio, evaporator airflow rate, and various other user inputs, such as cooling loads and physical characteristics of the cabin. The mass and energy balance equations which were the core of the dynamic simulator were explicitly stated. It was shown that the dynamic simulator was able to run drive cycles, such as the NEDC, as well as pull down tests and cyclic tests with compressor on/off cycling. Instead of focusing only on compressor power consumption, the dynamic simulator allowed for real time monitoring and recording of refrigerant pressure and temperature, as well as air-side temperature and relative humidity. Cabin temperatures during NEDC cycle, as well as superheat and subcooling information were presented.

M. B. Yahia and C. Petitjean [14] performed dynamic tests on a test bench. NEDC cycle, as well as steady state tests, based on European climate were performed. Two windtunnels, together with a variable speed compressor stand were used to test an NEDC cycle. The research focused on energy consumption of the compressor, however the control of the compressor speed was not well refined. Yahia and Petitjean found that average compressor power consumption during an NEDC differed about 5% from the steady state weight calculated average value. Test bench results and results from climatic windtunnel tests with actual cars did not agree well, and test conditions of the test bench had to be adjusted so that test bench results would resemble climatic windtunnel results

tested under the original test conditions. The authors concluded that if the A/C system could be controlled in short enough time intervals there should be little effect of transients on energy consumption, however no proof of this theory was provided in the test data shown.

1.2 Transient Modeling of Automotive Air-Conditioning Systems

C. Huang [15] conducted dissertation research on a dynamic simulation model for automobile passenger compartment climate control and evaluation. The objective of the dissertation was to develop a mathematical model to simulate dynamic features of mobile air-conditioning systems while predicting temperature and relative humidity inside the passenger cabin. The model consisted of two modules, one of them being the A/C network, and the other one being the passenger compartment. The passenger compartment was modeled as a lumped capacitance model. The model consisted of energy and mass balance equations that took the various loads, as well as the thermal and physical parameters of the cabin into consideration. Huang was able to transiently model the passenger cabin, showing the dynamic behavior of cabin temperature and relative humidity during a pull down procedure.

M. Wang, D. Farley, and L. Leitzel [16] investigated head pressure spikes during vehicle acceleration by experiment and simulation. Head pressure spikes occur during gear shifts due to sudden acceleration of the compressor rpm and are a concern for system durability and passenger comfort requirements. Head

pressure spikes are mainly a mass balance phenomenon between the expansion device and the compressor, where the compressor pumps refrigerant faster than the expansion device can accommodate. The research focused on a mathematical transient model with application to A/C systems with scroll compressor. The developed model was able to simulate head pressure spikes effectively and allow conclusions on the phenomenon. It was found that scroll compressors have significant head pressure spikes due to their high volumetric efficiency. It was also found that the type of expansion device, as well as ambient conditions and heat transfer performance at the condenser during acceleration significantly affect the magnitude of head pressure spikes.

T. Hendricks [17] conducted optimization of vehicle air-conditioning systems using transient air-conditioning performance analysis. The Sinda/Fluint analysis software was used to capture two-phase flow effects in evaporator and condenser, as well as system mass effects, air-side heat transfer, vehicle speed effects and temperature dependent properties. The A/C model was integrated with a simplified cabin model. Single-variable and multi-variable design optimizations were performed on COP, cabin cool down time, and system heat load capacity. The simplified cabin model was able to predict cabin and panel outlet temperatures during transient cool down periods and steady state operation. Combining the A/C system model and the cabin model allowed the prediction of drive cycle behavior and vehicle idle performance. Examples were presented in form of an optimization of COP, based on condenser tube diameter and transport line diameter.

R. Marzy, J. Hager, and C. Doppelbauer [18] investigated the optimization of vehicle warm-up, using the 1-D simulation tool KULI. To investigate vehicle warm-up, sub models for the vehicle engine, the HVAC system, and the vehicle cabin were combined into one model. A 3-D computational fluid dynamics (CFD) airflow simulation for the front end to model complex flows at the radiator and engine was added. Resistance curves were used on the air-side for the various heat exchangers and elements of the HVAC system in the 1-D model, which allowed for flexibility in adding or taking out components to model different system designs. Although the implementation of this software model was described and some transient simulation results were shown, validation of the model with experimental data was not provided.

C. Tian and X. Li [19] evaluated the transient behavior of automotive air-conditioning systems using a variable displacement compressor. They built a mathematical model to evaluate variation of stroke length, based on change of suction pressure. As a result of their simulation effort, a time lag between system change and compressor wobble plate response of less than three seconds was found. Similarly, a time lag between piston stroke length and refrigerant mass flow rate was found to be less than five seconds. Experimental evaluation of transient response of variable displacement compressor parameters, such as rotary speed, piston stroke length, suction pressure and MFR was conducted. Both, experimental results and modeling results, showed that transient effects of the wobble plate are negligible and a variable displacement compressor can be modeled as a steady state component for transient modeling of HVAC systems.

H. Tummelscheit and D. Limperich [20] published information about the Air-Conditioning Library in the Dymola development environment for simulation of advanced A/C systems. The simulation tool Dymola, based on the language Modelica, was chosen by German original equipment manufacturers (OEMs) as the preferred tool for model development and library development. The A/C library is a commercial package which contains a complete range of component models and templates of typical A/C system architectures and refrigerants. Dymola has steady-state, as well as transient simulation capabilities and includes a dynamic process interface to show dynamic ph-diagrams and other visualization techniques. A model encryption allows the selective hiding of model source code, which unfortunately prevents convenient modification of existing models and addition of own code. Tummelscheit and Limperich used the Air-Conditioning Library with Dymola to compare the performance of R134a and Fluid "H". They concluded that fluid "H" shows lower capacity and COP and higher superheat and therefore cannot be used as drop-in refrigerant for R134a.

I. Bayraktar [21] conducted research on time dependent simulation methods for vehicle thermal management. Underhood and HVAC optimization were considered, and both 1-D and 3-D calculations of component temperatures were conducted. Air flow and heat transfer were evaluated using 3-D CFD tools, namely Fluent and RadTherm software packages. Model results were compared to experimental results from a passenger compartment model in a climate chamber, instrumented with more than 100 thermocouples and a large number of pressure transducers on air- and refrigerant-side. To verify the model, the target

was to minimize difference between experimental and computational results for a cabin cool down process at four checkpoint locations (10, 20, 40 and 50 minutes). The author concluded that 1-D simulation can provide valuable first predictions, but higher fidelity 3-D CFD models are needed to analyze transient behavior of the entire thermal system of a vehicle.

B. Li and A. Alleyne [22] presented a full dynamic system model with switched moving boundary components, which was able to accommodate severe transients in heat exchanger dynamics. The research was focused on start/stop cycles, specifically the phenomenon of compressor clutch cycling. Heat exchanger models were implemented in Thermosys, a Matlab toolbox. The dynamic system model was created in Matlab/Simulink and was successfully validated using an experimental test stand. In the moving-boundary modeling framework, heat exchangers were divided into control volumes or zones in terms of fluid phase. The location of the boundary between zones is a key dynamic variable that captures the essential multi- phase flow dynamics. It was shown that switching schemes between different representations (i.e. subcooled liquid, superheated vapor, or two-phase) handle the transitions of dynamic states while keeping track of vapor and liquid refrigerant regions during start-stop transients. The authors concluded that their model enables the adjustment of hysteresis set points on compressor cycling (i.e. at which temperatures the compressor turns on and off) in simulation before experimental testing is required. System responses like space temperature, refrigerant cycle pressure and superheat condition were successfully predicted by the model.

K. Sandhu, C. Chatham and A. Milosevic [23] developed a model to study the impact of various A/C circuit configurations on A/C performance of a Land Rover vehicle. In hybrid or electric vehicles, the A/C system design and resulting power consumption significantly affects driving range and cooling performance of batteries and electric systems. The simulation software GT-Suite was used. The model was validated at several steady-state conditions against experimental results from an R134a A/C system. A multi-evaporator design was studied with 3 cooling loads, one of them being an intermediate heat exchanger cooling a secondary loop for battery and inverter cooling. Refrigerant R1234yf was used in the model. Transient pull down tests were simulated by integrating the A/C system model with a vehicle cabin model. A target evaporator temperature was calculated, based on ambient temperature, blower speed, solar intensity, recirculation mode and battery cooling demand. The target evaporator temperature was subsequently used to control compressor speed. Results of a pull down simulation in form of transient cabin temperature and transient compressor power were presented. However, no comparison with experimental data was provided.

1.3 Alternative Refrigerants in Air-Conditioning and Refrigeration

Table 1.1 shows properties of five flammable refrigerants, along with R134a properties as baseline. Isobutane (R600a) is a hydrocarbon refrigerant, mostly used for medium- and low-temperature domestic refrigeration applications. With a low Global Warming Potential (GWP) of 8, an Ozone Depletion Potential

(ODP) of 0, and an Atmospheric Life Time (ALT) of less than a year, R600a has excellent environmental properties. R600a is in the safety classification A3 of the ASHRAE Standard 34 [24], meaning that it is highly flammable. It has a lower flammability limit (LFL) of 1.7 vol.%, which makes it the easiest to ignite among the refrigerants in the table. The acute toxicity exposure limit (ATEL) is a value used by ASHRAE Standard 34 [24] and ISO 817 [25] to establish the maximum refrigerant concentration limit for a refrigerant in air. It is calculated from the acute toxicity data using methods determined in accordance with the standards.

Table 1.1: Alternative Refrigerants and Characteristics (Wang et al.) [26]

Refrigerants	R134a (HFC)	R290 (HC)	R600a (HC)	R290/R600a mix. (HC)	R152a (HFC)	R1234yf (HFO)
Global Warming Potential (GWP)	1,430	11	8	7	140	4
Ozone Depletion Potential (ODP)	0	0	0	0	0	0
Atmospheric Life Time [a]	14	<1	<1	<0.04	2	<0.05
Acute Toxicity Exp. Level [ppm]	50,000	50,000	25,000	40,000	50,000	101,000
Lower Flammability Limit [vol.%]	-	2.2	1.7	2.0	3.9	6.5
Minimum Ignition Energy [mJ]	-	0.25	0.25	N/A	0.38	>1000
Safety Group	A1	A3	A3	A3	A2	A2L
Molar Mass [kg/kmol]	102.03	44.096	58.122	N/A	66.051	114.042
Vapor Density (25°C) [kg/m^3]	32.35	20.65	9.12	N/A	18.47	37.94
Critical Temperature [°C]	101.1	96.8	135	114.8	113.3	94.7
Critical Pressure [kPa]	4,061	4,247	3,647	4,040	4,522	3,382
Normal Boiling Point [°C]	-26.11	-42.11	-11.78	-31.5	-24.0	-29.48
Vapor Spec. Heat (25°C) [kJ/kg K]	1.0316	2.0724	1.8189	1.77	1.2536	1.053

Propane (R290) is a hydrocarbon (HC) refrigerant used for high-, medium- and low-temperature applications in commercial and industrial refrigeration, air conditioning, as well as heat pumps and chillers. With a GWP of 11, an ODP of 0, and an ALT of less than a year, R290 is an environmentally friendly choice. A

LFL of 2.2 vol.% puts it in the safety classification A3 with a MIE of 0.25 mJ required for ignition.

An HC zeotropic mixture, a blend of R290 and R600a, is mostly used in high- and medium-temperature commercial, automotive and residential applications. As its constituents are R290 and R600a, it has a small GWP of 7, an ODP of 0, and a negligible ALT. Its LFL of 2.0 vol.% is in the typical range of a HC refrigerant, so that the assigned safety classification is A3. Due to flammability and safety concerns, this HC mixture, as its constituents, should be used in a SL system when used in MACs.

1,1-Difluoroethane (R152a) is a HFC refrigerant, and was investigated for use in MACs, as well as household refrigerators. Its GWP of 140 is quite high compared to that of HCs, but is beneath the upper limit of 150, set by the European Council[27]. An ALT of about 2 years makes it less environmentally friendly compared to HCs, yet far superior to the currently used R134a. The advantage of R152a is the higher LFL of 3.9 vol.% and the resulting safety class A2.

2,3,3,3-Tetrafluoropropene (HFO1234yf), proposed by American chemical companies, is currently investigated for use in MACs by Spatz and Minor [28]. Its GWP of 4 is the lowest among the reviewed flammable refrigerants. As R1234yf has zero ODP and a negligible ALT, it is the most environmentally friendly of the reviewed flammable refrigerants. A LFL of 6.5 vol.% and a MIE of greater than 1000 mJ make it the safest choice among the assorted classification of

refrigerants in terms of flammability. The safety class to be designated is expected to be A2L. Due to its low LFL and MIE as compared to HCs, chemical companies proposed to apply R1234yf to DX systems without using a SL as a safety measure when used in MACs.

Granryd[29] and Corberan et al. [30] summarized the environmental safety considerations and standards applied for the safe use of flammable refrigerants. Both ASHRAE Standard 34 [24] and European standard prEN378 (CEN, 2006) [31] classify refrigerants in three classes 1–3, where Class 1 is used for non-flammable fluids and Class 3 for highly flammable fluids. The group of Class 3 refrigerants, which includes HCs, is currently limited in use for industrial applications in the USA and France, due to restrictive regulations. Some European standards, such as prEN378 (CEN, 2006), British standard BS EN378-1 (BSI, 2008) [32] and German standard DIN 8975 (DIN, 2004) [33], allow for a broader range of applications if certain safety requirements are met. As a result, the use of HCs in household refrigerators, freezers and small heat pumps has increased in European countries.

Furthermore, Granryd [29] compared the performance of HCs, such as R600a and R290 and their mixtures to the well established refrigerants R12, R22 and R134a. Blends of R290 with R600a could achieve vapor pressures close to that of R134a and would hence be a suitable replacement. While R290 has a higher volumetric cooling capacity, R600a and the HC blends have a lower volumetric cooling capacity compared to R134a. As a refrigerant with a high

volumetric cooling capacity will provide a high cooling capacity for a given swept volume of the compressor, R290 shows superior characteristics.

Colbourne [34] summarized a study analyzing over 50 published technical documents comparing the performance of fluorinated refrigerants and HCs. A significantly higher number of tests showed an increase in performance when using HCs as compared to using fluorinated refrigerants, as shown in Colbourne and Suen [35]. The average improvements in Coefficient of Performance (COP) resulting from the use of HCs were 6.0% for domestic refrigeration applications, 15.0% for commercial refrigeration applications, 8.8% for air-conditioning and 9.6% for heat pumping as shown in Table 1.2.

Table 1.2: Comparison of Performance of Hydrocarbons per Application [26]

Applications	Proportion of cases where HCs improved COP				Average Improvement
	< 10% Improvement	10% - 20% Improvement	> 20% Improvement	Total	
Domestic Refrigeration	63.9%	13.9%	5.6%	83.7%	6.0%
Commercial Refrigeration	51.6%	12.9%	25.8%	90.3%	15.0%
Air-Conditioning	63.0%	25.9%	3.7%	92.6%	8.8%
Heat Pumping	58.6%	37.9%	3.4%	100%	9.6%

Colbourne and Ritter [36] investigated the compatibility of non-metallic materials with HC refrigerant and lubricant mixtures. Experiments were performed in compliance with European standards for the testing of elastomeric materials and ASHRAE material compatibility test standards. Test results were presented for swell rates, hardness rating, mass changes and the change of tensile strength. A R290/R600a HC blend in combination with various lubricants

VG32 Mineral Oil, VG100 Mineral Oil and VG46 Polyol Ester Oil, was tested. The chosen materials for testing were common materials, such as Buna N, HNBR, EPDM, Viton and Neoprene. Results for Buna N, HNBR, Viton and Neoprene indicated that linear and volumetric swell was minimal and acceptable. Buna N, HNBR, Neoprene and Silicone were found to show only minimal amount of mass change. The authors concluded that Buna N, Viton, Neoprene and HBNR, as well as Mylar as a plastic, were all suitable elastomers for use with HC refrigerants.

Maclaine-Cross and Leonardi [37] compared the refrigerant performance of HCs based on refrigerant properties and concluded that the COP improvements, commonly reported in literature, were consistent with better thermodynamic properties of HCs. R600a properties and their influences on system performance were discussed. In refrigeration systems, the evaporator has to withstand pressures similar to those in the condenser during the off period. Since the typical condensing pressures of R600a is about 50% smaller than that of R134a and other refrigerants, the thickness of the heat exchanger material can be reduced. This helps the heat transfer in heat exchangers through a reduction of thermal resistance, and thus reduces capital costs and environmental impact. Additionally, the low compressor discharge temperature of R600a allows for a cheaper and more efficient design of the electric motor. They suggested that although performance differences between ideal cycles using R600a and common refrigerants were small, the flow and heat transfer parameters were typically better by a factor of two for R600a. This explains the 20% energy

savings reported in literature. Through redesign of components, similar improvements can be achieved in other small applications.

Joudi et al. [38] studied the performance of MAC systems with alternative refrigerants. A computer model was developed to determine the most suitable alternative refrigerant to R12. The influence of evaporating temperature, condensing temperature and compressor speed in an ideal cycle was considered. Four refrigerants were studied: R134a, R290, R600a and an R290/R600a mixture. The model predicted the R290/R600a mixture as the most suitable alternative to R12. A subsequent experiment with a prototype MAC system compared R290, the HC blend and R12 performance. It was observed that R290 outperformed R12 by approximately 8.3% in terms of COP, depending on condensing temperatures, whereas the R290/R600a mixtures had a similar performance to R12. For the pull-down time at soaking temperatures, a superior performance of the HC blend was recognized for all test conditions. The power consumption of the HC mixtures was slightly higher for all operating conditions investigated, resulting in slightly lower COPs between 0.86% and 2.27%, based on operating conditions.

Ghodbane [39] investigated the use of R152a and HCs in MACs. Based on thermophysical data, a quantitative analysis of MACs with flammable refrigerants was proposed. R290 having the lowest normal boiling point (NBP) was expected to have the highest operating pressure, while R600a was expected to have the lowest operating pressure. R152a was expected to have a similar operating pressure to R134a since its NBP is closest to R134a. Critical

temperatures of R152a, R290 and R600a are all above 93.3°C. An ideal performance comparison with respect to R134a was performed over a wide range of evaporating and condensing temperatures. The cooling capacity of the system was set to be 3.7 kW. Pressure drop was neglected and the compressor isentropic efficiency was set to be 100%. Results showed that over the whole range of evaporating temperatures, R152a had the highest COP in the range of 37.8–54.4°C condensing temperature, which is the desired range for MACs. The COP of R152a was increased about 6–19% as compared to R134a, depending on condensing temperature. R152a showed a higher hot discharge gas temperature compared to other refrigerants, resulting in 6.6–14.1 K higher temperatures compared to R134a. Despite the higher discharge temperature, R152a was chosen by Ghodbane as the most suitable flammable refrigerant to replace R134a in MACs, due to its superior performance. A more realistic evaluation of the refrigerants under operating conditions in a vehicle with simulation of road load conditions followed. R152a remained the best performer with a performance increase over R134a of 11% at road load conditions and 8% at idling conditions. R152a had a condensing heat transfer coefficient of about 1.33 times higher than R134a under the prescribed conditions for idling (1.26 for road load). The evaporative heat transfer coefficient of R152a increased to 1.04 times of R134a at the same ambient conditions under idling (1.14 times for road load). The highest increase in evaporative heat transfer coefficient was reported for R290 with 1.43 times of R134a for idling (1.51 times for road load). Two-phase flow pressure drop data showed that the HCs, as well as R152a, have a

considerably low pressure drop, with R152a having 50% less pressure drop than R134a.

Risk assessment

In their research ‘‘Hydrocarbon Refrigerant Risk in Car Air-Conditioning’’, Maclaine-Cross and Leonardi [40] provided an overview of the potentially dangerous scenarios that need to be considered when employing flammable HC refrigerants in MAC systems. Principal hazards associated with refrigerants were determined to be: explosion in space, fire, asphyxiation or poisoning, flying debris resulting from an explosion, cold burns and damages due to chemical reactions. Several safety standards were adopted in Europe, Australia, Asia and the USA, which restrict the use of flammable refrigerants based on the charge amount, safety design of the system, as well as the individual properties of the refrigerants. Based on the necessary precautions demanded by these standards, the authors believe that R600a and mineral oil mixtures require the least expenditure on precautions for MAC systems. This combination is already commonly used in household refrigerators.

Razmovski and Rajasekariah [41] experimentally evaluated possible ignition sources in a car by connecting a welding torch to a HC refrigerant cylinder. The refrigerant streaming out of the welding torch was then tested for more than 15 min on the hot engine, electrical wiring, exhaust system, ignition, switches, fan motor and internal cigarette lighter. It was found that none of the

aforementioned sources ignited the torch and a lit up match or external butane cigarette lighter was the only possible ignition source for the HC refrigerant in a car. One scenario that particularly causes concerns is an explosion of flammable refrigerant within the passenger compartment through rupturing of a pipe just before the expansion valve, which releases a refrigerant cloud into the passenger compartment. It is expected that a fatigue fracture of the liquid line could be a likely cause of this scenario.

Maclaine-Cross and Leonardi [40] concluded from their experiments that safe operation of HC refrigerants in cars is possible. In a study about HC refrigerant leakages in car passenger compartments, Maclaine-Cross referred to a report made by Arthur D. Little Ltd. [42], who noted that serious injury to occupants through use of flammable refrigerant would only be possible if the car crashed, due to overpressure in the compartment after a fatigue damage of the liquid line. The risk level of such an event, which could also occur with non-flammable refrigerants, was estimated to be 4.16×10^{10} per car year. Most refrigerants, not only HCs, are asphyxiants and causes drowsiness and driver fatigue. The potential hazards implied are thousands of times more frequent than the ignition of refrigerants and have a higher potential to entail damage through possible crashes. Peak concentrations in fractions of the LEL were determined for a variety of Australian cars, built from 1970 to 1989. For models built in the 1970s, the concentration in the cabin was found to be above the LEL only for an instantaneous complete fracture. In all cars built in the 1980s, the possible concentration after one of the aforementioned events was well below the LEL.

A report from Dieckmann et al. [43] for the USA Department of Energy was reviewed, which assessed the risk of using flammable refrigerants in MACs. Field data from car crashes and car fires was used as basis for the analysis. The extent of damage to the refrigerant circuits in crashed cars was visually inspected. A fault tree analysis allowed for risk estimates.

A similar risk assessment, performed by Elbers and Verwoerd [44], considered an R290 heat pump system used for residential heating. The estimated risk in terms of fatalities is provided in above table. To provide a context for these safety estimates, Ritter and Colbourne [45] published a review on HC risk assessment from 1991 to 1998. The use of background risks as a basis for comparison of the risk of fire with HC was presented. The background risks are then taken as a datum for comparison with the risk of a fire due to the use of flammable refrigerant. Several systems were considered by Ritter and Colbourne, including MAC, supermarket cold storage rooms, supermarket line chest freezers and integral unit chillers. A typical MAC system with a charge of 400 g of HC mixture was assessed to have a risk level of $3.0x10^{7}$ per car year. The risks considered included minor burns from jet fires, cloud fires and overpressure. The risk level of a car crash, resulting from leakage of a HC mixture was subsequently estimated to be $9.91x10^{8}$ per car year. This number is negligible compared to the background risk of fire frequency in cars, which is $3.29x10^{3}$. Based on the foregoing comparison, Ritter and Colbourne [45] concluded that the risks of flammable refrigerant leakages and possible

subsequent fires, evaluated for numerous systems, are mostly negligible when compared to background risks.

Jetter et al. [46] used a fault tree analysis to estimate the number of refrigerant exposures of automotive service technicians and vehicle occupants in the USA. The estimated number of exposure for occupants in a vehicle is smaller than the exposure for technicians. Furthermore the largest best estimate was a leakage following a collision. The authors claimed that a common concern, the leakage from the evaporator in the passenger compartment following a collision, might be overrated because for parked vehicles and those standing still after an accident, refrigerant leaking out of the evaporator would flow through the condensate drain due to its high density compared to air and would not enter the passenger compartment in a significant amount.

A quantitative risk assessment model was developed by Colbourne and Suen [47] to examine the influence of design, installation of equipment and external conditions on the frequency of ignition and the associated consequences for indoor refrigeration and air-conditioning units using HC refrigerants. The output of the model was evaluated with a sensitivity analysis of the parameters to show their relative impact on the overall risk level. Key aspects in terms of design were shown to be refrigerant charge quantity and installation height due to their impact in the event of quick dispersion. Also the refrigerant selection itself showed a noticeable impact on the risk value, where R600a showed the highest risk.

The above literature review on low GWP refrigerants showed that flammable refrigerants are safely used in a variety of industrial, commercial and residential (mostly Europe/ Asia) settings. Cars with MACs running with Propane (R290) exist in Australia. Simulation and experimental research on flammable refrigerants in MACs shows that R152a and R290, as well as mixtures of R290 and R600a are promising candidates to be used in future automotive air-conditioning systems. Hydrocarbons, such as R290 and R600a, are superior with regard to environmentally friendly operation. At the same time the supply of HCs can be reliably guaranteed in most parts of the world. Risk assessment studies showed that the risk of fire due to the use of hydrocarbons as refrigerant in direct expansion systems (DX) is low compared to background risks. It is generally agreed upon that it is safe to use hydrocarbons in MACs if safety measures are taken. The secondary loop is one of these safety measures which, in addition to fire hazard mitigation, includes other advantages, such as cold storage and enabling of multiple cooling loads.

1.4 Secondary Loop Systems in Air-Conditioning and Refrigeration

The vapor compression cycle of a secondary loop (SL) system consists of a compressor, a condenser, an expansion device and an intermediate heat exchanger, often called chiller. The chiller cools down a working fluid in the secondary loop, which in turn cools down the air by exchanging heat in the cooler, a liquid to air heat exchanger. One or more pumps cycle the coolant in the secondary cooling circuit.

Primary Loop Equipment

Most of the components used in DX systems can also be used for SL systems, which is also true for the compressor. Palm [48] reported that HC producers listed the compressor manufacturers whose compressors are compatible with HCs, including 23 compressor manufacturers. After taking an internal evaluation of safety aspects, Danfoss [49] decided to supply compressors used in small hermetic systems with HC charge of 150 g or less. Corberan et al. [50] investigated the performance of a positive displacement hermetic refrigerant piston compressor working with R290 as refrigerant. The cooling capacity of an R22 compressor that was switched to R290 operation decreased by 13% to 19%. However, the COP of the system increased from 2 to 6% at the same time.

The intermediate heat exchanger, often called chiller, is of special interest in SL systems. Pellec et al. [51] tested two types of heat exchangers (brazed- and platular-welded-plate heat exchangers) working with ammonia and silicone heat transfer fluid as a secondary refrigerant. With the same mass flow rate on the secondary refrigerant-side, the heat transfer coefficient is about five times less for the platular- welded-plate heat exchanger compared to the brazed plate heat exchanger, due to the plate patterns. Setaro et al. [52] tested and compared heat transfer and pressure drop for a brazed plate heat exchanger and a tube-and-fin coil using two different refrigerants, R22 and R290 in an air-to- water heat pump system. Both, the heat transfer coefficient and pressure drop of R290, are lower than R22 in the two types of heat exchangers which were studied. Hrnjak

and Hoehne [53], who studied charge minimization in SL systems, reported that an air to R290 minichannel heat exchanger developed for a 2 kW cooling capacity refrigeration system needed less than 0.13 kg of R290 due to its smaller internal volume compared to traditional fin-and-tube heat exchangers. Fernando et al. [54] studied liquid-to-refrigerant heat exchangers using flat multiport with 1.4 mm hydraulic diameter tubes and showed a lower charge compared to plate heat exchangers. Fernando et al. ([55], [56], [57]) also carried out comprehensive tests on performance of minichannel aluminum tube heat exchangers working as evaporator and condenser. Correlation equations of refrigerant-side (R290) heat transfer coefficient were compared and validated with experimental results.

Primary Loop Refrigerants

Primary refrigerants for commercial systems can be distinguished into Ammonia, hydrofluorocarbons (HFCs) and HCs. A lot of examples exist for Ammonia and HFCs as primary refrigerants, including American manufacturers, as shown by Likes [58], who established an early SL system for supermarkets. The primary refrigerant was R22 and the secondary refrigerant was a water-propylene glycol solution, 65/35% by mass. Preliminary test results showed that the performance of the secondary system for the medium temperature case was satisfactory, but the energy consumption was higher than expected. Rolfsman [59] reported a supermarket in Sweden which was converted to a SL system. NH3 was used as the primary refrigerant and CO_2 was used as the secondary refrigerant for freezing. Five of the same systems were installed and had been

operating successfully for a year. Evenmo [60] cited a supermarket in the United Kingdom using R407C as the primary refrigerant and a commercial fluid as the secondary fluid, since first opened in February 1997. In the same year, Horton et al. [61] tested a drop-in SL refrigeration system for medium temperature supermarket applications. The primary refrigerant was R22 and the secondary refrigerants were a 50/50% mixture of water-propylene glycol, and hydro-fluoroether. Comparison of the performance of the R22 baseline vapor compression cycle and SL systems showed that the COP of the primary loop in the SL setup was about 1.5–2 times higher compared to the baseline. Nyvad and Lund [62] reported on a supermarket in Denmark replacing its existing (H)CFC-plant with a new indirect SL system. In this system, NH3 was used as the primary refrigerant and Tyfoxit (Tyforop Chemie Gmbh [63]) was used as the secondary refrigerant. The experimental results showed that average energy consumption of the SL system with NH3 as the primary refrigerant was 35% less compared to the old system using (H)CFC as the refrigerant. Arias and Lundqvist [64] reported field test results of advanced systems in three supermarkets. Two of them used a cascaded SL system with R404A as primary refrigerant and potassium formate brine solution as secondary refrigerant. The third system had individual SL refrigeration units in each display case which were all connected to a central building chiller for heat rejection. Faramarzi and Walker [65] tested the performance of a SL refrigeration system in USA supermarkets. The primary refrigerant was R507 and secondary refrigerant was Dynalene. The energy consumption of this SL refrigeration system was 4.9% less compared to the

baseline multiplex system. Minea ([66], [67]) reported a supermarket refrigeration system with SLs installed near Montreal, Canada. This advanced system involved secondary fluid loops on both refrigerating and condensing sides, heat recovery with brine- to-air heat pumps and passive heat exchangers. The primary refrigerant was R507 and the secondary refrigerants for low temperature freezing loop and medium temperature refrigeration loop were potassium formate and propylene glycol (50/50% by mass), respectively. The secondary fluid on the condensing side was ethylene glycol/ water mixture (50/50% by mass). The total quantity of the primary refrigerant was reduced by 61% compared to a baseline multiplex refrigeration systems.

Examples for HCs as primary refrigerant include Rivers [68], who reported on an SL refrigeration system designed for a supermarket in Greenwich, England. An HC was chosen as primary refrigerant. Propylene glycol was employed as the medium temperature secondary refrigerant, while an organic potassium salt solution was chosen for the low temperature loop. Baxter [69] reported a case study for a small Danish supermarket where the old refrigeration plant had been replaced with a cascade plant. R290 was used as the high temperature refrigerant (14/30°C) while CO_2 was used as the low temperature refrigerant (32/11°C). CO_2 was used directly to perform the cooling in the freezers while propylene glycol was used in the coolers. Total energy consumption was decreased by 10% with the new plant.

Primary refrigerants mostly used in residential and automotive air-conditioning are HCs, CO_2, or R152a (used in MACs). Examples for

hydrocarbons include Choi et al. [70], who evaluated the performance of R22, R290, R290/600a (70/30%), and R32/152a (50/50%) used in a water-to-water residential heat pump for space cooling and heating. The secondary fluid was a 60/40% mixture of water and ethylene glycol. For the same system capacity, R32/152a proved to be the best performer due to a good temperature glide matching in the heat exchangers and its excellent thermodynamic and transporting properties. The HC mixture R290/600a had the highest COP at a given compressor speed, but its COP at the constant-capacity criterion was the lowest. Chang et al. [71] reported the performance and heat transfer characteristics of a heat pump system charged with HC refrigerant (R290, R600a, R1270 and binary mixture of R290/ R600a and R290/R600). The secondary fluid was ethyl alcohol. Test results showed the heating and cooling capacity of R290 was slightly less than that of R22. The COP of R290 was slightly higher compared to R22. The heating and cooling capacities of R290/600a and R290/600 mixtures were nearly linear with respect to mass fraction of R290. Pelletier and Palm [72] tested a domestic heat pump using R290 as compared to the R22 baseline system. For R290, the heating capacity was 7–10% lower, while the heating COP was 4–5% higher than R22. Payne et al. [73] investigated and compared the performance of R22, R290 and zeotropic mixtures of R32/R290 and R32/152a. The secondary fluid was 70/30% mixture of water and ethylene glycol. In the cooling mode at a constant capacity, the R32/290 (50/50%) mixture resulted in the highest COP, 8% higher than R22. In the heating mode, the COP of R290 was the highest, 6–8% higher than that of the remaining fluids.

Examples using CO_2 as primary or secondary refrigerant in residential systems include Stene [74], who investigated the performance of a residential brine-to-water CO_2 heat pump for combined low temperature space heating and hot water heating. The system heating capacity was 6.5 kW. Yanagisawa et al. [75] investigated a SL refrigeration system, using a vapor compression NH3 cycle as the primary loop and a CO_2 thermosiphon loop as the SL. In the SL, CO_2 was circulated between the intermediate heat exchanger and the cooler by the difference in density between liquid and vapor lines. The experimental SL with the CO_2 liquid head of 0.9 m operated at a cooling capacity of 3.5 kW and COP of 3.7.

In automotive air-conditioning, natural refrigerants, such as HCs, are considered due to the currently used refrigerant, R134a being phased out by 2011 in the European Union. HCs present a potential alternative to R134a due to their good thermodynamic and transport properties, heat transfer characteristics, material compatibility, low cost, low toxicity and low GWP (Corberan et al. [30]; Domanski and Yashar [76]; Fernando et al. [54]; Mani and Selladurai [77], Palm [48]). The chemical industry has been working to synthesize new chemicals and mixtures of chemicals that have a GWP below the required threshold, such as R152a (Ghodbane [39]) and R1234yf (Hill [78]; Spatz and Minor [28]). The HCs, R152a, and NH3, have received less attention compared to other refrigerants because of safety concerns, such as flammability or toxicity. The USA Environmental Protection Agency (EPA) does not explicitly forbid the retrofit of R134a systems with Hydrocarbons, though some states do [79]. However, HCs

are declared unacceptable substitutes on the basis of a current lack of adequate assessment of their flammability risk by the U.S. EPA as of 2010 [80]. Therefore, most published papers on these refrigerants being employed in automotive direct expansion systems are theoretical in nature. However, one way of safely employing HCs, R152a or NH3 in MACs is to use them in conjunction with a SL system. An SL system would prevent the primary refrigerants from entering the passenger cabin and thereby mitigate any fire hazard for vehicle occupants.

Secondary Refrigerants

There are two kinds of secondary refrigerants: single phase fluids and two-phase fluids. Single phase fluids generally include some kind of antifreeze solution, corrosion inhibitor, or biocides. A series of glycol-, potassium acetate-, and potassium formate-based secondary refrigerants have been applied in SL refrigeration systems (Ure [81]). There are few SL refrigeration systems that use a two-phase mixture as secondary refrigerant. Two-phase secondary refrigerants take advantage of the high latent heat during the phase change process from liquid to solid or from liquid to gaseous state (Delventura et al. [82]). The higher the percentage of refrigerant undergoing the phase change, the higher the energy stored per kilogram of refrigerant. The freezing point is the most important physical property to consider when choosing among fluids. Usually the freezing point of the chosen secondary refrigerant is not less than 5–10 K below the system operating temperature. Aqueous solutions, due to their high specific heat and good heat transfer coefficients, are widely used as working fluids in the

secondary circuit. Most commonly used aqueous solutions with their thermophysical properties are listed in Table 1.3 (Melinder [83]).

Table 1.3: Characteristics of Aqueous Solutions as Secondary Refrigerants [26]

Aqueous Solutions	c_A [wt.%]	t_F [°C]	t [°C]	ρ [kg/m^3]	cp [kJ/kg K]	k [W/m K]	μ [mPa s]
Ethylene Glycol	36.19	-20	-10	1058	3.494	0.415	7.99
Propylene Glycol	39.41	-20	-10	1045	3.620	0.384	21.67
Ethyl Alcohol	29.73	-20	-10	970	4.127	0.393	12.22
Methyl Alcohol	24.87	-20	-10	969	3.914	0.431	5.42
Glycerol	46.28	-20	-10	1129	3.155	0.460	2.94
Ammonia	13.46	-20	-10	953	4.239	0.460	2.94
Potassium Carbonate	30.95	-20	-10	1322	2.877	0.519	6.25
Calcium Chloride	20.82	-20	-10	1196	2.992	0.530	4.48
Magnesium Chloride	16.59	-20	-10	1151	3.192	0.505	5.58
Sodium Chloride	22.62	-20	-10	1182	3.305	0.530	4.22
Lithium Chloride	13.66	-20	-10	1083	3.405	0.522	3.97
Potassium Acetate	27.91	-20	-10	1155	3.232	0.467	5.67
Potassium Formate	28.94	-20	-10	1192	3.121	0.506	3.55

Other secondary refrigerants, which are widely used include ice slurries and CO_2. Ice slurries consist of a number of ice particles in an aqueous solution where the diameter of ice particles is equal or smaller than 1mm, as stated by Egolf and Kauffeld [84]. The smaller the ice particles are, the better the slurries can be transported. The cooling capacity of an ice slurry is four to six times higher than that of conventional chiller water, depending on the ice fraction (Ure and Mashrae [85]). Often cooling point depressants, such as salts or ethanol are used, as researched by Meewisse and Ferreira [86] who compared two freezing point depressants, sodium chloride and ethanol. The results showed that economic performance of SL cooling cycle utilizing sodium chloride as freezing point depressing substance was at most 8% higher than that of ethanol.

Examples of successful integration of ice slurries in SL systems include Wang and Goldstein [87], who applied an ice slurry system for cooling in railway transportation, Christensen and Kauffeld [88], who described the application of ice slurry as secondary refrigerant in a SL system with the use of an ice slurry accumulation tank, and Wang et al. [89] who studied an SL ice slurry system using ethylene glycol-water binary solution in the Ritz Carlton Plaza Hotel in Japan. Fukusako et al. [90] reviewed studies related to the cold thermal storage systems and components using ice slurries and recent research activities on ice slurries in Japan. The types of ice storage systems were categorized into five groups by the process of ice manufacturing. Saito [91] reviewed recent research on cold thermal energy storage including a SL ice slurry system. The ice making process, ice storage process, transportation and utilization of stored ice, as well as the whole process were identified as important future research topics.

Recently more and more attention has been paid to Carbon Dioxide (CO_2), which shows several benefits as a two-phase secondary fluid. The advantages of utilizing CO_2 as a secondary refrigerant are lower pumping power (zero pump power when thermosiphon is used), smaller pipe size, excellent heat transfer properties, and good material compatibility with the additional benefit of the low cost of the fluid compared to conventional single-phase secondary refrigerants. The main disadvantage of CO_2 appears to be relatively low critical temperature and limited availability of components (Hinde et al. [92]). A few applications that utilize CO_2 as a volatile secondary refrigerant have been implemented in low-temperature applications in supermarket systems in Sweden (Melinder [93];

Pachai [94]; Pearson [95]). Pearson [96] submitted patents on the use of CO_2 as a volatile secondary refrigerant, including a novel hot gas defrost system.

Further examples on CO_2 as secondary refrigerant include Christensen [97], who investigated a SL system using CO_2 as primary and secondary refrigerant in supermarket applications. Tests showed that CO_2 was a suitable alternative to HFCs in supermarket applications. Pachai [94] reported a SL system installed in Helsingborg, Sweden. The primary refrigerant was a HC, a mixture of R290 and R170, and the low- and intermediate-temperature side secondary refrigerants were CO_2 and propylene glycol, respectively. The system had successfully been running since 1997 and more than fifty shops have been installed with similar systems in Sweden. Nilsson et al. [98] reported an ice rink refrigeration system with CO_2 as the secondary fluid with a cooling capacity of 15 kW. Also in 2006, a British company implemented an air-conditioning system to protect computer servers against overheating for a bank at its London office, as reported by Jahn [99]. The chilled water circuit condensed CO_2 at 6°C. Then, CO_2 was pumped out to the server cabinets by centrifugal pumps, evaporated, and returned to the condenser to begin the process again. The cooling capacity of the whole system was 300 kW. Hinde et al. [92] reported that at least nine low-temperature CO_2 systems were operational in the USA and Canada in early 2008. All systems utilized CO_2 as a low-temperature two-phase secondary refrigerant. The stores ranged in size from small neighborhood markets to large supercenters and warehouse-style stores. The system's cooling capacities ranged from 22 to 160 kW.

Secondary Loop Systems in Automotive Applications

Examples of secondary loop systems in MACs include Ghodbane[39], who investigated the potential of R152a and HC refrigerants as alternative refrigerants to R134a and published a comparative assessment of a SL system applied to MACs. The assessment showed that the SL for MACs requires less development time compared to other alternatives, such as CO_2, air cycle, etc. Ghodbane expected the SL system to have higher mass and cost than the baseline R134a system, but to offer the potential of being lower mass and cost compared to the other alternatives to R134a systems. The performance of a SL MAC with R152a or HCs as primary refrigerant and ethylene glycol-water mixture in 50/50 wt.% as secondary refrigerant was compared theoretically to a traditional DX system using R134a. Based on the theoretical comparison, the author decided to experimentally test a SL system using R152a as primary refrigerant. Comparison of the performance of the SL system with a production R134a system as baseline is shown in Table 1.4 at 87.5 km/h road load and ambient conditions of 37.8°C and 40% RH. The SL system COPs were decreased by 5–19% while the condenser capacities were increased by 6% when R152a was used as a primary refrigerant. The contributor to higher compressor power and higher condenser capacity for the SL system was a low suction condition, which was dictated by the cooling capacity requirement. Added pump power in combination with the indirect contribution from low suction conditions were found to result in a low COP compared to DX systems.

Table 1.4: Comparison of R152a to R134a in an Automotive Secondary Loop System [39]

Parameter	Refrigerant / System			
	R134a DX	**R152a DX**	**R134a 2LP**	**R152a 2LP**
Ambient Temperature [°C]	37.8	37.8	37.8	37.8
Ambient Relative Humidity [°C]	40	40	40	40
Humidity Ratio [kg/kg dry air]	0.017	0.017	0.017	0.017
Evap. Air Flow Rate [m^3/h]	424.8	424.8	424.8	424.8
Evap. Air Mass Flow Rate [kg/min]	7.8	7.8	7.8	7.8
Evap. Outl. Air Temperature [°C]	10	10	10	10
Cond. Air Flow Rate [m^3/h]	3,398	3,398	3,398	3,398
Cond. Air Mass Flow Rate [kg/min]	62.6	62.6	62.6	62.6
Cond. Outl. Air Temperature [°C]	47.8	47.2	48.3	47.8
Refrigerant Charge [kg]	0.96	0.62	0.96	0.62
Refr. Mass Flow Rate [kg/min]	3.14	1.82	3.28	1.88
Comp. Suction Pressure [kPa]	300	295	214	213
Comp. Suction Temperature [°C]	3.6	4.4	-5.6	-5.0
Comp. Discharge Pressure [kPa]	1,723	1,544	1723	1,544
Comp. Discharge Temperature [°C]	90.6	107.2	95.6	123.3
Comp. Isentropic Efficiency	60%	60%	60%	60%
Comp. Power [kW]	3.24	2.89	4.03	3.89
Cond. Outl. Pressure [kPa]	1,640	1,510	1,640	1,510
Cond. Outl. Temperature [°C]	50.6	51.7	50.6	51.7
Cond. Capacity [kW]	10	9.6	10.8	10.6
Evap. Inl. Pressure [kPa]	368	326	263	235
Evap. Inlet Temperature [kPa]	6.7	5.6	-2.8	-3.3
Evaporator Effectiven./Overall Eff.	85%	85%	62%	62%
Evap. Latent Load [kW]	3.1	3.1	3.1	3.1
Evap. Sensible Load [kW]	3.6	3.6	3.6	3.6
Evap. Cooling Capacity [kW]	6.7	6.7	6.7	6.7
Comp. Power [kW]	3.2	2.9	4.0	3.9
Comp. Power Loss [kW]	0.097	0.087	0.12	0.12
A/C Blower Power [kW]	0.28	0.28	0.28	0.28
System Power [kW]	3.6	3.3	4.6	4.4
Cycle COP [-]	2.072	2.322	1.666	1.726
System COP [-]	1.863	2.065	1.464	1.51

Dentis et al. [100] compared the SL system with R152a and HC refrigerants to an R134a system on a test bench, and demonstrated that the performance of SL system was similar to, and in some cases exceeded, the

performance of an R134a system. Ghodbane [101] also compared the performance of MAC SL systems to conventional R134a systems used in a small size passage car under the same test conditions in a windtunnel and in road performance tests. The SL system delivered equal or better performance and comfort levels compared to the production R134a system.

Ghodbane and Baker [102] received a patent on the SL system for passenger compartment heating and cooling. Another patent was issued to Kadle and Ghodbane [103] for a heat pump using SL air-conditioning system. An R152a SL system with pre-prototype components installed in a sport utility vehicle was demonstrated by Ghodbane et al. [104]. They built and tested the performance of an R152a SL system, in a compact passenger car. The energy consumption of the MAC compressor in the SL system was shown to be 13–16% lower compared to the production R134a system when applying a capacity control algorithm. The global warming impact of direct refrigerant emissions of the R152a SL system was claimed to be lower by at least 94% compared to an equivalent R134a system.

1.5 Literature Review Summary

- Few researchers did transient tests with MACs in controlled laboratory environments. Transient tests, such as drive cycle tests, are usually performed in a climatic windtunnel, which is associated with high expenses. At the same time, climatic windtunnel tests limit the amount of instrumentation and the accuracy of results that can be obtained.

- Researchers which performed dynamic tests with MACs usually operated in narrow operating conditions, often limited by the employed equipment. In few cases where drive cycle research was conducted, the drive cycle control was rigid and of limited accuracy.
- A. Gado developed a cabin model which enabled transient testing of MAC components without the need for industry scale climatic windtunnels.
- Most pure modeling research and simulation studies are limited to simple transient studies, such as pulldown scenarios.
- Commercial software was used in many cases which limits access to the source code and the flexibility of adding own component models.
- The software Dymola shows a potential to be universally employable in transient studies of MAC systems. Dymola is based on a modular approach with a variety of component libraries which can be updated by adding new components or altering the source code of existing components.
- In general, publications on research in automotive air-conditioning are rare when compared with other fields. The automotive industry often chooses to not disclose complete statements of testing conditions or exact system parameters.
- The review on low GWP refrigerants showed that mildly flammable to flammable refrigerants are safely used in a variety of industrial, commercial and residential (mostly Europe/ Asia) settings. Cars with direct expansion MACs running with Propane (R290) exist in Australia.
- Simulation and experimental research on flammable refrigerants in MACs shows that R152a and R290, as well as mixtures of R290 and R600a are promising candidates to be used in future automotive air-conditioning systems.

- Hydrocarbons, such as R290 and R600a, are superior with regard to environmentally friendly operation. At the same time the supply of HCs can be reliably guaranteed in most parts of the world.

- Risk assessment studies showed that the risk of fire due to the use of hydrocarbons as refrigerant in direct expansion systems (DX) is low compared to background risks. It is generally agreed upon that it is safe to use hydrocarbons in MACs if safety measures are taken. The use of secondary loop system is one of these safety measures.

- A variety of alternative flammable refrigerants can be used as primary refrigerants in SL systems. Considering the desired characteristics for automotive systems, such as normal boiling point and specific volume, R152a and R290 have been shown to operate well in SL systems.

- Experimental research on R152a SL MAC systems was done by Ghodbane et al., who showed the viability of automotive SL systems, whereas R290 has only been used in commercial applications and not yet in automotive applications.

- Though limited experimental research was done, no studies on the typical characteristics and strengths of secondary loop system (i.e. cold storage, multiple cooling loads, delayed pull down, etc.) were found in published literature.

- For simplicity and reliability, aqueous mixtures of water and ethylene glycol work well as secondary refrigerants in automotive SL systems. The high specific heat and high heat transfer coefficient of water favor mixtures with high water content, such as a 68/32% water ethylene glycol mixture.

2 Research Objectives

The overarching goal of this thesis is to study the performance of secondary loop systems, in particular thermal storage potential and benefits in terms of transient performance. Based on the reviewed literature, as well as developments in state-of-the-art automotive air-conditioning units, the following research objectives have been identified:

1. Characterize performance of secondary loop systems using low-Global Warming Potential (GWP) refrigerants
    - Build a test facility which enables steady-state and transient performance measurements with high accuracy for direct expansion, as well as secondary loop systems
    - Quantify performance characteristics of secondary loop systems, such as cooling capacity, coefficient of performance (COP), energy consumption and pull down time
    - Investigate the performance of environmentally friendly low-GWP refrigerants, such as R152a and R290 in secondary loop systems
2. Quantify potential benefits of thermal storage, as well as measures to reduce A/C energy consumption
    - Quantify the effect of thermal storage on thermal comfort and power consumption during off-cycle operation
    - Investigate the role of phase change thermal storage to reduce energy consumption of secondary loop systems
    - Evaluate alternative measures of reducing energy consumption, such as compressor and pump controls, as well as cabin pre-conditioning
3. Model and simulate a secondary loop system for steady-state, as well as transient operation with Modelica
    - Model a passenger cabin, a direct expansion system and a secondary loop system
    - Validate models based on experimental data

- Simulate effects of coolant volume and composition on transient system performance

A test facility was built to accommodate direct expansion and secondary loop systems. The test facility, the sensing equipment, and modifications made to the facility for different tests are described in Chapter 3. Data acquisition and controls of the facility, as well as the cabin model needed for transient testing, are discussed in Chapters 4 and 5.

Experimental results to quantify the performance of secondary loop systems in relation to direct expansion systems, as well the test procedures used for steady-state and transient performance testing are discussed in Chapter 7.

The performance of alternative refrigerants, such as R152a and R290 in the secondary loop system is discussed in Chapter 8. Steady-state, as well as transient experimental results are provided with respect to the R134a direct expansion system.

Thermal storage of secondary loop systems during off-cycle period, as well as the development of suitable test procedures is discussed in Chapter 9, as well as an evaluation of ice storage with regards to thermal comfort and energy saving in electric vehicles.

Chapter 10 introduces possible control strategy to reduce energy consumption during the operation of the air-conditioning unit in electric vehicles. The benefits of different control strategies and cabin pre-conditioning are investigated and discussed.

Models of a direct expansion system, a secondary loop system, and an automotive passenger cabin were built in the Modelica language. Details of the models and their validation with experimental data are shown in Chapter 11. Simulations were carried out to study the effect of coolant volume and coolant composition on transient system performance.

3 Experimental Test Facility

Chapter 3 is divided into three parts, each introducing a variation of the experimental facility, which was build to perform tests on mobile air-conditioning systems (MACs). While chapter 3.1 acquaints the reader with the basic direct expansion (DX) system, also referred to as the baseline system, Chapters 3.2 and 3.3 introduce variations which enable experimental research on secondary loop systems. Specifically, the secondary loop (2LP) test facility, and the combined secondary loop ice storage (IS) facility. Each facility allows for the use of different refrigerants in the vapor compression cycle.

3.1 Direct Expansion Test Facility

Figure 3.1 shows the direct expansion (DX) baseline facility. The test rig features a basic vapor compression cycle (VCC), including a compressor (1), a condenser (2), an electronic expansion valve (3) and an evaporator (4). The automotive compressor is belt driven by an electric motor (5), similar to the operation in cars using internal combustion engines (ICEs). The motor is driven by a variable frequency drive (VFD), enabling a variable speed control of the compressor. A torque meter in between the electric motor and the compressor, combined with an rpm meter in front of the compressor clutch, allows for measurement of compressor power consumption. A receiver (6) was installed after the condenser for a stable refrigerant charge management during changing operating conditions. A mass flow rate meter, placed at the lowest point of the

test facility after the receiver, measured mass flow rate of subcooled liquid refrigerant to determine refrigerant-side cooling capacity.

For the purpose of automotive air-conditioning testing, the test facility allowed for two independent climatic environments, namely the ambient and the passenger cabin. This was accomplished by housing the condenser windtunnel (9) in a climatic chamber and installing the evaporator in a psychrometric loop featuring an air handling unit (AHU) (8). The condenser windtunnel, as well as the evaporator psychrometric loop served the purpose of air flow rate and air-side capacity measurements at the respective heat exchangers. In addition to nozzles (7), needed for air flow rate measurement, both the windtunnel and the psychrometric loop featured thermocouple mesh grids, relative humidity measurements, flow turbulators, and flow straighteners in accordance with AHSRAE standard [105].

Figure 3.1 contains a legend, which details system components and sensing equipment used in the direct expansion baseline facility.

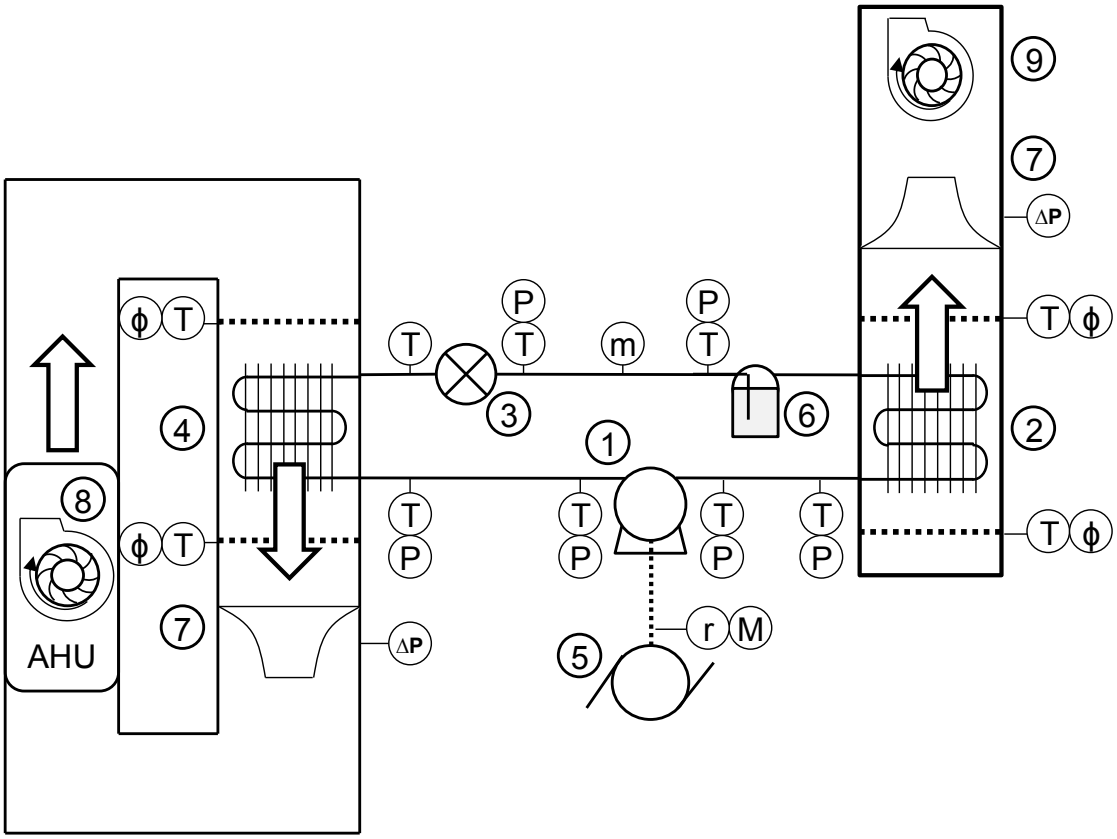

Component Symbols	Component/Sensor
1	Compressor
2	Condenser
3	Expansion Valve (electronic)
4	Evaporator
5	Electric Motor
6	Receiver
7	Air Flow Nozzle
8	Air Handling Unit
9	Fan
Sensor Symbols	
m	Mass Flow Rate Meter
M	Torque Meter
P	Pressure Transducer
ΔP	Differential Pressure Transducer
r	RPM Meter
T	Thermocouple
ϕ	Relative Humidity Sensor

Figure 3.1: Direct Expansion (DX) Test Facility Schematic

3.2 Secondary Loop Test Facility

Figure 3.2 shows a schematic of the secondary loop (2LP) experimental test facility. Compared to the baseline direct expansion facility, several modifications were made to the facility. The evaporator of the VCC was replaced with an intermediate plate type heat exchanger (4). Instead of the evaporating refrigerant cooling down the air of the passenger cabin directly, the intermediate heat exchanger cools down a secondary working fluid.

About 5.5 kg of a water-ethylene glycol mixture were used in the current research, prepared to 32 wt% ethylene glycol and 68 wt% water. The use of a water glycol mixtures is common in automobiles and was chosen due to its balance between frost prevention, high specific heat capacity, cost effectiveness, and safety. The mass fraction of water and glycol was chosen to prevent pipe bursts due to freezing at low ambient temperature while maximizing water content in the mixture, due to the superior heat transfer characteristic of pure water. Furthermore, this specific mass fraction was chosen to allow for comparison with previous research by Ghodbane et al. [104].

A variable speed pump (8) was used to circulate the chilled coolant from the intermediate heat exchanger through a liquid to air heat exchanger, called the cooler (5). In the experimental test facility, the cooler cools down the air in the psychrometric loop. In an automobile, the cooler would be located underneath the dashboard to provide cool air to the passenger cabin. A reservoir (9) was used as pressure expansion tank. Temperatures and coolant mass flow rate

were measured to determine capacities of the intermediate heat exchanger and the cooler in the secondary loop.

In automobiles, this configuration allows for the entire vapor compression cycle to be placed underneath the hood. This results in a significant reduction of refrigerant charge, a reduction of refrigerant-side pressure drop, and an increase in safety when using flammable or high pressure refrigerants. On the other hand, more components (heat exchangers, pump, coolant) result in an increase in mass and consequently fuel consumption, A/C power consumption, as well as a thermal delay in passenger cabin cool down. Some of these disadvantages may be offset by a smart choice of refrigerants and thermal storage controls to balance the need for capacity to deliver passenger comfort and the goal of achieving a reduction in long term A/C power consumption.

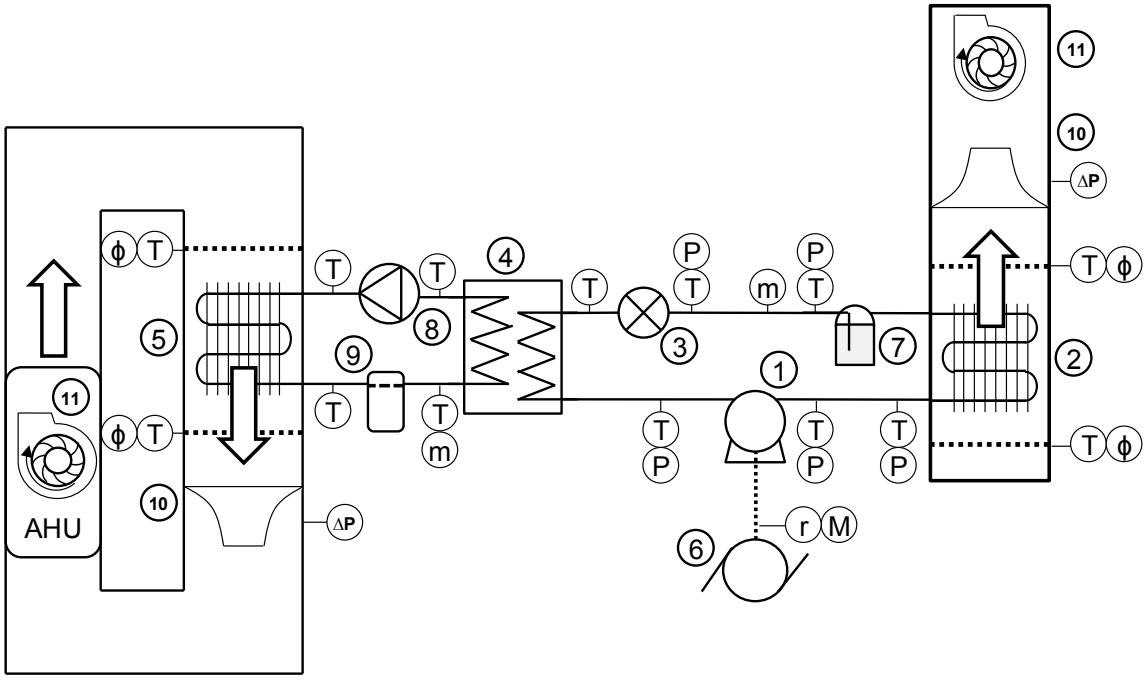

Component Symbols	Component/Sensor
1	Compressor
2	Condenser
3	Expansion Valve (electronic)
4	Intermediate Heat Exchanger
5	Cooler
6	Electric Motor
7	Receiver
8	Coolant Pump
9	Coolant Reservoir
10	Air flow Nozzle
11	Air Handling Unit
12	Fan
Sensor Symbols	
m	Mass Flow Rate Meter
M	Torque Meter
P	Pressure Transducer
ΔP	Differential Pressure Transducer
r	RPM Meter
T	Thermocouple
ϕ	Relative Humidity Sensor

Figure 3.2: Secondary Loop (2LP) Test Facility Schematic

3.3 Secondary Loop combined with Ice Storage Test Facility

Figure 3.3 shows the test facility schematic for a secondary loop test facility including ice storage (IS). The figure omits the primary loop, i.e. the VCC, since the refrigerant-side was not modified. The main change to the secondary loop facility, introduced in Chapter 3.2, is the addition of an ice storage box (3) and the integration of three sets of ball valves (6) to bypass each heat exchanger.

The ice storage heat exchanger, shown in Figure 3.4 was custom designed and built in the laboratory for the purpose of producing ice from 15 Liters of water and using the ice to assist the VCC in cooling the passenger cabin. Based on transient performance data from the baseline and secondary loop system, the heat of fusion of 10 to 15 L of ice was found to provide enough energy for cooling the passenger cabin during a 20 minute commute without the need for a vapor compression system. However, this idealized approximation did not account for the challenge of distributing the heat fast and evenly throughout the ice so as to harvest the cooling capacity in a quick and homogenous fashion. During realistic operation, the ice would melt quickly around the tubes of the heat exchanger, giving rise to sensible heating of liquid water around the tubes. The estimated 10 to 15 L of ice would not suffice as a standalone source of cooling, but would rather be helpful in taking part of the load away from the VCC. To increase heat transfer, fins were added to the ice storage heat exchanger, though with a significantly larger fin spacing compared to air-side fins.

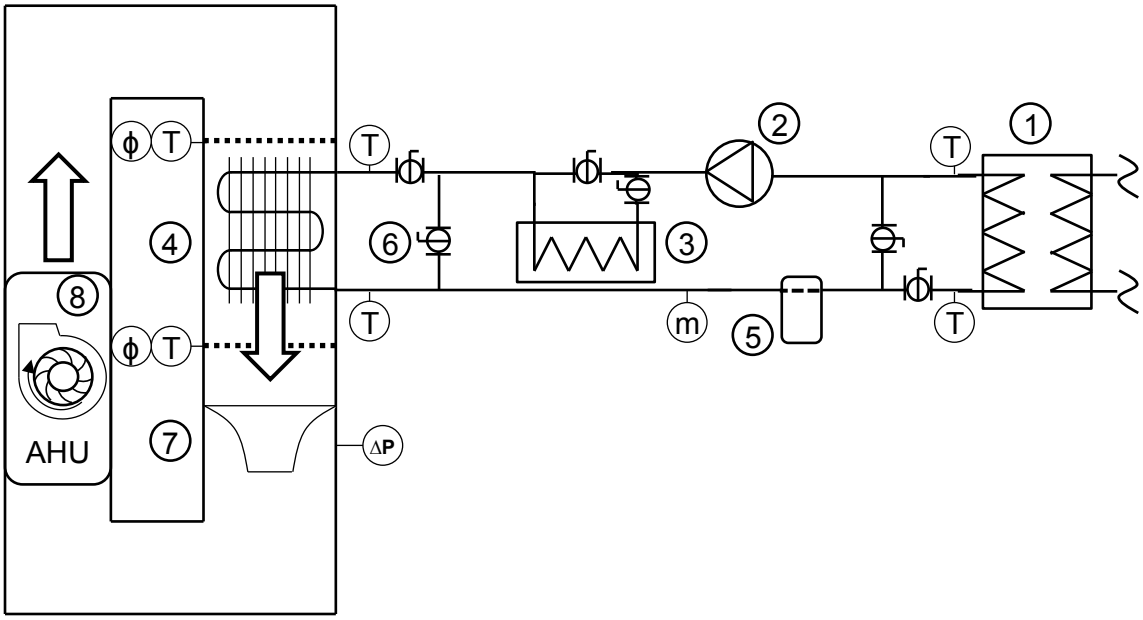

Component Symbols	Component/Sensor
1	Intermediate Heat exchanger
2	Coolant Pump
3	Ice Storage Heat Exchanger
4	Cooler
5	Coolant Reservoir
6	Ball Valve
7	Air Flow Nozzle
8	Air Handling Unit
Sensor Symbols	
m	Mass Flow Rate Meter
ΔP	Differential Pressure Transducer
T	Thermocouple
ϕ	Relative Humidity Sensor

Figure 3.3: Ice Storage (IS) Test Facility Schematic

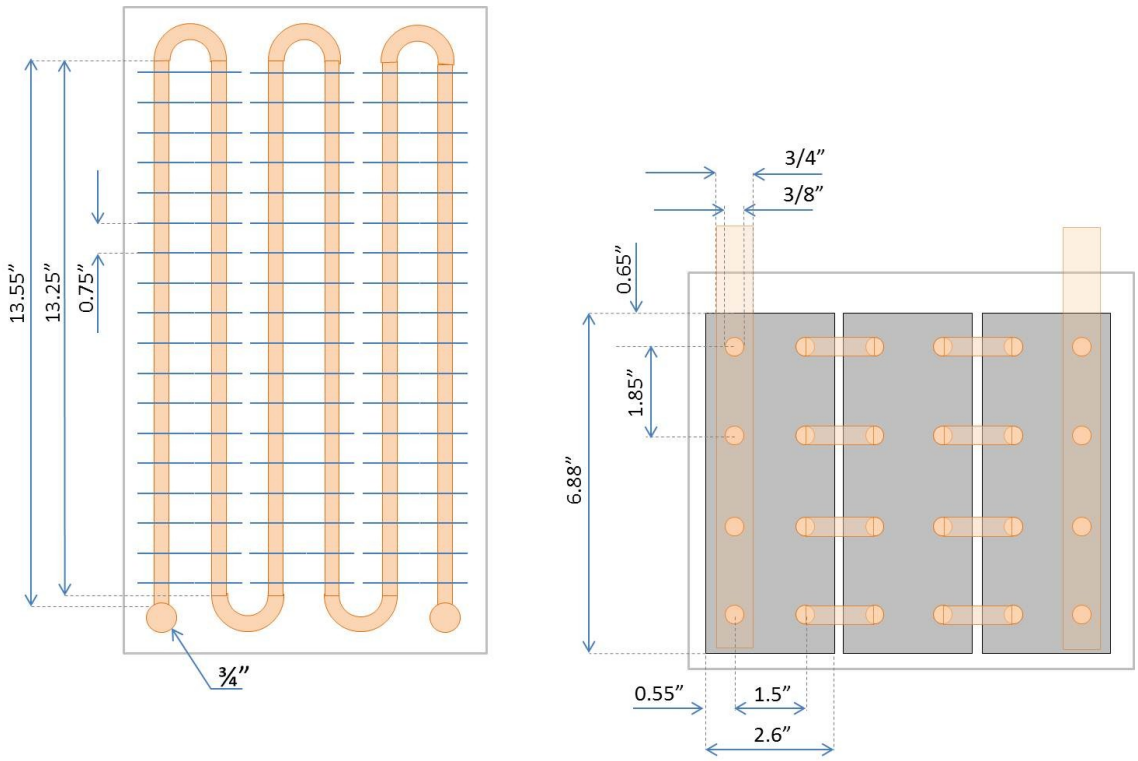

Figure 3.4: Ice Storage Heat Exchanger Schematic

The ice storage heat exchanger, made solely of copper, was manufactured in the laboratory according to the following design goals:

- to allow for manual construction using soldering connections
- to create a large surface area for heat transfer, while remaining structurally stable
- to fit into and sufficiently use the volume of a 15 liter plastic box

Figure 3.5 provides information on the operational modes of the ice storage test facility. Bypasses, controlled by ball valves, allow for four operational modes of the facility. Mode (a) bypasses the ice storage heat exchanger, so as to use only the basic secondary loop system for cooling. Mode (b) is a charging

mode, in which the cooler is bypassed to allow the entire cooling capacity of the VCC to be used for ice production. Mode (c) enables the combination of VCC and ice storage to cool the passenger cabin. Mode (d) forces the ice storage box to cool the passenger cabin alone, by bypassing the chiller.

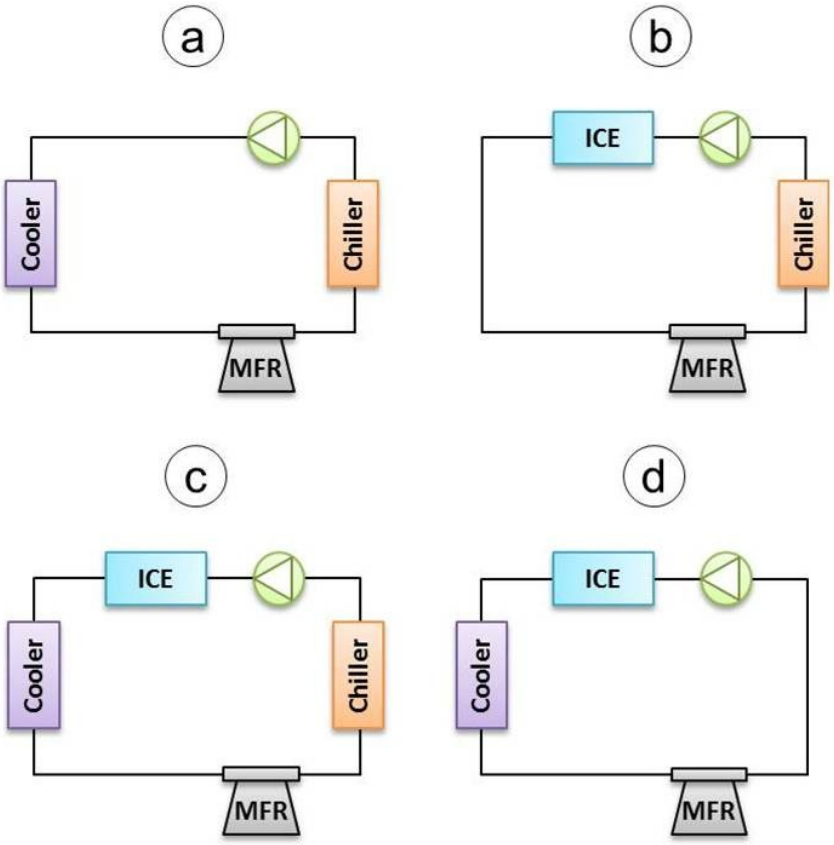

a) Vapor Compression cooling only (2LP)
b) Ice Storage charging
c) 2LP plus Ice Storage cooling (2LP + IS)
d) Ice Storage cooling only (IS)

Figure 3.5: Ice Storage Facility Operation Modes

Specifications of the sensing equipment used throughout the three variations of the experimental test facility are provided in Table 3.1. The type of sensing equipment, as well as manufacturer and model, are shown. The table further provides information on operating range and systematic uncertainty, based on manufacturer's data.

Specifications of system components, such as compressor, expansion valves, and heat exchangers are provided in Appendix A.

Table 3.1: Sensing Equipment Specifications

Sensor	Manufacturer/Model	Operating Range	Systematic Uncertainty
Refrigerant-side			
Thermocouple	Omega / T-type	-200 : 350 °C	± 0.5 K
Pressure Transducer	Setra / 280E	0 : 250 psig	± 0.13% FS
	Setra / 280E	0 : 500 psig	± 0.13% FS
Mass Flow Rate Meter	MicroMotion	0 : 1,300 kg/h	± 0.05% AR
Air-side			
Thermocouple-grid	Omega / T-type	-200 : 350°C	± 0.3 K
Relative Humidity Sensor	Vaisala / HMD 30YB	2 : 100%	± 2 %
	Vaisala / HMD 60Y	2 : 100%	± 2 %
Differential Pressure Tr.	Setra / 264	5.0" WC	± 1% FS
Refrigerant-side			
Thermocouple	Omega / T-type	-200 : 350 °C	± 0.5 K
Mass Flow Rate Meter	MicroMotion/ R025	0 : 2,720 kg/h	± 0.5% AR
Compressor/Pump Power			
RPM Meter	Shimpo / RS-220H	0 : 500 Hz	± 0.1% AR
Torque Meter	Himmelstein 28002T	56.5 Nm	± 0.1% FS
Watt Meter	Ohio Semitronics / PC5	0 : 750 W	± 0.5% FS

4 Data Acquisition and Analysis

Chapter 4 introduces the data acquisition process, as well as the data reduction process and uncertainty analysis.

4.1 Data Acquisition Process

Figure 4.1 shows the structure of the data acquisition process (DAQ). The sensing equipment (1), introduced in Chapter 3, sends output signals of 4-20 mA or 0-5 VDC to National Instrument Field Point modules (2) [106]. Field Point modules collect the signals and transfer them to a data acquisition personal computer (PC) (3). National Instrument's LabVIEW software reads in the signals for further processing. Several LabVIEW programs (4) were written, some of which are introduced in Chapter 5. The programs allow for reading sensor signals, converting them to the unit of measure (i.e. pressure or mass flow rate) and employing data reduction techniques. In addition to the standard LabVIEW library, the PID Control Toolset, as well as a sub-program, XProps [107], were used. XProps is a software distributed by Optimized Thermal Systems and is based on NIST's REFPROP-8 [108] refrigerant property database. Furthermore, sub-programs for moist air and for water-glycol mixtures were used in the data reduction process. Part of the processed data was used to control equipment in the test facility (5) (6), as well as visualize processes real time on the PC monitor (7). Controls can be distinguished into continuous controls, using analog output modules (used for EXV opening, compressor rpm, etc.), or the control of discrete

events, using digital output modules (used for compressor clutch, pump on/off, etc.). An array of all collected data and processed data was written to a Microsoft Excel spreadsheet (8). Custom Microsoft Excel analysis spreadsheets were used for further data analysis and visual formatting.

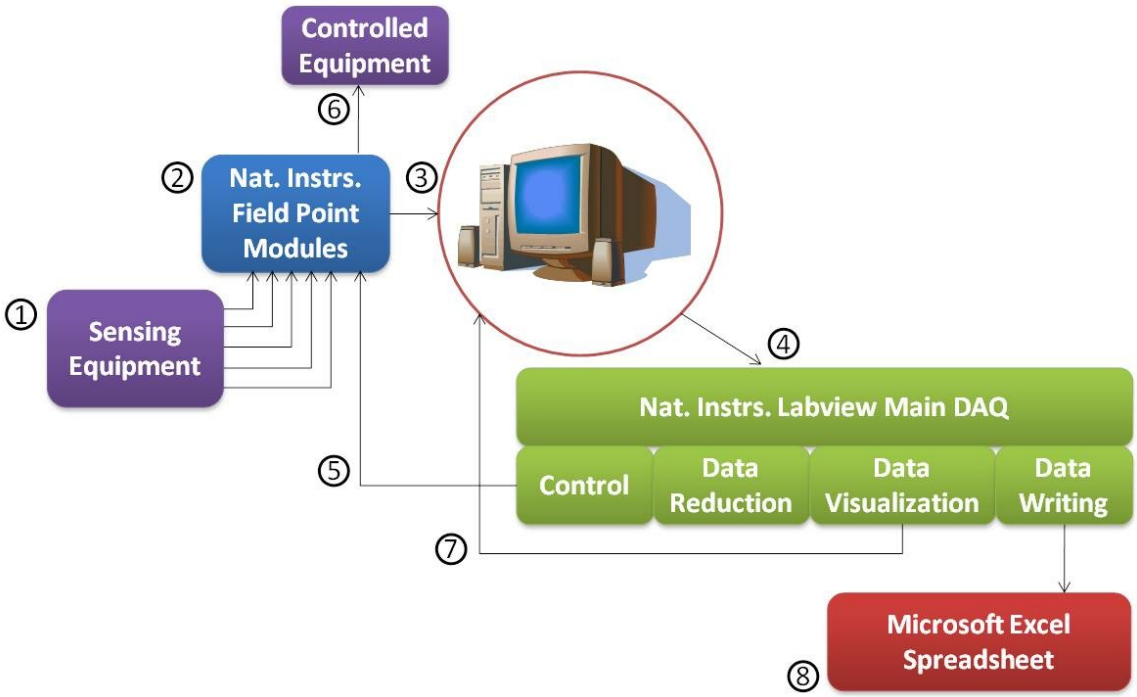

Figure 4.1: Data Acquisition Process Structure

4.2 Data Reduction Process

Data reduction was performed within the LabVIEW data acquisition program. Property subroutines are an essential part of converting measurables, such as temperature and pressure, into calculated parameters, such a density, specific heat capacity, enthalpy, and others. A refrigerant property subroutine, a moist air property subroutine, as well as a property subroutine for aqueous mixtures of glycol were used in LabVIEW to calculate fluid properties. The

refrigerant property subroutine is based on XProps [107]. The moist air property subroutine was developed by Hwang and Aute in the Center for Environmental Energy Engineering. The glycol property subroutine was written specifically for this research. Equations and coefficients used in the subroutine were borrowed from M. Conde Egineering [109]. A visual representation of all subroutines, showing the respective inputs and outputs, is provided in Figure 4.2.

Air flow rates across cooler and condenser were determined by pressure drop measurement across nozzles in the condenser windtunnel and the evaporator psychrometric loop. The calculation of air flow rates, and subsequently the calculation of air-side heat exchanger capacities, were based on the "Standard Methods for Laboratory Airflow Measurement", ANSI/ASHRAE 41.2-1987 (RA92) [105].

Airs side mass flow rates were calculated based on air flow rate and local density using Equation (1).

$$\dot{m} = \dot{V}_{Nozzle} \times \rho_{Nozz,In} \quad (1)$$

Air-side capacity was determined for the evaporator and cooler using mass flow rate and enthalpy difference, while condenser air-side capacity was determined using mass flow rate, specific heat capacity, and temperature difference, as shown in Equations (2) and (3), respectively.

$$\dot{Q}_{Evap,Air} = \dot{m}_{\mathrm{Evap,Air}} \left(\Delta \mathrm{h}\right) \quad (2)$$

$$\dot{Q}_{Cond,Air} = \dot{m}_{\mathrm{Cond,Air}} \times c_p \left(\Delta T\right) \quad (3)$$

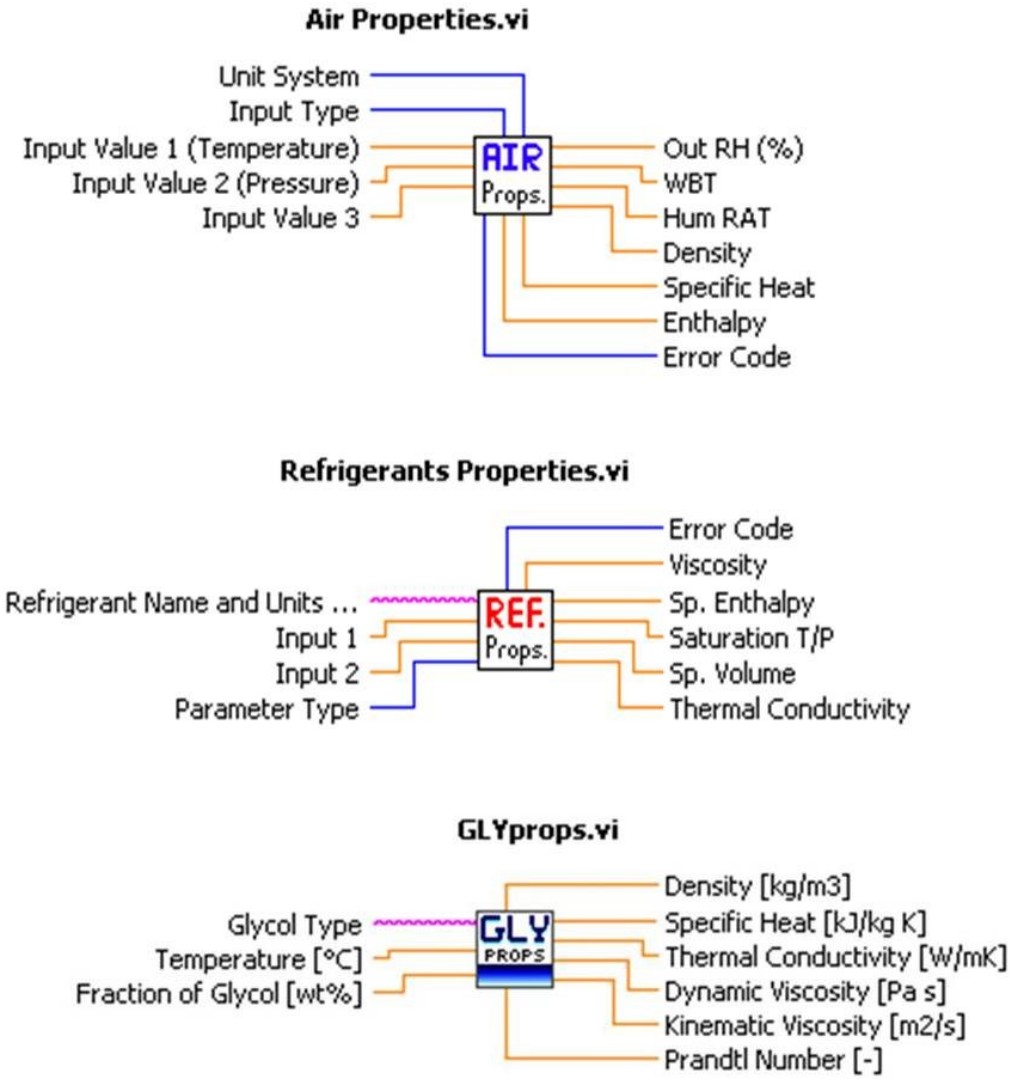

Figure 4.2: Moist Air / Refrigerant / Glycol Property Sub Routines

Evaporator or cooler air-side capacity can be further distinguished into sensible and latent capacity. Sensible capacity constitutes the portion of heat transfer which is used to decrease the temperature across the evaporator or cooler, while latent capacity denotes the portion used to dehumidify the air. A common parameter used in air-conditioning is the Sensible Heat Factor (SHF), which decribes the amount of total heat used for sensibly changing the

temperature of a given quantity of air. Sensible and latent capacity, as well as the sensible heating factor are shown in Equations (4), (5), and (6).

$$\dot{Q}_{sensible} = \dot{m} \times c_p \Delta T \quad (4)$$

$$\dot{Q}_{latent} = \dot{Q}_{total} - \dot{Q}_{sensible} \quad (5)$$

$$SHF = \frac{\dot{Q}_{sensible}}{\dot{Q}_{total}} \quad (6)$$

Refrigerant-side capacities for evaporator, intermediate heat exchanger, and condenser were determined using refrigerant mass flow rate and enthalpy difference, as shown in Equation (7).

$$\dot{Q}_{\mathrm{Ref}} = \dot{m}_{\mathrm{Ref}} (\Delta \mathrm{h}) \quad (7)$$

Calculation of energy balance for refrigerant-to-air heat exchangers, as well as refrigerant-to-coolant and coolant-to-air heat exchangers, were determined to proof proper operation of the system and ensure consistency of measured data. Equation (8) gives an example of an energy balance calculation for the evaporator in the baseline DX system.

$$EB_{Evap} = \frac{\left(\dot{Q}_{Evap,\mathrm{Ref}} - \dot{Q}_{Evap,Air}\right)}{\dot{Q}_{Evap,\mathrm{Ref}}} 100 \quad (8)$$

Compressor power was determined by torque and rpm measurements, as shown in equation (9). Pump electrical power was measured directly using a wattmeter.

$$P_{Comp} = Torque \times rpm \quad (9)$$

Compressor isentropic and volumetric efficiencies were calculated using experimentally measured data. Isentropic efficiency was determined using Equation (10), where the numerator denotes ideal enthalpy difference achieved through isentropic compression, and the denominator describes the experimentally measured enthalpy difference. The volumetric efficiency was determined by Equation (11), where MFR is the refrigerant mass flow rate, $\rho_{suction}$ is the suction density, rpm is the compressor speed, and V_D is the compressor displacement.

$$\eta_{isentropic} = \frac{h_{discharge,ideal} - h_{suction}}{h_{discharge,measured} - h_{suction}} \quad (10)$$

$$\eta_{volumetric} = \frac{MFR}{V_D \times \rho_{suction} \times \frac{rpm}{60}} \quad (11)$$

System efficiency, determined by the coefficient of performance (COP), was calculated by comparing refrigerating effect to the power consumed by the system. Equations (12) and (13) introduce the COP, where Q is cooling capacity, and P is power consumption. In case of a secondary loop system, two COPs can be distinguished. The primary COP, Equation (12), is the efficiency of the primary refrigeration cycle, where Q is refrigerant-side cooling capacity at the intermediate heat exchanger, and P is power consumption of the compressor. Total COP, Equation (13), was determined by air-side cooling capacity and combined power consumption of compressor and coolant pump.

$$COP_{prim} = \frac{\dot{Q}_{Chiller,\mathrm{Ref}}}{P_{Comp}} \quad (12)$$

$$COP_{Total} = \frac{\dot{Q}_{Cooler,Air}}{P_{Total}} \quad (13)$$

Up to this point, the discussed equations dealt with performance measurements during steady state operation. However, air-conditioning operation in an automobile is often highly transient, which is reflected by the majority of the experimental tests conducted in this research. To assess and compare transient performance, performance parameters, such as power consumption and cooling capacity, are integrated over the duration of the respective tests. Similarly to the coefficient of performance for steady state operation, a transient COP, the transient performance factor (TPF), was defined to compare system performance during transient operation. The TPF is defined in Equation (14).

$$TPF = \frac{\int_{t=0}^{t} \dot{Q}_{air}}{\int_{t=0}^{t} P_{total}} \quad (14)$$

While ice storage is used in connection with the secondary loop system, two additional performance parameters can be introduced: cooling capacity of the ice storage heat exchanger, Equation (15), and ice storage charging COP, Equation (16). Cooling capacity of the ice storage heat exchanger can only be measured on the refrigerant-side and not on the ice-side, due to phase change.

$$\dot{Q}_{ICE} = \dot{m} \times c_{p,coolant} (\Delta T)_{coolant} \quad (15)$$

$$COP_{ICE,charging} = \frac{\dot{Q}_{ICE}}{P_{total}} \quad (16)$$

4.3 Uncertainty Analysis

Uncertainty analysis was performed on both, steady state, as well as transient data. The total uncertainty of a parameter can be distinguished into two contributors, the so called systematic uncertainty and random uncertainty. The systematic uncertainty is a bias error, which causes the mean of a measured parameter to be significantly different from its "true" value. Systematic uncertainty can be caused by imperfections in the measurement instrument, imperfections of the calibration of the instrument, and unexpected changes in the environmental conditions which cannot be accounted for. Calibration with a more precise instrument can be used to remove part of the systematic error of an instrument. Random uncertainty is based on the fact that repeated measurements of the same parameter using the same instruments under the same operating conditions will randomly and unpredictably differ in magnitude. Random uncertainty is closely related to the precision, i.e. the resolution of the instruments used for measurement. For a finite repeated set of measurements, the higher the precision of the instruments, the smaller the variance around the mean of the measurand. If a measurement under identical operating conditions and with identical instruments would be repeated indefinitely, the random uncertainty would be expected to be null, due to a statistically normal distribution. The total uncertainty of a parameter can subsequently be determined by linear summation of the systematic and random uncertainty. Figure 4.3 strives to visualize the concepts of systematic uncertainty, random uncertainty, and calibration.

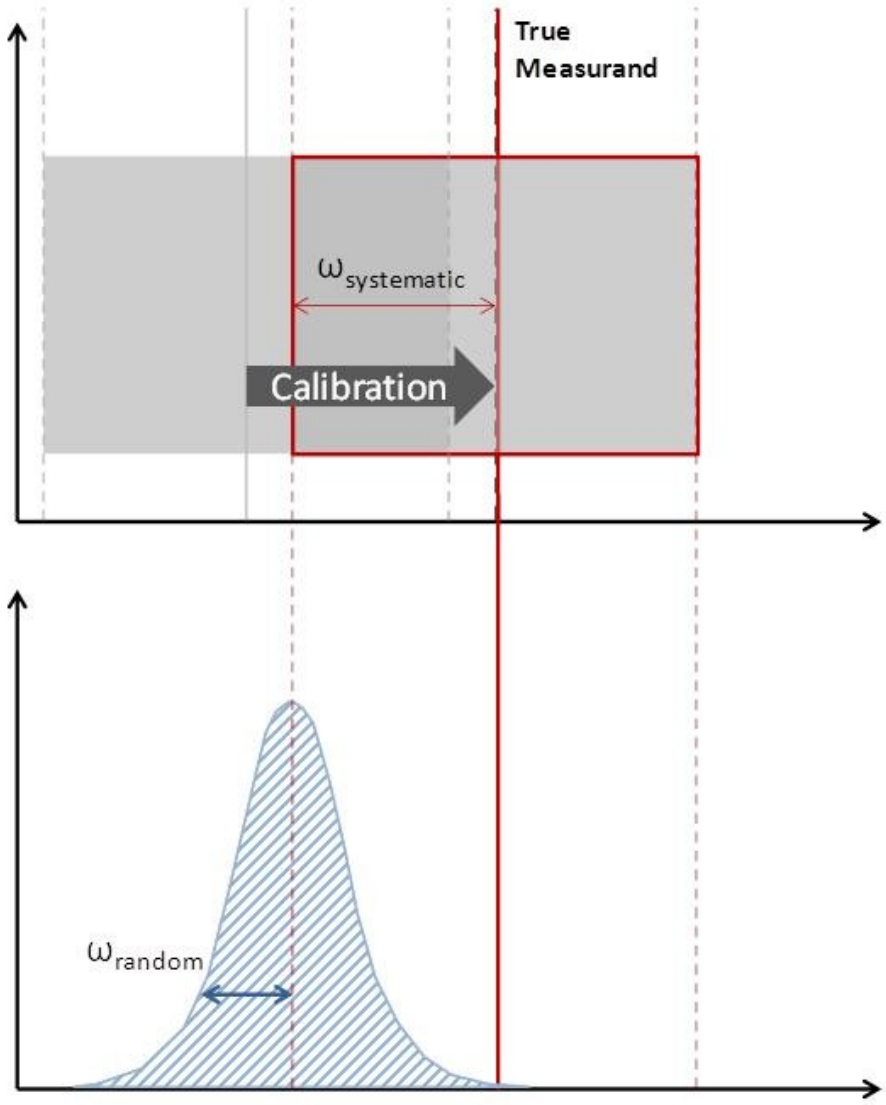

Figure 4.3: Systematic and Random Uncertainty

During the data reduction process, non-measurable fluid properties, such as enthalpy or specific heat, were calculated based on measured physical properties, such as temperature and pressure. These non-measurables were further used to determine system performance metrics, such as cooling capacity and COP. Random uncertainty of non-measurables and performance metrics can be computed as their respective standard deviation, using Equation (17).

$$STD_{x_1,x_2,..,x_n} = \left(\frac{1}{n}((x_1 - \bar{x})^2 + (x_2 - \bar{x})^2 + .. + (x_n - \bar{x})^2)\right)^{\frac{1}{2}} \quad (17)$$

For any calculated parameter, the systematic uncertainty needs to be propagated by means of Pythagorean Addition, shown in Equation (18) for a function f and coefficients x_i from x_1 through x_n.

$$\omega_{f(x_1,x_2,..,x_n)} = \left(\left(\frac{\partial f}{\partial x_1}\omega_{x_1}\right)^2 + \left(\frac{\partial f}{\partial x_2}\omega_{x_2}\right)^2 + .. + \left(\frac{\partial f}{\partial x_n}\omega_{x_n}\right)^2\right)^{\frac{1}{2}} \quad (18)$$

Equation (18) implies that the relationship of any calculated parameter, i.e. enthalpy, to its measurable components, i.e. temperature and pressure, be known. A flexible approach of finding the uncertainty of calculated parameters is the use software which allows for propagation of uncertainty of fluid properties, such as Engineering Equation Solver (EES).

Table 4.1 provides an example of systematic and random uncertainty for a steady state test of the secondary loop system (2LP), using Propane (R290) as primary refrigerant. The table shows systematic, random, and total uncertainty of performance parameters at idling compressor speed and at compressor speed related to highway driving. Uncertainties of three different cooling capacities are given: refrigerant-side cooling capacity at the intermediate heat exchanger, refrigerant-side cooling capacity at the cooler, and air-side cooling capacity at the cooler. Total uncertainty was lowest on the refrigerant-side, due to a low systematic uncertainty. High systematic uncertainty caused the air-side capacity to exhibit the highest total uncertainty. Random uncertainty was typically highest on the refrigerant-side, due to vibrations in the compressor belt drive and PID

control of the EXV. The thermal mass of the coolant allowed coolant and air-side measurements to have decreased fluctuations and consequently lower random uncertainty. In general, relative uncertainty of cooling capacity for idling speed tests was about twice as high compared to high way speed tests. This was due to reduced absolute magnitudes of measurands compared to fixed absolute uncertainties (e.g. decreased ΔT across heat exchanger, while thermocouple uncertainty of 0.5 K stays constant). Uncertainty of power consumption was dominated by random uncertainty for the reasons mentioned above. Uncertainty of primary or refrigerant-side COP was about 5-6%, mostly dominated by random uncertainty. Uncertainty of total system COP on the refrigerant-side was about 6% for highway speed tests and about 10% for idling speed tests.

Table 4.1: Relative Systematic and Random Uncertainties (R290 2LP, T35RH40)

Performance Parameter	Idling			Highway		
	Systematic [%]	Random [%]	Total [%]	Systematic [%]	Random [%]	Total [%]
Capacity (refrigerant)	0.7	2.5	3.2	0.7	1.1	1.7
Capacity (coolant)	4.6	1.3	5.9	2.2	0.5	2.8
Capacity (air)	14.5	1.7	16.2	7.7	1.2	8.8
Power Consumption	0.4	4.1	4.5	0.4	3.7	4.1
COP (refrigerant)	0.9	4.8	5.7	0.8	3.9	4.6
COP (coolant)	6.5	3.3	9.8	2.7	3.4	6.1

Due to lower uncertainty compared to air-side measurements, refrigerant-side COP was used to describe steady-state system performance of the direct expansion system, while coolant-side COP was used to describe steady-state system performance of the secondary loop system.

Table 4.2 provides a summary of total relative uncertainties of performance parameters during steady state operation. Uncertainties are given for different refrigerants (R134a, R152a, R290), different system layouts (DX, 2LP), a range of ambient temperatures and relative humidities (15°C/80%, 25°C/50%, 35°C/40%, 45°C/20%), and different compressor speeds (idle, highway). Across various refrigerants, system layouts, and operating conditions, several characteristics can be observed: Refrigerant-side capacity typically showed a relative uncertainty in the range of 3%, often less at highway speed and more at idle speed. For the secondary loop system, refrigerant-side capacity was in the range of 3% at highway speed and in the range of 6% at idle speed. Relative uncertainty of power consumption was on the order 3% at highway speed and on the order of 5-7% at idle speeds. In a few cases, moslty when idling at low ambient temperatures, relative uncertainty was significantly higher than above mentioned values. At these conditions the lack of cooling load, which made EXV PID control difficult, resulted in fluctuations in MFR, which increased random uncertainty of cooling capacity.

Table 4.2: Summary of Steady-state Relative Uncertainty of Performance Parameters

Refrig./System	R134a DX							
Amb. Conditions	T15 RH80		T25 RH50		T35 RH40		T45 RH20	
Speed	idle	hwy	idle	hwy	idle	hwy	idle	hwy
Capacity (ref) [%]	1.2	-	1.3	1.3	1.4	1.6	1.5	1.5
Capacity (col) [%]	-	-	-	-	-	-	-	-
Capacity (air) [%]	12.8	-	15.5	8.5	19.1	10.0	20.0	13.6
Power [%]	6.7	-	6.1	3.4	6.5	2.9	6.9	2.7
COP (ref) [%]	7.0	-	6.4	3.6	6.8	3.3	7.4	3.2
COP (col) [%]	-	-	-	-	-	-	-	-
Refrig. /System	R152a DX (drop-in)							
Amb. Conditions	T15 RH80		T25 RH50		T35 RH40		T45 RH20	
Speed	idle	hwy	idle	hwy	idle	hwy	idle	hwy
Capacity (ref) [%]	14.1	-	3.1	1.8	2.8	2.0	2.5	6.8
Capacity (col) [%]	-	-	-	-	-	-	-	-
Capacity (air) [%]	13.6	-	13.3	7.5	17.0	9.3	18.7	12.1
Power [%]	42.2	-	6.6	3.7	6.3	3.2	7.0	3.0
COP (ref) [%]	16.5	-	7.3	4.2	7.0	3.8	7.4	7.7
COP (col) [%]	-	-	-	-	-	-	-	-
Refrig./System	R290 DX (drop-in)							
Amb. Conditions	T15 RH80		T25 RH50		T35 RH40		T45 RH20	
Speed	idle	hwy	idle	hwy	idle	hwy	idle	hwy
Capacity (ref) [%]	-	-	2.3	-	2.6	3.3	2.9	2.6
Capacity (col) [%]	-	-	-	-	-	-	-	-
Capacity (air) [%]	-	-	12.6	-	14.2	8.1	16.3	11.3
Power [%]	-	-	4.6	-	4.8	2.3	5.0	2.0
COP (ref) [%]	-	-	5.3	-	5.5	4.0	6.1	3.4
COP (col) [%]	-	-	-	-	-	-	-	-
Refrig. /System	R152a 2LP (drop-in)							
Amb. Conditions	T15 RH80		T25 RH50		T35 RH40		T45 RH20	
Speed	idle	hwy	idle	hwy	idle	hwy	idle	hwy
Capacity (ref) [%]	4.4	-	2.2	2.7	4.3	1.5	4.3	2.7
Capacity (col) [%]	7.0	-	6.5	3.5	5.4	2.9	5.1	2.8
Capacity (air) [%]	11.4	-	14.0	7.8	17.0	9.6	18.9	12.4
Power [%]	6.6	-	5.1	2.8	6.1	2.4	6.9	2.4
COP (ref) [%]	7.8	-	5.5	4.0	7.5	2.8	8.2	3.7
COP (col) [%]	13.1	-	10.9	5.2	10.2	4.6	9.9	4.4
Refrig. /System	R290 2LP (reduced speed)							
Amb. Conditions	T15 RH80		T25 RH50		T35 RH40		T45 RH20	
Speed	idle	hwy	idle	hwy	idle	hwy	idle	hwy
Capacity (ref) [%]	5.8	-	3.2	1.9	3.2	1.7	3.0	2.0
Capacity (col) [%]	9.0	-	6.1	3.1	5.9	2.8	5.5	2.7
Capacity (air) [%]	14.7	-	12.8	7.1	16.2	8.8	17.5	11.7
Power [%]	4.7	-	4.7	4.1	4.5	4.1	4.1	4.5
COP (ref) [%]	7.4	-	5.7	4.6	5.7	4.6	5.1	5.1
COP (col) [%]	15.6	-	10.8	6.3	9.8	6.1	8.9	6.4

For transient measurements the principle of random uncertainty, by which a parameter is repeatedly measured under the same conditions, becomes irrelevant. since all parameters are deliberately changing in time. As a result, uncertainty of transient tests can only be evaluated by systematic uncertainty, though it's calculation is more involved. The absolute magnitude of a measurand can change significantly during the course of a test. Systematic uncertainty was evaluated at every timestep during the test and integrated over the time of the experiment to determine the total uncertainty of accumulated performance parameters, such as energy consumption or energy availability for cooling.

Transient uncertainty analysis was performed using the uncertainty propagation table method in the Engineering Equation Solver software (EES). An example of transient uncertainty is given in Figure 4.4, showing absolute uncertainty of performance parameters during a New European Drive Cycle test (NEDC) for the R152a secondary loop (2LP) system. The uncertainty of air-side capacity followed uncertainty of the temperature difference across the cooler, and was consequently decreasing as the test progressed. Uncertainty of refrigerant-side uncertainty followed fluctuations in MFR, which were determined by the compressor speed profile. During sharp transients superheat can be lost and refrigerant-side uncertainty can spike. Uncertainty of power consumption directly followed the NEDC compressor speed profile.

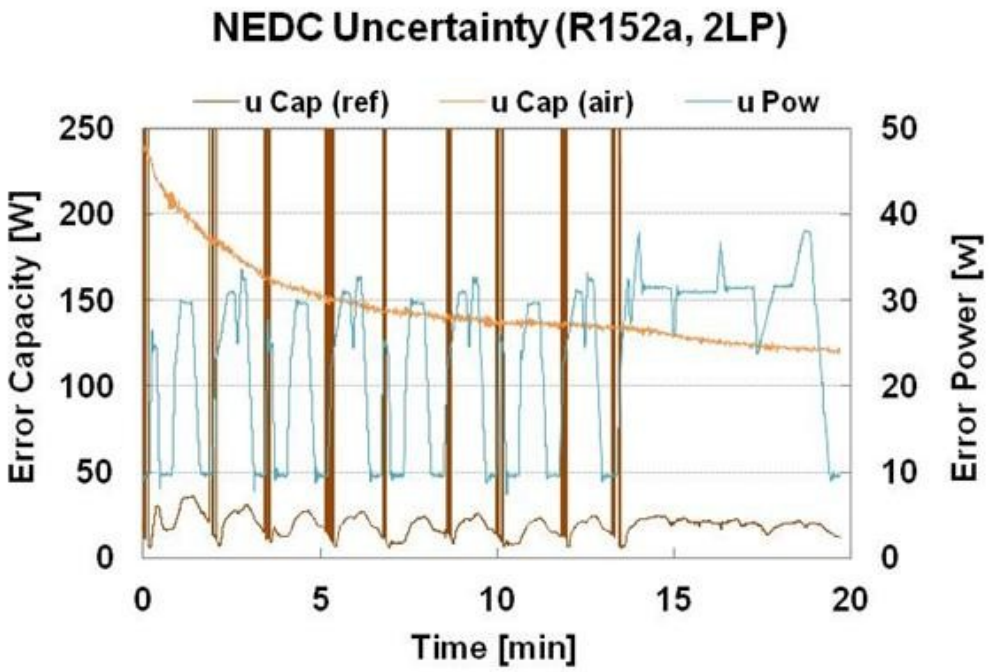

Figure 4.4: Transient Uncertainty Example - New European Drive Cycle

Similar to the analysis of transient performance data, discussed in Chapter 4.2, transient uncertainty data can be integrated over time to find the accumulated uncertainty over the duration of a transient test. With accumulated uncertainties of air-side capacity (19) and power consumption (20), uncertainty of the transient performance factor (TPF) can be determined, based on Pythagorean summation (21).

$$\omega_{Q_{air},\mathrm{acc}} = \int_{t=0}^{t} \omega_{Q_{air},instantaneous} \qquad (19)$$

$$\omega_{P_{total},\mathrm{acc}} = \int_{t=0}^{t} \omega_{\mathrm{P}_{total},instantaneous} \qquad (20)$$

$$\omega_{\mathrm{TPF}} = \sqrt{\left(\frac{1}{\mathrm{P}_{\mathrm{total,acc}}} \times \omega_{Q_{air},\mathrm{acc}}\right)^2 + \left(\frac{\mathrm{Q}_{\mathrm{air,acc}}}{\mathrm{P}_{\mathrm{total,acc}}{}^2} \times \omega_{P_{total},\mathrm{acc}}\right)^2} \qquad (21)$$

Uncertainty of steady state experimental results, as well as accumulated uncertainty of transient experimental results, are provided by means of error bars in the charts shown in Chapters 7, 8, and 9.

5 Automation and Control

Chapter 5 provides information about automation and control of the data acquisition system and test facility. The chapter discusses the passenger cabin model, which allows transient testing of MAC components, as well as the controls implemented for drive cycle testing, and the controls implemented for research on energy saving strategies through alternative control of the air-conditioning system.

5.1 Structure of the Data Acquisition Control

Figure 5.1 shows the structure of the Main LabVIEW Data Acquisition program (main DAQ). The main DAQ consisted of six modules, which followed separate tasks and can be scheduled independently.

The first module scheduled the data reduction process, the control of the cabin model, the visualization of all data in real time on screen, and the recording of data to an Excel spreadsheet. The data reduction process was introduced in Chapter 4.2, while the Cabin Model and associated controls will be introduced in Chapter 5.2.

The second module was used to manually control the temperature, relative humidity, and air flow rate in the condenser wind tunnel and evaporator psychrometric loop, respectively.

The third module scheduled the drive cycle controls. Various components and parameters in the system can be controlled by predefined drive cycles, as opposed to constant control or PID control. Details of the drive cycle control will be introduced in Chapter 5.3

Modules 4 through 6 controlled components in the system directly. While module 4 controled the compressor clutch and compressor speed, module 5 controled the pump speed and it's actuation, and module 6 controled the opening of the EXVs, based on evaporator superheat. Component control modules will be introduced in Chapter 5.4.

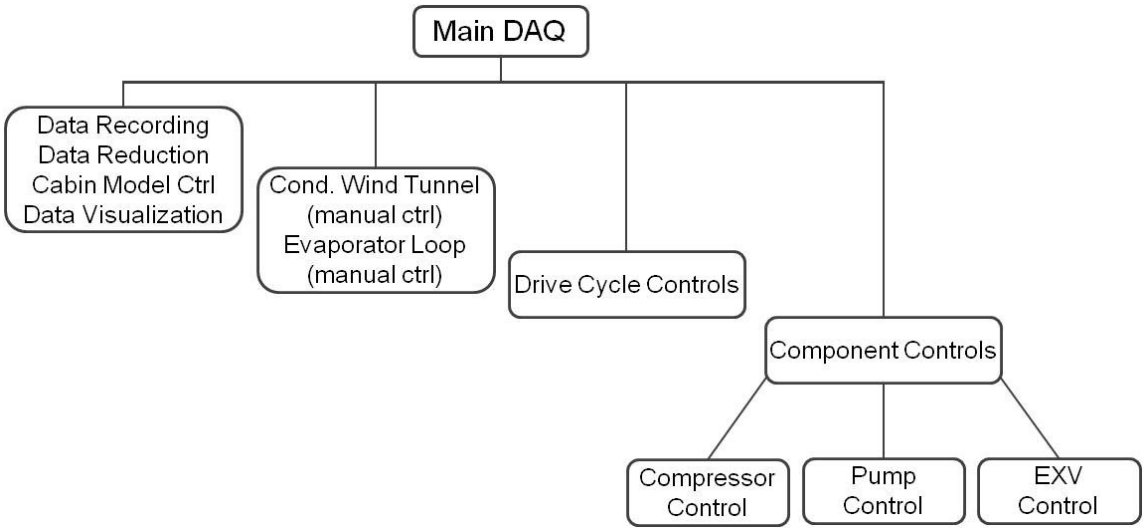

Figure 5.1: Main Data Acquisition Structure and Control in LabVIEW

5.2 The Cabin Model

The Cabin Model is a lumped model of the automotive passenger cabin to simulate thermal and psychrometric processes. The main function is real-time communication with the controller of the air-handling unit of the psychrometric

loop to control the state of the air upstream of the evaporator (DX) or cooler (2LP).

The core of the model consists of a set of energy and mass balance equations, which are solved by the Gauss-Jordan Method. This method was first developed by Gado [12]. For details on the equations used in the model, the reader is referred to Gado [12]. Since the core of the model did not change, the current model was successfully validated against data from Huang [15], using the same procedures outlined by Gado.

The Cabin Model enables transient testing by a process described in Figure 5.2. At every timestep, temperature, relative humidity, and air flow rate downstream of the evaporator (DX) or cooler (2LP) were measured. Based on physical and thermal characteristics of the cabin, as well as thermal loads, the cabin model determined temperature of the cabin air, temperature of interior mass, and relative humidity inside the cabin. The cabin air was then allowed to mix with ambient air, based on a pre-defined recirculation ratio, which lead to the state of the return air. The return temperature and relative humidity determined by the cabin model were subsequently used as set points for the PID control of the air handling unit (AHU), which controlled the condition of the air upstream of the evaporator (DX) or cooler (2LP). After the air was cooled down by the evaporator/cooler, the process was reiterated at the next timestep. All thermal and physical characteristics of the passenger cabin can be set by the user in the LabVIEW graphical user interface, which makes the Cabin Model a versatile instrument for testing MAC components in various automotive scenarios.

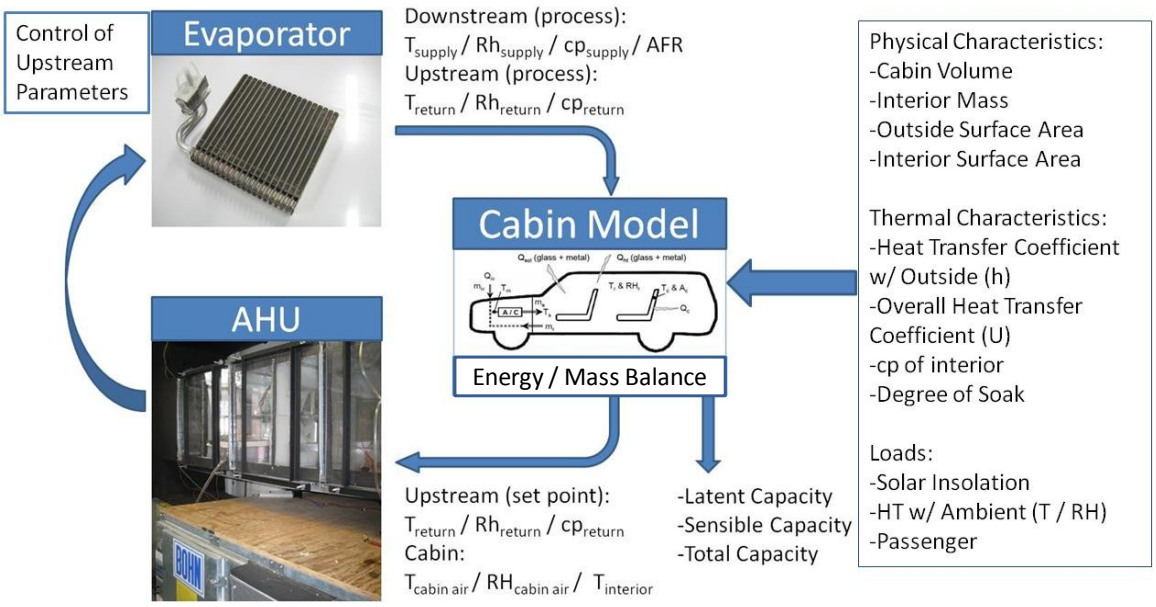

Figure 5.2: Cabin Model Operational Schematic

A flow chart of the Cabin Model is shown in Appendix B. Several control strategies used in automotive air-conditioning were implemented to increase versatility of the Cabin Model for simulation of subjective evaluation drives.

An evaporator fan speed control was implemented to decrease air flow rate across the evaporator/cooler as cabin temperature approaches comfort temperature, set by the user. A five step control was used to vary face velocity from 2.47 m/s for hot soaked conditions to 1.83 m/s for cabin temperatures within 2°C of comfort setting.

A thermostat control, using a virtual heater core, was added to be able to keep the cabin at comfort temperature once the air-conditioning system pulled the cabin temperature below comfort setpoint. In an actual automotive air-conditioning unit, the total air stream would pass through the evaporator. After

being cooled down and dehumidified, part of the air stream would be routed through a heater core for reheating in order to control for comfort temperature. The heater core utilizes hot engine coolant to reheat the air, while the supply temperature to the cabin is controlled by a mixing flap after the evaporator, which controls the fraction of flow rate passing through the heater core. As the current test facility lacked the ability to house a heater core and mixing chamber, a virtual heater core was added to the Cabin Model to enable thermostat functionality. The virtual heater core used a software side PID controller which added a certain magnitude to the actual, measured supply temperature downstream of the evaporator/cooler. The cabin model energy and mass balance equations therefore received an artificially higher supply temperature signal. This resulted in an increase of the calculated return temperature in the model, and therefore the upstream evaporator air temperature, controlled by the model. Therefore, within one timestep, the virtual heater core would lead to a real increase in process temperature, enabling the facility to work as if an actual heater core were present. Heater core load was subsequently determined by using the virtual temperature difference across the heater.

Drive cycle controls, described in Chapter 5.3, were added to the Cabin Model. Instead of using a fixed ambient temperature, relative humidity, and solar insolation, the user could choose to use pre-determined drive cycles as input. This allowed for transient changes in ambient temperature, humidity and insolation, which is a key feature of a new drive cycle test, developed to showcase the versatility of the test facility. The development of drive cycles, as

well as system operation during a long term evaluation drive, the I-95 test, is explained in detail in Appendix C.

5.3 Drive Cycle Control

Drive cycle modules were developed to control components of the test facility in a predefined way, using software side PID controls. The New European Drive Cycle (NEDC) is one example of a predefined sequence of vehicle speed over time. The cycle consists of several UN/ECE Elementary Urban Cycles and one UN/ECE Extra-Urban Driving Cycle, as provided by the USA Environmental Protection Agency[110]. This predefined sequence of vehicle speed was used to determine a compressor speed profile and condenser fan frequency profile. Appendix C gives a more detailed overview about the conversion process. Inputs to a drive cycle module are:

- Process value
- Set point array
- Time step
- Cycle length

The set point array is a text file, which holds an array of time vs. set points. The cycle length could be manually set by the user, to abort drive cycle operation after a set amount of time. The set point fed to the PID control is an adjusted set point, as a feed forward factor was implemented in all drive cycle modules for a tighter control of the process value. The feed forward factor can be tuned by the user, in a similar manner as tuning PID gains. For a feed forward factor of zero,

the set point of the PID control is the original set point, while for a feed forward factor of one, the adjusted set point will be the set point for the next time step in the set point array. This allowed the PID control to "know" a set point ahead of time and therefore helped to smooth out over- and undershooting.

To simplify the task of reading in drive cycle profiles into LabVIEW, drive cycle modules included a reader which read out setpoint and time information from an Excel spreadsheet. For long drive cycles specifying each setpoint and time individually can get tedious, as drive cycles were typically controlled to a 0.5 second timestep. Instead, only the corner points of a profile were specified in the Excel spreadsheet, as seen in Figure 5.3, and the drive cycle reader interpolated between these points. Based on the desired time step, the interpolation between the corner points of the profile was fine or coarse.

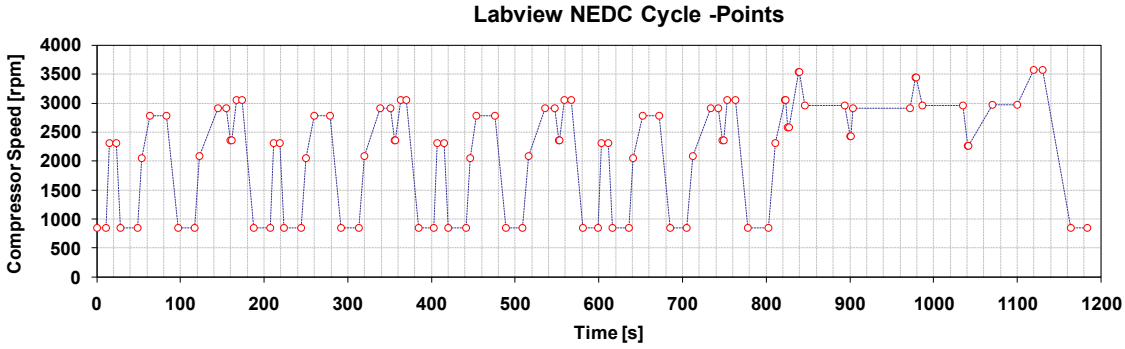

Figure 5.3: NEDC Cycle Input to LabVIEW Cycle Reader

Drive cycles modules could be turned on and off individually. The following parameters could be controlled by drive cycle modules:

- Compressor speed
- Compressor clutch actuation
- Condenser fan speed
- Ambient temperature
- Ambient relative humidity
- Solar insolation

For NEDC tests, only compressor rpm and condenser fan frequency cycles are necessary. For off-cycle Start/Stop and SS3xl tests a clutch actuation profile has to be added. A rather complex drive cycle was developed to simulate a car driving down the I-95 corridor from Maine to Florida on the United State east coast. The test facility was able to simulate changes in climate, day and night cycles, driving patterns, and rest stops, using fully automated drive cycle control. Towards this purpose, drive cycles for ambient temperature, relative humidity, and solar insolation were added, based on TMY2 data [111]. Appendix C provides more detail about the I-95 test and associated test results.

During shakedown tests, the NEDC compressor rpm profile was used in the compressor rpm drive cycle module to verify the fidelity of the setpoint following of drive cycle modules. Figure 5.4 shows compressor rpm, as well as condenser fan speed, and the discrepancy between set points (predetermined profile) and process value. The compressor rpm followed drive cycle set points with high fidelity. Deviations from the drive cycle profile occurred for a short time during fast acceleration and deceleration due to inertia of the compressor and the motor, as well as due to pressure balance across the compressor. The short

deviations had no significant effect on power consumption measurements. The condenser fan control showed a high fidelity, even during sharp transients.

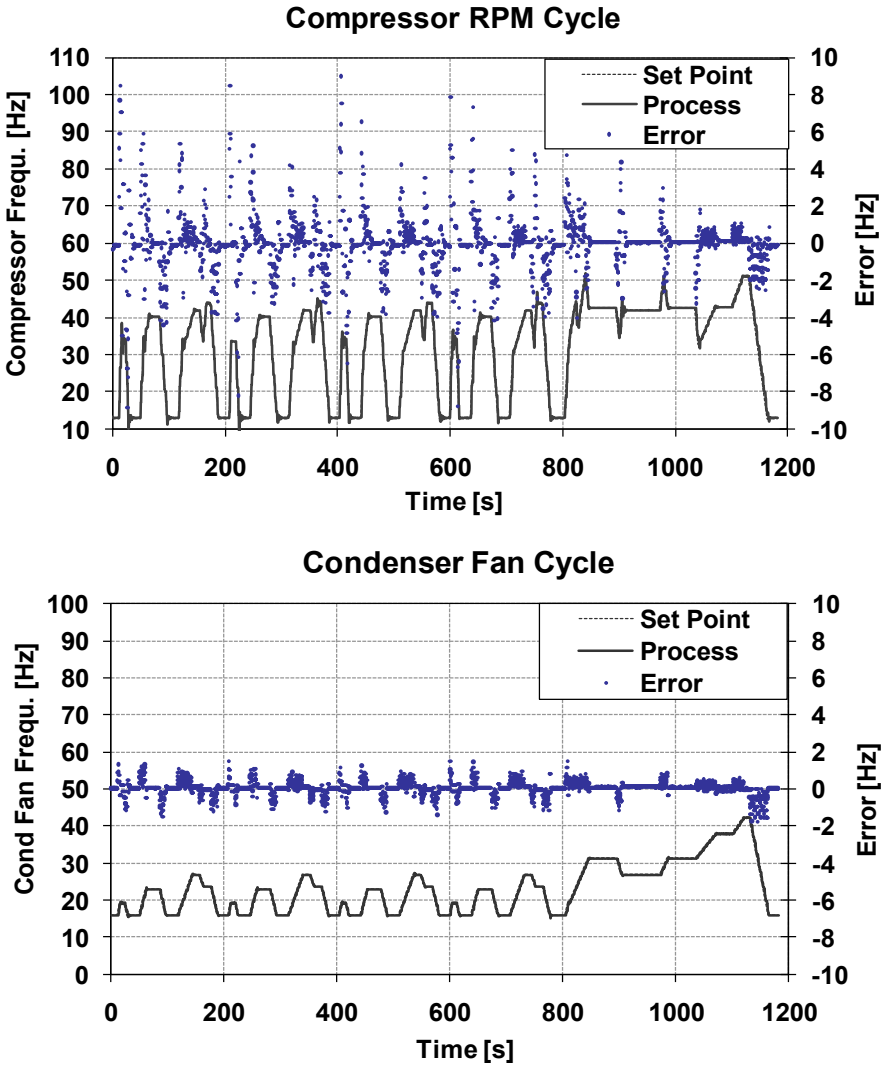

Figure 5.4: NEDC Cycle PID Control Verification

5.4 Component Control

Two electronic expansion valves (EXVs) were used for superheat control at the evaporator (DX) or the intermediate heat exchanger (2LP). The two valves were installed in parallel and fitted with separate controls, which allowed for a

continuous control of opening area of the smallest opening of one valve to the largest opening of both valves combined. This enabled the test facility to accommodate the different needs of various refrigerants and a wide range of operating conditions. Appendix B provides more detailed information about the EXV control, which was developed for this research.

The coolant pump was controlled in either manual or automatic control mode. In manual mode, pump speed could be set by the user, while automatic control employed a software side PID control. Automatic control was used mostly when controlling cabin temperature during comfort control tests utilizing ice storage. More detailed information on coolant pump control, as well as a control flow chart, is provided in Appendix B.

The control of compressor speed and clutch actuation was the most versatile, since each test needed a different control strategy. The different modes of compressor control are:

- Manual
- Pump - temperature control
- Drive cycle
- Pull down
- Comfort (Frost cycling)
- Comfort (Relative Humidity cycling)
- Comfort (Relative Humidity continuous)

A detailed summary of the compressor controls developed for this research, as well as their respective flow charts, is provided in Appendix B.

6 Refrigerant Comparison

One of the objectives of the present research was the evaluation of performance of alternative refrigerants, in both a direct expansion system, as well as in a secondary loop system. Before conclusions can be drawn from experimental results, the thermophysical characteristics of the refrigerants have to be compared to establish a foundation for their evaluation. Two alternative refrigerants were compared with the properties of R134a as reference. HFC-134a has been used in MACs since the early 1990's as a replacement for the more environmentally harmful CFC-12. While it has been used for the past two decades, recent regulations (MAC directive) resulted in its ban in all new automotive units in the European Union, starting from 2011. As a possible alternative, HFC-152a was introduced by Ghodbane et al. in the late 1990's [39]. To mitigate the flammability of R152a, the use of a secondary loop system was proposed by Ghodbane et al. [112]. Due to a lack of incentives for the automotive industry, the use of R152a in secondary loop systems has not been investigated further until recently. Hydrocarbons, such as R290, R600a, or mixtures of the two, are yet another environmentally friendly alterative. R290 has been used by car owners in Australia, as well as USA, within the past decades for direct expansion system retrofits, which is illegal in some states. Both R152a, as well as R290, were investigated in this research for use in secondary loop systems MACs.

A comparison of refrigerant properties is shown in Table 6.1. Both, R152a, as well as R290 (Propane) have an Ozone Depletion Potential (ODP) of zero.

The Global Warming Potential (GWP) of R152a GWP_{R152a}=140 is significantly lower than R134a GWP_{R134a}=1430, and is within the limits set forth for new refrigerants by the European Union (GWP < 150). R290 has an even lower GWP GWP_{R290}=11, making it the most environmentally friendly choice amongst the three refrigerants used in this research.

Table 6.1: Refrigerant Property Table

Parameter	R134a	R152a	R290
ODP	0	0	0
GWP	1400	140	11
NBP	-26.11	-24.0	-42.11
T_{cr}	101.1	113.3	96.68
P_{cr}	4059	4520	4247
Cp(0°C)	0.894	1.147	1.779
L (0°C)	198.7	306.6	374.5
ρ vapor (0°C)	14.42	8.381	10.34
ρ liquid (50°C)	1102	830.5	448.6
μ (0°C)	$1.09x10^{-5}$	$9.045x10^{-6}$	$7.79x10^{-6}$
Molar Mass	102.03	66.051	44.096

For use in MACs, the normal boiling point (NBP) of a refrigerant is a good indicator for its suitability of operating pressure. NBP, The normal boiling point of R134a is NBP_{R134a}=-26.11°C. The normal boiling point of R152a is very similar NBP_{R152a}=-24.0°C, indicating that R152a will work at similar, though somewhat lower pressures as R134a. R290 has a significantly lower NBP of NBP_{R290}=-42.11°C. It is therefore expected that R290 operates at higher pressures compared to R134a. During drop-in tests in the direct expansion system, R290 operated at about 43% increased pressure at the evaporator, compared to R134a.

Specific heat of saturated vapor at 0°C of R152a is about 28% increased compared to R134a. Specific heat capacity of R290 at the same conditions is about 99% increased compared to R134a. Both, R152a, as well as R290, will have lower superheat, as well as lower subcooling, all other things considered equal. However, since the test facility uses EXVs, superheat stayed the same, but EXV opening was about 20% to 35% increased for R152a, and about 45% to 60% increased for R290.

A density comparison shows that R290 has a saturated liquid density which is about 60% reduced from the saturated liquid density of R134a. The liquid density of R152a is about 24% reduced compared to R134a at a temperature close to 50°C (liquid line). As a result, the refrigerant charges in the BSL facility of both, R152a and R290, were decreased by 20% and 56%, respectively. Saturated vapor density at 0°C is reduced 28% and 42% for R290 and R152a, respectively. When operating a compressor with same displacement volume and same rpm, MFR for these refrigerants is expected to decrease accordingly, sans minor deviations based on changes in volumetric efficiency. Experimental results for the DX facility show a decrease in MFR of -29% for R290 and -41% for R152a, which supports the theoretical values.

A comparison of viscosity shows that liquid line viscosity can be reduced by 10% to 15% for R152a and as much as 50% for R290. For saturated vapor, R152a viscosity can be reduced by 10% to 15% in comparison to R134a, while R290 viscosity can be reduced by 25%to 30%. A smaller frictional pressure drop can be expected throughout the system for both R152a and R290 when

compared to R134a. These magnitudes could not be verified experimentally, as the pressure drop in the vapor and liquid lines were mostly within measurement uncertainty.

Figure 6.1 shows the P-h Diagram for R134a, R152a and R290. For the temperature range of interest (~ -10°C through +15°C), the latent heat of R152a is increased by roughly 55% compared to R134a, whereas the latent heat of R290 is increased by roughly 88%. Figure 6.1 also shows a comparison of isentropic lines (*) in the upper left corner of the figure. R290 isentropic lines show the smallest slope, possibly leading to an increase of discharge temperature and isentropic losses.

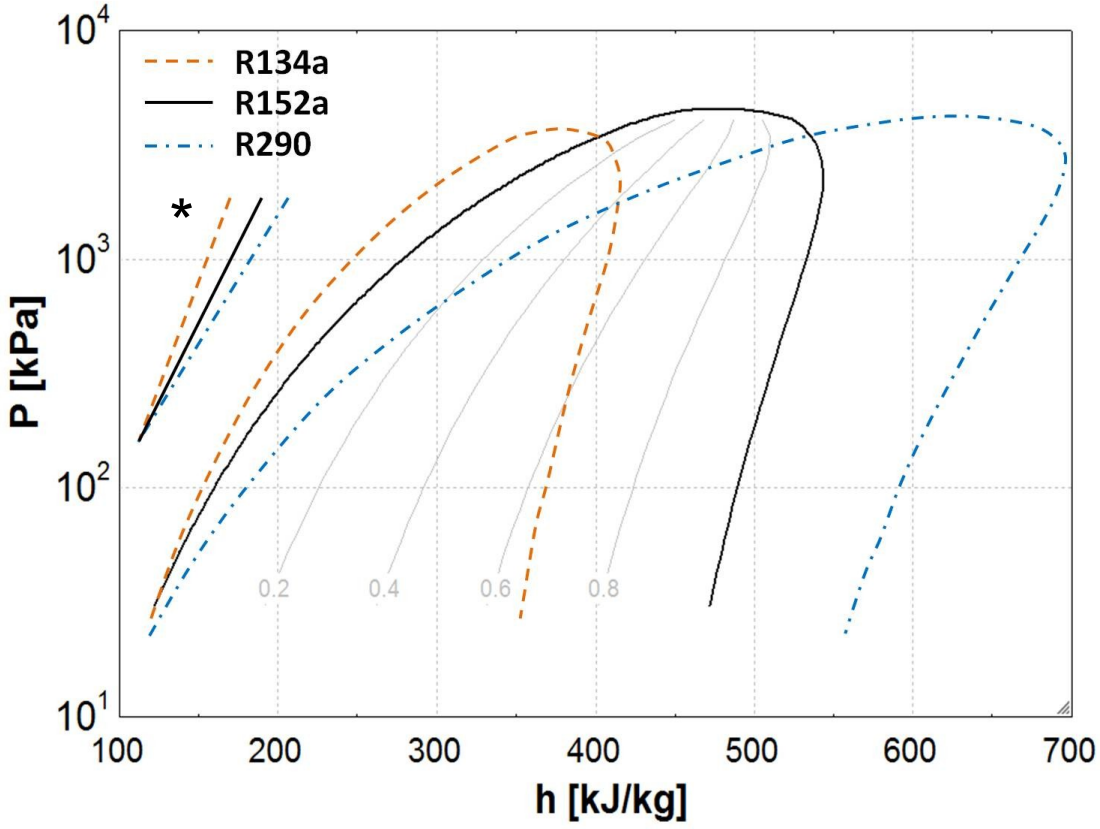

Figure 6.1: Refrigerant P-h Diagram

Figure 6.2 shows the T-s Diagram for R134a, R152a, and R290. The T-s Diagram can be very useful to compare expected refrigerant performance in terms of cooling capacity and efficiency. Didion [113] discussed the importance of the vapor dome shape in the T-s Diagram. An important characteristic location is the critical point. When comparing refrigerants, a high critical pressure typically indicates a decrease in cooling capacity due to a lower suction density, resulting in a decreased MFR and subsequently volumetric capacity. The theoretical volumetric capacity for R152a is decreased by 10%, while the volumetric capacity of R290 is increased 35% compared to R134a. Similarly, the normal boiling point (NBP) is related to the critical temperature and a good indicator for working pressure. Refrigerant property data, shown in Table 6.1 supports these indications. On the other hand, McLinden and Didion [114] point out that high critical temperatures often indicate increased COP. Since the condensation process is further removed from the critical point, excessive compressor superheat, as well as flash gas losses, can be avoided. While the specific heat capacity affects the shape of the vapor dome, it often has less of an effect on performance than NBP. However, since drop-in refrigerants, or refrigerants for the same application, are likely to be chosen to have similar NBPs, specific heat capacity can be a first indicator of cycle performance. Vapor-liquid lines featuring a smaller inclination angle are usually an indicator for better cycle performance. The slopes of vapor liquid lines are compared in the upper right corner of Figure 6.2 (**) for R134a, R152a, and R290.

An alternative way to compare cycle performance of different refrigerants was introduced by Alefeld [115]. Alefeld devised a method to determine theoretical cycle efficiency using the second law of thermodynamics. A more accurate statement of efficiency η_2, based on enthalpy differences, as well as a highly simplified statement, η_6, were introduced, as shown in Equations (22) and (23)

$$\eta_2 = g_c \frac{h_6 - h_3}{h_5 - h_6} \quad (22)$$

$$\eta_6 = g_c(\eta_r - \frac{cT_1}{2r}) \quad (23)$$

where g_c is compressor isentropic efficiency, η_r is carnot efficiency, c is specific heat capacity, and r is latent heat. The simplified statement has the advantage that in fact only very little information about the refrigerant is needed and prior experimental testing to determine cycle efficiency can be omitted. Various assumptions and simplifications were introduced on the way from η_2 to arrive at η_6. Values for both are shown in Figure 6.3 for R152a and R290 with respect to R134a as function of evaporating temperature. It can be concluded that, assuming an isentropic efficiency of g_c=0.75, R152a will result in a slightly increased COP, while the use of R290 will result in a slightly decreased COP. In both cases, the comparison of refrigerant efficiency based on Alefeld's method shows no significant variations beyond ± 5%.

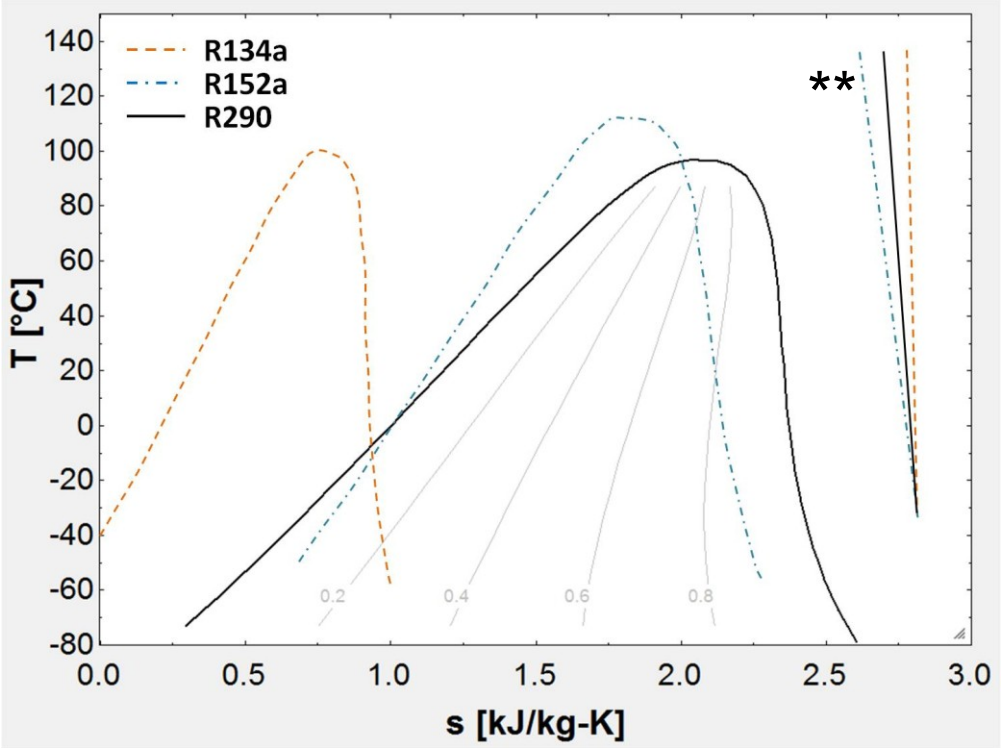

Figure 6.2: Refrigerant T-s Diagram

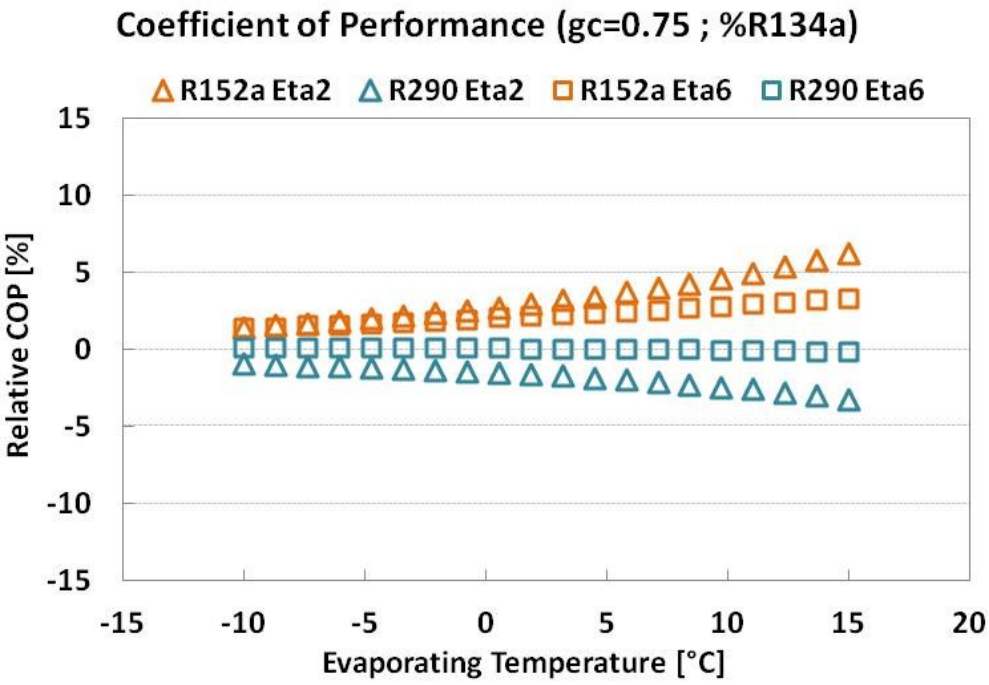

Figure 6.3: Alefeld Refrigerant Efficiency with Respect to R134a

7 Experimental Results: Secondary Loop Versus Direct Expansion

Chapter 7 presents experimental results, which provide a foundation to compare automotive secondary loop and direct expansion systems. Experimental results were obtained from steady state, as well as transient tests. Table 7.1 shows a test matrix, including compressor speeds and ambient conditions, as well as air-side face velocities at the heat exchangers. Experimental tests on the direct expansion system were performed using R134a and R152a as refrigerants, while tests on the secondary loop system were performed using R152a. Test conditions were chosen based on typical conditions encountered in the industry.

Table 7.1:Test Matrix - Secondary Loop Versus Direct Expansion System

System/ Refrigerant	Test	Compr. Speed	Ambient Temp/RH	Evap. Face Vel.	Cond. Face Vel.
R134a DX /R152a DX /R152a 2LP	Steady-state Performance	idle	15°C/80%	2.3 m/s	1.5 m/s
		idle	25°C/50%		
		idle	35°C/40%		
		idle	45°C/20%		
		highway	15°C/80%	2.3 m/s	3.0 m/s
		highway	25°C/50%		
		highway	35°C/40%		
		highway	45°C/20%		
	NEDC	NEDC profile	30°C/50%	2.3 m/s	NEDC profile
	Pulldown Performance	idle	30°C/50%	2.3 m/s	1.5 m/s
		idle	41°C/32%		
		highway	30°C/50%	2.3 m/s	3.0 m/s
		highway	41°C/32%		

The variable speed coolant pump used in the experimental facility is a low efficiency gear pump. The pump, along with the three phase motor, was oversized to allow for a wide range of mass flow rates and pressure drop conditions. Electrical pump power consumption measured with a wattmeter was in the range of 330 W. A typical secondary loop pump, recently developed for research and pre-development of a new kind of automotive thermal management systems, shows a peak power consumption of 90 W and a rated power of 30 - 80 W at mass flow rates similar to the present research for a 50wt% water-ethylene glycol solution. This value was confirmed through [116], as well as personal oral communication with a person working on the development of such pumps. Due to the pump in the present research being oversized for an actual automotive system, system COP suffered, especially at idling conditions where compressor power consumption was reduced and pump power consumption had a larger impact on total power. Therefore, experimental power consumption and COP results for the secondary loop system in the present research were adjusted to 70 W coolant pump power consumption instead of the experimentally measured 330 W (average) throughout all steady-state and transient performance results.

7.1 Charge Optimization - Secondary Loop Versus Direct Expansion

Charge optimization for the baseline direct expansion system (DX), as well as for the secondary loop system (2LP) was conducted according to the SAE International Surface Vehicle Standard for the “Procedure for Measuring System

COP of a Mobile Air Conditioning System on a Test Bench" [117]. The operating conditions, detailed in the standard, are shown in Table 7.2.

Table 7.2: Charge Optimization Operating Conditions

Parameter	Magnitude
Ambient Temperature [°C]	40
Ambient Relative Humidity [%]	40
Compressor Speed [rpm]	2000
Condenser Subcooling [K]	>5
Evaporator Face Velocity [m/s]	2.7
Condenser Face Velocity [m/s]	3.5

Charge optimization results for the baseline system are shown in Table 7.2 for the R134a direct expansion system (DX), R152a DX, and R152a 2LP. For R134a, a charge of 1,730 g was found to results in the best system performance, balancing cooling capacity and COP. The use of R152a reduced the charge by roughly 19%. Changing the system to a secondary loop system decreased the charge 28% from the original R134a DX system. When comparing refrigerant charges in this research, it is implied that the refrigeration cycles, both for DX and 2LP systems, are larger compared to typical MAC cycles. In the present research, the layout of the laboratory facilities resulted in an increased length of vapor and liquid lines, compared to an original automotive vapor compression cycle.

Table 7.3: Charge Optimization Results: 2LP Versus DX

Refrigerant /System	Optimized Charge [g]	Charge (% R134a DX)
R134a DX	1,730	0%
R152a DX	1,400	-19%
R152a 2LP	1,240	-28%

Figure 7.1 shows a theoretical estimate of a more realistic charge for direct expansion and secondary loop systems. It was assumed that an original MAC system would not include the liquid line MFR meter, and would feature a reduced receiver and filter dryer volume compared to the present test facility. Heat exchanger volume, compressor volume, and vapor line volumes were kept the same as in the present research. Liquid line size was varied within reasonable boundaries. It can be observed that R152a charge may be reduced by as much as 25%, if all other components remain the same.

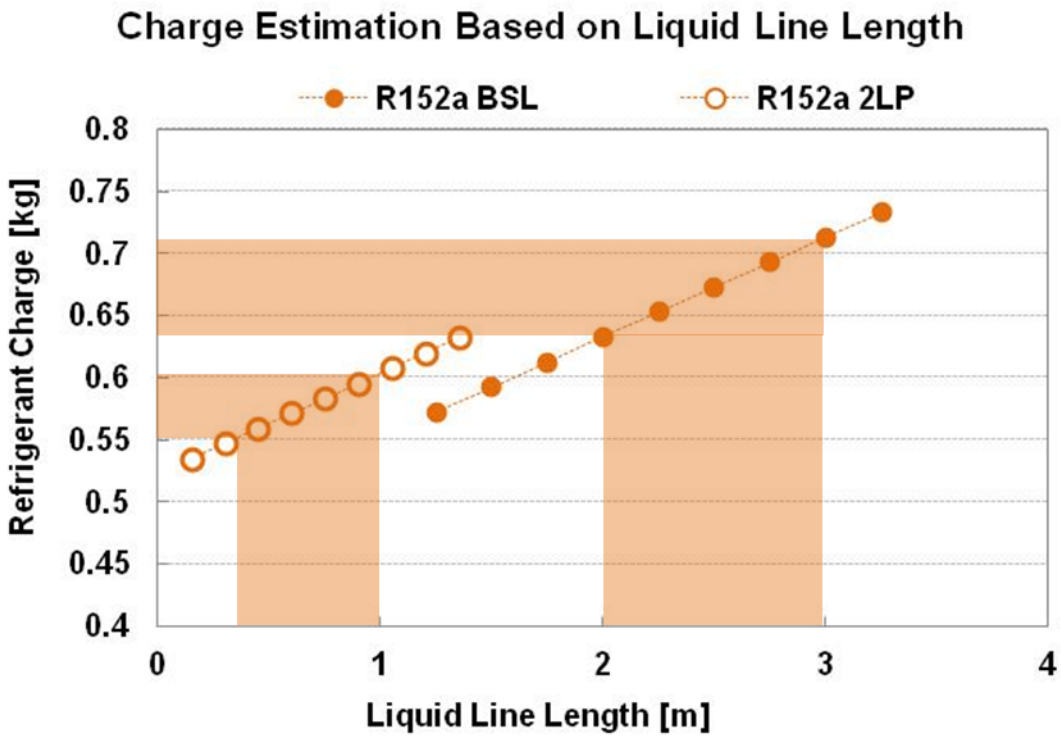

Figure 7.1:Estimated Charge Savings for R152a Secondary Loop Systems

7.2 Steady-state Performance - Secondary Loop Versus Direct Expansion

Steady-state performance measurements were conducted to compare the 2nd loop system to a DX system without the introduction of transient effects. Comparison of steady-state cooling capacity and power consumption are important measures to evaluate suitability of alternative refrigerants and operating systems.

Figure 7.2 shows an illustration of the difference between the expected COP of a secondary loop system and a direct expansion system. Given the same refrigerant, primary loop components, and operating conditions, the COP of a secondary loop system is expected to be smaller compared to a DX system, due to the additional pump work, more surface area for heat losses (or heat introduction), and a small amount of heat introduced to the coolant by the pump.

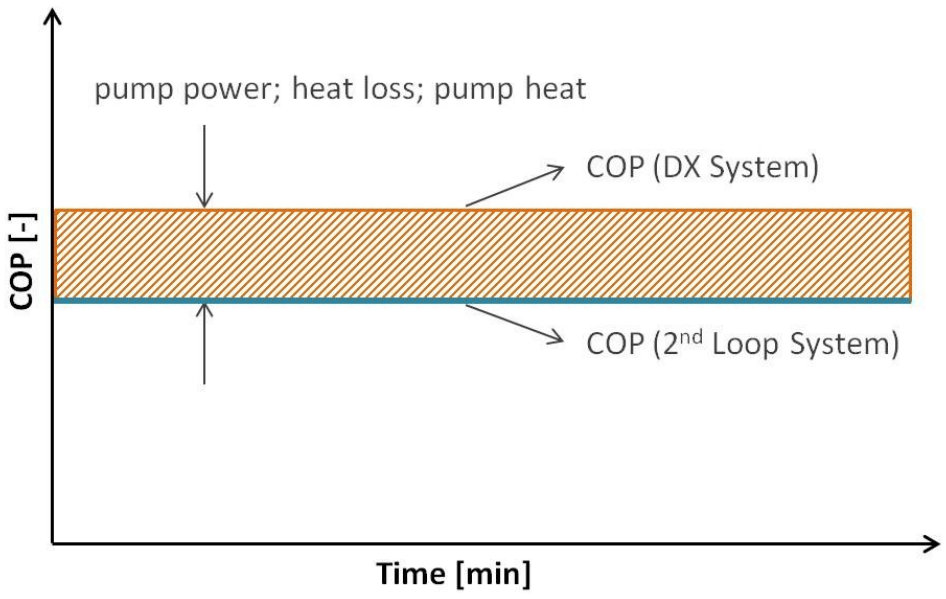

Figure 7.2: Secondary Loop Steady-state COP Illustration

Figure 7.3 shows system temperatures and pressures at various state points throughout the vapor compression system. R152a is working at a significantly decreased pressure compared to R134a. When switching from direct expansion to secondary loop system, pressure was elevated only slightly, mostly due to reduced pressure drop and different heat transfer area at the intermediate heat exchanger. Temperatures were changing only slightly when using R152a instead of R134a. Condensing temperature was elevated by 1 K, while evaporating temperature remained the same. When operating the secondary loop system, condensing temperature stayed the same within the uncertainty of measurement, while evaporating temperature decreased by 2.5 K, due to the replacement of the evaporator with the intermediate heat exchanger.

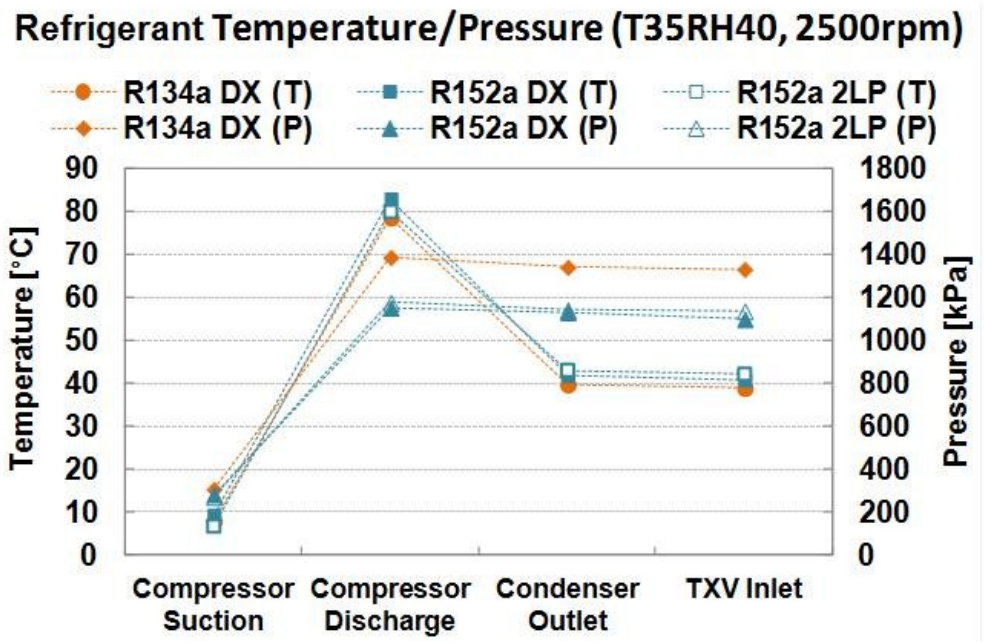

Figure 7.3: System Temperature and Pressure State Point Profiles (2LP Versus DX)

Figure 7.4 shows a summary of steady-state results for the comparison of R152a direct expansion (R152a DX) and R152a secondary loop system (R152a 2LP) to an R134a direct expansion system (R134a DX). Results are provided relative to R134a DX results. For reference, absolute steady-state data for the R134a DX system is provided in Appendix I. R152a was used as a drop-in, effectively working under the same operating conditions in the same equipment. Measurements were recorded for a range of ambient temperatures from 15°C through 45°C. However, Figure 7.4 shows only 35°C data, while a more comprehensive summary of steady-state data for the 2LP versus DX comparison is given in Appendix D. Compressor speed of 2,500 rpm was used to simulate highway driving, while a compressor speed of 900 rpm was used for idling tests.

Figure 7.4 a) shows a comparison of performance metrics, specifically cooling capacity, power consumption, and COP. Cooling capacity of R152a in a direct expansion system was virtually the same as R134a for highway speed tests, and about 8% decreased for idle tests. At idle speed, the secondary loop system showed a capacity similar to the R152a DX system, while a slightly decreased capacity was observed at highway speed, possibly due to increased heat introduction at the coolant piping and increased heat introduction by the pump. Power consumption of R152a DX was reduced by more than 10% at highway speed and idle speed, respectively. R152a 2LP power consumption increased only slightly compared to R152a DX, mainly due to power consumed by the coolant pump, but decreased more than 10% compared to R134a DX. At idling speed, pump power maked up for a greater fraction of total power, resulting

in a slightly larger deviation from R152a DX power. COP of R152a DX was more than 10% increased above R134a DX COP, for both highway and idle tests. COP of secondary loop system was reduced, compared to R152a DX, but between 5% and 10% greater compared to R134a DX. Due to smaller absolute magnitudes and more fluctuation in superheat control, relative uncertainties were greater during idling speed tests compared to highway speed tests.

Figure 7.4 b) shows a comparison of volumetric and isentropic efficiencies. While at idling speed the volumetric efficiencies for the R152a DX and R152a 2LP were effectively the same compared to R134a DX, the volumetric efficiency of R152a was increased 5% and 12% for DX and 2LP, respectively. Isentropic efficiency of R152a DX wais about 10% increased while idling, while it was slightly decreased during highway driving. R152a 2LP isentropic efficiency was increased by 13% and 5% during idling and highway driving, respectively.

Figure 7.4 c) shows a comparison of sensible and latent cooling performance at the evaporator (DX) and cooler (2LP). Sensible cooling capacity of R152a DX was within 5% of R134a DX for both, idling and highway driving. The R152a 2LP system showed a similar sensible performance compared to the R134a DX system for idling and about 7% decreased for highway driving. Latent capacity for both, R152a DX and R152a 2LP was similar to the R134a DX case. During idling, both R152a DX and 2LP showed a significant decrease of -20%, albeit these measurements are associated with high uncertainties and a concrete conclusion cannot be drawn. The sensible heating factor (SHF), both at idling and highway speed, did not deviate from the R134a DX SHF.

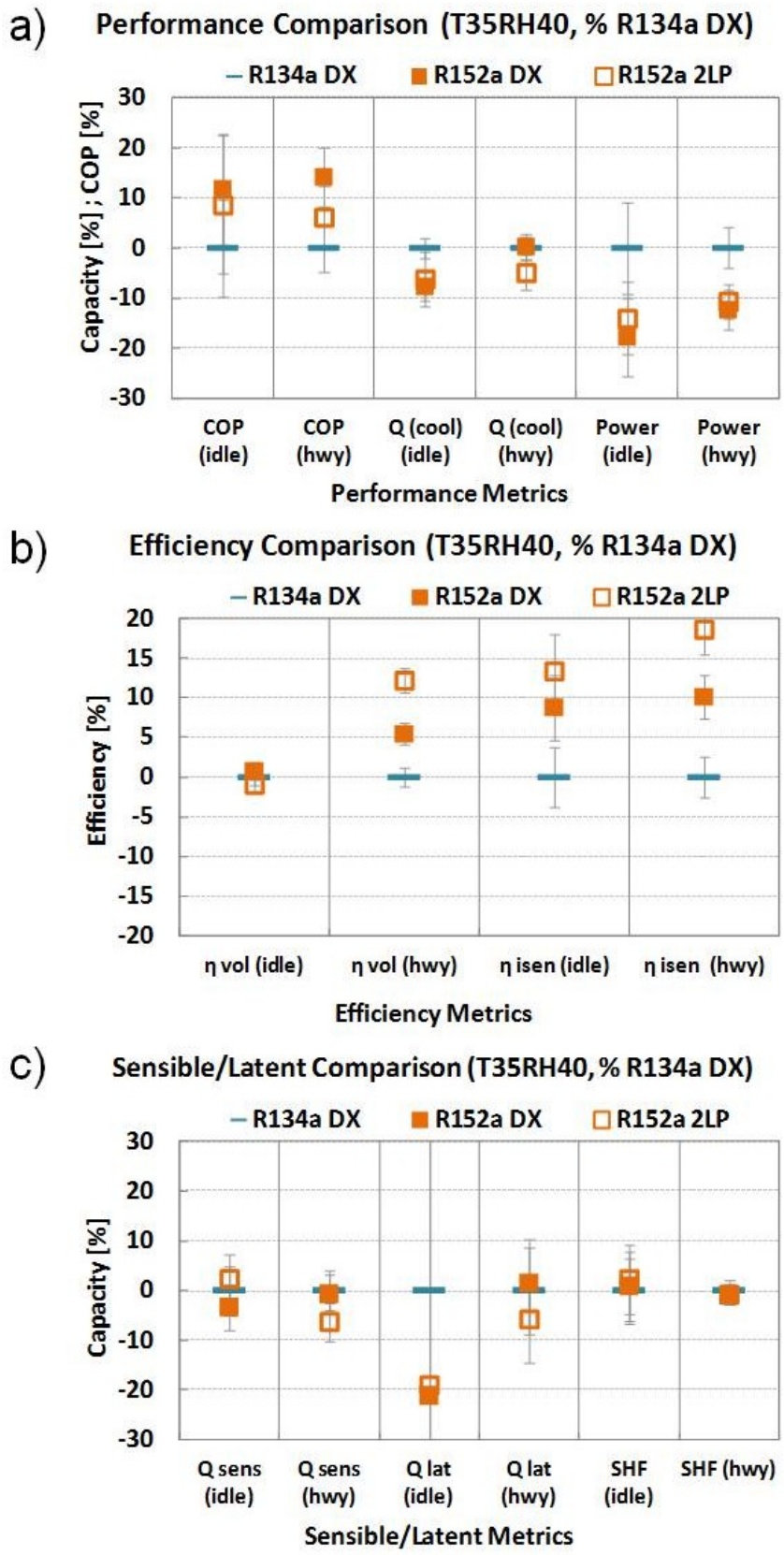

Figure 7.4: Steady State Performance Results (2LP Versus DX)

7.3 Transient Performance - Secondary Loop Versus Direct Expansion

Chapter 7.3 provides experimental results about the transient performance of the R152a secondary loop system with respect to a direct expansion system. Secondary loop systems have an inherent transient performance penalty, when compared to a direct expansion system. The performance penalty is explained by Figure 7.5, which illustrates typical transient trends of cooling capacity during a pull-down test. Cabin temperature is high initially, resulting in a high cooling capacity. As the cabin is cooled down temperature difference decreases, consequently resulting in a decrease in cooling capacity. Since thermal mass, such as pipes and heat exchangers, is being cooled down, only part of the total cooling capacity of the refrigerant-side will be available to cool down the air. Eventually, as the system approaches steady-state, capacity available on the refrigerant-side is close to capacity delivered on the air-side. The area below the capacity curve is the total energy used for cooling over the test. Secondary loop systems have an increased thermal mass, due additional heat exchangers, coolant pipes, and the coolant itself. Therefore, an additional decrease of energy available to cool down the air can be expected.

Figure 7.6 shows an illustration of COP over time during a pull-down test. Due to high initial cooling capacity, COP is high when the passenger cabin is warmed up. As the cabin cools down, COP decreases according to the decrease in cooling capacity. Therefore, pull-down tests tend to show a higher average COP for short tests, while longer tests tend to show a lower average COP.

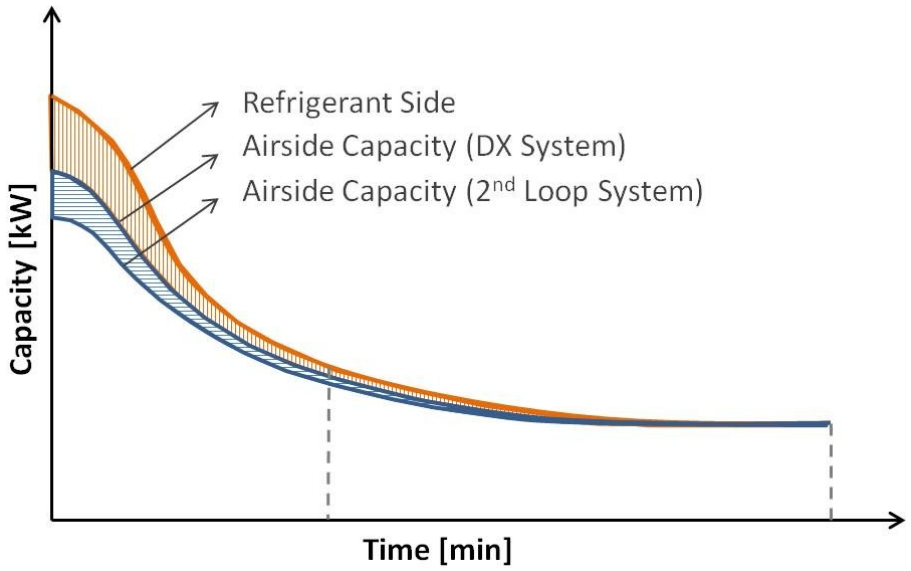

Figure 7.5: Secondary Loop Transient Cooling Capacity Illustration

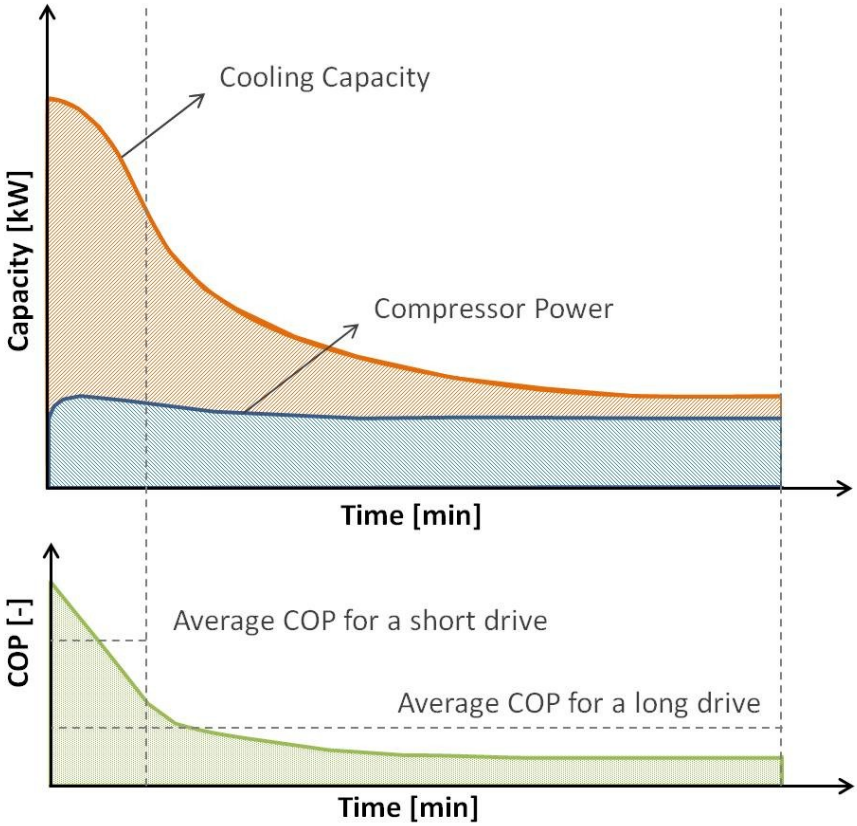

Figure 7.6: Secondary Loop Transient Capacity and COP Illustration

7.3.1 Pull-down Performance - 2LP Versus DX

Pull-down tests were performed to evaluate cooling capacity and time needed to pull the cabin down to comfort temperature. Tests were started with the cabin in a soaked condition, meaning that cabin temperature was elevated above ambient temperature. As the air-conditioning system was turned on, the compressor delivered cooling capacity to start decrease the supply air temperature to the cabin. Depending on compressor speed, ambient condition, and cooling loads, the time taken to pull the cabin down to comfort setpoint varied. The comfort temperature, after reaching which a test was aborted, was defined as 24°C.

Figure 7.7 shows a comparison of time taken to pull the cabin down to comfort temperature. Time is given relative to the time required by the R134a DX system. Using R152a as a drop-in in the direct expansion system either reduced or kept constant the time required to achieve comfort condition. At high ambient temperatures and highway speed, time to comfort was reduced by more than 15%, while at 30°C time to comfort equaled the result for the R134a DX system. At 30°C ambient temperature idling, R152a DX decreases time to comfort by less than 10%. Using the secondary loop system increased time to comfort for highway driving speed. At 30°C, time increased by 22%, while at 40°C time increased by 12%. At 30°C idling, time to comfort for the secondary loop system was similar to the R152a DX system. The system under test lacked the capacity to pull the cabin down to comfort temperature while idling at 41°C ambient

temperature. Therefore, idling pull down at 41°C was aborted after 60 minutes for both systems and time to comfort showed no relative deviation.

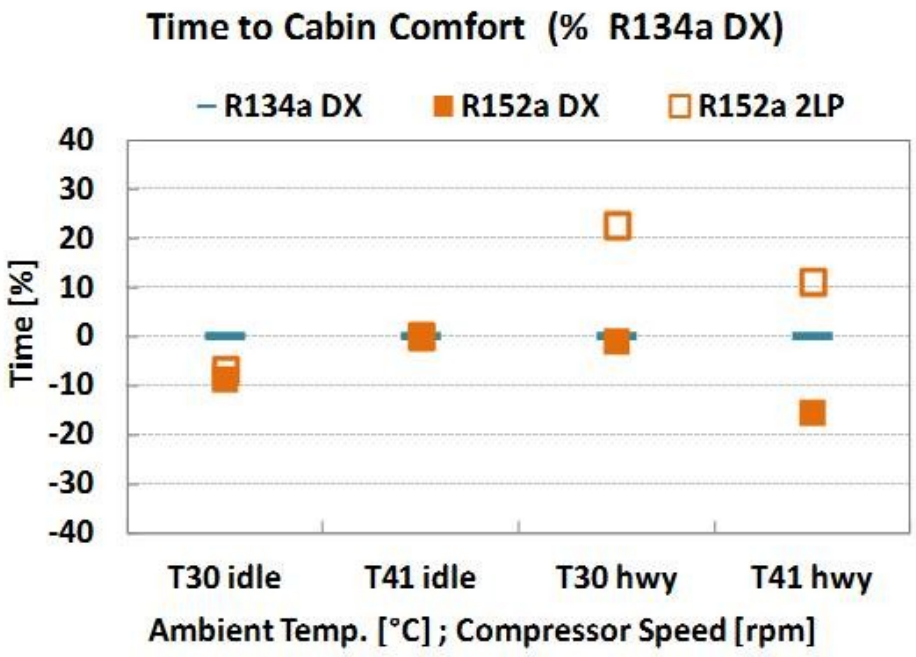

Figure 7.7: Pull-down - Time to Cabin Comfort (2LP Versus DX)

Figure 7.8 shows accumulated pull-down performance results. As described in Chapter 4.2, capacity and power consumption were integrated over the time of testing and a transient performance factor was determined. The accumulated performance metrics are therefore not decoupled from the time to comfort (i.e. testing time). Figure 7.8 a) shows the total energy which is available to cool the cabin air, relative to the total cooling energy of the R134a DX system. For the R152a DX system, the trends directly correlate with the time to comfort results for the respective operating conditions. As less cooling energy is available on the air-side when using secondary loop systems, accumulated capacity

decreases compared to R134a DX and R152a DX when time to comfort is the same, i.e. when idling at 41°C ambient temperature. During other tests, it simply takes a longer time to pull down the cabin, which increases the total energy required to achieve comfort temperature. Figure 7.8 b) shows a comparison of total energy provided by the compressor (DX) or compressor and coolant pump (2LP) during pull down tests. Accumulated power consumption follows the time to comfort trend. The R152a DX system required significantly less energy, between 15% and 28%, depending on compressor speed and ambient temperature. Due to additional coolant pump power, as well as increased time to comfort, the secondary loop system required a higher energy input compared to the R152a DX system. At idling speed, the energy input was 10% to 15% below R134a DX energy input, while at highway speed the energy input was 6% to 17% increased. Since time to comfort is short at highway speed as compared to idling speed, the relative difference in energy input between direct expansion and secondary loop systems was more pronounced. The relative transient performance factor, shown in Figure 7.8 c), was about 20% increased in all tests for R152a as a drop-in in direct expansion systems, when compared to R134a DX. For the R152a secondary loop system, TPF was within 5% of R134a DX TPF for both idling and highway speed, as well as for both ambient temperatures.

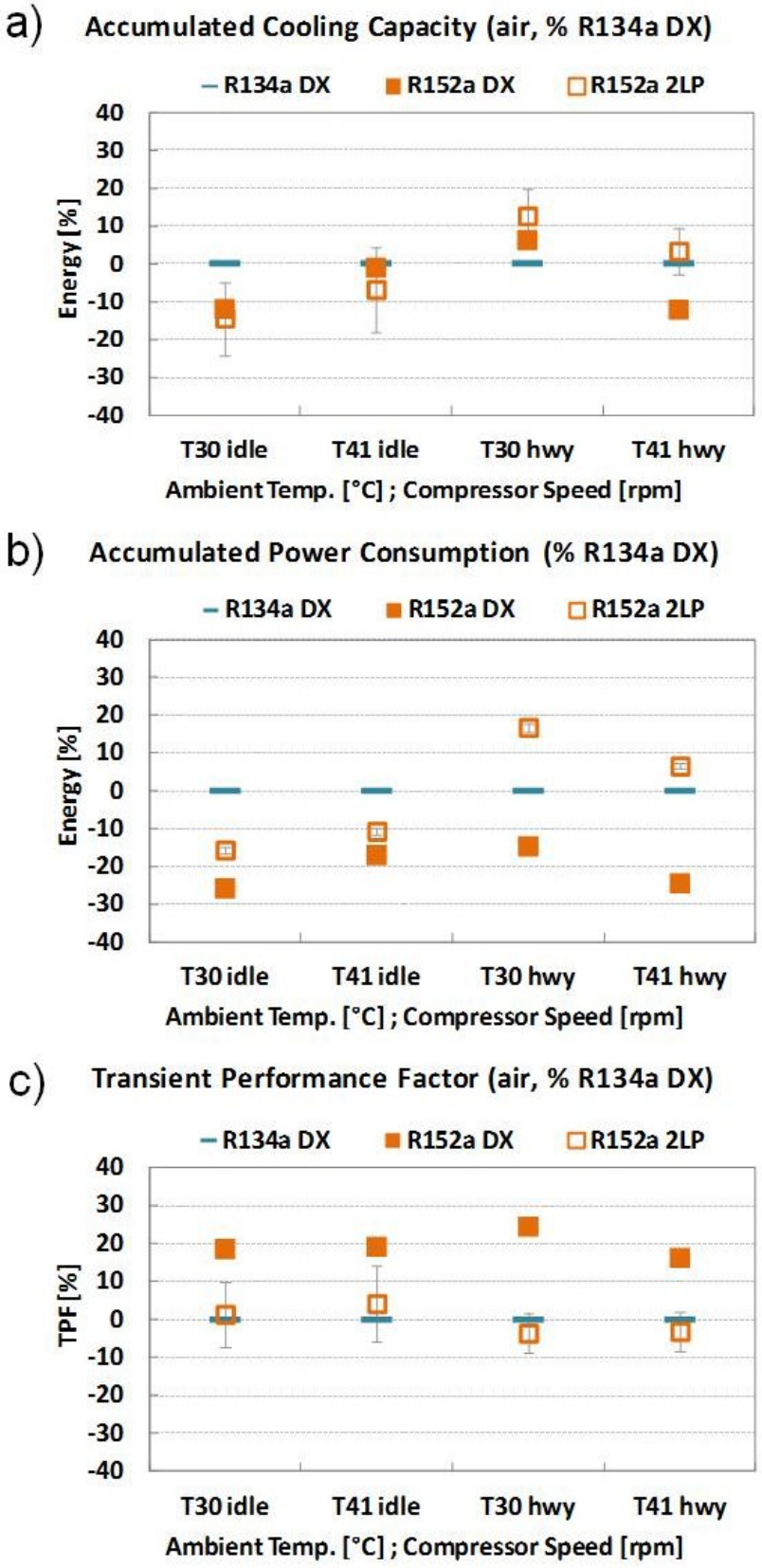

Figure 7.8: Pull-down Performance Results (2LP Versus DX)

Another way to evaluate pull-down performance is to normalize performance parameters with respect to time. When time-normalized, as shown in Figure 7.9 a) and b), transient performance factor of the secondary loop system was observed to be 20% and 13% lower at 30°C and 41°C ambient temperature, respectively. TPF of the R152a DX system was 25% and 38% increased above R134a DX TPF.

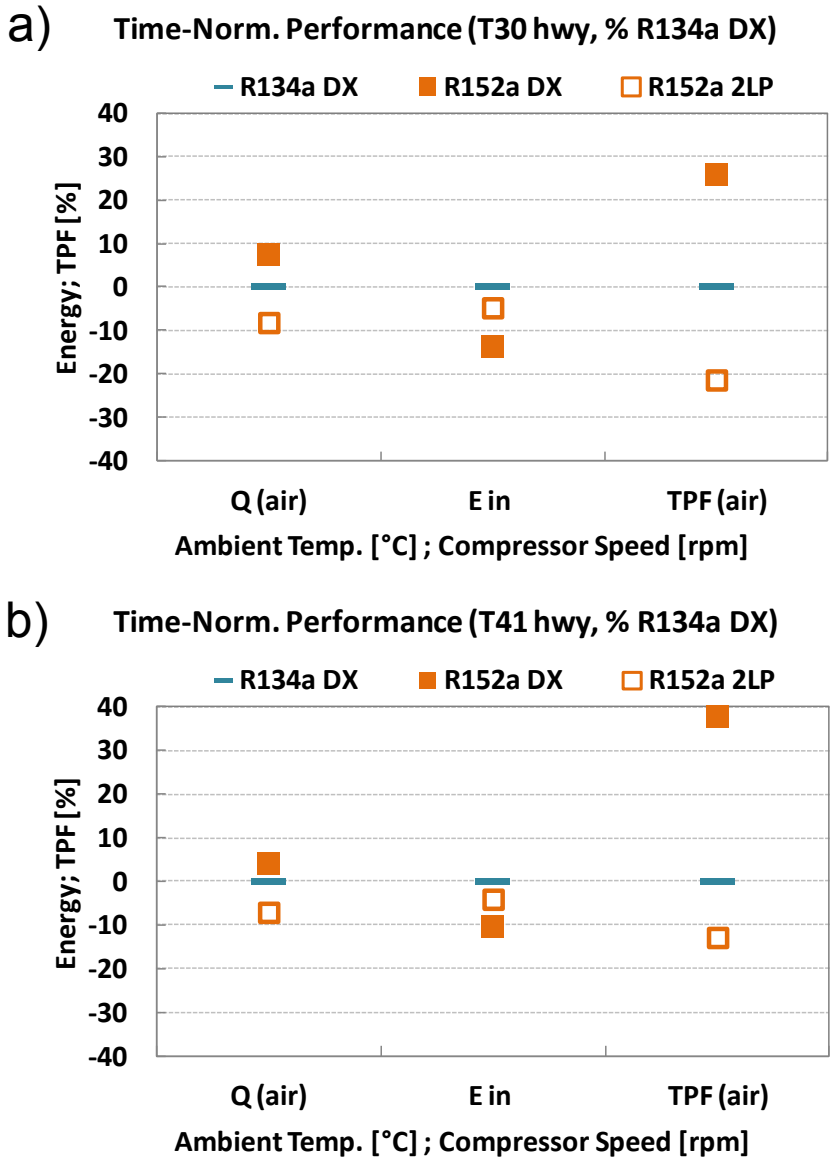

Figure 7.9: Pull-down Time-normalized Performance Results (2LP Versus DX)

7.3.2 New European Drive Cycle Performance - 2LP Versus DX

A comparison of transient behavior and performance during the New European Drive Cycle (NEDC) is provided in Chapter 7.3.2. The NEDC is used to evaluate power consumption of the air-conditioning unit at quasi-realistic, but standardized driving conditions. Due to large transients in compressor speed and condenser air flow rate, considerable fluctuations in cooling capacity, and consequently cabin supply temperature are introduced. As a secondary loop system has a larger thermal mass, drive cycle performance, as well as cabin air conditions may vary from the performance of a direct expansion systems. Transient trends, as well as accumulated performance data are discussed.

Figure 7.10 shows a transient comparison of supply temperature. As can be observed, using R152a as a drop-in in the direct expansion system reduced cabin supply temperature slightly, but not significantly. Due to the additional thermal mass of the secondary loop system, initial cool down of supply temperature was hindered and can be increased as much as 8°C during the initial minutes of the cycle. Close to the end of the highway section of the NEDC, R152a 2LP supply temperature approached the supply temperature of the direct expansion system. At the same time, secondary loop supply temperature was not subject to the same fluctuations supply temperatures of the direct expansion system experiences.

Further transient trends are shown in Figure 7.11, including trends in air-side cooling capacity, system power consumption, and dehumidification. As can be observed in Figure 7.11 a), R152a DX transient cooling capacity profile is

similar to the R134a DX capacity profile. R152a 2LP air-side capacity was significantly decreased during the first minutes of the cycle. During the middle section of the NEDC, the average capacity was observed to be close to the direct expansion system average, while showing less fluctuations. During acceleration, the secondary loop system capacity was slower to respond, while during deceleration, cooling capacity was preserved above the magnitude observed for the direct expansion system. After an extended time into the test, during the highway section of the cycle, secondary loop system capacity was on par with the direct expansion system capacity. Figure 7.11 b) shows transient profiles of power consumption. R152a as a drop-in in the direct expansion system showed decreased power consumption throughout the drive cycle. The R152a 2LP system power consumption was strongly increased during the first minutes of the cycle, as the refrigerant-side capacity was significantly higher compared to the direct expansion system (although air-side capacity was decreased). The R152a 2LP power consumption remained higher than power consumption of the R134a DX system throughout the drive cycle.

Figure 7.11 b) shows a comparison of transient dehumidification during the NEDC. Dehumidification profiles follow inverted profiles of cooling capacity, with R152a performing slightly worse than R134a DX, especially during the high speed portions of the cycle. During the mid section of the NEDC cycle, the direct expansion system experienced re-evaporation of condensate from the evaporator surface during idling. In comparison, the secondary loop system

performed worse in the beginning, but prevented re-evaporation during the mid section of the cycle for the most part.

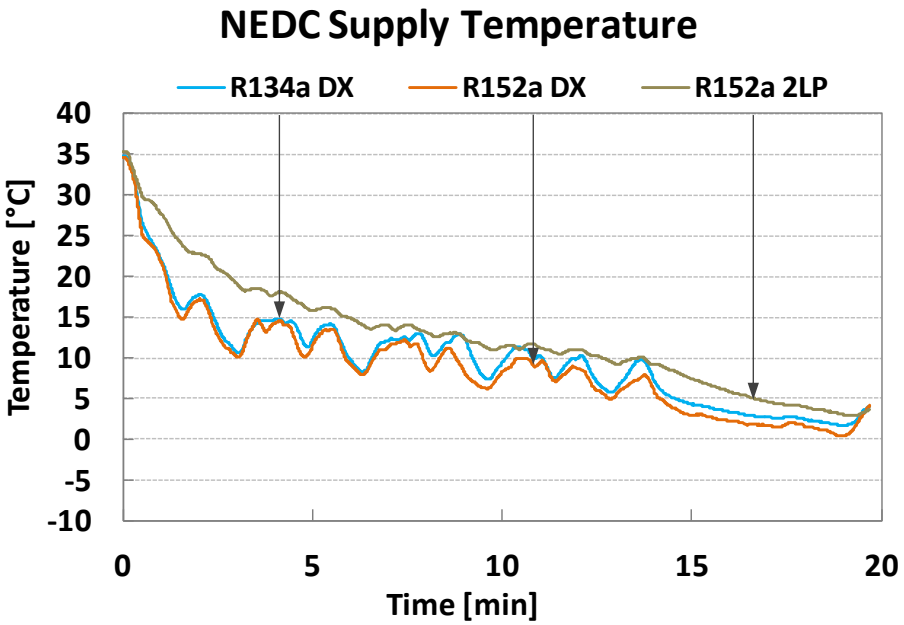

Figure 7.10: NEDC Supply Temperature Trend (2LP Versus DX)

Figure 7.12 provides a comparison of accumulated NEDC performance data, as well as a comparison of sensible and latent performance. Figure 7.12 a) shows refrigerant-side, as well as air-side accumulated performance parameters. R152a DX refrigerant-side, as well as air-side energy available for cooling were similar to the R134a DX system. Due to a decreased energy input in terms of compressor power, transient performance factors of R152a DX were about 10% increased above R134a DX TPF. The secondary loop system showed a significant increase of 25% in the energy available for cooling on the refrigerant-side. However, considerably less energy, -10%, was available on the air-side.

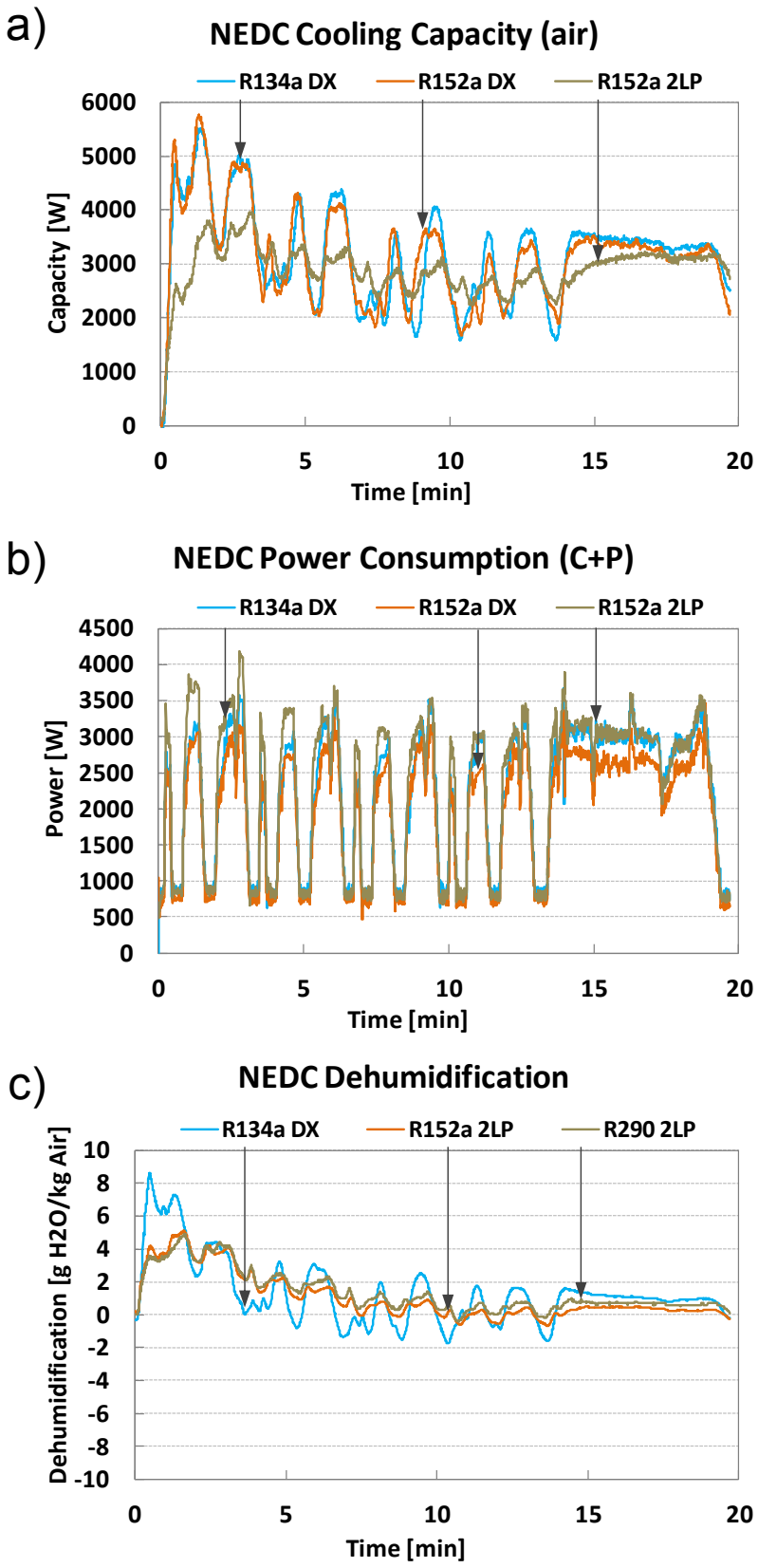

Figure 7.11: NEDC Performance Metrics Trend (2LP Versus DX)

Since the NEDC cycle is only little more than 18 minutes long, a significant amount of total energy is spent on cooling thermal mass of the system. Since the total energy input to the secondary loop system was increased by about 5%, the air-side transient performance factor was decreased by 14%. Figure 7.12 b) shows accumulated sensible and latent capacity. It can be observed that the sensible performance of R152a DX was similar to R134a DX. 2LP accumulated sensible capacity was decreased by 10%, following the trend of the accumulated air-side capacity. Accumulated capacity for both the R152a DX and the R152a 2LP system were reduced by 20%. The total amount of latent capacity integrated over the NEDC test time was small compared to sensible capacity. At the same time, measurement uncertainty of latent performance is high. The dehumidification performance follows the measurement of the latent capacity. The R152a DX as well as the R152a 2LP systems showed 20% reduced dehumidification performance as compared to R134a DX.

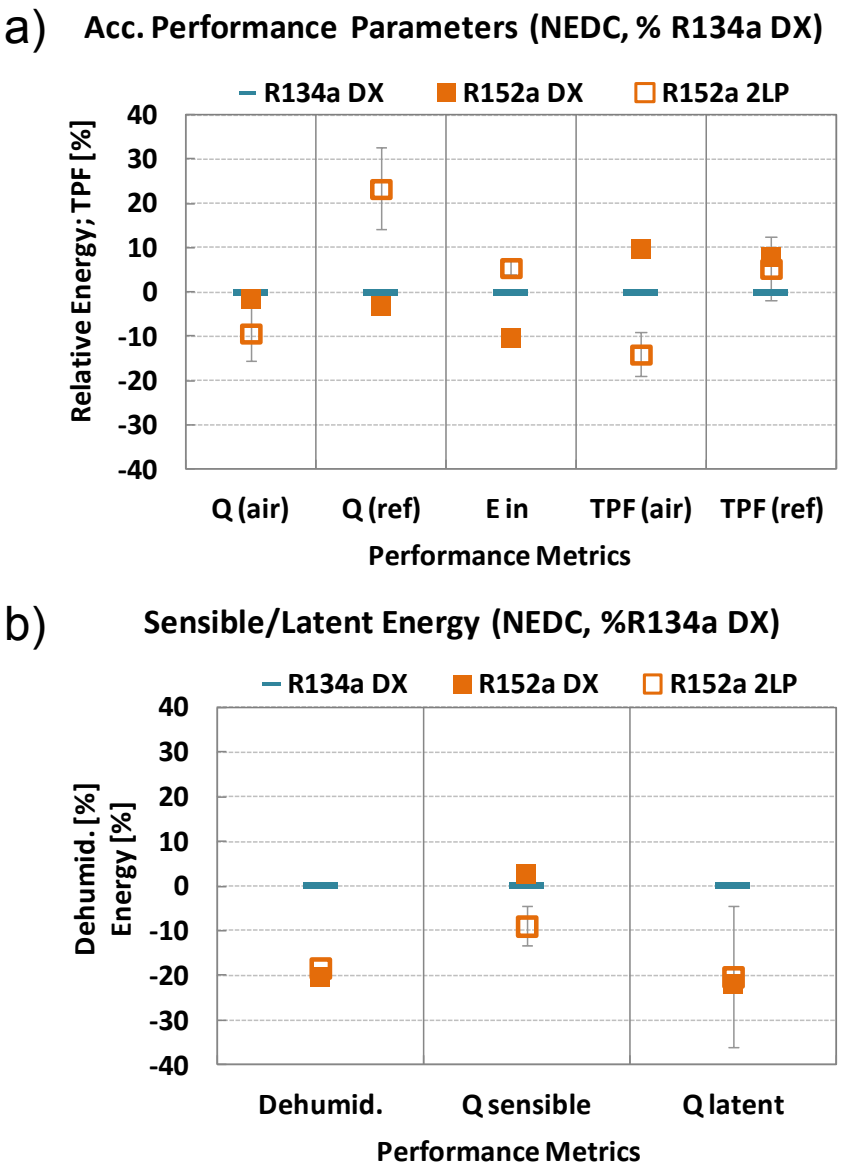

Figure 7.12: NEDC Accumulated Performance Metrics Results (2LP Versus DX)

7.4 Summary of Results: Secondary Loop Versus Direct Expansion

- Charge optimization for the R152a 2LP system showed a 28% reduction in refrigerant charge compared to the R134a DX system. A theoretical estimation of charge reduction for units built into a small to mid-size vehicle showed that by changing from R134a to R152a the charge can be reduced by about 24%, based on liquid line density.

When switching from R152a DX to R152a 2LP, an additional 25% of charge can be saved.

- Steady-state results showed that the cooling capacity of secondary loop systems was similar to the direct expansion system using the same refrigerant. R152a power consumption was more than 10% reduced compared to R134a, which allowed the R152a 2LP system to have 5% to 10% higher COP compared to the R134a DX system. Compressor isentropic and volumetric efficiencies were determined to be similar or higher compared to R134a. Sensible and latent cooling performance was within 10% of the R134a DX system. At idling conditions, latent cooling capacity might be decreased, but high uncertainties prevent a definite statement.

- Transient pull-down results showed that as expected, time to pull down to comfort set point was increased for secondary loop systems. For the amount of coolant in the present research (~ 5.5 kg), the increase can be as much as 25% from R152a DX to R152a 2LP at highway driving conditions. Consequently, the accumulated power during a pull down was increased by about 30% from R152a DX to R152a 2LP, and therefore also increased above R134a DX results. The transient performance factor for pull-down was within 5% of R134a DX and about 20% decreased compared to R152a DX.

- During NEDC operation, the energy provided to cool down the supply air was decreased by about 10% from R134a DX. At the same time, energy consumption was increased by about 5%. Consequently, air-side TPF was decreased by more than 10%. Latent energy used for dehumidification was reduced by about 20% for both, R152a DX and R152a 2LP. Sensible energy for the secondary loop system was reduced by 10%, due to sensible cooling of the additional thermal mass.

8 Experimental Results: Propane in Secondary Loop Systems

Chapter 8 shows experimental results which provide a basis for understanding the performance of Propane (R290) in mobile air-conditioning systems (MACs) as an alternative to R152a. As a low-GWP refrigerant with excellent thermophysical characteristics, Propane has been gaining attention in residential and commercial applications in recent years. Due to its high flammability, the use of an indirect system, such as the secondary loop system, is imperative for its use in automotive air-conditioning.

The normal boiling point of R290, as shown in Table 6.1, is significantly lower compared to both, R134a and R152a. As a result, R290 operates at higher pressures. R290 shows a significant increase in compressor power consumption, as well as a significantly increased volumetric capacity.

Figure 8.1 shows relative drop-in performance of R290 in the direct expansion system. Both at idling and highway driving, R290 showed an increase in power consumption by 40% above R134a results. Cooling capacity was increased by about 22%. In contrast, R152a showed a power consumption which was decreased by 12% - 18%, while cooling capacity was similar to R134a. As a result, COP of R290 was observed to be between 10% and 15% decreased compared to R134a, while COP of R152a was increased by about the same amount.

As a result of increase of capacity and the decrease of COP during drop-in tests, subsequent tests with Propane in the secondary loop system were

performed with reduced compressor speeds. The compressor rpm for R290 2LP tests was modified to result in similar cooling capacities and transient cooling performance compared to R134a DX. R134a and R152a were operated at speeds of 2,500 and 900 for highway driving and idling. For R290, compressor speeds were reduced to 1,550 and 650 rpm for highway driving and idling, respectively. In an automobile this could be achieved by either using a compressor with smaller displacement volume, or by changing pulley size at the engine to adjust the gear ratio between engine and compressor.

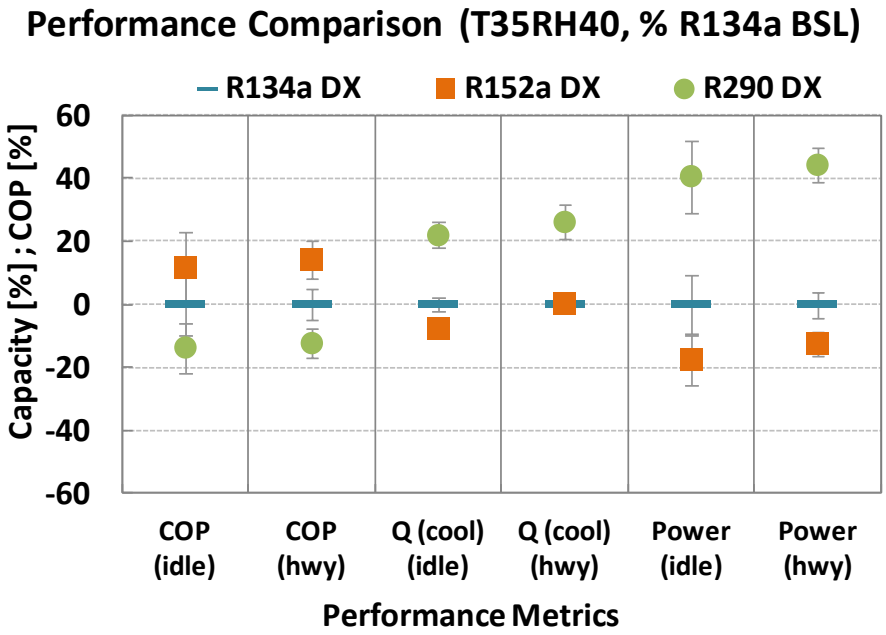

Figure 8.1: R290 Drop-in Performance in the Direct Expansion System

8.1 Charge Optimization: Propane in Secondary Loop Systems

Due to lower liquid density, Propane was found to have a decreased optimum charge compared to R134a and R152a. Table 8.1 shows charge

optimization results for the R290 secondary loop system in comparison to the R134a baseline and the R152a secondary loop system. A charge reduction of 60% was observed when changing the R134a DX system to a R290 2LP system. The decrease in charge is roughly twice the amount observed for the R152a 2LP system. This amounts to a 44% decrease in charge when replacing R152a with R290 in the secondary loop system.

Table 8.1: Charge Optimization Results: R290 2LP

Refrigerant /System	Optimized Charge [g]	Charge (% R134a DX)
R134a DX	1,730	0%
R152a 2LP	1,240	-28%
R290 2LP	700	-60%

Figure 8.2 shows the estimated charge savings, considering realistic pipe lengths in an automobile. For this estimation, vapor line lengths remained the same as in the 2LP test facility, but liquid line length was varied within reasonable boundaries, as shown in Figure 8.2. Additionally, the volume of the mass flow rate meter was omitted, and the volumes of filter-drier and receiver in the liquid line were reduced to fit commercially available products. Based on above assumptions, Propane charge could be reduced to as little as 380 g for baseline systems, and 320 g for secondary loop systems. It is estimated that a realistic charge of Propane in secondary loop systems could stay below 350 g. On average, this could result in a charge reduction of roughly 43% when replacing R152a in secondary loop systems.

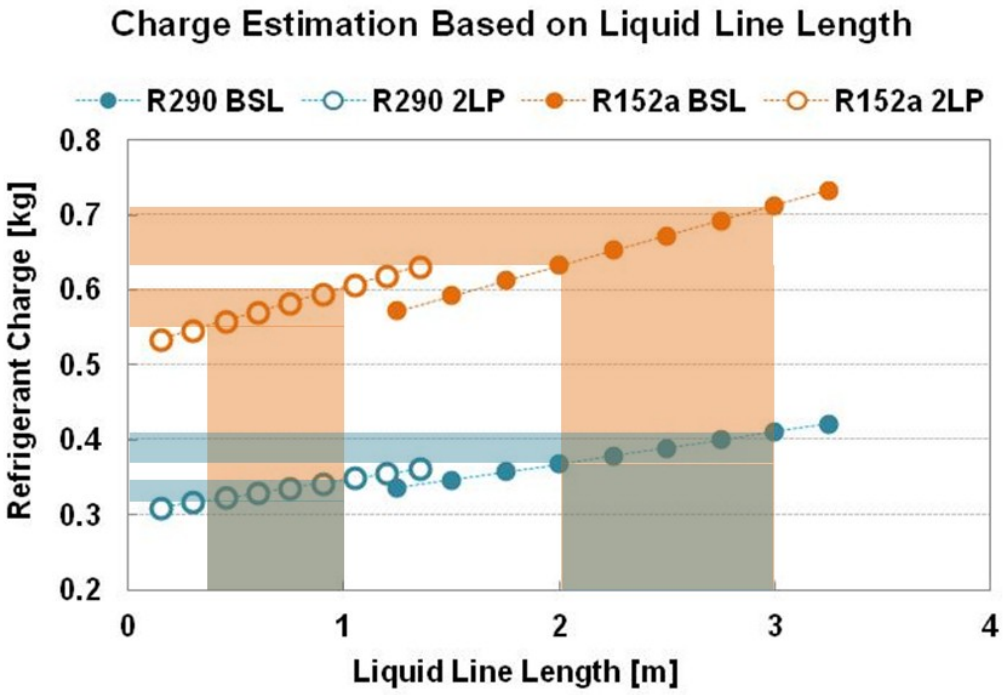

Figure 8.2: Estimated Charge Savings for R290 Secondary Loop Systems

8.2 Steady-state Performance: Propane in Secondary Loop Systems

Chapter 8.2 shows relative steady-state performance results of R290 in the 2LP system, as compared to R134a DX and R152a 2LP results. System performance, compressor efficiencies, and sensible/latent capacity are provided.

Figure 8.3 shows temperature and pressure at several locations in the refrigeration cycle when operating at highway driving speed and ambient conditions of 35°C and 40% relative humidity. Temperature is shown on the first y-axis, while pressure is shown on the second y-axis. Propane operates at pressures well above R134a pressures. Suction pressure increased to about 500 kPa, while high side pressure increased to about 1,750 kPa. Suction temperature

was very similar to suction temperature of R134a DX and R152a 2LP, while discharge temperature was significantly reduced (8 K) with respect to R134a DX.

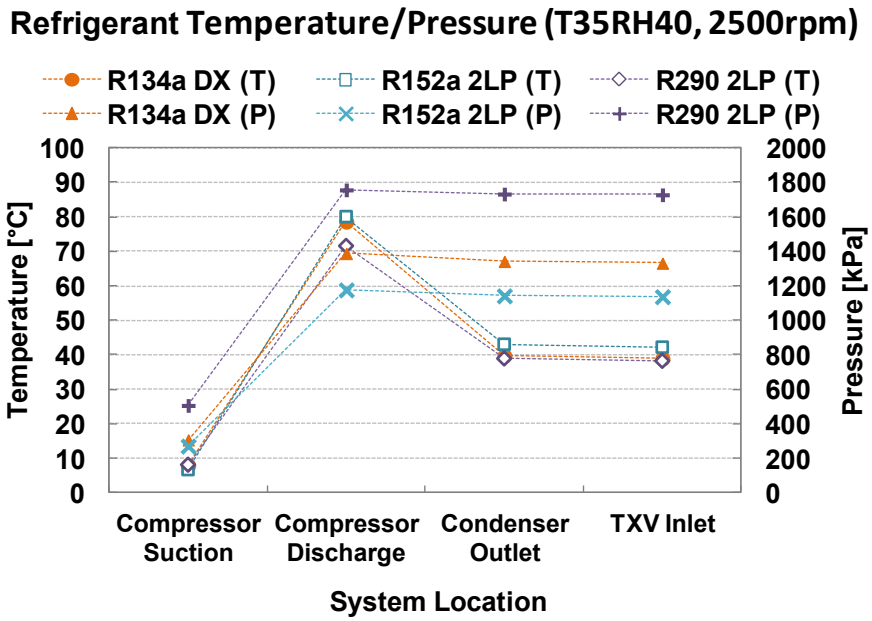

Figure 8.3: System Temperature and Pressure State Points (R290 2LP)

Figure 8.4 shows R290 2LP performance metrics, compressor efficiencies, and sensible/latent performance relative to R134a DX. For reference, absolute steady-state data for the R134a DX system is provided in Appendix I. Figure 8.4 a) provides experimental results for cooling capacity, power consumption, and COP during highway driving and idling conditions. Since R290 2LP compressor rpm was adjusted, as described in Chapter 8, performance results are not drop-in results. R290 2LP capacity was adjusted to show similar transient performance as the R134a DX system. Steady-state cooling capacity was observed to be reduced by about 10% for highway driving speed and about 20% for idling, while R152a 2LP cooling capacity stayed within -5% for both driving conditions. Due to

the reduction in rpm for R290 2LP, power consumption decreased accordingly, resulting in a decrease of roughly 15% and 5% for highway and idling conditions, respectively. At the same time, R152a 2LP showed a 5% smaller decrease at highway speed conditions and a significantly higher decrease of 15% at idling conditions. Consequently, COP for R290 was increased by more than 5% at highway driving condition. During idling, R290 2LP COP was observed to be decreased by about 15%, though measurement uncertainty was increased when operating at idling conditions. Figure 8.4 b) shows relative changes in isentropic and volumetric efficiency. R290 2LP displayed a 10% increase in both, isentropic, as well as volumetric efficiency with respect to R134a DX. However, during idling a significant decrease of 20% and 25% was observed for volumetric and isentropic efficiency, respectively. It was determined that if compressor efficiencies at idling were similar to R134a DX efficiencies, due to optimization of the compressor for R290, idling COP would be increased 15% above R134a DX.

Figure 8.4 c) shows a comparison of sensible and latent cooling performance for idling and highway speed driving conditions. R290 2PL sensible capacity was similar to R134a DX and R152a 2LP sensible capacity during idling, while it was decreased by about 8% under highway driving conditions, much similar to R152a 2LP. Latent capacity for R290 2LP was measured to be zero during idling, while latent capacity of R134a DX and R152a 2LP were measured to be 280 W and 230 W, respectively. However, latent capacity during idling was associated with high measurement uncertainties, leaving the R290 2LP latent performance comparison without a definite conclusion.

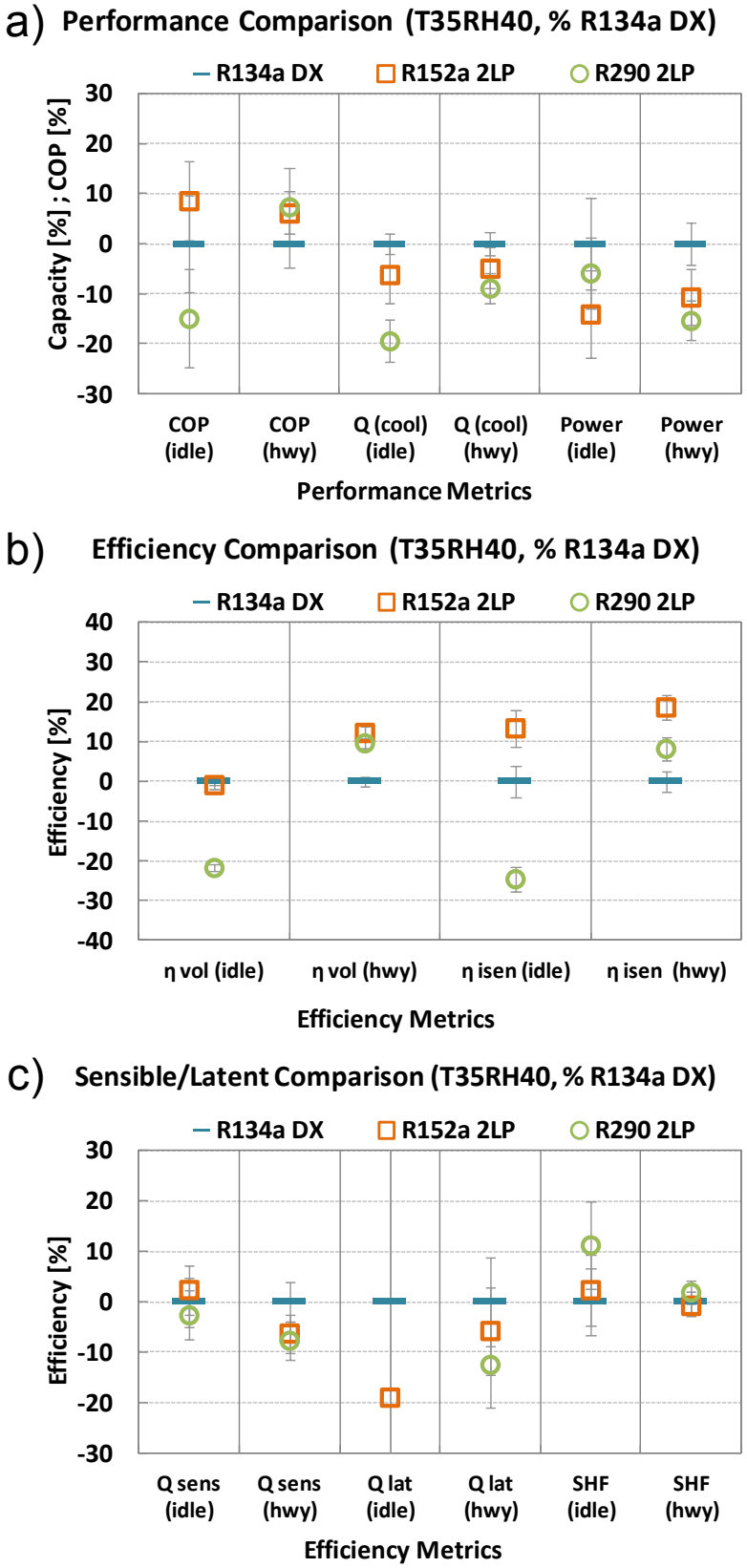

Figure 8.4: Steady-state Performance Results (R290 2LP)

The sensible heat factor of R290 2LP was similar to R134a DX SHF when operating at highway conditions and increased by roughly 10% during idling.

Based on the assumption that compressor design could be changed to achieve idling efficiencies similar to R134a DX efficiencies, a theoretical estimate on possible R290 2LP performance was performed using Engineering Equation Solver. It was furthermore assumed that suction state properties, as well as discharge pressure would not change from the previously measured values. With isentropic and volumetric efficiencies similar to the R134a DX experimental values, idling capacity would change significantly, while power consumption would stay nearly the same. As a result, R290 2LP idling COP would increase to about 15% above R134a DX COP, as observed in Figure 8.5, which would also translate into enhanced transient drive cycle performance.

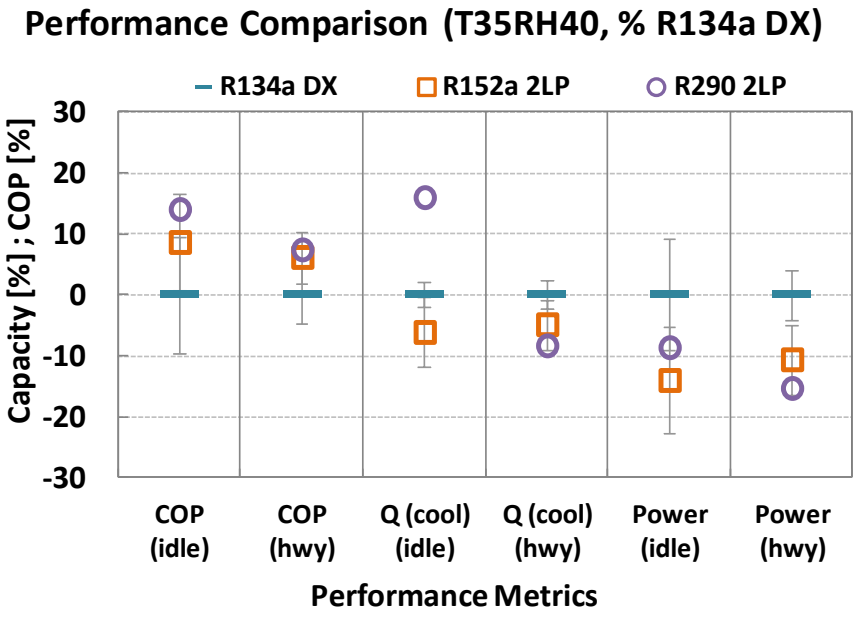

Figure 8.5: Theoretical R290 2LP Performance Results with Increased Idling Compressor Efficiencies

8.3 Transient Performance: Propane in Secondary Loop Systems

Chapter 8.3 provides transient experimental results for the R290 secondary loop system in comparison to the R134a DX and the R152a 2LP systems. Pull-down performance at several ambient conditions and compressor speeds, as well as NEDC drive cycle performance, are discussed.

8.3.1 Pull-down Performance: Propane 2LP

Figure 8.6 shows time to comfort information for R290 2LP, relative to the R134a DX system. At highway speed, time to comfort was increased by 30% and 20% for 31°C ambient temperature and 41°C ambient temperature, respectively. At both conditions, the R290 2LP time to comfort was increased by about 10% with respect to R152a 2LP measurements. At 41°C idling, the air-conditioning system was not able to pull the cabin down to comfort setpoint, resulting in the abortion of the test for all systems after 60 minutes. Therefore, no difference in time to comfort can be observed at 41°C idling conditions. At 30°C idling, the R290 2LP system showed an increase of time to comfort above 60%. This was a result of the poor steady-state performance at low and moderate temperatures during idling. However, pull-down results may change, depending on how compressor rpm, compressor displacement, or pulley ratio are adjusted. The adjustment of compressor rpm for R290 2LP added to the increase in time to comfort. Therefore, time to comfort should not be taken as final result for the R290 2LP system, but rather as a parameter which can be adjusted.

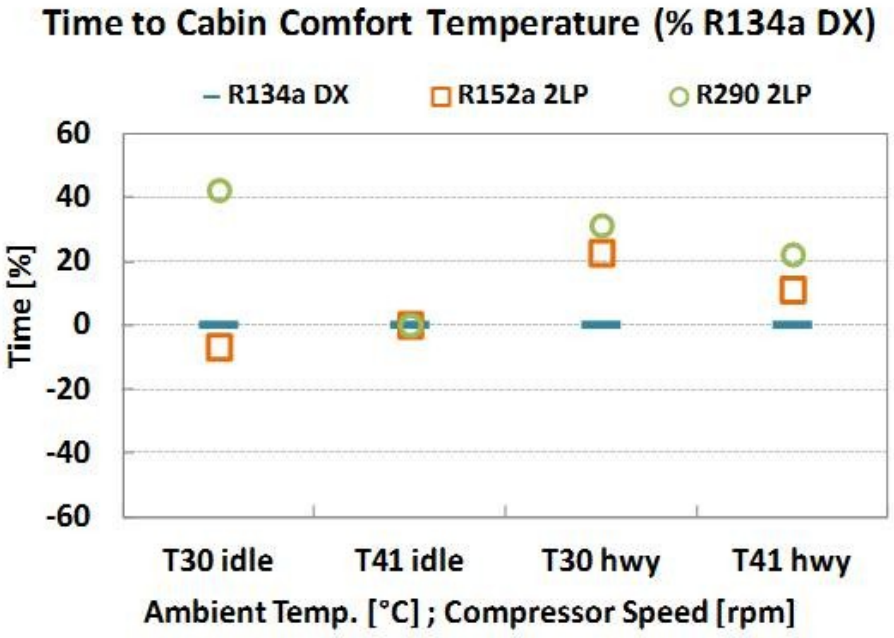

Figure 8.6: Pull-down Time to Cabin Comfort (R290 2LP)

Figure 8.7 shows relative results for accumulated performance metrics. Accumulated cooling capacity, power consumption, and transient performance factor results are shown. Due to accumulated capacity and power consumption being heavily influenced by time to comfort (i.e. length of the test), the rpm adjustment for R290 2LP affects capacity and power consumption. However, since both are affected in the same way, it can be expected that transient performance factor results retain their validity when rpm is adjusted within reasonable boundaries. Figure 8.7 a) shows relative results of energy available for cooling cabin air over the time of a pull-down test. At highway driving conditions, the R290 2LP system showed a 20% and 15% increased capacity for 30°C and 40°C ambient temperature, respectively. In both cases, cooling energy was elevated above R152a 2LP values. Accumulated cooling capacity trends

followed the trends for time to comfort. At idling conditions, accumulated cooling capacity was decreased by 16% at 41°C. As test time is constant for the three systems, trends resemble steady-state results. However, at 30°C, R290 2LP accumulated capacity was increased by more than 40%, due to the long testing time. Figure 8.7 b) shows relative results for a comparison of power consumption. At highway speeds, the R290 2LP system showed an increase in power consumption of about 25%. While the power consumption matched R152a 2LP power consumption at moderate temperatures, it increased by 10% over the R152a 2LP power consumption at 41°C ambient temperature. At idling conditions, R290 2LP power consumption was 15% higher compared to R134a DX for 41°C ambient temperature, while R152a 2LP consumption was about 9% increased. At 30°C ambient temperature, R209 2LP power consumption is increased by about 100% compared to R134a DX consumption. Figure 8.7 c) shows a relative comparison of air-side transient performance factor. At highway speed, R290 2LP was performing as well (41°C) or better (30°C) as R134a DX and R152a DX. However, at idling speed transient performance was reduced by about 10% to 15%.

Figure 8.8 shows time-normalized results at highway driving conditions for ambient temperatures of 30°C and 41°C with respect to R134a DX performance. When time-normalized, accumulated cooling capacities were reduced by 9% (30°C) and 7% (41°C). The time-normalized R290 2LP results for cooling capacity were matching R152a 2LP results. Time-normalized energy consumption was decreased by 11% (30°C) and 6% (41°C).

a) Accumulated Cooling Capacity (air, % R134a DX)

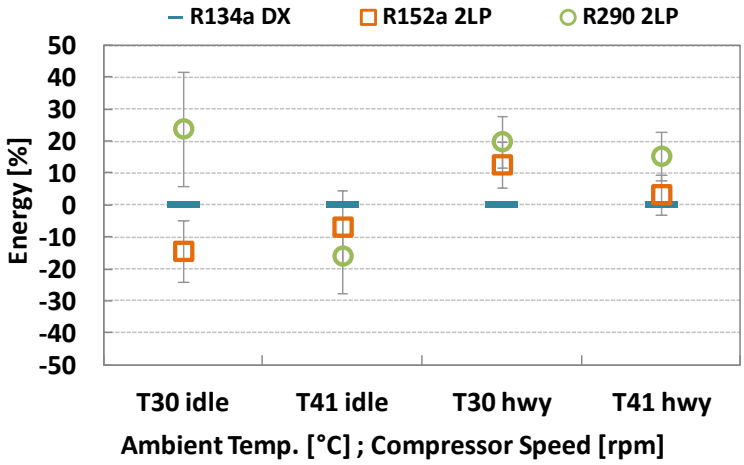

b) Accumulated Power Consumption (% R134a DX)

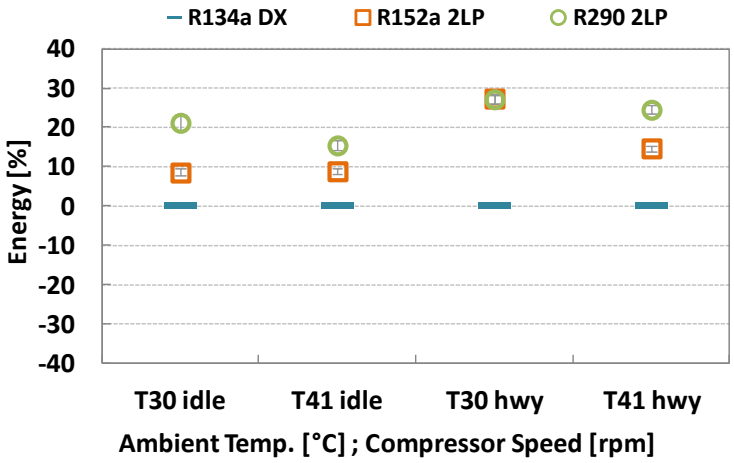

c) Transient Performance Factor (air, % R134a DX)

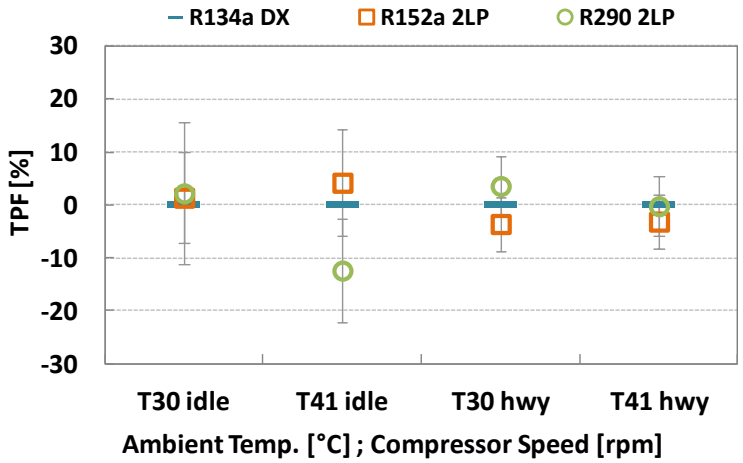

Figure 8.7: Pull-down Performance Results (R290 2LP)

In the case of 30°C ambient temperature, R290 2LP time-normalized energy consumption was 7% lower compared to R152a 2LP. The time-normalized transient performance factor of R290 2LP was decreased by about 20% for both ambient temperatures. In the case of 41°C, R290 2LP time-normalized TPF was about 6% lower compared to R152a 2LP.

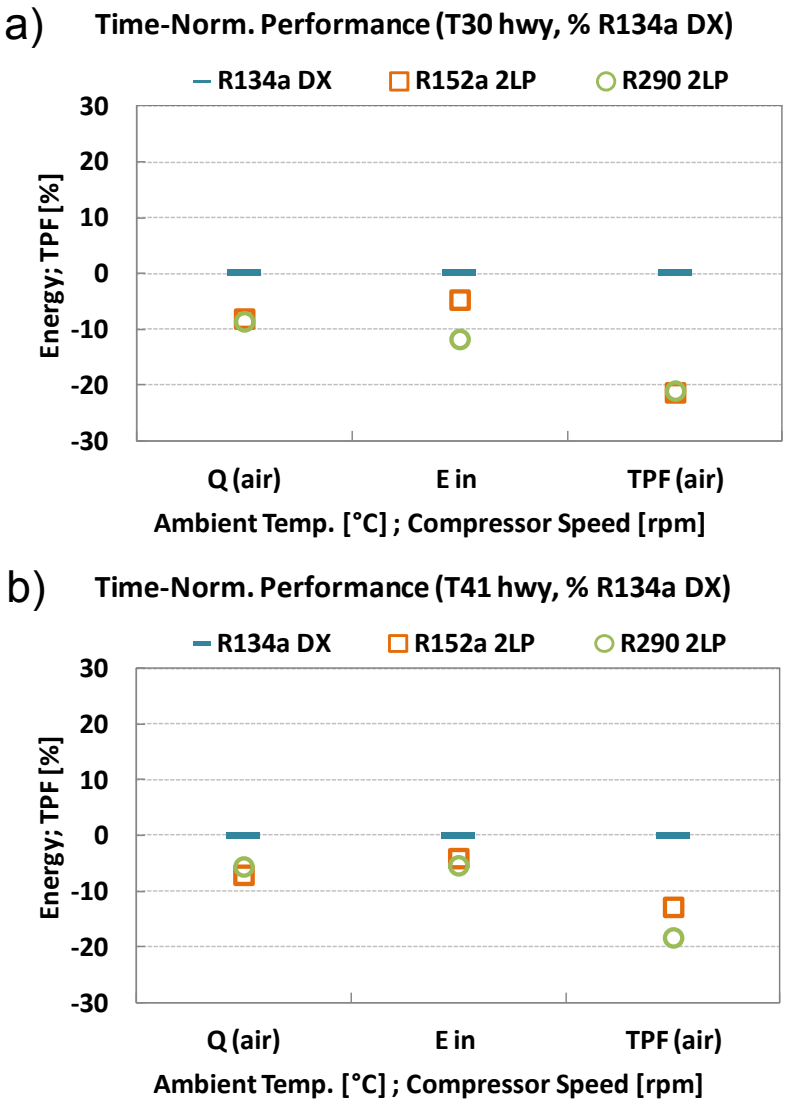

Figure 8.8: Pull-down Time-normalized Performance Results (R290 2LP)

8.3.2 New European Drive Cycle Performance - Propane 2LP

Figure 8.9 shows transient trends for cabin supply temperature. The supply temperature profile of R290 2LP showed the same trends as the R152a 2LP profile, but was elevated by about 1 K to 1.5 K. This was due to the adjusted compressor rpm for R290 2LP tests. Both for R152a 2LP and for R290 2LP the supply temperature profile showed less fluctuations compared to the R134a DX profile, due to the thermal mass of the coolant in the secondary loop. At the end of the drive cycle, supply temperature of R290 2LP was within 1 K of the supply temperature of the R134a DX profile.

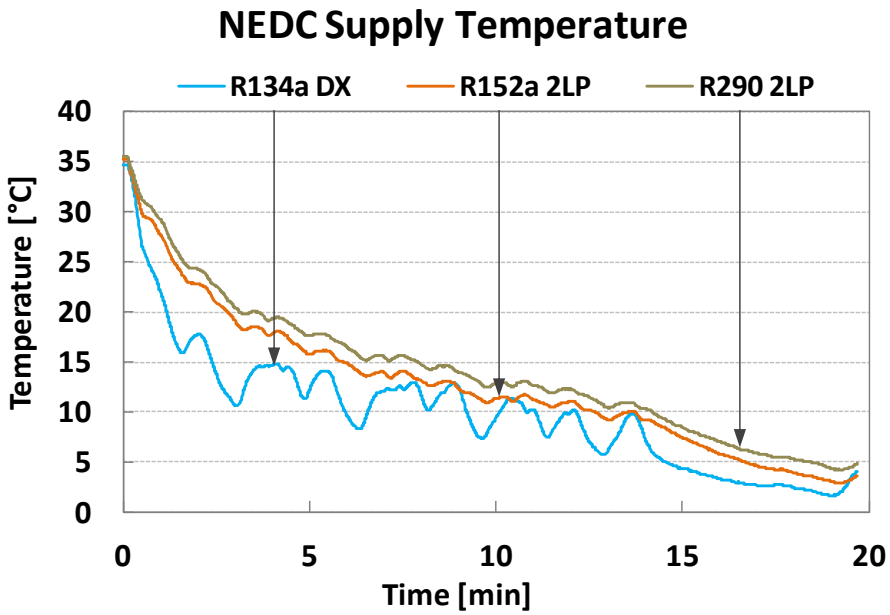

Figure 8.9: NEDC Supply Temperature Trend (R290 2LP)

Figure 8.10 shows a comparison of relative performance metrics results. As can be observed in Figure 8.10 a), the cooling capacity of the R290 2LP system follows the same profile as the R152a 2LP system. R290 2LP, as well as

R152a 2LP air-side cooling capacity was decreased significantly during the first minutes of the cycle, due to the thermal mass of the secondary loop system. R290 2LP power consumption, shown in Figure 8.10 b), followed the same profile as R134a DX power consumption. R290 2LP power consumption was lower than R152a 2LP power consumption during the high rpm sections of the cycle. The R290 2LP dehumidification profile, shown in Figure 8.10 c), showed the same trend as the R152a 2LP profile, though with a slightly increased dehumidification throughout the drive cycle. Again, the differences to the direct expansion dehumidification trend, specifically reduced fluctuation due to a decrease in re-evaporation, become apparent.

Figure 8.11 introduces relative accumulated NEDC performance results for the R290 2LP system. Air-side capacity was reduced by 10%, similar to R152a 2LP air-side capacity. However, the power consumption was reduced by 5%, resulting in a decrease of TPF of 5% with respect to R134a DX. This is a small improvement, +8%, with respect to R152a 2LP. As discussed in previous chapters, the refrigerant-side TPF was increased compared to R134a, while the air-side TPF was decreased. The largest contributors to this phenomenon are the thermal mass of the secondary loop, which reduces the accumulated air-side capacity, and the pump power, which steadily increases the accumulated total power consumption of the system.

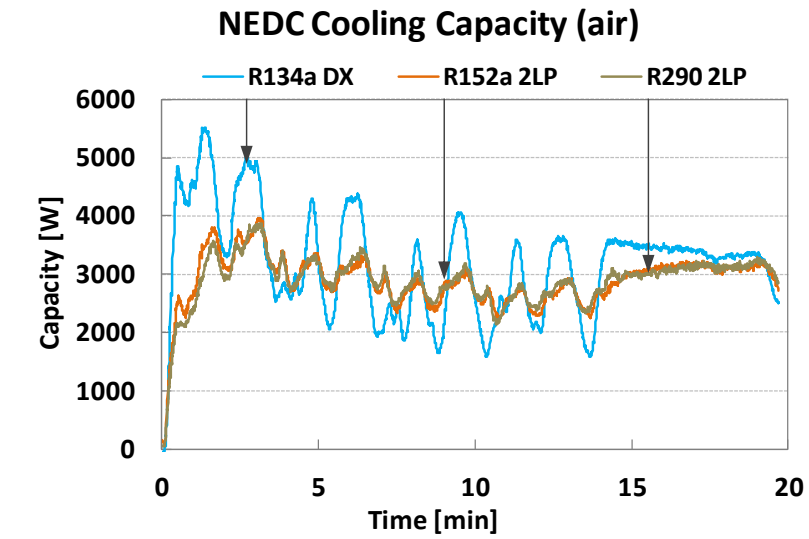

b)

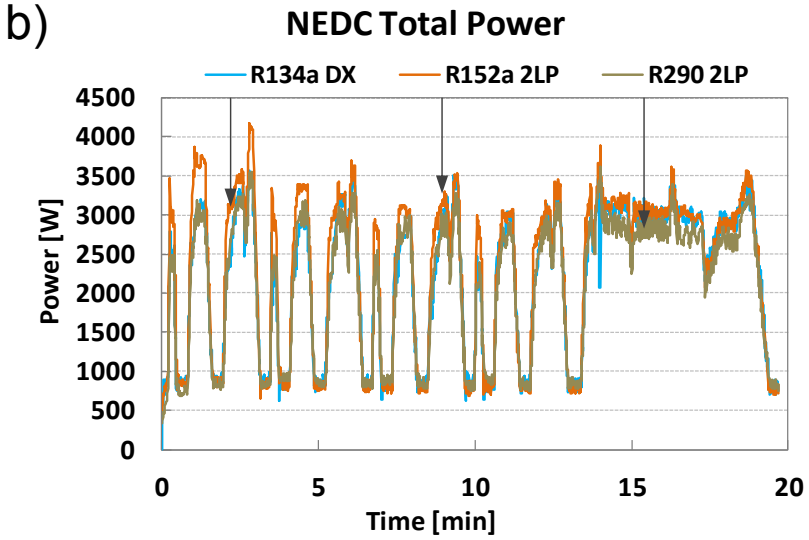

c)

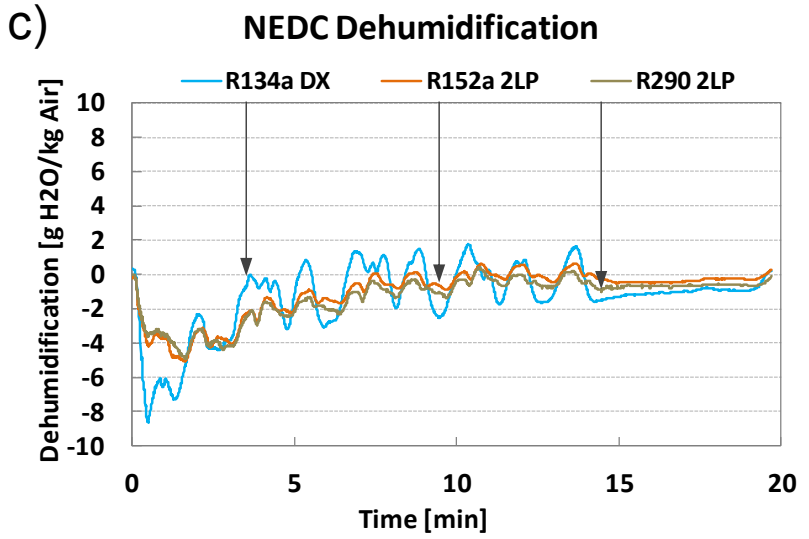

Figure 8.10: NEDC Performance Metrics Trends (R290 2LP)

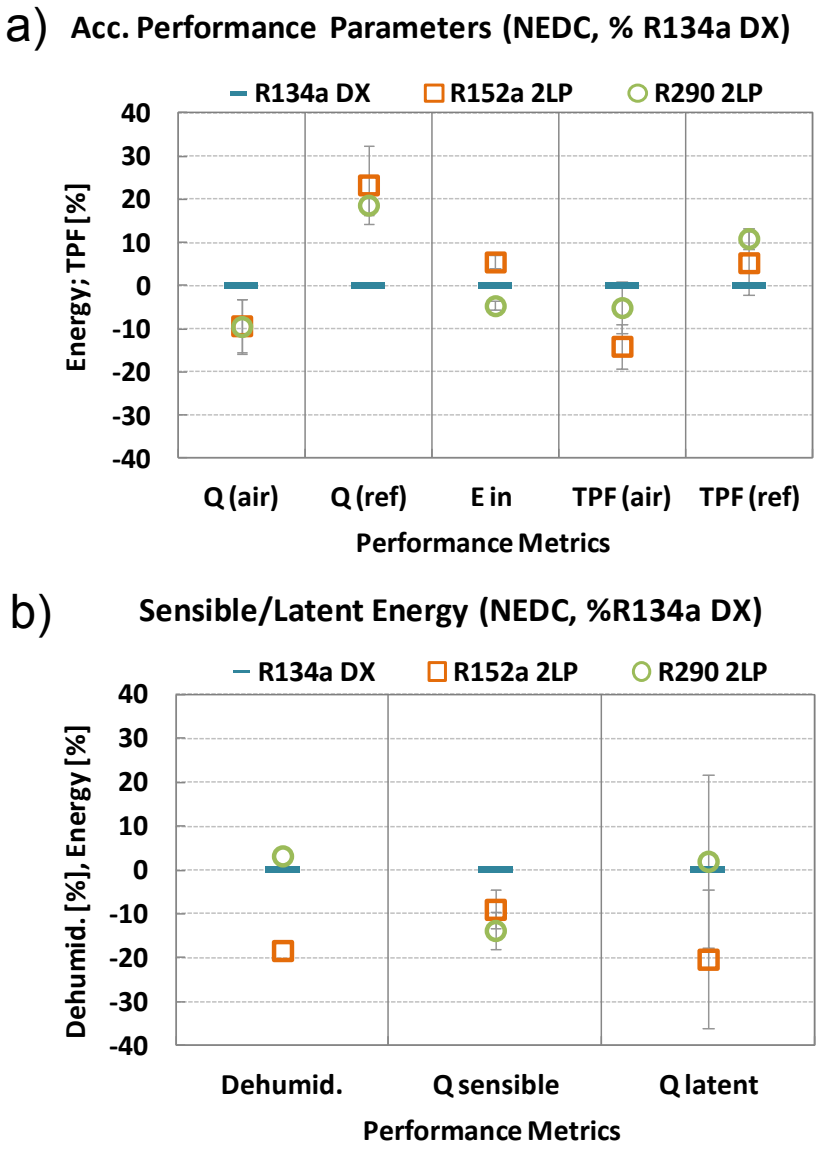

Figure 8.11: NEDC Accumulated Performance Metrics Results (R290 2LP)

8.4 Summary: Propane as Refrigerant in Secondary Loop Systems

- Using R290 as a drop-in with components optimized for R134a under the same operating conditions resulted in increased cooling capacities and increased power consumption. R290 2LP COP during drop-in tests was reduced by more than 10% compared to R134a DX. Therefore, R290 tests were carried out with reduced compressor rpm

to simulate a smaller compressor and decrease cooling capacity to comparable levels.

- Charge optimization for R290 2LP reduced refrigerant charge by 60% in comparison to R134a DX. A theoretical estimation showed that R290 charge may be about 60% smaller compared to R134a, based on liquid density. In an air-conditioning system for a small to mid-size vehicle, charge may be reduced by an additional 20% for secondary loop systems in comparison to direct expansion systems.

- Steady-state performance of R290 in secondary loop systems changed significantly with compressor speed. At highway driving conditions, R290 2LP COP was about 8% higher than R134a DX COP, and therefore similar to R152a 2LP COP. At idling conditions, R290 2LP COP was reduced by 15% from R134 DX COP. This was due to volumetric and isentropic compressor efficiencies, which were reduced by up to 25% compared to R134a DX. If compressor efficiencies could be increased to R134a DX levels by using a compressor which is optimized for R290, COP would be increased 14% above R134a DX. Sensible and latent cooling capacity were decreased slightly from R152a 2LP results, due to a decrease in overall cooling capacity caused by the reduction in compressor rpm.

- Transient pull-down results showed that time to comfort increased by 20% to 30% for highway driving in comparison to R134a DX. This was due to the choice of reduced rpm and the subsequent availability of cooling capacity. Therefore, experimental results for pull down accumulated cooling capacity will vary, based on which rpm (or in a car: which compressor size) is chosen. However, TPF results show that transient performance of R290 2LP was similar or better than R134a DX during highway driving conditions. At idling conditions, TPF was decreased by 10% to 15%. A compressor designed specifically for R290 can significantly increase TPF at low compressor speeds.

- NEDC results show that R290 2LP transient performance was decreased by 5% with respect to R134a DX, as opposed to nearly 15% for R152a 2LP. Sensible capacity was about 14% decreased, which was influenced by the reduction in rpm. Latent capacity was about the same as R134a DX results, although measurement uncertainty was significant.

- It was shown that R290 2LP steady-state COP, as well as transient TPF could be similar or higher, compared to R134a DX. However, reduced COP at low compressor speeds prevent the R290 2LP NEDC TPF to increase above R134a DX TPF. If components were used, which were optimized for use with R290, steady-state, as well as transient performance could improve well above R134a DX performance.

Based on measurements of the components used in the experimental test facility, as well as a reasonable estimate of refrigerant and coolant line lengths in an mid-size sedan, the mass of the secondary loop system was assumed to be increased by about 24%, compared to a DX system. The increase of mass is due to the adding of coolant, coolant tubing, and secondary loop components, such as the coolant pump and an intermediate heat exchanger. Fischer [118] estimated an annual increase in fuel consumption of about 3.4 gallons (12.7 liters) due to the mass of a regular air-conditioning system. Due to the estimated increase in mass by 24%, when switching to a secondary loop system (as discussed above), an additional 0.82 gallons (3.1 liters) of fuel consumption might be expected per year.

Green-Mac-LCCP [119], a software which was peer reviewed and globally accepted as a credible method of comparing the climate performance of mobile air conditioning systems, was used to estimate the impact of secondary loop systems on the Life Cycle The model takes into account the change of mass of the system, the change of charge due to different refrigerants and system layouts, as well as other characteristics associated with the change of life cycle climate performance when using different refrigerants. Figure 8.12 shows a comparison of CO_2 equivalent emissions per lifetime per vehicle for a range of U.S cities in colder, as well as warmer climate. A secondary loop system using R152a or R290 as refrigerant will reduce the CO_2 equivalent emissions per lifetime per vehicle by roughly 12% to 20% (R152a) or 13% to 22% (R290) as compared to a R134a DX system. The decrease in CO_2 equivalent emissions is mainly due to decrease of direct contributions (i.e. due to the decrease in negative impact the refrigerant itself has on the environment). Inputs to the Green-MAC-LCCP model were based on experimentally measured cooling capacity and COP. A secondary loop system which is optimized for R290 as primary refrigerant would possibly reduce CO_2 equivalent emissions even beyond the results shown in Figure 8.12.

A theoretical comparison of refrigerants in Chapter 6 showed that the cycle efficiency, or COP, of R290 should be expected to be 0% to 5% decreased compared to an R134a system. However, experimental steady-state results showed an increase of 10% during highway driving conditions and a 15% decrease during idling conditions. During transient NEDC operation, where compressor speeds are much higher than idling speeds for a majority of the time,

the R290 2LP system faired similar to the R134a DX system despite capacity disadvantage due to increased thermal mass. This discrepancy can be explained by taking compressor efficiencies into account. Alefeld [115] distinguished irreversibilities into two categories: irreversibilities caused by fluid properties and by system design. System design irreversibilities are partially reflected in the isentropic compressor efficiency term in Equations (22) and (23) in Chapter 6. As observed in Chapter 8, R290 2LP isentropic efficiency during highway driving is 10% increased compared to R134a DX. If this increase would have been included in the term g_c in Equations (22) and (23), theoretical analysis and experiment would agree within 2%.

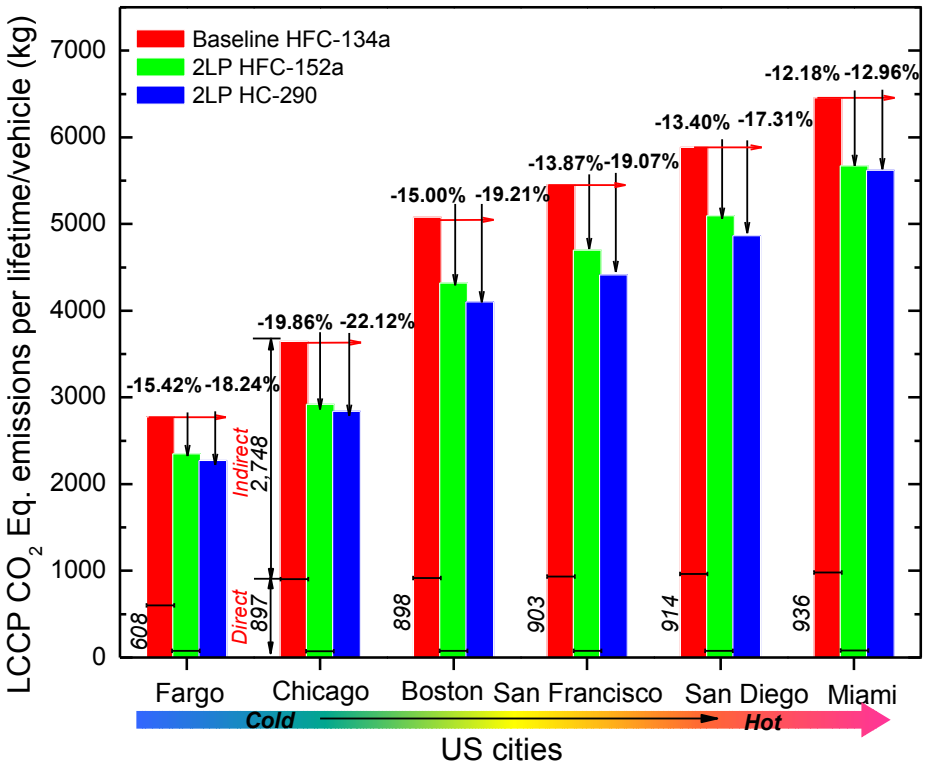

Figure 8.12: Impact of Secondary Loop Systems on Life Cycle Climate Performance of a Mid-size Passenger Car

9 Thermal Storage During Off-Cycle Test Results

Chapters 7 and 8 introduced transient performance results of the secondary loop system. Thermal lag during pull-down tests and NEDC drive cycle tests, due to an increased thermal mass, were characterized and discussed. While this can be a disadvantage for a fast cabin pull-down and consequently thermal comfort, it can be turned into an advantage during off-cycle operation. If the automobile idles and the compressor either runs with reduced rpm, or is turned off for short periods of time, cooling capacity is reduced. The thermal mass of the secondary loop system can preserve capacity and therefore thermal comfort during off-cycle periods.

Chapter 9 provides experimental results to quantify the effect of thermal storage of a secondary loop system during off-cycle periods. Two experimental test procedures were developed, namely the Start/Stop drive cycle and the off-cycle cabin warm-up after pull-down. The Start/Stop drive cycle is a modified version of the NEDC. The idling periods were replaced by off periods, simulating the start/stop operation of many modern cars. A further modification of the Start/Stop cycle is the Start/Stop 3x Idling drive cycle (SS3xI). All idling periods, or for that matter off-cycle periods, were tripled in length to determine how changes in off-cycle time affect the performance of secondary loop systems with respect to the performance of direct expansion systems. The second test procedure developed for thermal storage characterization is the cabin warm-up test. For this test, a regular pull-down test is performed. When the cabin temperature reaches are pre-determined comfort setpoint, the compressor is

turned off and the cabin is allowed to warm up. Cabin air and supply air temperature, as well as relative humidity, are measured during the warm-up period. Appendix E provides more detailed information about the thermal storage test procedures.

In addition to the secondary loops thermal storage, ice storage was investigated as part of advanced thermal storage options. To this end, an ice storage heat exchanger (IS), introduced in Chapter 3.3, was built and integrated into the secondary loop test facility. Chapter 3.3 also details the modifications made to the facility and resulting operating modes, such as IS charging, IS only cooling, and 2LP+IS cooling mode. Chapter 9.2 shows experimental results for pull-down with ice storage, and thermal storage cabin warm-up tests.

9.1 Secondary Loop Thermal Storage Performance

Chapter 9.1 provides experimental test results, which characterize the thermal storage effect of secondary loop systems. Start/Stop drive cycle results, as well as cabin warm-up after pull-down results are discussed. Thermal storage tests were performed with 5.5 kg of ethylene glycol as coolant, as detailed in 3.2. In a commercial vehicle, results may vary based on the amount of coolant. A comparison of thermal storage performance based on coolant mass fraction and based on secondary loop coolant volume is provided in Chapter 11 as part of the transient simulation effort in Modelica.

9.1.1 Secondary Loop Start/Stop Drive Cycle Performance

Start/Stop drive cycle tests are a modified version of the New European Drive Cycle (NEDC). Due to turning off the compressor, instead of running at idling speed, fluctuations in temperature and relative humidity during the city portion of the cycle are more pronounced. Over the course of the start/stop cycle, less energy is consumed compared to the NEDC, which was the reason why start/stop operation was introduced to commercial vehicles in the first place (though rather for fuel saving than for A/C energy saving). At the same time, less energy is available for cooling the cabin, due to the off-times of the compressor.

Figure 9.1 shows a comparison of cabin supply air temperature and relative humidity profiles for R134a DX, R152a 2LP, and R290 2LP. Similar to the NEDC results, the secondary loop lagged behind in cooling down the supply air during the first minutes. The capacity, and subsequently the supply temperature, of the R290 2LP system were determined by the reduced rpm, which was chosen in order to give a similar transient performance to R134a DX systems. Although the supply temperature of R290 was shown to be 1 K - 1.5 K higher compared to R152a, this can be adjusted by choosing an appropriate compressor displacement or compressor speed (for internal combustion engine vehicles: engine/compressor gear ratio). Supply air temperature of the secondary loop was up to 5K higher during the course of the drive cycle. However, the thermal mass of the secondary loop stabilized supply air temperature, as well as relative humidity in comparison to the direct expansion (DX) system. In Figure 9.1 b), it can be observed that R134a DX supply relative humidity increased rapidly during

off-cycle periods, due to re-evaporation of condensate. At the end of the city portion of the cycle, supply air may be saturated or close to saturation, which might decrease the thermal comfort level of passengers and increase the threat of windshield fogging under certain operating conditions. Due to its thermal storage potential, the secondary loop could retain cooling capacity during off-cycle periods, which prevented excessive re-evaporation and stabilized supply relative humidity.

Figure 9.2 shows a comparison of accumulated performance results for the start/stop drive cycle with respect to R134a DX performance. Accumulated cooling capacity, as well as accumulated power consumption, and transient performance factor (TPF), are shown in Figure 9.2 a). While secondary loop system results, R152a 2LP and R290 2LP, show a 8% decrease in energy available for cooling, cooling energy increased 2% to 3% compared to NEDC results, discussed in Chapter 8.3.2. This is due to the secondary loop system retaining cooling capacity during off-cycle periods. Based on the energy input required for R152a 2LP and R290 2LP, TPF decreased by roughly 10% (R152a 2LP), or was similar to R134a DX (R290 2LP). Although the secondary loop energy consumption was increased, due to the coolant pump operation during off-cycle periods, the cooling capacity advantage due to thermal storage resulted in a higher TPF, compared to NEDC operation. Figure 9.2 b) shows accumulated sensible and latent performance during the start/stop cycle. Energy available for sensibly cooling the air was up to 10% reduced (R290 2LP) as compared to R134a DX, while latent energy available to dehumidify the air was reduced by up

to 30% (R152a 2LP). Measurement uncertainty for latent performance was significantly increased compared to uncertainty of sensible performance and may distort the results for latent cooling and dehumidification.

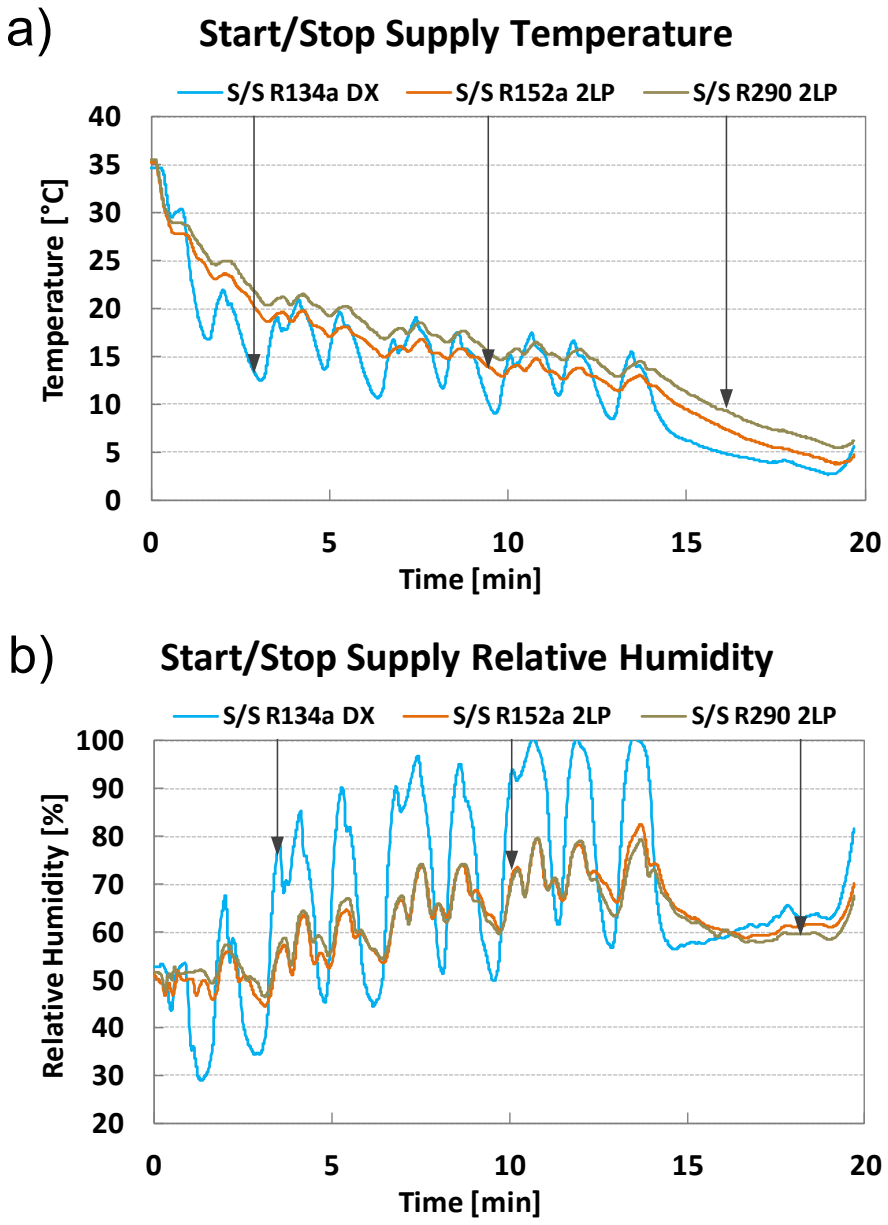

Figure 9.1: Start/Stop Drive Cycle Supply Air Profiles

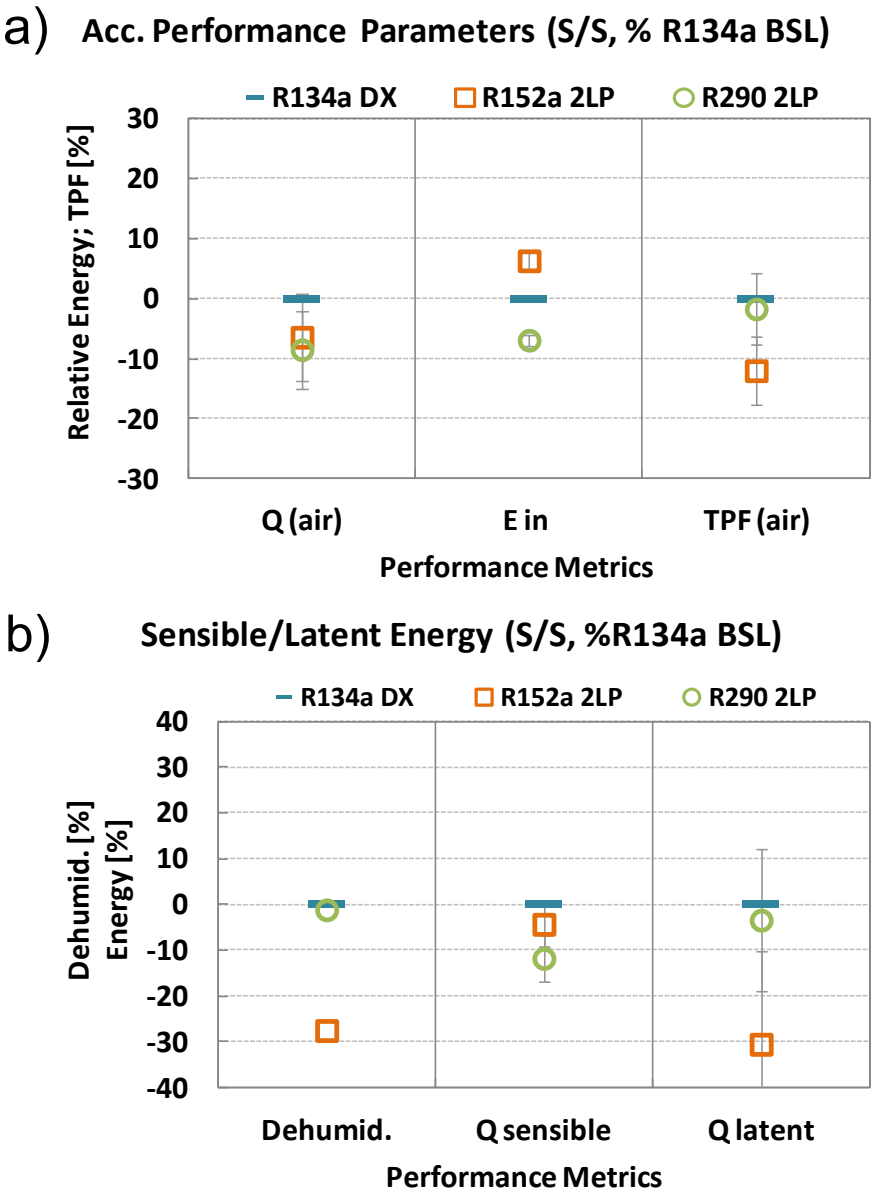

Figure 9.2: Start/Stop Drive Cycle Accumulated Performance Results

The start/stop drive cycle was modified by increasing the length of off-cycle periods. NEDC and start/stop drive cycles feature idling periods of roughly 20 seconds length. For the Start/Stop 3x Idling (SS3xI) drive cycle, the off-cycle

periods were tripled, featuring a length of roughly 60 seconds. This was felt to be still within a realistic boundary for traffic light stops during city driving.

Figure 9.3 shows a comparison of transient supply temperature and relative humidity profiles for the SS3xI drive cycle operation. It can be observed that the fluctuations in supply temperature and relative humidity are more pronounced compared to regular start/stop operation. For a direct expansion system, increase in supply temperature during off-cycle periods could be as high as 10 K, while the secondary loop system was able to limit the fluctuations in supply temperature to about 2 K. The average increase of R152a 2LP or R290 2LP supply temperature compared to R134a DX supply temperature was not as clear cut as observed in the NEDC or Start/Stop results. Figure 9.3 b) shows R134a DX supply humidity to increase well beyond the saturation limit during the second half of the city portion of the cycle. Although there was a significant increase for R152a 2LP and R290 2LP supply humidity as well, relative humidity never reached 100% throughout the SS3xI drive cycle.

A comparison of accumulated performance parameters for the Start/Stop 3x Idling drive cycle, as well as accumulated sensible and latent performance, are shown in Figure 9.4. As can be observed in Figure 9.4 a), the energy available for cooling the air was on par with R134a DX for R290 2LP and was increased by about 4% for R152a 2LP. In comparison to NEDC and Start/Stop drive cycle, the long off-cycle periods of the SS3xI allowed the secondary loop to catch up in air-side cooling energy, despite the disadvantage of having to cool

down more thermal mass. Consequently, R290 2LP TPF increased by 10% above R134a DX, and R152a 2LP TPF was measured to be similar to R134a DX.

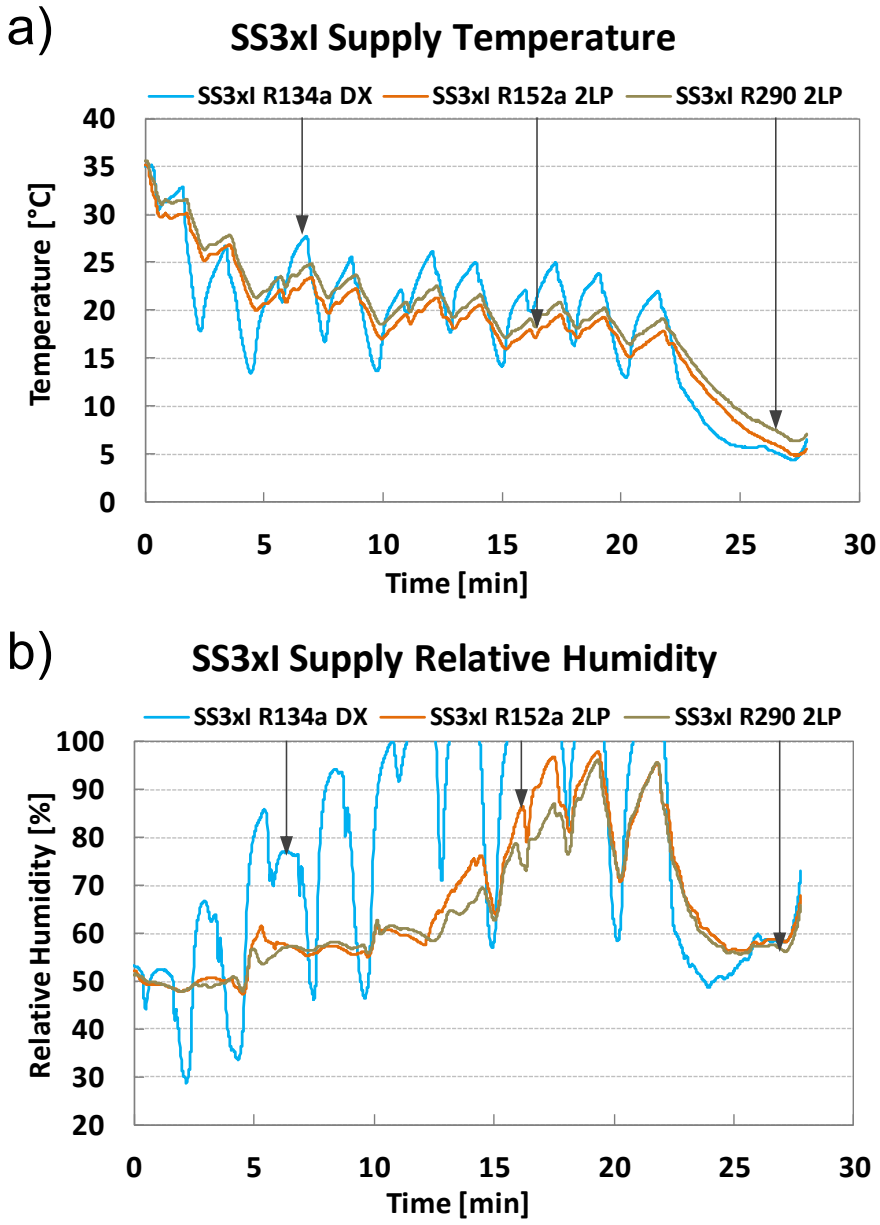

Figure 9.3: Start/Stop 3x Idling Drive Cycle Supply Air Profiles

Sensible cooling performance for both secondary loop refrigerants, shown in Figure 9.4 b), equaled R134a DX sensible cooling performance. Latent cooling

was still reduced compared to the direct expansion system. R152a 2LP and R290 2LP latent cooling were reduced by about 40% and 25%, respectively.

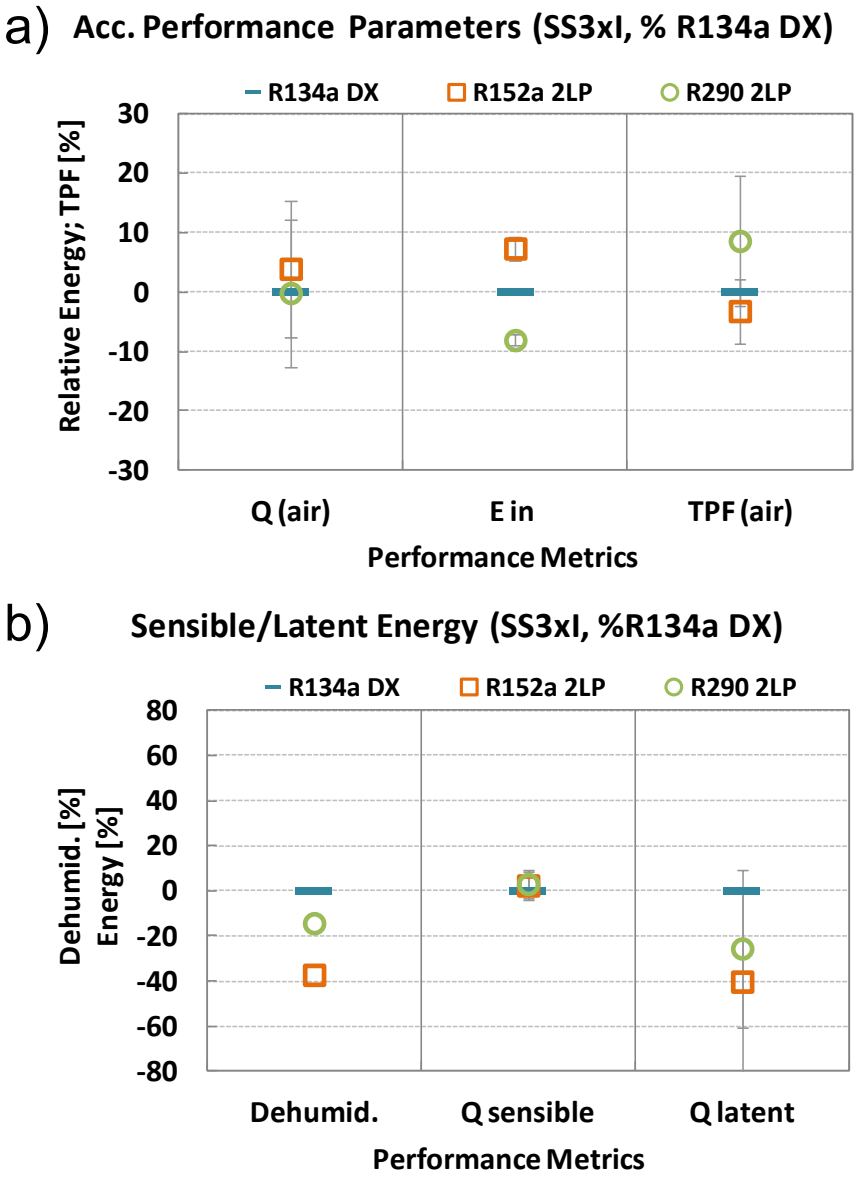

Figure 9.4: Start/Stop 3x Idling Drive Cycle Accumulated Performance Results

A comparison of the three cycles may show the difference between direct expansion and secondary loop systems more conclusively. Figure 9.5 shows an

accumulated performance comparison between all three systems for both, Start/Stop with respect to NEDC performance, and SS3xI with respect to NEDC performance. It can be observed that the R134a DX system "loses" 12% of air-side cooling energy when moving from regular NEDC operation to Start/Stop operation, while the secondary loop system accumulated cooling capacity decreases by 10%. The difference is well within measurement uncertainty. As off-cycle periods increase in length, as is the case for the SS3xI drive cycle, R134a DX "loses" nearly 40% of air-side cooling energy. At the same time, cooling energy of the secondary loop system decreased by only 33%. The reduction in energy consumption when switching from NEDC to Start/Stop operation is about 5% for both, direct expansion and secondary loop system. The reduction in energy for 2LP systems when switching to SS3xI is less compared to direct expansion system, due to the increased impact of pump work with increasing off-cycle periods. Nevertheless, decrease in TPF favors secondary loop systems, especially for longer off-cycle periods. It can be concluded that city driving with start/stop operation favors secondary loop systems with increasing off-cycle periods in terms of energy consumption and thermal comfort.

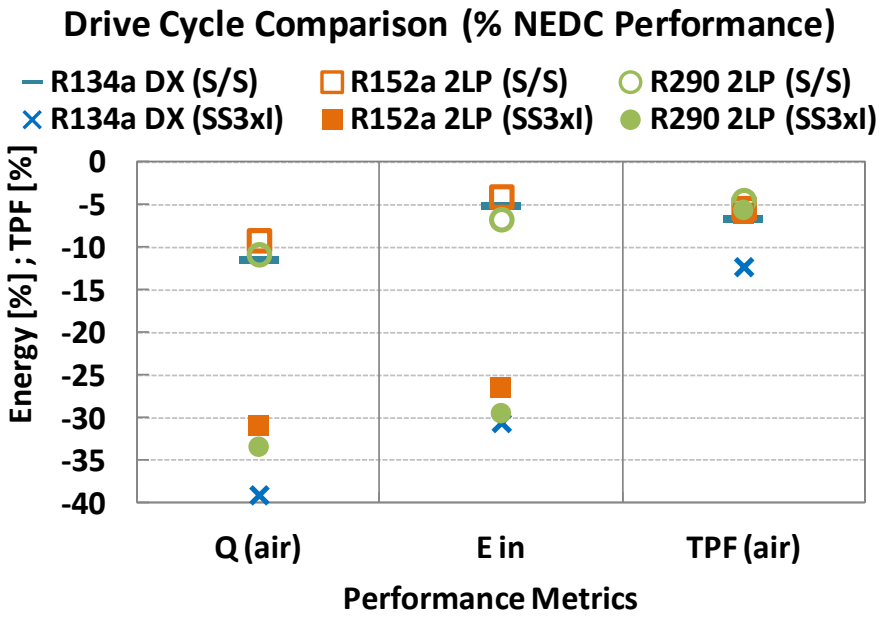

Figure 9.5: Drive Cycle Accumulated Performance Results Comparison

9.1.2 Secondary Loop Off-Cycle Cabin Warm-up Performance

Cabin warm-up tests evaluate the development of cabin temperature and relative humidity during extended off-cycle periods. To this end, the cabin was pulled down to comfort condition, at which point the compressor was turned off and the cabin was allowed to warm back up. The airflow over the evaporator (DX) or cooler (2LP) was kept constant and the coolant pump was kept running for the secondary loop system.

Figure 9.6 shows a comparison of cabin and supply temperatures during an extended off-cycle period. Trends for the increase of cabin temperature are shown in Figure 9.6 a). While the cabin temperature increased immediately for the direct expansion system, 2LP cabin temperature stayed at comfort setting (24°C) for a period of about 2 - 2.5 minutes. After the first minute of compressor

shut down, the difference in cabin temperature between the direct expansion system and the secondary loop system was about 1 K. Further along the cabin warm-up, the temperature difference increased to about 2.5 K and 3 K at 5 minutes and 15 minutes, respectively. The temperature difference between direct expansion and secondary loop system seemed to stay fairly constant thereafter for an extended period of time. The difference in cabin temperature can be traced back to the difference in cabin supply temperature, shown in Figure 9.6 b). While the cabin supply temperature started to increase immediately after compressor shut down, due to loss of cooling capacity, the rate of increase was far higher for the direct expansion system. This was especially true for the first one to two minutes of the cabin warm-up process. The steep increase in supply temperature might partially be a result of condensation of refrigerant vapor inside the evaporator. While condensation might happen at the intermediate heat exchanger of the secondary loop system as well, the thermal mass of the coolant is able to compensate. During the initial minutes of the warm-up process, 2LP supply temperature was about 7 K lower compared to R134a DX supply temperature. During later stages of the warm-up process the temperature difference decreased to roughly 5 K.

Another aspect of extended off-cycle periods is the re-evaporation of condensate off the outer surface of the evaporator (DX system) or cooler (2LP system). Figure 9.7 shows supply relative humidity profiles, as well as dehumidification at the heat exchanger. DX supply relative humidity rose fast and reached saturated conditions after about 30 seconds, while it took about 2

minutes for 2LP supply relative humidity to achieve saturation. It was observed that direct expansion re-evaporation humidified the air with approximately 5 gram of water per kg of moist air within the first three minutes of the cabin warm-up process.

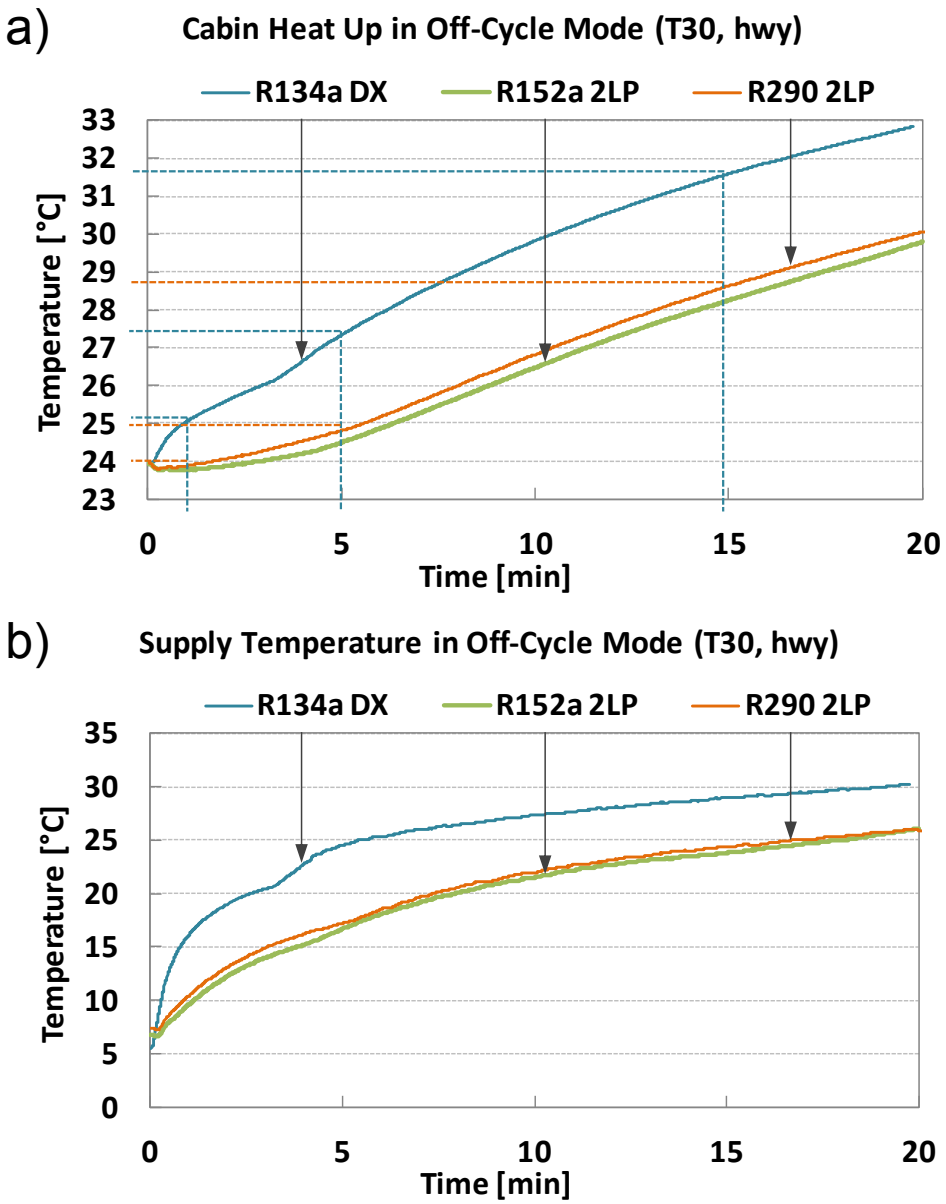

Figure 9.6: Secondary Loop Off-cycle Cabin Warm-up Profiles

Secondary loop thermal storage decelerated this process. A rate of 4 gram of water per kg of moist air was reached after about 3 minutes. Starting from 6 minutes, the humidification for both the DX and 2LP system was reduced to about 2 g/kg and reduced slowly thereafter. The cabin was humidified at a slow rate for an extend period of time, mostly through the remaining condensate in the drain bin and drain pipe of the facility. Humidification during off-cycle periods should be avoided as much as possible, since the moisture results in an increased latent load when the compressor turns back on. At the same time, excessive humidity combined with rising temperatures might lead to reduced passenger comfort. The secondary loop system has a clear advantage compared to direct expansion systems in terms of decelerating re-evaporation and cabin humidification. However, even when employing a secondary loop system, off-cycle periods longer than a few minutes will lead to undesirable humidification.

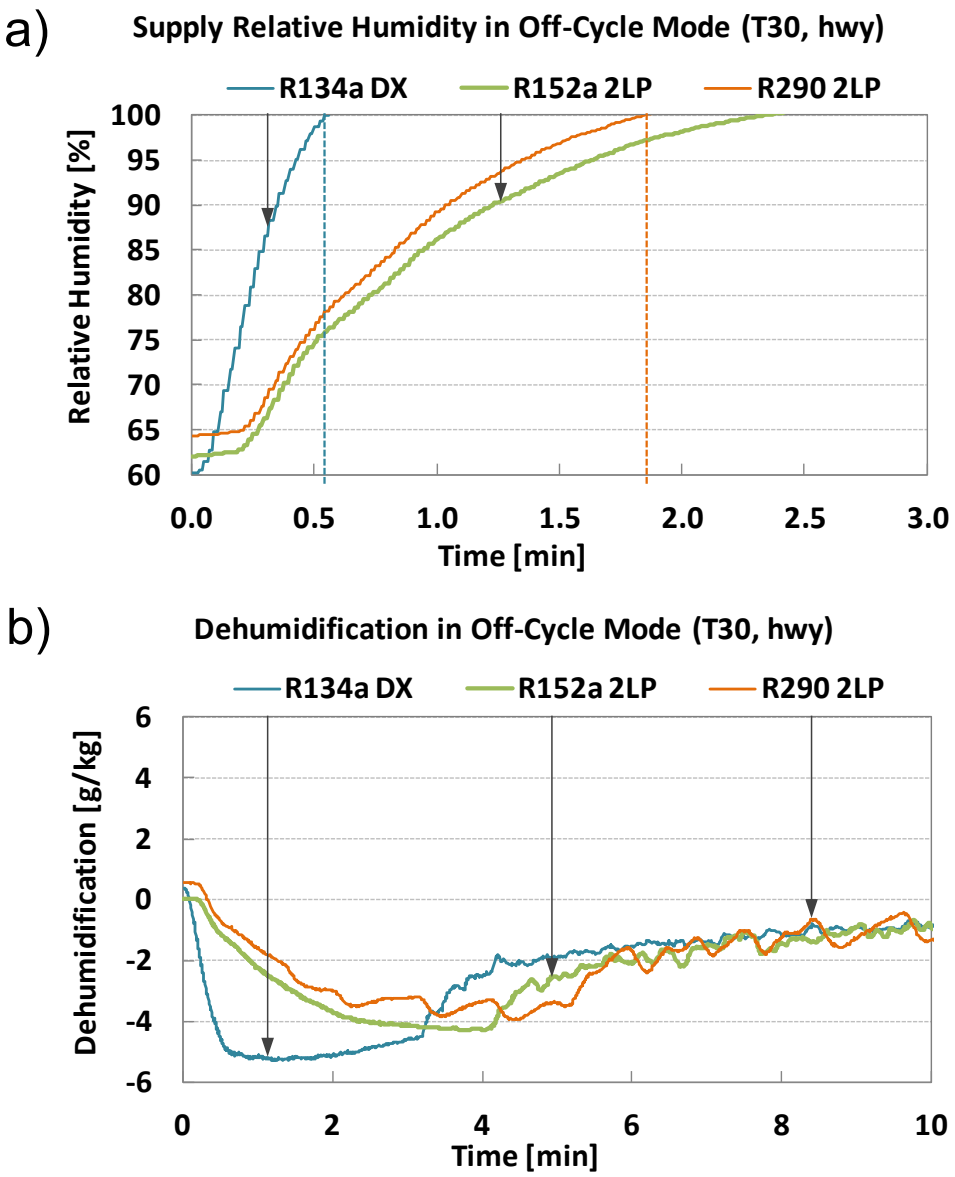

Figure 9.7: Secondary Loop Off-cycle Relative Humidity Profiles

9.2 Ice Storage Thermal Storage Performance

Advanced thermal storage options, such as phase change materials (PCMs), can be used to extend passenger comfort, as well as partially prevent excessive humidification of the cabin air during off-cycle periods. Depending on charging and releasing strategies, phase change materials might also assist the

vapor compression cycle during cabin pull-down, essentially reducing time to comfort. One of the least expensive and widely available phase change materials, operating within the acceptable temperature range, is water, H_2O. While water in frozen form can assist the air-conditioning system during the cooling period in the summer, it may also assist as a low temperature reference point for automotive heat pump systems in the winter to increase cycle efficiency when outdoor temperatures are well below 0°C. In the present research, ice storage was used for cooling purposes as part of a secondary loop automotive air-conditioning system. A custom ice storage box, introduced in Chapter 3.3, was built and integrated into the coolant loop. In the present research it was assumed that the ice storage box would be used in an electric vehicle, which allows the charging of ice at reduced electricity rates during the night. The ice would subsequently be used during the day to decrease A/C power consumption and reduce the effect of air-conditioning on the range of electric vehicles. Several options of how to charge the ice box exist. In an actual vehicle, ice could be produced by a dedicated facility outside of the vehicle, or while the ice storage box is installed in the vehicle. In the present research the ice was produced by the R290 2LP system, while the storage box was installed in the secondary loop.

Studies on driving patterns show that an average commute in the USA lasts about 25 minutes, while 80% of commutes fall within 34 minutes of travel time [120]. In European countries this might reduce significantly. In France, an average commute lasts less than 15 minutes, while about 95% of commutes fall within a 30 minute time frame [121]. Since a usual pull-down from soaked cabin

condition to comfort temperature lasts about 15 minutes, even at highway speed, a large part of the commute will be spent at an uncomfortably high cabin temperature. The ice storage box was built with experimental pull-down results from previous R134a DX pull-down tests in mind. The energy consumption of the A/C system during the first 20 minutes of a pull-down was measured to be between 4,500 and 5,000 kJ. The mass of ice in the ice storage box was chosen based on the assumption that the ice storage box might be able to either cool the cabin without the vapor compression cycle (VCC), or at least help increase thermal comfort and reduce VCC power consumption significantly during pull-down. Consequently, a mass of 15 kg of ice was chosen, since this covered the energy needed for cooling during a 20 to 25 minute commute, as seen in Figure 9.8.

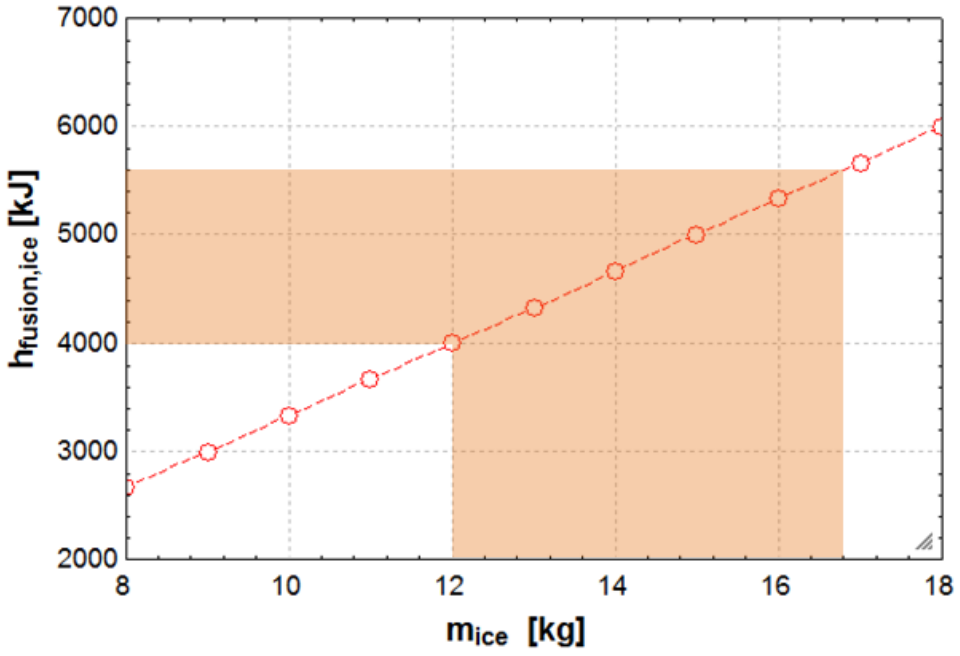

Figure 9.8: Enthalpy of Fusion Based on Mass of Ice

While adding such a large mass to a vehicle will undoubtedly increase vehicle fuel consumption, the overall impact on fuel consumption might not be so clear cut when taking fuel consumption due to A/C power consumption into account. Reynolds [122] showed that the change in fuel consumption per 100kg for internal combustion engine vehicles (ICEVs) is about 0.7 l/100km, while it is 0.4 l/100km for hybrid electric vehicles (HEVs). For the 15 kg ice storage box, this results in an increase in fuel consumption of roughly 0.1 l/100km for ICEVs and 0.06 l/100km for HEVs. For a ICEV which could drive 15 km per liter of fuel, this would result in a reduction of 0.22 km/l. At the same time, Clodic [121] and Johnson [123] determined that an A/C system typically uses 2,000 W to 3,000 W during steady-state cooling operation (peak power can be double). Farrington [124] shows that each vehicle experiences a fuel consumption penalty of roughly 1 less mile per gallon per 400 W auxiliary load. For 2,400 W A/C load, this results in a 6 mpg fuel consumption penalty (2.55 km/l). If the ice storage box can cover only a third of the A/C load and gets used roughly a third of the year, it will have more than made up for the additional fuel consumption due to its mass, not speaking of the benefit of enhanced passenger comfort.

9.2.1 Ice Storage Charging Performance

Figure 9.9 details the performance of the vapor compression system when charging the ice storage box. To form ice, the cooler of the secondary loop was bypassed and the vapor compression cycle cooled part of the secondary loop to sub zero temperatures. The water-glycol mixture was routed through the ice

storage heat exchanger charge the ice storage box. Figure 9.9 a) shows charging time with respect to initial average temperature in the ice storage box. Six thermocouples were placed in the storage box to evaluate average temperature during the charging and the cooling processes. It can be observed that charging time for the ice storage box was about 60 minutes if the initial average temperature was above 10°C. Sensibly cooling the ice took a small portion of the overall time, so that charging time did not increase significantly at higher initial temperatures. At initial temperatures close to 0°C, the storage box may still hold ice, while the mass fraction of liquid water to frozen ice cannot be determined with certainty. Thus any correlation of charging time over initial temperature must be very weak at low initial temperatures. Figure 9.9 b) shows energy used for charging the ice storage box with respect to initial average storage box temperature. It was observed that about 1,500 Wh were needed to freeze the 15 L of water and subcool the ice to -6°C average storage box temperature. Transient performance factor, shown in Figure 9.9 c) did not change significantly with initial average temperature. On average, ice charging TPF was between 0.55 and 0.7. Ice charging TPF and charging time may be improved by optimizing the ice storage heat exchanger and designing the VCC for the conditions which are prevalent during the charging process.

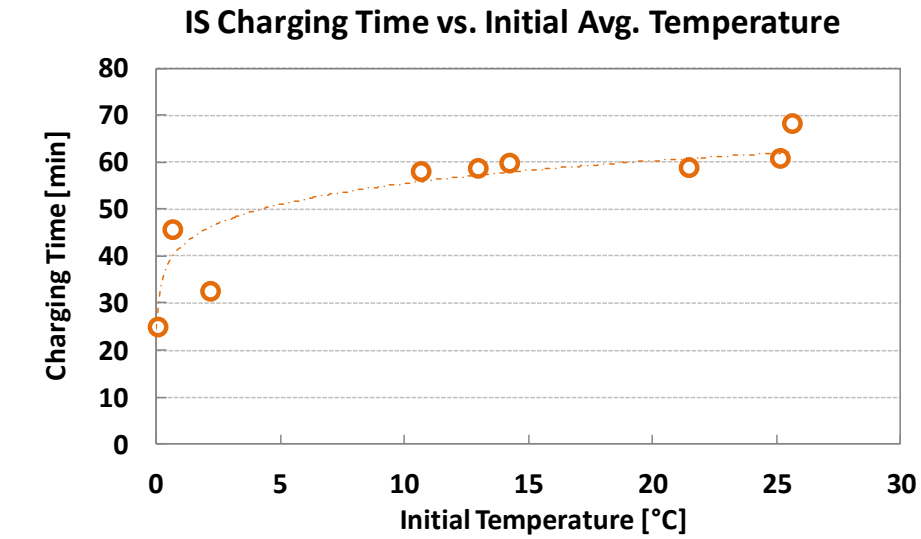

b)

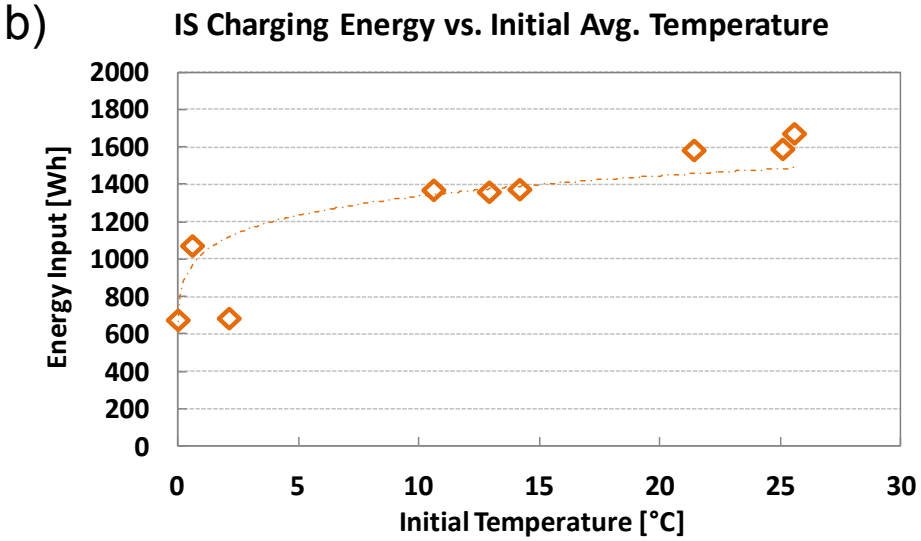

c)

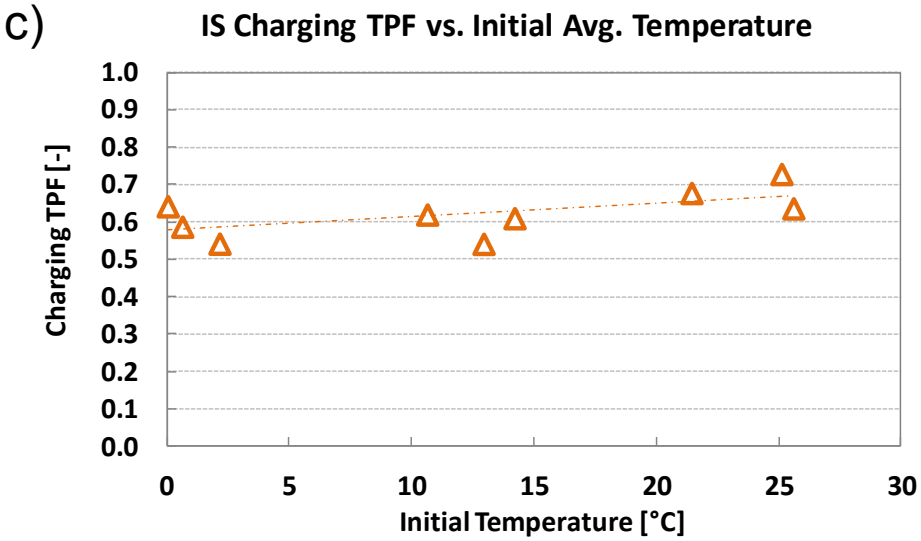

Figure 9.9: Ice Storage Charging Performance

9.2.2 Ice Storage Pull-down Performance

Chapter 9.2.2 9.2.2provides an example of using ice storage during cabin pull-down to assist the secondary loop system. In this operation mode, the water-glycol mixture is cooled by the VCC in the intermediate HX, subsequently routed through the ice storage box to be cooled down further, and finally cools down the cabin supply air at the cooler.

Figure 9.10 through Figure 9.12 show a performance comparison of a cabin pull-down test with the R290 2LP system, labeled 2LP, and a pull-down test assisted by the ice storage box, labeled 2LP+IS. The test detailed in this chapter is a pull-down test at highway driving condition and ambient conditions of 30°C/50% relative humidity. At the beginning of the test, the cabin was soaked to 42°C, which is indicated by the label (S).

Figure 9.10 shows the cabin and supply temperature profiles for the pull-down comparison between 2LP and 2LP+IS system operation. It was observed that ice storage has the greatest effect during the first minutes of the pull-down test. Right from the start, the supply air temperature of the 2LP+IS system was significantly lower compared to the 2LP system supply air temperature. After about 8 minutes, the supply air temperatures of both systems approached a similar value. This is reflected in the cabin temperature, which was decreased by about 1.5 K in the initial minute and remained 2 K below 2LP cabin temperature throughout the remainder of the test. As a result, more than 2 minutes could be shaved off time to comfort by using the ice storage system.

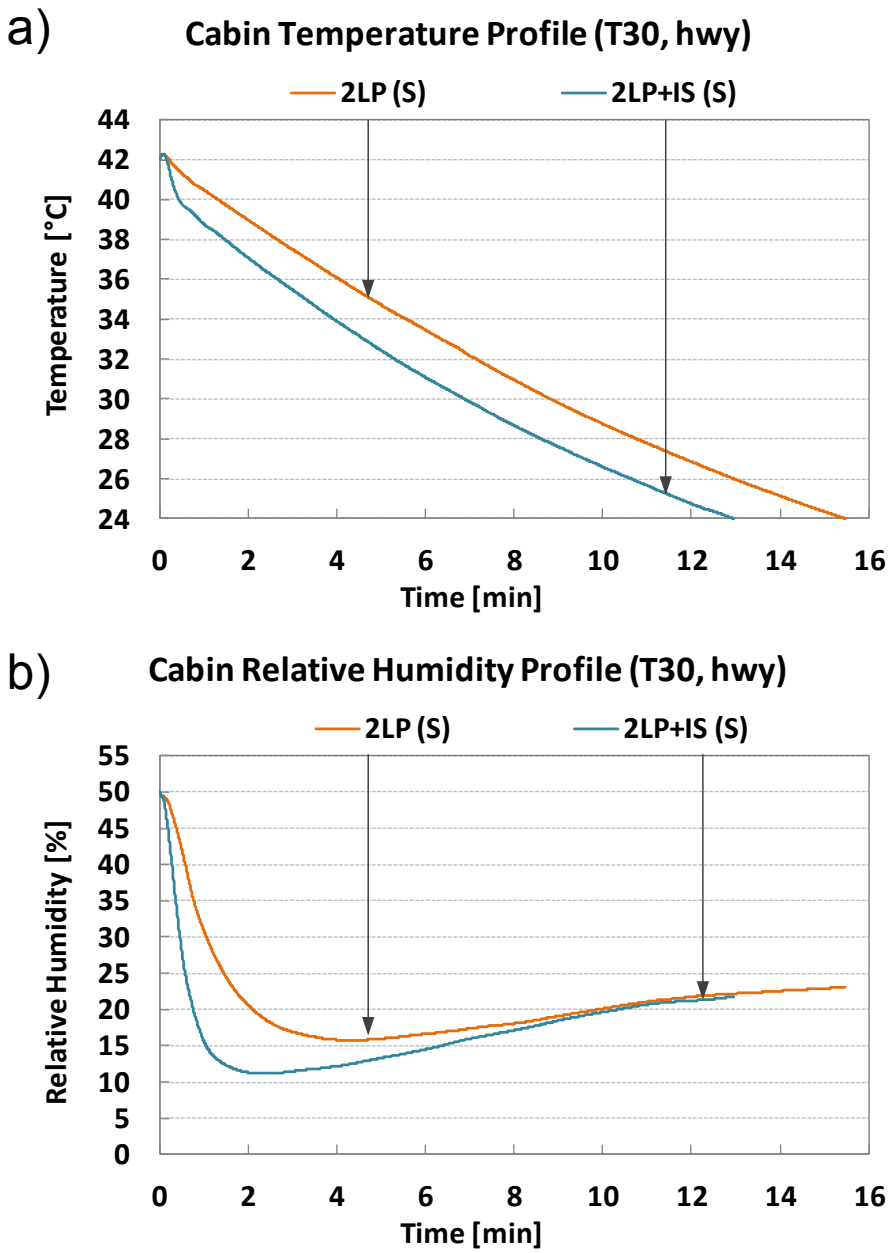

Figure 9.10: Ice Storage Pull-down Cabin Air Profiles

Figure 9.11 shows a comparison of transient profiles of cooling capacity and power consumption during a pull-down test. For the 2LP system, air-side cooling capacity is shown in Figure 9.11 a), while for the 2LP+IS system total air-side cooling capacity, as well as ice storage heat exchanger cooling capacity are

shown. The trends for cooling capacity support the conclusions drawn from the supply air and cabin air temperature profiles. In the initial minutes, the ice storage heat exchanger added additional cooling capacity to the total capacity available on the air-side. However, after about 4 minutes the cooling capacities for 2LP and 2LP+IS became identical and 2LP+IS capacity continued to decrease below the cooling capacity of the 2LP only system. On one hand this was due to a faster decreasing temperature difference for the 2LP+IS system. On the other hand, it was also due to the evaporation temperature reaching low enough values, resulting in the ice storage system hindering a further rapid pull-down (due to the water/ice mixture remaining at 0°C). This was observed at an advanced stage after 10 minutes, when the value for ice storage cooling capacity becomes negative, indicating that the ice storage box was charged by the 2LP cycle, instead of assisting in cooling cabin supply air. Figure 9.11 b) shows a comparison of power consumption profiles for both 2LP and 2LP+IS. While power consumption was highest for the 2LP only system during the initial minutes of the test, when the compressor and the pump were started, power consumption of the 2LP+IS system was lowest during the start-up phase. After about 4 minutes, the trends of power consumption of both systems were the same, with the power consumption of the 2LP+IS system being slightly reduced by about 100 W. Overall, the ice storage system allowed for energy saving during cabin pull-down when assisting a vapor compression cycle, but energy savings did not add up to a significant amount.

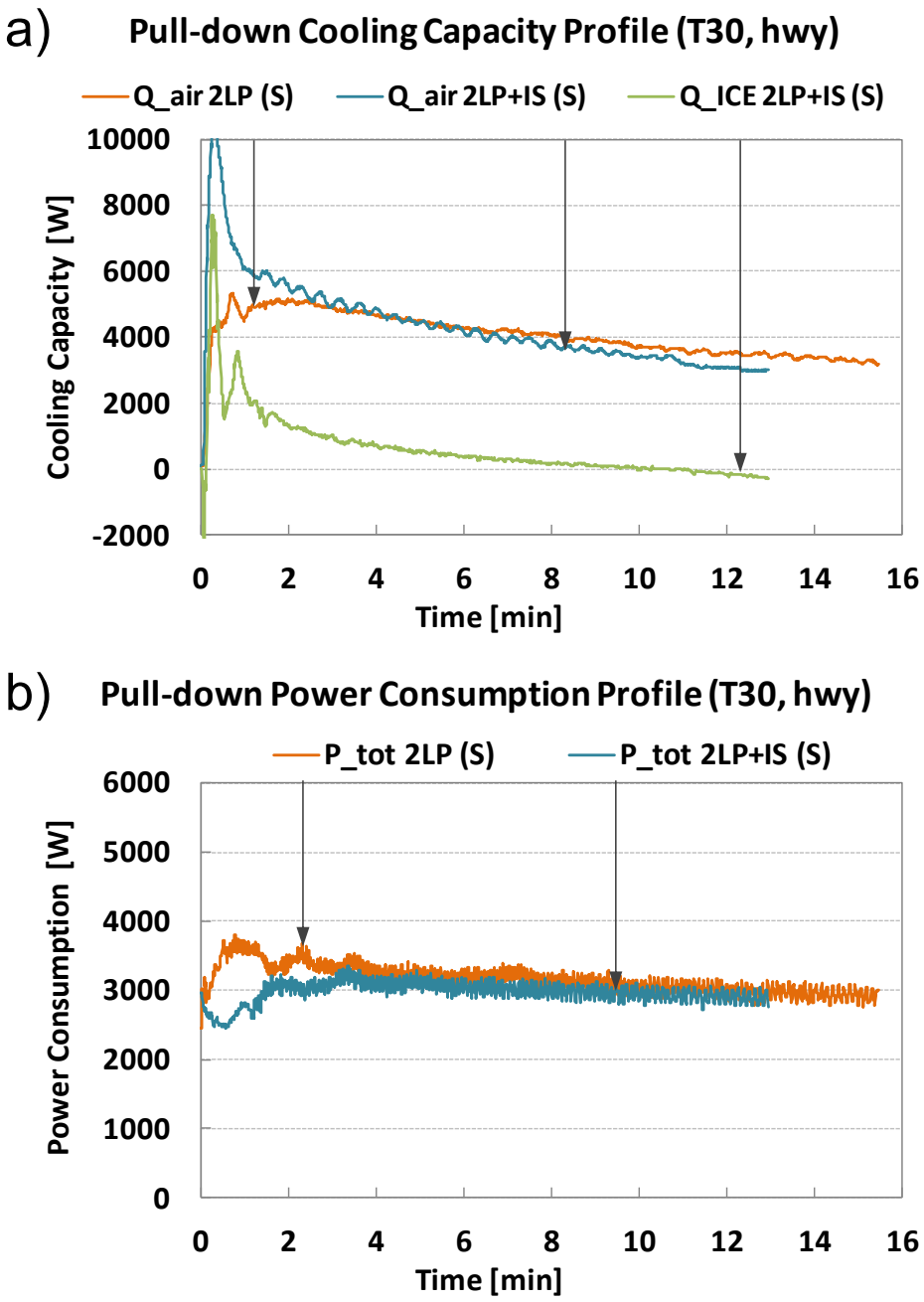

Figure 9.11: Ice Storage Pull-down Transient Performance Profiles

Figure 9.12 shows the accumulated performance results of the 2LP+IS system with respect to the performance of the 2LP system. It can be observed that time to comfort was decreased by about 16%. Consequently, energy

available to cool cabin supply air was reduced by about 10%, due to the reduced testing time. The 2LP+IS system was able to save about 21% of power consumption with respect to the power consumption of the 2LP system. The overall TPF increased by 15%.

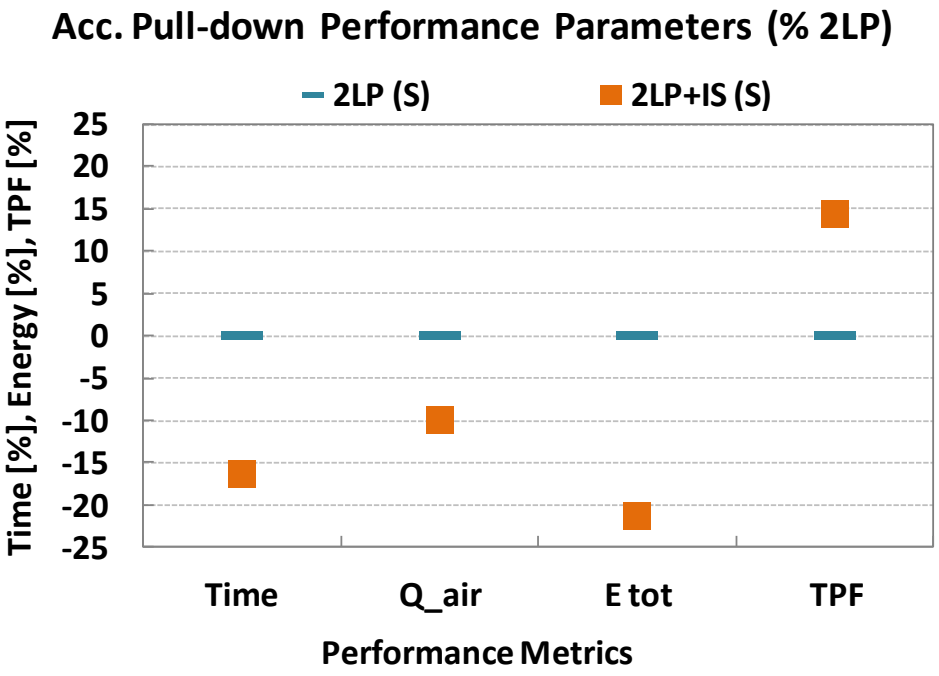

Figure 9.12: Ice Storage Pull-down Accumulated Performance Results

9.2.3 Ice Storage Off-cycle Cabin Warm-up Performance

Chapter 9.2.3 9.2.3discusses thermal storage performance of the ice storage system during a cabin warm-up test. Temperature, as well as relative humidity results for the R290 2LP+IS system are compared to R290 2LP results and R134a DX results. The test was performed at highway driving speed and ambient conditions of 30°C/50% relative humidity. The cabin was soaked to 42°C

at the start of the pull-down, which preceded the cabin warm-up portion of the test.

Figure 9.13 shows cabin, as well as cabin supply temperature trends during the cabin warm-up test. Throughout the pull-down procedure enough ice remained frozen in the ice storage box to provide cooling capacity to keep the cabin temperature at comfort set point or slightly lower for an extended amount of time. Cabin temperature increased to 28°C and 31.5°C after 15 minutes for R290 2LP and R134a 2LP, respectively. At the same time, R290 2LP+IS cabin temperature remained below 23.5°C at 15 minutes into the test. This was reflected in the cabin supply temperature profile, which did not increase above 15°C 15 minutes into the test, remaining roughly 10 K and 15 K below R290 2LP and R134 DX supply temperature, respectively.

The differences in thermal storage performance are illustrated by Figure 9.14, which shows a comparison of accumulated sensible capacity over the duration of a cabin warm-up test. Energy available for cooling was the same for the R134a DX, the R290 2LP, and the R290 2LP+IS system within the first 30 seconds. After the first half minute the capacity of the direct expansion system started to decrease significantly compared to secondary loop system capacity, resulting in a decrease of slope of the R134a DX cooling energy, as shown in Figure 9.14. For the first three minutes the ice storage system (2LP+IS) showed no advantage in comparison to the regular secondary loop system. However, after three minutes the secondary loop system cooling capacity decreased, while the cooling capacity of the ice storage system stayed constant (resulting in a

steady increase of cooling energy with time). Consequently, the ice storage system had a significant advantage over the unmodified secondary loop systems in terms of thermal comfort for extended off-cycle periods.

Figure 9.13 shows supply relative humidity trends, as well as dehumidification during off-cycle cabin warm-up.

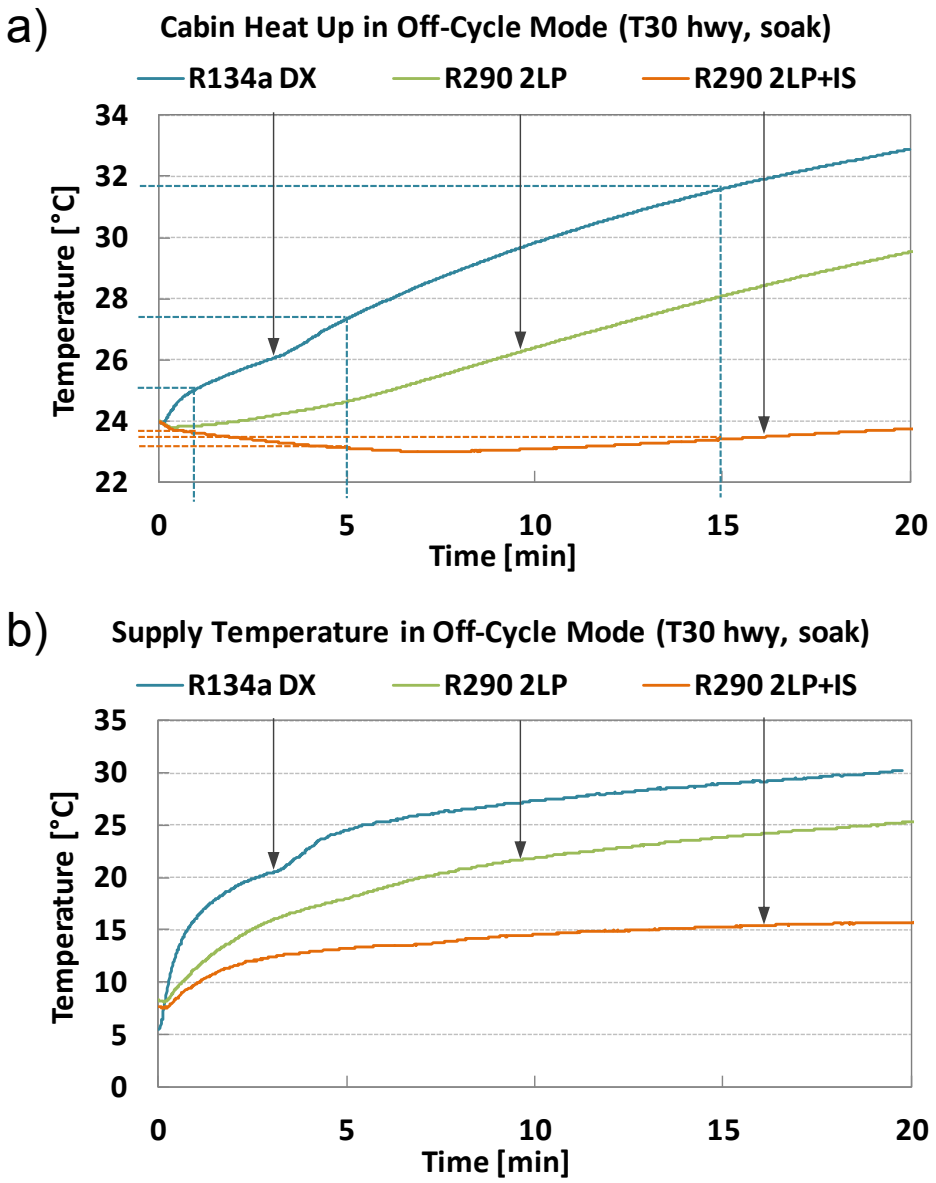

Figure 9.13: Ice Storage Off-cycle Cabin Warm-up Temperature Profiles

It was observed that the ice storage system retained enough latent capacity to reduce re-evaporation at the cooler to a degree which allowed the supply air to stay below 95% relative humidity for an extended period of time. This was supported by the dehumidification profile, which showed a severe decrease in humidification of cabin supply air during the first 7 minutes of the cabin warm-up test, compared to R290 2LP and R134a DX. The secondary loop, with the assistance of the ice storage box, was able to preserve passenger thermal comfort, as well as prevent excessive cabin air humidification for a period longer than 20 minutes after compressor shut down.

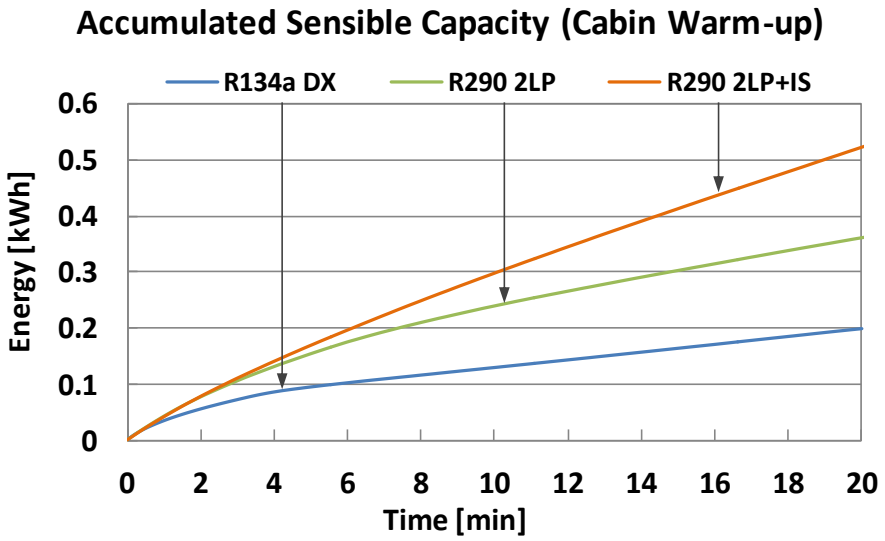

Figure 9.14: Cabin Warm-up Accumulated Sensible Capacity Comparison

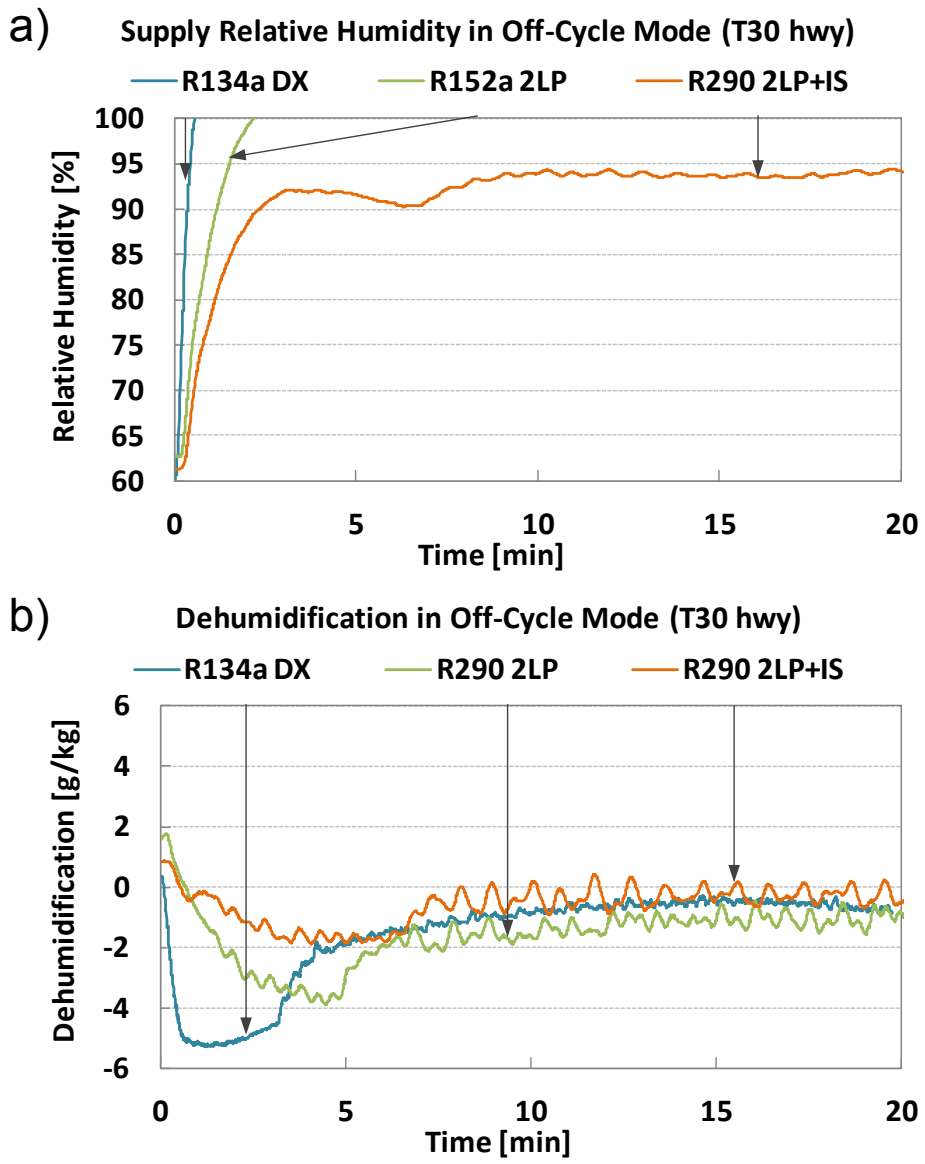

Figure 9.15: Ice Storage Off-cycle Cabin Warm-up Humidity Profiles

9.3 Summary: Thermal Storage in Secondary Loop Systems

- Several test procedures were designed to test the effect of thermal storage with respect to extension of thermal comfort and transient performance improvement during off-cycle operation.

- During Start/Stop operation, a regular direct expansion system experiences large fluctuations in cabin supply temperature and relative humidity. Fluctuations in humidity are mostly due to re-evaporation of condensate from the evaporator (DX) or cooler (2LP) surface, once the compressor is turned off. The thermal mass of the secondary loop decreases fluctuations in supply temperature and humidity and therefore improves stability of supply and cabin conditions, which can be related to an increase in thermal comfort.

- During Start/Stop operation, the energy available for cooling the supply air was reduced due to the larger thermal mass of the secondary loop. However, cooling energy was reduced by less than 10% in comparison to R134a DX, while R290 2LP TPF was equal to R134a TPF.

- When the Start/Stop drive cycle was modified by increasing off-cycle periods by three times, the secondary loop system outperformed the direct expansion system in terms of dehumidification, as well as efficiency. With increasing idling (or off-cycle) periods, the direct expansion system was prone to re-humidifying the cabin while the compressor was turned off. The secondary loop system prevented excessive cabin humidification and kept cabin temperature stable during off-cycle periods. The energy available to cool the cabin supply air was the same compared to the R134a direct expansion system. Therefore, R290 2LP TPF increased to 9% above R134a DX TPF. The sensible energy available was the same compared to the R134a direct expansion system, while the latent energy was smaller, due to the increased dehumidification needed by the direct expansion system. When switching from a car without start/stop to a car with start/stop automatic operation, less cooling energy will be available over the course of the drive cycle. Due to thermal storage, secondary loop systems face less of a penalty compared to direct expansion systems.

- If the compressor is turned off after pull down to comfort temperature, the secondary loop reduces the heating up of the cabin. During an extended time of 20 minutes, secondary loop cabin temperature was consistently 2.5 to 3 K below direct expansion cabin temperature during cabin warm-up. At the same time, the secondary loop could not prevent excessive humidification of the cabin after the compressor was turned off, but it was able to delay it by about 1.5 minutes longer than the direct expansion system. Taking cabin humidification into consideration, the secondary loop can be useful for short off-cycle periods of a few minutes.

- An ice storage box with an ice to water-glycol heat exchanger was designed and built. 15 L of water were used in the ice storage box, which resulted in a charging time of about one hour and a charging energy of about 1.5 kWh. Since the regular vapor compression system was used for charging, the unusually low temperature conditions resulted in an average TPF of 0.65 during charging.

- Ice storage assisted in pulling down the cabin to comfort temperature by decreasing power consumption and decreasing time to comfort. However, ice storage was only advantageous during the first minutes of the pull-down test. With increasing time the ice storage system becomes less profitable, as evaporating temperature decreases and the ice storage system inhibits higher cooling capacity. TPF was increased by 15%. The biggest advantage of the ice storage system comes to bear during off-cycle cabin warm-up, where the ice storage system could keep the cabin at comfort temperature for periods of 20 minutes, while preventing excessive cabin humidification.

10 Experimental Results - A/C Controls and Cabin Preconditioning

Chapter 10 provides experimental results of research done in the area of air-conditioning systems control and cabin preconditioning in combination with secondary loop systems and ice storage. In previous chapters, pull-down tests were used to compare time to comfort and cooling energy available on the air-side. The present chapter focuses on A/C energy consumption during tests of 60 minutes, including the initial pull-down. The A/C control tests strive to determine energy savings when different control strategies for the compressor and coolant pump are used. Cabin preconditioning tests focus on energy savings which may be achieved when the cabin is prevented from soaking by pre-conditioning cabin air to either ambient temperature or comfort temperature. While the results of A/C control experiments and cabin preconditioning are universal to all types of cars, they have their biggest impact in electric vehicles (EVs). On the one hand, cabin preconditioning may be more conveniently realized in EVs, while some of the discussed compressor control strategies are applicable only to electric compressors. On the other hand, results for cabin preconditioning and compressor control strategies explicitly focus on reducing A/C power consumption during vehicle operation and therefore have an immediate effect on driving range of EVs. It will be discussed how cabin preconditioning and thermal storage (here ice storage) can work together with alternative control strategies to reduce overall A/C power consumption, including heater (or PTC element) power consumption.

Reducing A/C energy consumption is especially important for electric vehicles, as shown by Farrington and Rugh [124]. While an internal combustion vehicle ICEV) may have a fuel penalty of 5 mpg for 2,000 W auxiliary load -a very conservative estimate for A/C systems-, fuel consumption of an advanced electric hybrid vehicle could see a penalty of as much as 34 mpg and range could reduce by 27%. This analysis did not include the PTC heater or other heating device for dehumidifying and series reheating the air. As Clodic [121] showed, a PTC heater alone can reduce EV range to below 90% at 35°C ambient condition. At high ambient conditions of 45°C driving range could reduce to roughly 75%. Umezu and Noyama [125] gave some information on the air-conditioning system and controls for the electric vehicle Mitsubishi i-MiEV in 2010. The i-MiEV uses a dedicated coolant cycle with a 5.0 kW PTC heating element to reheat the air after the evaporator. With A/C and heater on, A/C power consumption may increase by 30% to 40%, while cruising range may decrease from 160 km to 90 km (A/C and heater on, 35°C ambient temperature). The next important steps for Mitsubishi at the time were to look into cabin preconditioning and improving PTC control to reduce PTC energy usage.

While the above paragraph clearly stated the importance of reducing energy consumption for EVs, the question remains how to do so. This chapter introduces two possibilities: alternative A/C compressor and heater controls, as well as cabin preconditioning. Both solutions have been evaluated under different circumstances by other researchers before. Forrest and Bhatti [126] looked into control of the recirculation ratio (or mixing ratio with fresh air), as well as series

reheat reduction. Instead of cycling the compressor to prevent frost at the evaporator, an externally controlled variable displacement compressor was used to decrease capacity when it was not needed. As a result, cabin relative humidity increased from about 30% steady-state value at comfort condition to 45% to 50%. It was estimated that the reheat reduction potential could reduce 28% of cooling capacity, which would not have to be delivered by the compressor. Experimental tests with the externally controlled compressor and series reheat reduction found a 60% (city) and 52% (highway) A/C fuel consumption reduction. However, the authors stated that due to the complexity of the test vehicles, tests were difficult to reproduce and there were high uncertainties due to an abundance in variables for vehicle conditioning. Furthermore, the study was focused on the reduction of ICEV fuel consumption, which does not translate well into energy savings an range preservation for EVs. Therefore, the current research focuses on a comprehensive investigation of energy saving potential due to alternative compressor and heater controls in a laboratory environment with high accuracy measurement capabilities.

Cabin preconditioning was investigated by Roy et al. in 2003 and 2005. In a simulation study [127] and an experimental study [128] the influence of cabin preconditioning strategies on the soaking profile and cabin temperature profile during cool down was evaluated. The study focused on comparing different pre-conditioning strategies, such as forced ventilation, vacuum panels, or special glazing for windows. It was found that combinations of various technologies could reduce soak and achieve energy savings of about 15% to 20%. The study did not

elaborate on how the energy savings were determined. Instead of focusing on temperature profiles and technologies to achieve preconditioning, the current research focuses on energy savings achievable during driving, given a certain preconditioning. Experimental results are focused on a combination of cabin preconditioning and alternative A/C controls to gain significant reductions in compressor and heater energy consumption for EVs and providing insight into the circumstances which make cabin preconditioning beneficial.

10.1 A/C Control Performance and Benefits

The A/C controls discussed in this chapter focus on the reduction of compressor power consumption and the reduction of re-heating during extended driving. The different control strategies are based on the assumption that a fixed displacement compressor, such as the compressor used in this research, can either be cycled, or can be speed-controlled externally. The latter assumption is true only for compressors which are not belt-driven by an internal combustion engine, and therefore is geared towards hybrid electric vehicles and full electric vehicles.

For each control test the cabin is initially pulled down to comfort temperature and the different control strategies evolve around keeping cabin temperature at comfort set point during an extended amount of time. Traditionally, this was done by leaving the compressor turned on, while the air-side evaporator outlet temperature decreased below the temperature needed to preserve thermal

comfort. Consequently, air leaving the evaporator was reheated. The compressor is cycled off only to prevent frost at the evaporator. Hence, frost cycling (F cyc) tests serve as a reference point for the alternative control strategies discussed in this chapter, namely the relative humidity cycling (RH cyc) and relative humidity continuous control (RH ctn) tests. A more detailed introduction to the test procedures is given in Appendix E.

Figure 10.1 shows a comparison of power consumption, cabin temperature, and cabin supply relative humidity for the R290 2LP system, utilizing the three above mentioned control strategies. Tests were conducted with the R290 2LP system at ambient conditions of 30°C ambient temperature and 50% relative humidity at highway driving conditions. Power consumption profiles for F cyc, RH cyc, and RH ctn control are shown in Figure 10.1 a). It was observed that F cyc had the overall highest power consumption. Once cabin temperature reached the comfort set point, the compressor remained running at full speed and soon thereafter heater power had to be used to keep the cabin at thermal comfort. Several minutes thereafter, the compressor started to cycle to prevent frost at the evaporator. The cycles occurred in intervals of 3-4 minutes, with the compressor on time being significantly longer than the compressor off times. RH cyc power consumption was significantly reduced compared to F cyc power consumption. The compressor cycled faster, since it controlled cabin/supply humidity, rather than preventing frost. Compressor off times were longer than compressor on times. Additionally, heater power consumption was significantly reduced compared to F cyc control. RH ctn control had the overall lowest power

consumption. Once thermal comfort temperature was achieved, the compressor speed, as well as the coolant pump speed were controlled by a PID controller. The compressor and the pump kept running continuously, though the PID controller reduced compressor speed significantly. Figure 10.1 b) shows the cabin temperature for the three control tests. It was observed that all three strategies were able to keep cabin temperature within a very narrow range (< 0.3 K) of comfort set point. F cyc supply relative humidity, shown in Figure 10.1 c), averaged at about 50% after thermal comfort was achieved. RH cyc, as well as RH ctn supply relative humidties were measured to be about 80% on average. At the same time, cabin relative humidty averaged at about 50%. While RH ctn supply relative humidity was more stable, compressor cycling during the RH cyc test introduced large fluctuations (< ±20%).

Figure 10.2 shows a comparison of accumulated performance results for three different control strategies. While Figure 10.2 a) compares results for R290 2LP only, Figure 10.2 b) compares accumulated performance results of the ice storage system. For 2LP only, A/C power consumption could be reduced about 40% and 60% for RH cyc and RH ctn control, respectively. This includes compressor, pump, and heater power (E in C+P+H). When including only compressor and coolant pump power (E in C+P), power consumption was reduced by about 30% and 55% for RH cyc and RH ctn control strategies, respectively. Due to reduced capacity delivered by the compressor and a reduced need for reheating, the energy available to cool the cabin supply air decreased by about 35%. This resulted in an overall increase in TPF of about 55%

for RH ctn, while RH cyc TPF decreased by about 50%. When RH cyc and RH ctn strategies using the ice storage system (2LP+IS) were compared with frost cycling using only the secondary loop system (2LP), power consumption was reduced significantly only for the RH cyc control strategy. Through the use of ice storage, power consumption during RH cyc control decreased to a similar level as power consumption druing RH ctn control (55%).

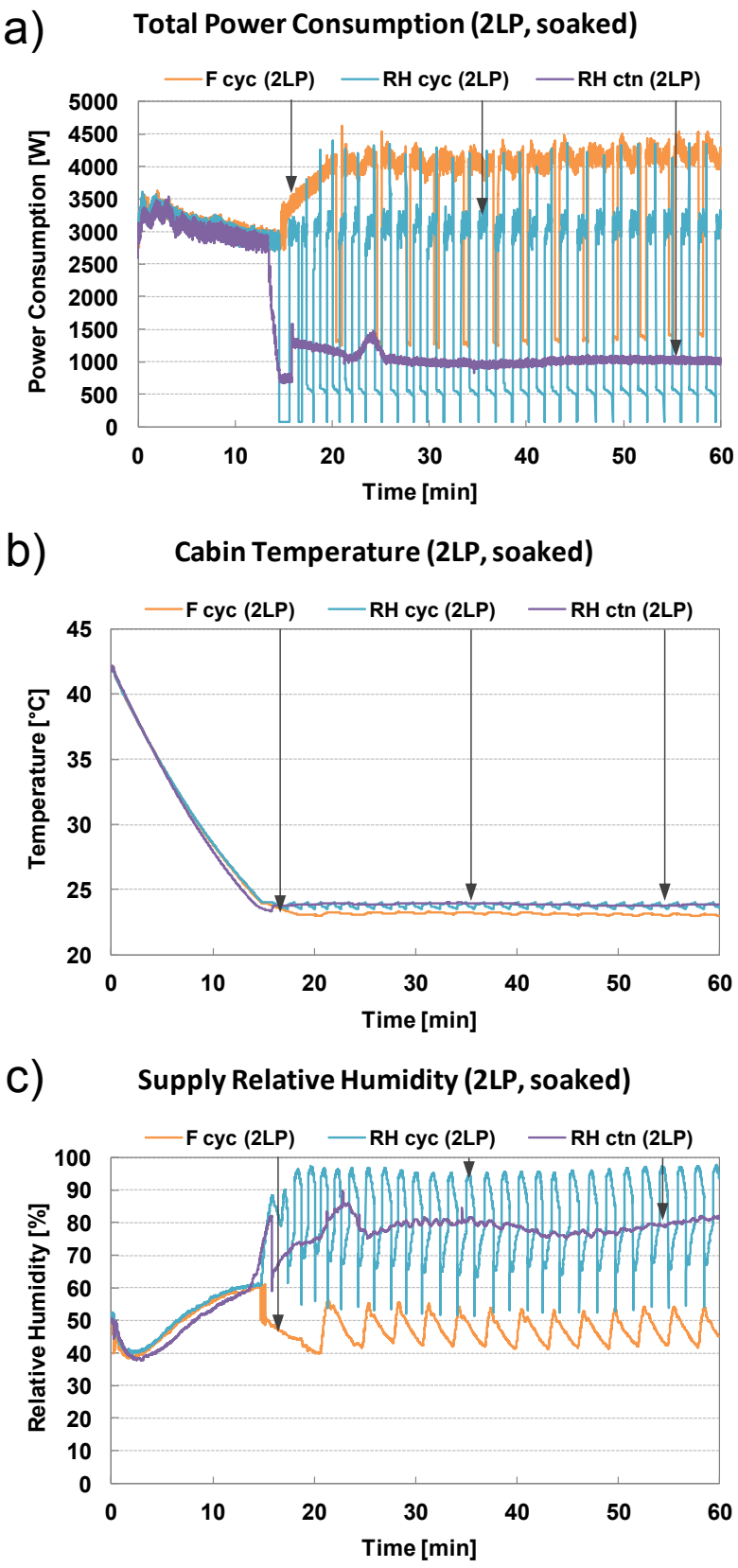

Figure 10.1: A/C Controls Power Consumption and Cabin Air Profiles Comparison

Power consumption of the RH ctn control strategy did not benefit from the ice storage system. At the same time, ice storage adds cooling capacity, which improves TPF for both, RH cyc and RH ctn control strategies. It can be concluded that RH ctn control strategy has the potential to reduce A/C energy consumption by as much as 60% at the given ambient and driving conditions. RH cyc control was able to reduce power consumption by about 40%. However, the increased start up currents for electric compressors when cycling were not taken into account, since the compressor used in the present research was a belt drive compressor. Therefore, results for compressor power consumption may vary for RH cyc operation in electric vehicles. Using thermal storage systems can benefit cyclic control, while it is of little benefit for the power consumption of a continuous, reduced speed compressor control. In the extreme case, there would be no need for a PTC element or other form of electrical reheating of the cabin supply air. This could be achieved by using the condenser heat from an indirectly cooled A/C condenser for reheating. This would be possible, since the condenser transferred -on average- 2.0 - 2.5 kW of heat during the time when re-heating was needed, based on experimental measurements. A theoretical evaluation of this possibility was performed, assuming a heater power consumption of zero (free heating) for the RH cyc and RH ctn cases. If using an indirectly cooled condenser, this modification would yield another 5% (RH cyc) and 7.5% (RH ctn) reduction of total energy consumption compared to the F cyc control baseline. This would add up to a 46% (RH cyc) and 64% (RH ctn) decrease in total energy

consumption. TPF would consequently increase to 26% (RH cyc) and 82% (RH ctn) above F cyc baseline TPF, as seen in Figure 10.3.

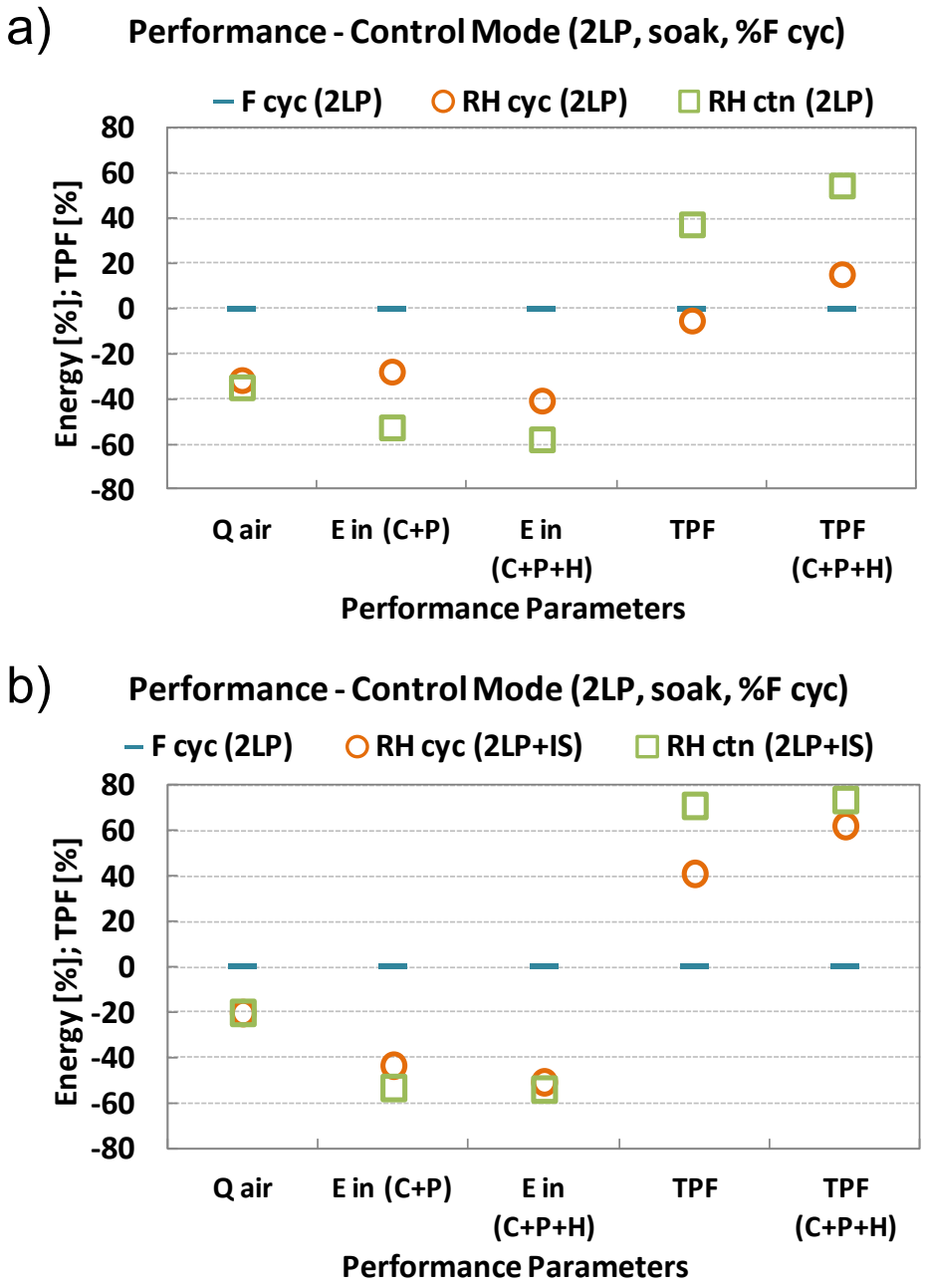

Figure 10.2: A/C Controls Accumulated Performance Results Comparison

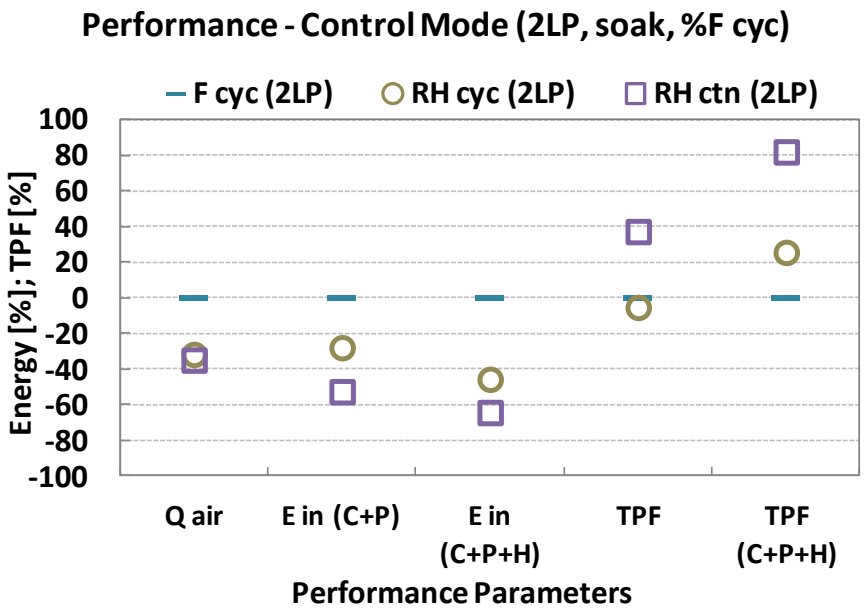

Figure 10.3: Theoretical Change in A/C Ctrl Accumulated Performance when Using an Indirectly Cooled Condenser for Supply Air Reheating

10.2 Cabin Preconditioning Performance and Benefits

Chapter 10.2 introduces a comparison of performance results for extended driving after pull-down when the passenger cabin was preconditioned to a certain temperature. Three initial cabin temperatures were compared: soaked condition (S) at 42°C, ambient condition (A) at 31°C, and comfort conditions (C) at 25°C. The initial cabin temperature was 1 K above ideal preconditioning temperature at ambient (A) and at comfort preconditioning (C). Cabin preconditioning can be achieved with a variety of techniques. Preconditioning close to ambient temperature may be achieved by simply parking in a garage, in some cases by forced convection, or by having an advanced glazing to reduce soak by reducing transmittance of the windows. Preconditioning close to comfort conditions may be achieved either by parking in

an air-conditioned or well ventilated parking garage, by intermittently running the vehicle air-conditioning system (when the EV is plugged in), or by using a charged thermal storage device while parking in the shade or in a garage.

A comparison of accumulated performance parameters for different cabin preconditioning settings is shown in Figure 10.4. The tests were performed at 30°C/50% ambient conditions, 950 W solar load, highway driving conditions, and a test time of 60 minutes. Figure 10.4 a) shows a comparison for Frost cycling control, while Figure 10.4 b) shows a comparison for RH cycling control. It was observed that cabin preconditioning did not decrease overall power consumption, when utilizing frost cycling control. While preconditioning decreased compressor power consumption by about 5% (E in C+P), it increased heater power consumption significantly, since the heater had to be employed much earlier in the test. This resulted in an overall increase of power consumption (E in C+P+H) of about 5% and 10% for ambient preconditioning and comfort preconditioning, respectively. This trends can be observed in Figure 10.5. It is assumed here that heating is not free, as it would be in the case of utilizing engine coolant from an internal combustion engine, which is at the same time the primary engine for the vehicle. The increase in heater energy over the course of a test resulted in a decrease of TPF of 4% for ambient preconditioning and 8% for comfort preconditioning.

However, when utilizing control strategies which reduce the need for reheating and allow the compressor to cycle or reduce its capacity, cabin preconditioning can achieve significant energy savings. As shown in Figure 10.4

b), compressor and pump power consumption could be reduced by as much as 30% for ambient preconditioning and 40% for comfort preconditioning. At the same time, overall power consumption, including heater power, was reduced by 25% - 30%. Overall TPF was similar to the unconditioned cabin, as the available energy for cooling was reduced by reducing compressor capacity and heater power.

Figure 10.5 shows transient profiles of system power consumption for cabin preconditioning scenarios while using frost cycling control in the R290 2LP system (no ice storage). The comparison of profiles explains the fact that cabin preconditioning does not help reduce power consumption when compressor and heater are used continuously, as is the case with frost cycling and reheating control. While initial compressor power decreases slightly when preconditioning the cabin to ambient and comfort temperature, the heater has to kick in earlier, since the cabin reaches thermal comfort condition faster.

The heater power necessary to reheat the supply air could reach up to 1.4 kW for comfort preconditioning. This resulted in a significant increase in overall power consumption during the initial 20 minutes of the test, until the compressor started to cycle to prevent frosting. At this point, thermal conditions were similar between tests and power consumption for the remainder of the cycle was alike.

Figure 10.6 a) shows a comparison of the cabin temperature profiles, as well as power consumption profiles, when only the charged ice storage box without the vapor compression cycle was used for air-conditioning. For a soaked

cabin, a solar load of 950 W and the load of one passenger, the ice storage box alone was unable to pull the cabin down to comfort set point.

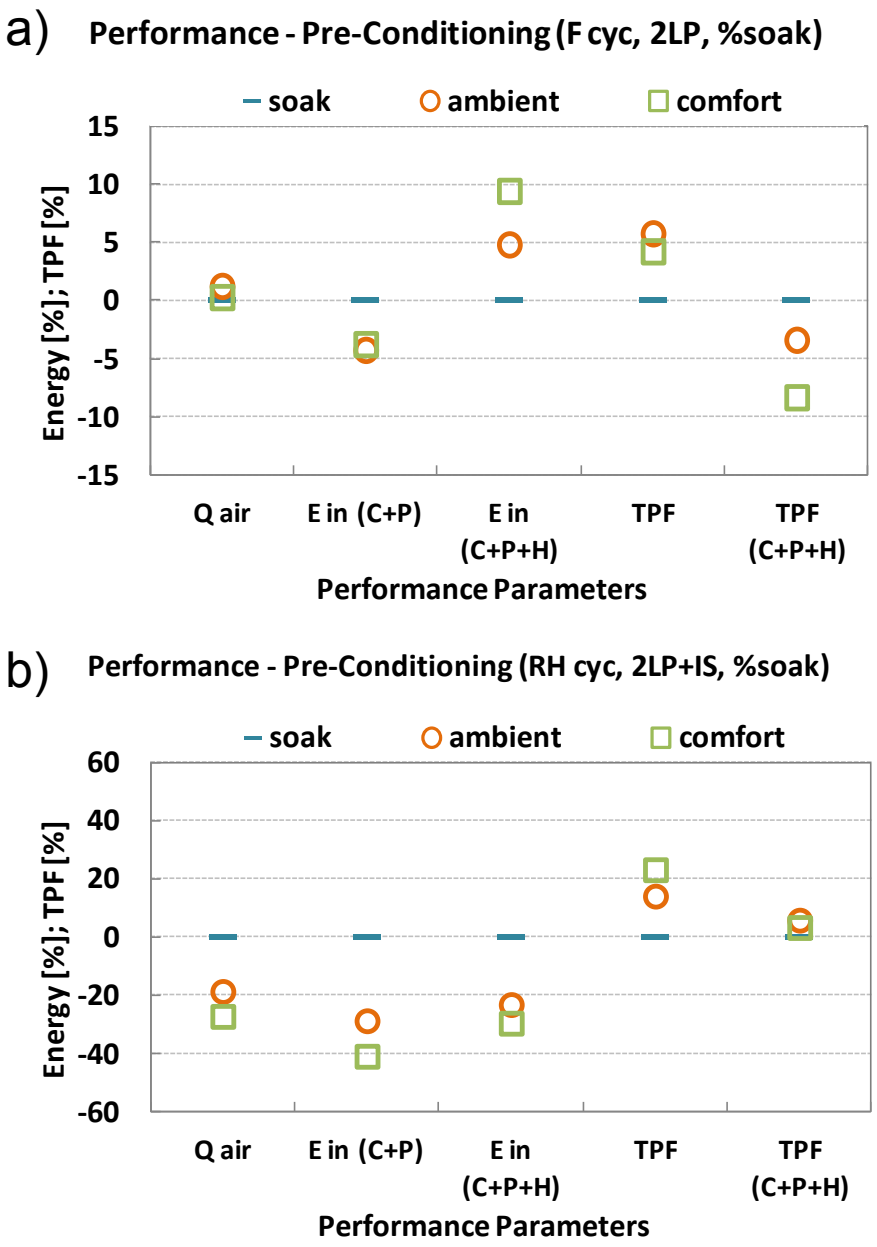

Figure 10.4: Preconditioning - Accumulated Performance Results Comparison

A similar result was observed when preconditioning the cabin close to ambient temperature. However, when preconditioning the cabin close to comfort temperature, the ice storage box was able to pull the cabin down to comfort set point and retain thermal comfort for an extended period (> 60 minutes).

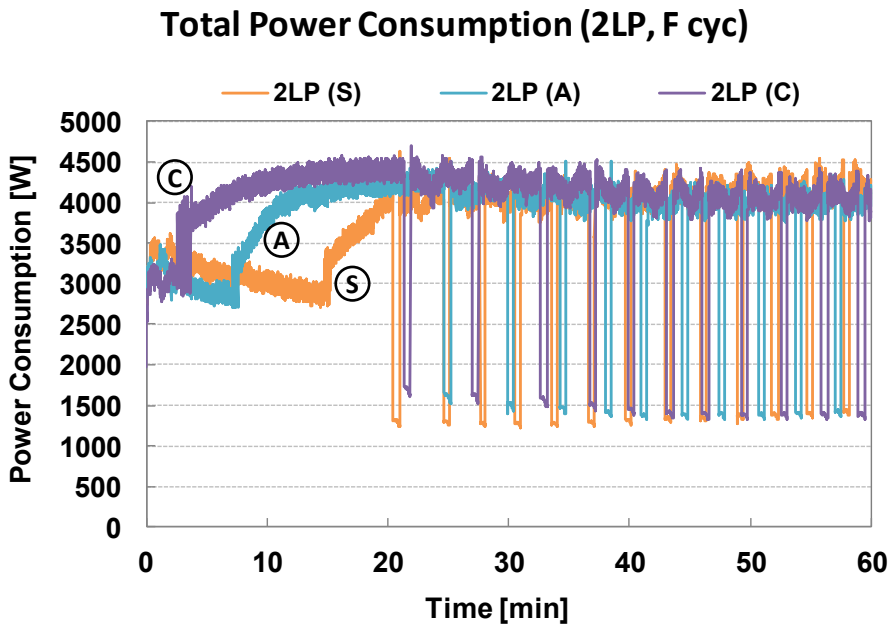

Figure 10.5: Preconditioning - Power Consumption Transient Profile Comparison

Figure 10.6 b) shows a comparison of power consumption profiles. The coolant pump was continuously on when the cabin was preconditioned to soaked and ambient temperature. When pre-conditioned to comfort temperature, cooling capacity was controlled by on/off control, as well as PID control during the on-times. It can be observed that the ice storage box was losing capacity towards the end of the test when PID control increased pump speed to retain thermal comfort in the passenger cabin.

This result has some interesting implications. First, there is no vapor compression system needed to keep the cabin at comfort temperature when the cabin is preconditioned. Second, although the ice storage box was not able to pull down the cabin from ambient preconditioning or higher initial starting temperatures, this is only a problem of heat exchanger optimization. The ice storage box provides enough energy for a cabin pull down in terms of fusion energy of the stored ice, but the heat transfer rate has to be increased by optimizing the ice storage heat exchanger for this application. Clodic [121] showed that the average commute in the US lasts about 25 minutes. A comparison of energy consumption relative to R290 2LP Frost cycle operation with soaked cabin preconditioning for a 25 minute commute is shown in Table 10.1. Approximately 15 minutes are spent on pull-down with the compressor permanently running, while the last 10 minutes are spent at comfort temperature with the compressor and heater controlling cabin temperature (and humidity in the RH cyc cases). As can be observed in Table 10.1, using alternative A/C controls (RH cyc) can reduce energy consumption by about 17%. Preconditioning the cabin at the same time to comfort condition results in combined energy savings of about 78% during the 25 minute commute. When using only ice storage and controlling cabin temperature by modulating coolant pump speed, energy savings of about 98% can be realized, which may preserve EV range to nearly the full extend. Essentially, nearly all of the A/C energy needed during a regular commute can be saved by preconditioning the cabin and

using latent storage without a VCC. The cabin relative humidity was fluctuating between 55% and 65%, which is at the high end of thermal comfort requirements.

Table 10.1: Comparison of Energy Consumption for a 25 Minute Commute Relative to 2LP F cyc (S)

2LP, F cyc (S)	2LP, RH cyc (S)	2LP, RH cyc (C)	IS (C)
0%	-16.8%	-77.7%	-97.6%

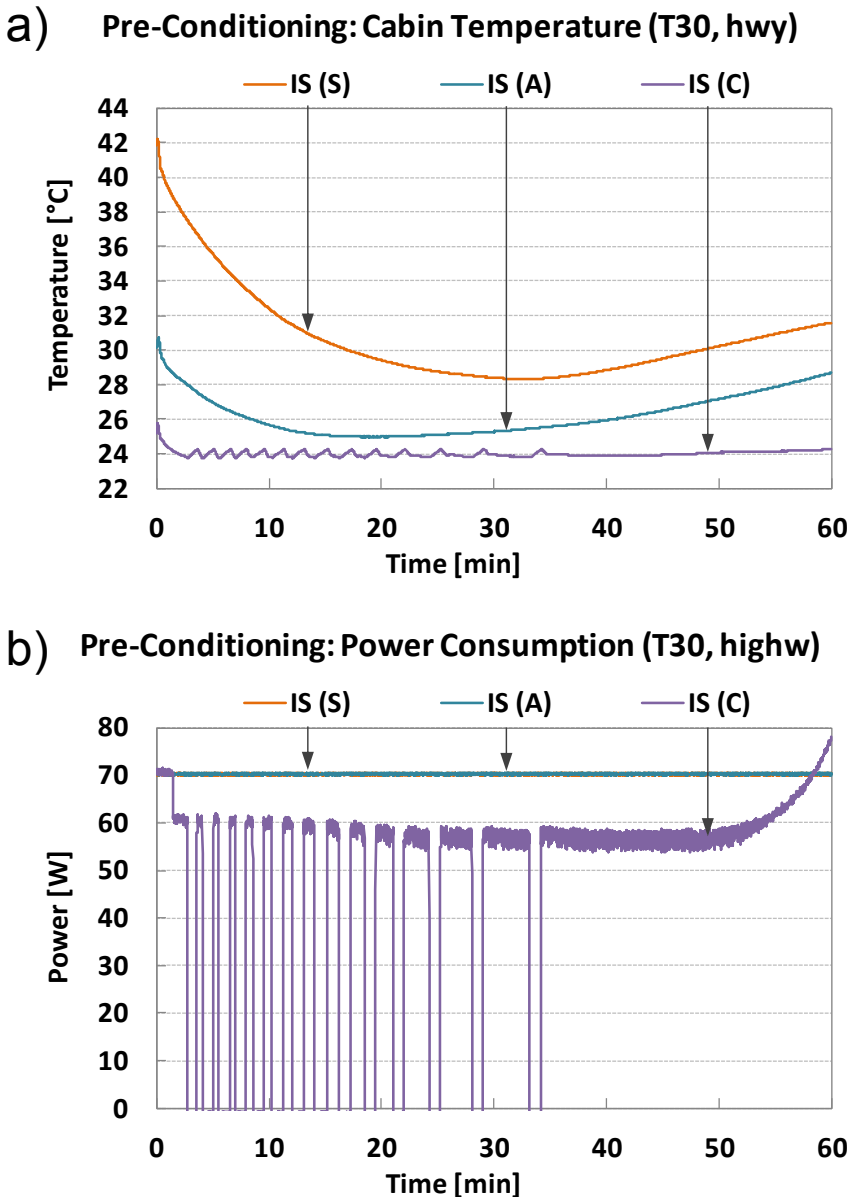

Figure 10.6: Preconditioning Ice Storage Performance Comparison

10.3 Summary: Benefits of A/C Controls and Cabin Pre-Conditioning

- Compressor and pump controls to reduce A/C power consumption were implemented. The control of humidity by the compressor, as well as the preconditioning of the passenger cabin were investigated as possible strategies to reduce power consumption.

- All three control strategies, Frost cycling, Relative Humidity cycling, and Relative Humidity continuous operation, were able to keep the cabin temperature at comfort set point after pull down. Relative Humidity cycling and Relative Humidity continuous operation kept the cabin supply relative humidity at 80% and the cabin relative humidity at 50% throughout the test.

- Energy consumption of the R290 secondary loop system, including heater power, could be reduced by as much as 40% for relative humidity cycling, and as much as 60% for relative humidity continuous control when compared to Frost cycling control. When using ice storage, energy consumption of relative humidity continuous did not decrease further. However, relative humidity cycling reduced the energy consumption by about 55%.

- Preconditioning the passenger cabin to ambient temperature or comfort temperature (instead of soaked condition) does not reduce overall power consumption (including heater power) for control strategies that rely on the compressor and heater being turned on for most of the time. However, when employing the relative humidity cycling control strategy, cabin preconditioning could reduce power consumption by 25% (A) and 30% (C).

- When operating only the charged ice storage box and the coolant pump without the vapor compression cycle, the cabin could not be pulled down from an initial hot soaked condition. However, when pre-conditioned to comfort temperature, the ice storage box was able to

keep the cabin at comfort temperature for one hour. Latent storage may therefore be used in combination with cabin preconditioning to either replace or significantly reduce the use of the vapor compression system during commutes.

11 Transient Simulation of Secondary Loop Systems

Modelica® is an object-oriented, equation based language used to model a variety of physical systems. Modelica® is heavily used in the automotive industry to design energy efficient vehicles, as well as design thermal management and air-conditioning systems. The programming environment Dymola was used to develop the secondary loop system, as well as perform transient simulation.

11.1 Cabin Model

A lumped model of a passenger cabin was developed in Modelica® to allow transient simulation of automotive air-conditioning systems. The cabin model developed by Gado [12] was used as a starting point and modified for the present research. The structure of the passenger cabin model, as well as the equations and modifications applied to Gado's model are discussed in the following chapter.

11.1.1 Cabin Model Equations and Structure

The heart of the model are a set of energy, mass, and moisture balance equations, which compute the psychrometric processes in a passenger cabin. The relevant equations are explained in the following paragraph. Table 11.1 provides an overview of the indices used in the cabin model equations.

Table 11.1: Cabin Model Equations - Index Explanation

Index	Explanation
c	Cabin air
i	Cabin interior
s	Supply air
r	Return air
m	Mixed air
a	Ambient air
sol	Solar (insolation)
ps	Passenger, sensible
pl	Passenger, latent

The set of equations contains a sensible sub set, as well as a subset for latent energy and mass balance. Equations (24) through (26) relate to the sensible portion, while Equations (27) through (29) related to the latent portion. Equation (24) describes the relation of cabin air and cabin interior thermal storage with the various loads on the cabin, such as solar insolation, sensible passenger load, and heat transfer with ambient. In comparison with Gado [12], the term which described the load on the evaporator, due to introduction of ambient air was left out, as it did not relate to load on the cabin itself. Equation (25) describes the change in interior temperature based on convective heat transfer with cabin air. Equation (26) describes the relation between the cabin air and the return air which leaves the cabin. The equation was modified from Gado's version by removing the influence of mixture with ambient air. In the present model, mixing with ambient air occurs after the air leaves the cabin and before it returns upstream to the evaporator (DX) or cooler (2LP). Energy, mass, and moisture balance for mixing are therefore not part of the cabin model. At the same time, an enthalpy balance was used due to a higher accuracy.

$$M_c C_{p,c} \frac{dT_c}{dt} + M_i C_i \frac{dT_i}{dt} = -m_s C_{p,s}(T_c - T_s) + Q_{sol} + Q_{ps} + U_o A_o (T_a - T_c) \quad (24)$$

$$M_i C_i \frac{dT_i}{dt} = -h_{ic} A_{ic} (T_i - T_c) \quad (25)$$

$$i_c = i_r \quad (26)$$

Equation (27) describes the moisture balance in the cabin, taking into account the storage of moisture in the cabin air, the introduction of moisture by the supply air, as well as the passengers, and the decrease of moisture due to the leaving return air. Equation (28) describes the relation between the humidity ratio of cabin air to the humidity ratio of return air leaving the cabin. As in previous equations, the influence of mixing with ambient air was omitted.

$$M_c h_{fg} \frac{dW_c}{dt} = m_s X_s - m_r X_r + Q_{pl} \quad (27)$$

$$W_c = W_r \quad (28)$$

Parameters X_s and X_r are mass fractions of water vapor to total mass of air. There relation to humidity ratio, W, is given by Equation (30).

$$W = \frac{X}{1-X} \quad (29)$$

Finally, since there is no mixing with ambient air inside of the cabin, the mass flow rate of return air equals the mass flow rate of supply air, as shown in Equation (30).

$$m_r = m_s \quad (30)$$

The air leaving the cabin is allowed to mix with ambient air, based on the recirculation ratio. To this end, an air splitter, as well as an air mixer were used. The air splitter splits up the air stream leaving the cabin into two streams, based

on a predefined recirculation ratio. One of the partial streams is mixed with ambient air, while the other is dumped to ambient. This is necessary to preserve mass balance with the added ambient air stream. Equations (31) through (33) determine the mass flow rate, energy flow rate, and moisture flow rate of the air stream which later mixes with ambient air and returning to the evaporator (out,2). Equations (34) through (36) shows the overall mass, energy and moisture conservation for the air splitter.

$$\dot{m}_{r,2} = recirc \times \dot{m}_{\mathrm{r}} \quad (31)$$

$$\dot{m}_{r,2} i_{\mathrm{r},2} = recirc \times \dot{m}_{\mathrm{r}} i_{\mathrm{r}} \quad (32)$$

$$\dot{m}_{r,2} X_{\mathrm{r},2} = recirc \times \dot{m}_{\mathrm{r}} X_{\mathrm{r}} \quad (33)$$

$$\dot{m}_{\mathrm{r},2} + \dot{m}_{\mathrm{r},1} = \dot{m}_{\mathrm{r}} \quad (34)$$

$$\dot{m}_{\mathrm{r},2} i_{\mathrm{r},2} + \dot{m}_{\mathrm{r},1} i_{\mathrm{r},1} = \dot{m}_{\mathrm{r}} i_{\mathrm{r}} \quad (35)$$

$$\dot{m}_{\mathrm{r},2} X_{\mathrm{r},2} + \dot{m}_{\mathrm{r},1} X_{\mathrm{r},1} = \dot{m}_{\mathrm{r}} X_{\mathrm{r}} \quad (36)$$

The air mixer adiabatically mixes fresh, ambient air with the partial return air stream leaving the cabin, based on the recirculation ratio. The mass flow rate of ambient air is determined by Equation (37). Equations (38) through (40) show the mass, energy and moisture balance for the mixing process. Following the adiabatic mixing process, the air is recirculated upstream of the evaporator.

$$\dot{m}_{\mathrm{a}} = (1 - \mathrm{recirc})\dot{m}_{\mathrm{s}} \quad (37)$$

$$\dot{m}_{\mathrm{a}} + \dot{m}_{\mathrm{r},2} = \dot{m}_{\mathrm{m}} \quad (38)$$

$$\dot{m}_{\mathrm{a}} i_{\mathrm{a}} + \dot{m}_{\mathrm{r},2} i_{\mathrm{r},2} = \dot{m}_{\mathrm{m}} i_{\mathrm{m}} \quad (39)$$

$$\dot{m}_{\mathrm{a}} X_{\mathrm{a}} + \dot{m}_{\mathrm{r},2} X_{\mathrm{r},2} = \dot{m}_{\mathrm{m}} X_{\mathrm{m}} \qquad (40)$$

Figure 11.1 shows the top level structure of the cabin model in Modelica®. Inlets for supply air, ambient air, solar insulation, as well as ambient temperature (for heat transfer) are present. Two air sinks serve as outlets in the bench test case. When combined with a direct expansion cycle, the supply air inlet would be connected to the outlet of the evaporator (DX) or cooler (2LP), while one of the outlets would be connected to the evaporator or cooler inlet.

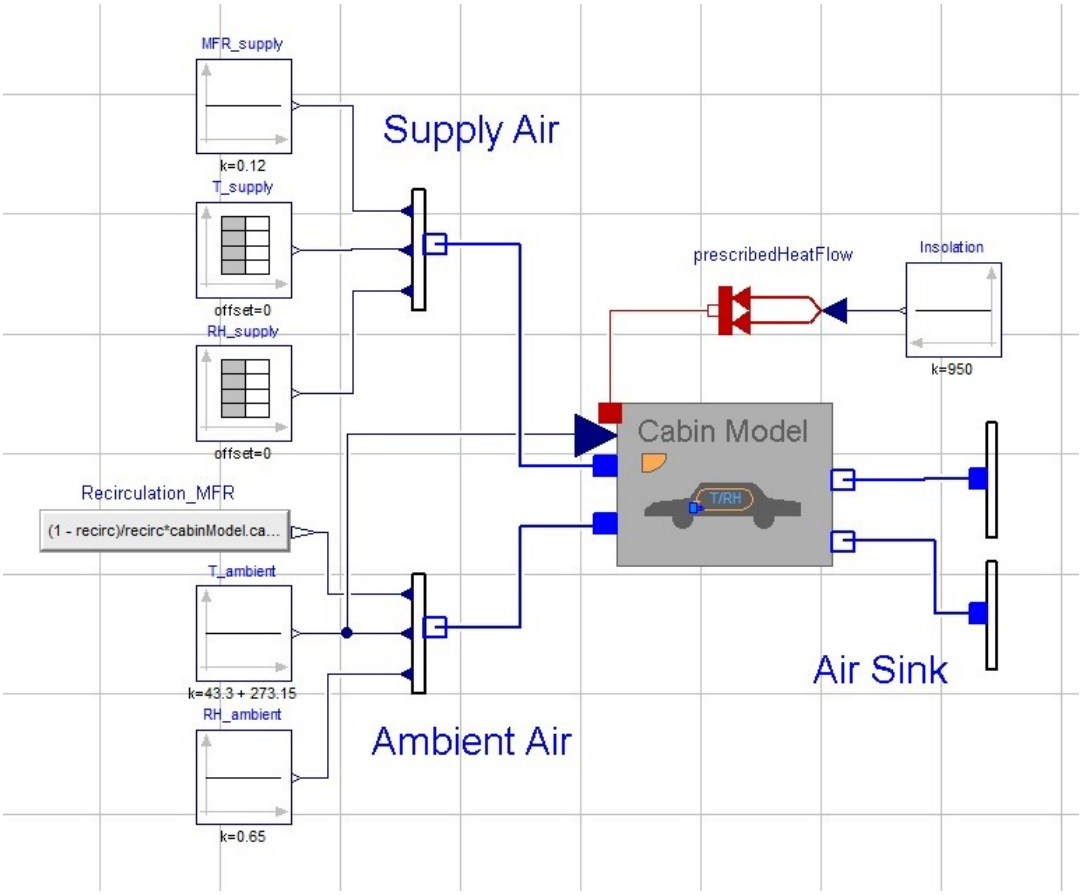

Figure 11.1: Modelica Passenger Cabin Model

11.1.2 Cabin Model Validation

The cabin model was validated, based on the process outlined in Gado [12]. A supply air temperature profile from Huang [15] was used as input to the cabin model. Based on the physical properties of the cabin used for validation, shown in Table 11.2, the cabin model calculates the state of the cabin air. The resulting cabin air profile is compared to the experimental values from Huang [15], as well as to the cabin model validation profile from Gado [12]. Figure 11.2 shows the comparison of cabin temperature profiles. It can be observed that the current cabin model (Eisele 2012) coincides with the validation results from Gado, despite the subtle differences introduced to the equations. Following the validation, the cabin model was used in the transient simulation of the direct expansion, as well as the secondary loop system.

Table 11.2: Cabin Model Validation Physical Parameters

Parameter	Magnitude	Source
Ambient Temperature [°C]	43.3	Huang (1998)
Ambient Relative Humidity [%]	65	Huang (1998)
Solar Insolation [W]	950	Huang (1998)
Degree of Soak [K]	16.7	Huang (1998)
Cabin Surface Area	30	Huang (1998)
Overall Heat Transfer Coefficient [W/m^{2}K]	2.5	Tuned
Internal Cabin Volume [m^3]	8	Huang (1998)
Interior Mass [kg]	200	Huang (1998)
Interior Specific Heat [J/kg K]	400	Huang (1998)
Interior Surface Area [m^2]	3	Typical Value
Convection Coefficient (interior) [W/m^2 K]	100	Tuned
Number of Passengers	0	Huang (1998)
Fresh Air Ratio	0	Huang (1998)
Supply Air Temperature [°C]	profile	Huang (1998)
Supply Air Relative Humidity [%]	profile	Typical Value

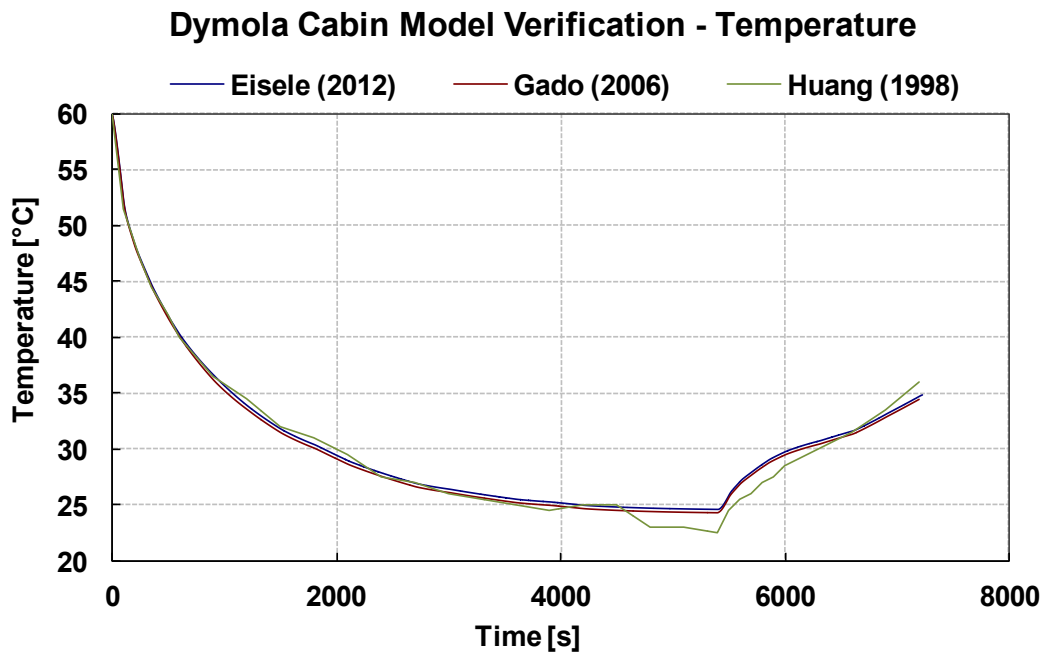

Figure 11.2: Cabin Model Validation Results

11.2 Direct Expansion System

As a first step towards transient simulation of secondary loop systems, an R134a direct expansion (DX) cycle was modeled and validated for steady-state, as well as transient operation. The direct expansion system was modeled after the experimental DX system, using microchannel refrigerant to air heat exchangers, a variable speed fixed displacement compressor, as well as a PID controlled electronic expansion valve. The refrigerant components were modeled by Qiao [129], a member of the Center for Environmental Energy Engineering (CEEE). For the present research, the components were combined to a direct expansion cycle and tuned to match experimental R134 DX system performance.

11.2.1 Direct Expansion Model and Components

Figure 11.4 shows the structure of a R134a DX stationary (steady-state) model in Dymola. The stationary model consists of a variable speed fixed displacement compressor (1), a microchannel condenser (2), a PID controlled electronic expansion valve (3), and a two pass microchannel evaporator (4). Refrigerant lines (5) permit heat transfer with ambient to take heat loss into account. Two types of boundaries, an air sink (6), and an air inlet boundary (7) are used to fix air-side conditions in the stationary model. The components of the direct expansion system were modeled by Qiao [129]. A brief description and summary of governing equations of the main direct expansion system component models is given in Appendix H.

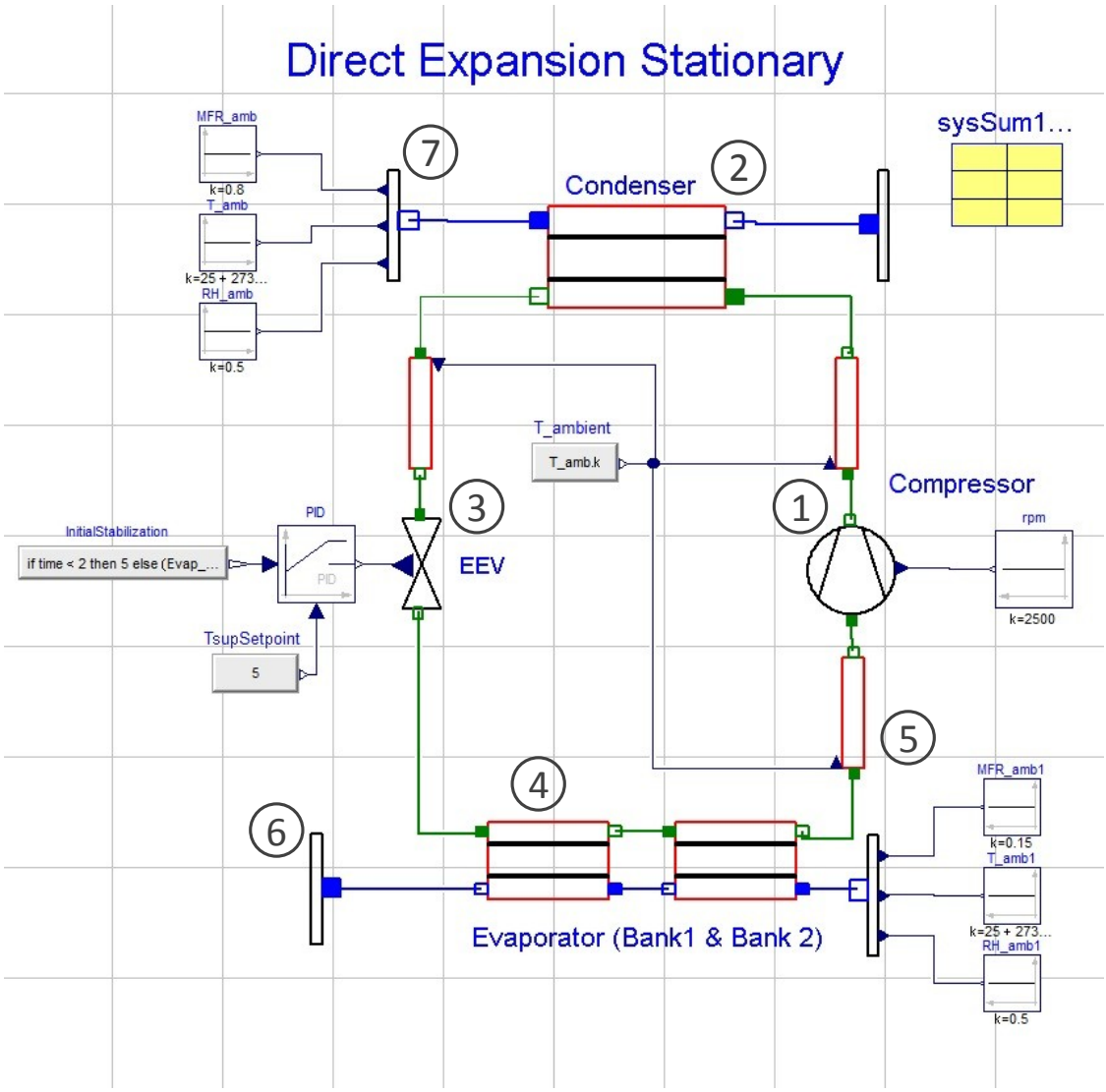

#	Component
1	Compressor, fixed displacement
2	Condenser, microchannel
3	Expansion Valve, PID controlled
4	Evaporator, microchannel
5	Refrigerant Piping
6	Air Sink
7	Air Boundary

Figure 11.3: Direct Expansion Steady-state System Model

Figure 11.4 shows the structure of the R134a DX transient system model. For the purpose of transient simulation, the DX model was combined with the automotive cabin model. The cabin model (6) replaces the air sink and inlet boundary of the stationary model evaporator, shown in Figure 11.3. The cabin model receives supply air from the second evaporator bank outlet. Ambient air for mixing is provided by an air inlet boundary (7), while heating by solar insolation is added through a heat transfer boundary (9). With this configuration, the R134a DX model is able to simulate transient pull-down, as well as drive cycle tests. While pull-down tests are performed at constant compressor speed and condenser air flow rate in the present research, drive cycle tests feature a predefined compressor speed and condenser air flow rate profile. Speed and air flow rate profiles are supplied to the compressor and the condenser model by time table modules, as shown in Figure 11.4.

The following chapter discusses validation results of the R134a DX system model for steady-state, as well as transient operation.

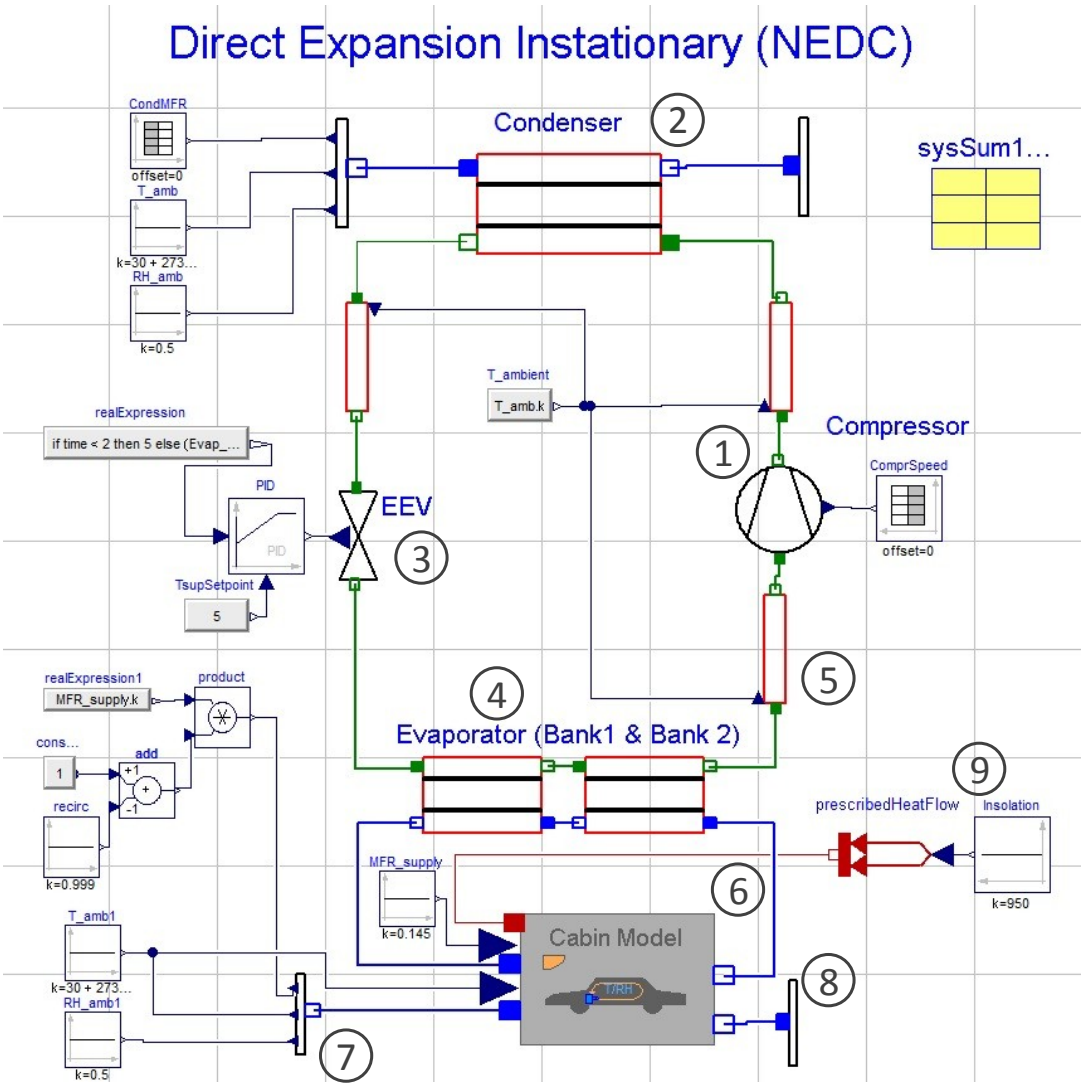

#	Component
1	Compressor, fixed displacement
2	Condenser, microchannel
3	Expansion Valve, PID controlled
4	Evaporator, microchannel
5	Refrigerant Piping
6	Cabin Passenger Model
7	Air Boundary
8	Air Sink
9	Heat Flow Boundary

Figure 11.4: R134a Direct Expansion Transient System Model

11.2.2 R134a Direct Expansion Model Validation

The R134a DX model was validated with experimental data for steady-state, as well as transient operation. The inner geometry of heat exchangers, expansion valve, and compressor (flow channels) were unknown. Steady-state experimental data was used to tune the component geometries, as well as the refrigerant charge of the system. Initialization of the model requires initial temperature, pressure, as well as initial enthalpy in the refrigerant components to be known. While the pressure can be assumed to be saturation pressure at the initial temperature if the system is charged correctly, initial enthalpy requires the knowledge of system volume and refrigerant charge to determine initial density. Initial volume can be estimated by measuring the combined volume of all components in the experimental system. However, estimation of refrigerant charge for transient simulation poses a challenge, although the charge is known for the experimental system. Refrigerant charge while the compressor is running (i.e. while there is a mass flow rate through the components) varies from initial charge, due to the behavior of the mass derivatives in the component models. Therefore, all system models need to be tuned by adjusting initial enthalpy (which is a function of initial refrigerant charge).

Table 11.3 shows the results of the steady state R134 DX model validation for two different ambient conditions, 25°C and 50% relative humidity, as well as 35°C and 40% relative humidity. At 35°C ambient temperature, the model was validated for idling conditions, as well as highway driving conditions. From Table 11.3 it can be observed that high side pressure is slightly

overpredicted at highway driving conditions, while low side pressure is slightly overpredicted at idling conditions. Discharge pressure is consistently underpredicted by as much as 7 K. However, cooling capacity is reasonably well predicted with an absolute deviation of as much as 50 W, which compares to a 1% relative difference compared to experimental data. Compressor power consumption was predicted by the model with a deviation of less than 1% throughout the three cases that were validated. As a result, system COP was predicted with less than a 1% deviation. Due to the excellent match of cooling capacity, compressor power consumption and consequently system COP, the tuned components were subsequently used in the transient simulation of pull-down and NEDC tests.

Table 11.3: R134a Direct Expansion Steady-state Model Validation Results

Parameter	Experiment	Simulation	Deviation [abs]
25°C / 50% ; highway			
High Side Pressure [kPa]	945.5	983.0	37.5
Low Side Pressure [kPa]	241.3	244.1	2.8
Discharge Temperature [°C]	65.2	58.1	-7.1
Cooling Capacity [W]	4724.2	4673.8	-50.4
Compressor Power [W]	2578.5	2558.7	-19.8
System COP [-]	1.83	1.83	0.0
35°C / 40% ; idle			
High Side Pressure [kPa]	1235.6	1233.1	-2.5
Low Side Pressure [kPa]	415.7	453.4	37.7
Discharge Temperature [°C]	65.0	61.0	-4.0
Cooling Capacity [W]	2965.6	3000.4	34.8
Compressor Power [W]	1167.6	1171.9	4.3
System COP [-]	2.55	2.56	0.4
35°C / 40% ; highway			
High Side Pressure [kPa]	1341.8	1382.8	41
Low Side Pressure [kPa]	306.9	310.0	3.1
Discharge Temperature [°C]	78.6	71.3	-7.3
Cooling Capacity [W]	5510.4	5456.3	-54.1
Compressor Power [W]	3397.2	3379.6	-17.6
System COP [-]	1.62	1.61	0.6

Figure 11.5 shows a comparison of simulation and experimental results of an NEDC drive cycle test, performed at 30°C/50% ambient condition and an initial soak of 5.6 K. Profiles of cabin temperature, cooling capacity, and power consumption are presented.

Figure 11.5 a) shows a comparison of cabin temperature profiles. During model validation, it was observed that the model would constantly underpredict the cabin temperature at the beginning of a pull-down (or NEDC) test, while the curves would run parallel during the mid to late section of the comparison. This can be explained by the thermal storage of the evaporator (DX)/cooler (2LP) windtunnel. The thermal mass of the windtunnel sensibly cools or heats the air between the point where it leaves the evaporator/cooler and the point where the thermocouple grid measures air-side outlet temperature. This thermal mass is unaccounted for in the Modelica® model. To adjust for this discrepancy, the cabin model physical parameters were tuned by adjusting the specific heat capacity of the interior, as well as the convection coefficient between the cabin air and the interior to reflect the behavior of the experimental system. From Figure 11.5 a) it can be concluded that after the tuning of the thermal mass of the interior, the model accurately predicts the cabin temperature profile during the NEDC test. Cabin temperature at the beginning of the cycle is still slightly lower compared to experimental results, but the overall profile is coherent.

Figure 11.5 b) shows a comparison of cooling capacity profiles. The overall trends for cooling capacity match well between the simulation and the experimental profiles. However, it can be observed that during the later parts of

the city cycle, significant deviations between the experimental and the simulation trends occur. The specific parts of the cycle were highlighted with a dotted circle in Figure 11.5 b). The deviations can be explained by the lack re-evaporation of condensate off the evaporator/cooler fins in the model. The experimentally observed cooling capacity during idling at later parts of the NEDC cycle includes the effect of re-evaporation and subsequent changes in the latent capacity. The model is not able to predict re-evaporation and consequently determines an increased total cooling capacity during idling periods.

Figure 11.5 c) shows a comparison of NEDC power consumption profiles. The overall trend of power consumption is well observed by the model. Small deviations occur at the points of load shifting at the end of an acceleration or deceleration phase. The model does not take the effects of inertia in the compressor, as well as in the electric motor which drives the compressor, into account.

Table 11.4 shows a comparison of accumulated performance parameters. Based on the comparison, the model is able to predict the total energy available for cooling the air within a deviation of 6.7%. The total energy put into the direct expansion system in the form of compressor power consumption was predicted with a deviation of 4.2%. The difference between the simulated and the experimental transient performance factor was observed to be 2.0%.

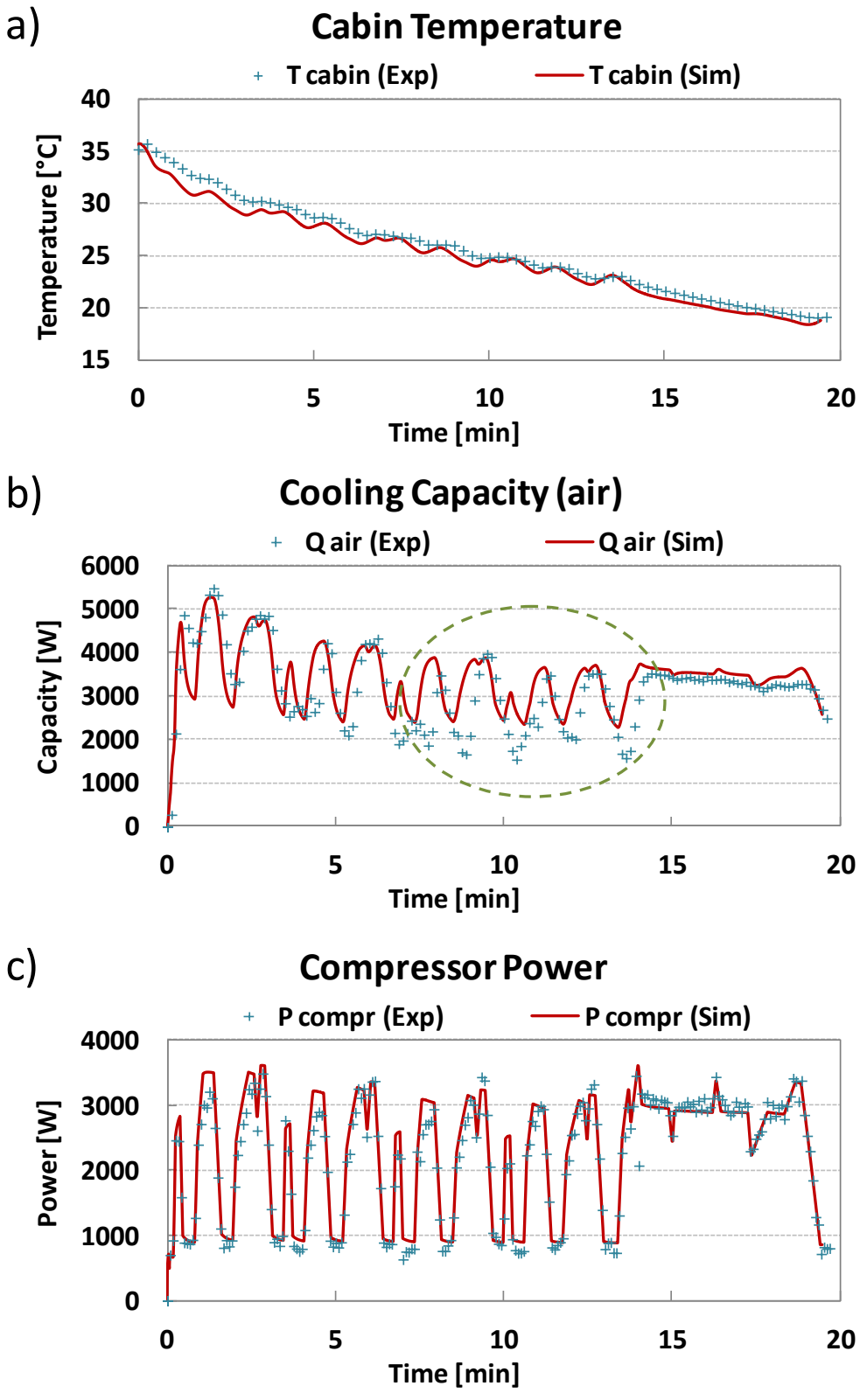

Figure 11.5: R134a Direct Expansion NEDC Validation Results

Table 11.4: R134a Direct Expansion NEDC Accumulated Performance Validation

Parameter	Experiment	Simulation	Deviation [%]
NEDC, 35°C/50%, 5.6 K soak			
Accumulated Capacity (air) [kWh]	1.04	1.11	*6.7*
Accumulated Compr. Power [kWh]	0.72	0.75	*4.2*
Transient Performance Factor [-]	1.45	1.48	*2.0*

Figure 11.6 shows a transient comparison of cabin temperature, cooling capacity, and power consumption for a pull-down test at 30°C/50% ambient condition and 2,500 rpm compressor speed, with an initial degree of soak of 12 K. With the tuning of components and cabin model, described in above paragraph, the model is able to predict pull-down performance reasonably well.

Figure 11.6 a) shows a comparison of cabin temperature profiles. The model predicted cabin temperature within 0.5 K, except during the initial minutes of the pull-down test. Figure 11.6 b) compares the experimental and simulated cooling capacity profiles. The initial transients in capacity are not well captured, possibly due to a difference in electronic expansion valve (EXV) behavior. During the remainder of the pull-down test cooling capacity is slightly overpredicted by the model. Experimental compressor power, shown in Figure 11.6 c), is well matched by the model. Again, initial transients are not captured, and the model slightly underpredicts compressor power consumption during the pulldown process.

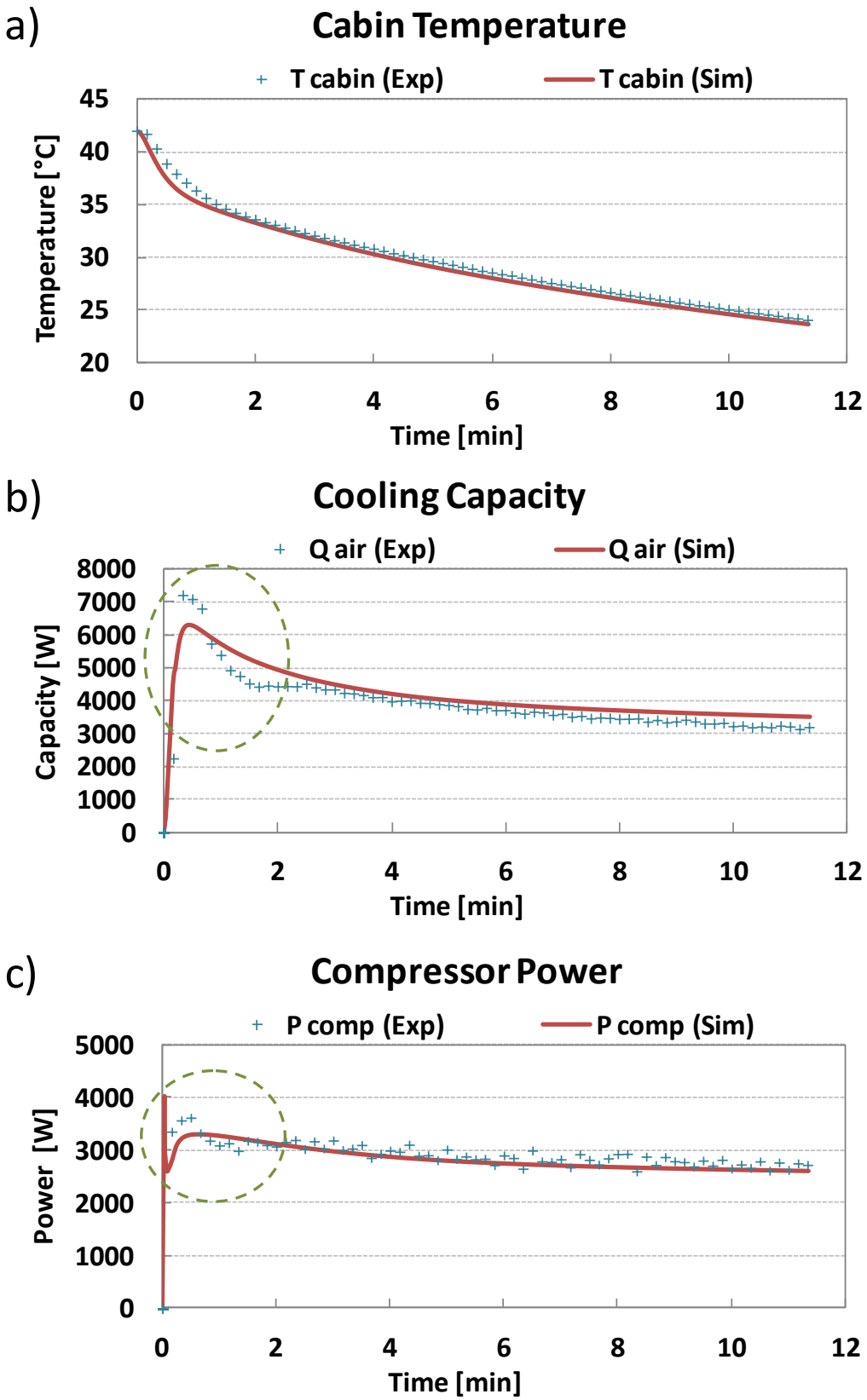

Figure 11.6: R134a Direct Expansion Pull-down Validation Results

Accumulated performance results are compared in Table 11.5. The model predicted accumulated capacity and accumulated power consumption to within 6%. Since cooling capacity was overpredicted and power consumption was underpredicted, the simulation TPF increased by 10.5% over experimentally measured TPF.

Table 11.5: R134a Direct Expansion Pull-down Acc. Performance Validation

Parameter	Experiment	Simulation	Deviation [%]
PIldn, 30°C/50%, 12K soak, 1550rpm			
Accumulated Capacity (air) [kWh]	0.744	0.788	*5.9*
Accumulated Compr. Power [kWh]	0.559	0.536	*-4.1*
Transient Performance Factor [-]	1.33	1.47	*10.5*

11.3 Secondary Loop System

To model the secondary loop system, several components had to be introduced in addition to the direct expansion cycle components. As part of this research, a generic glycol media package has been developed, as well as a coolant pump, coolant tubes, an intermediate heat exchanger, as well as a coolant to air heat exchanger. The following chapters introduce the coolant components and the validation of the secondary loop system model.

11.3.1 Coolant Cycle Model and Components

Figure 11.7 shows the secondary loop steady-state system model. Components previously described for the direct expansion system, such as compressor (1), condenser (2), expansion valve (3), and refrigerant lines (5) don't change. The length of the refrigerant lines was changed according to the

changes observed when the experimental test facility was switched from direct expansion to a secondary loop system layout. The evaporator was replaced by a refrigerant to coolant plate type heat exchanger (4). A coolant to air heat exchanger (6) was used to cool down the supply air. The coolant was circulated through the secondary loop by a coolant pump (7). Coolant lines (8) were used to connect the secondary loop components.

The glycol media package for aqueous solutions of ethylene glycol was developed based on equations from M. Conde Engineering [109]. Property equations and coefficients used for the present research are restated in Appendix G.

Governing equations for the coolant tubing are given by Equations (41), (42), (43), (44) and (45). Equation (41) provides information about the determination of the forced convection heat transfer coefficient for liquid coolant. The heat transfer coefficient for each segment i is a function of the inner diameter of the tube, thermal conductivity, dynamic viscosity, mass flow rate, and specific heat capacity. Equation (42) provides information about the pressure drop correlation used for the coolant tubing. The pressure drop for each segment in the Blasius type solution is a function internal tube diameter, segment length, mass flow rate, density and dynamic viscosity.

$$htc_i = DittusBolter(Di, k_i, \mu_i, \dot{m}, cp_i) \quad (41)\ [130]$$

$$\mathrm{dp}_i = \mathrm{Blasius}(Di, \frac{\mathrm{Lt}}{\mathrm{n_{Seg}}}, \dot{m}, \rho_i, \mu_i) \quad (42)\ [131]$$

Forced convection heat transfer in each tube segment was determined by Equation (43), where A_s was surface area, n the number of segments, T_w was wall temperature and T was the temperature of the coolant.

$$q_i = htc_i \frac{A_s}{n_{seg}} \left(T_{w,i} - T_i\right) \quad (43)$$

Mass and energy conservation equations were used for the coolant tube control volume, as shown in Equations (44) and (45). Equation (45) allows for thermal storage in the secondary loop components.

$$\dot{m}_{out} = \dot{m}_{in} \quad (44)$$

$$m_i \times cp_i \frac{dT_i}{dt} = q_i + \dot{m}(h_i - h_{i+1}) \quad (45)$$

The above equations used for the coolant tube control volume were employed for the coolant-side control volumes of the intermediate heat exchanger and the air cooler as well. Flow splitters and mixers were added before and after the control volume to model microchannel and plate type heat exchanger behavior.

A quasi-steady state, efficiency based model was used for the coolant pump. Equation (46) shows the energy equation for a generic pump, where p is pressure, ρ is density, v is velocity, g is gravitational acceleration and ht is height.

$$W_p = \frac{p_{out} - p_{in}}{\rho} + \frac{{v_{out}}^2 - {v_{in}}^2}{2} + g(ht_{out} - ht_{in}) \quad (46)$$

The electrical power consumed by the pump, depending on volumetric, hydraulic, and motor efficiency, is given by Equation (47). It was assumed that

half of the heat produced due to motor inefficiencies was introduced as heat gain into the fluid.

$$Q_e = \frac{\rho \times \dot{V} \times W_p}{\eta_{vol} \times \eta_{hydr} \times \eta_{mot}} \quad (47)$$

To simulate transient operation, the secondary loop model was combined with the cabin model (9) to enable pull-down and drive cycle testing, as shown in Figure 11.8. The cabin model receives supply air from the cooler air-side outlet, while the mixed air is returned back to the inlet of the cooler. Similar to the direct expansion cycle transient model, ambient air is introduced to the cabin model by an air inlet boundary (10).

The following chapter discusses the validation of the secondary loop model with experimental data for steady-state, as well as transient operation.

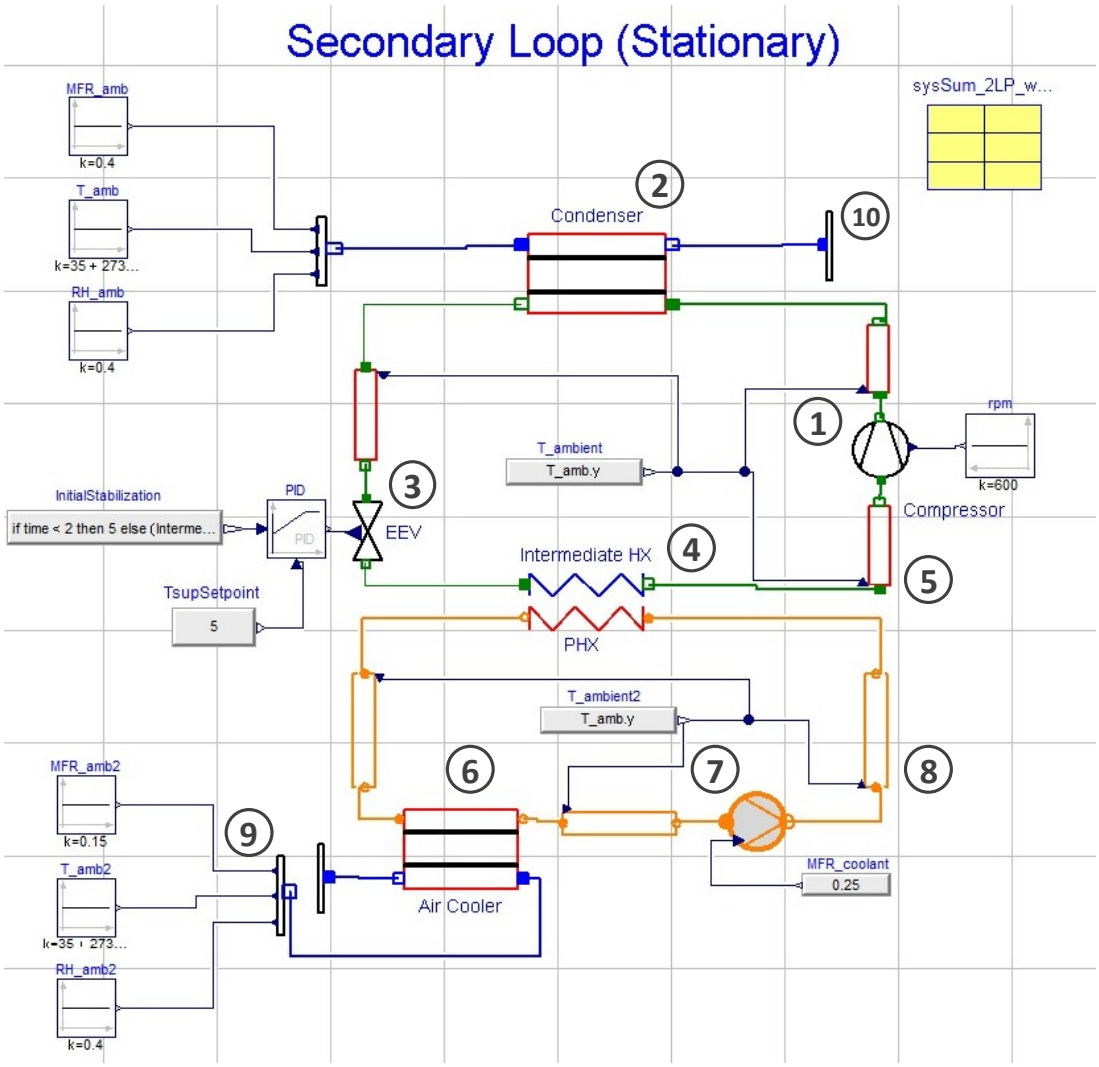

#	Component
1	Compressor, fixed displacement
2	Condenser, microchannel
3	Expansion Valve, PID controlled
4	Intermediate Heat Exchanger, plate type
5	Refrigerant Piping
6	Air Cooler, microchannel
7	Coolant Pump
8	Coolant Tubing
9	Air Boundary
10	Air Sink

Figure 11.7: Secondary Loop Steady-state System Model

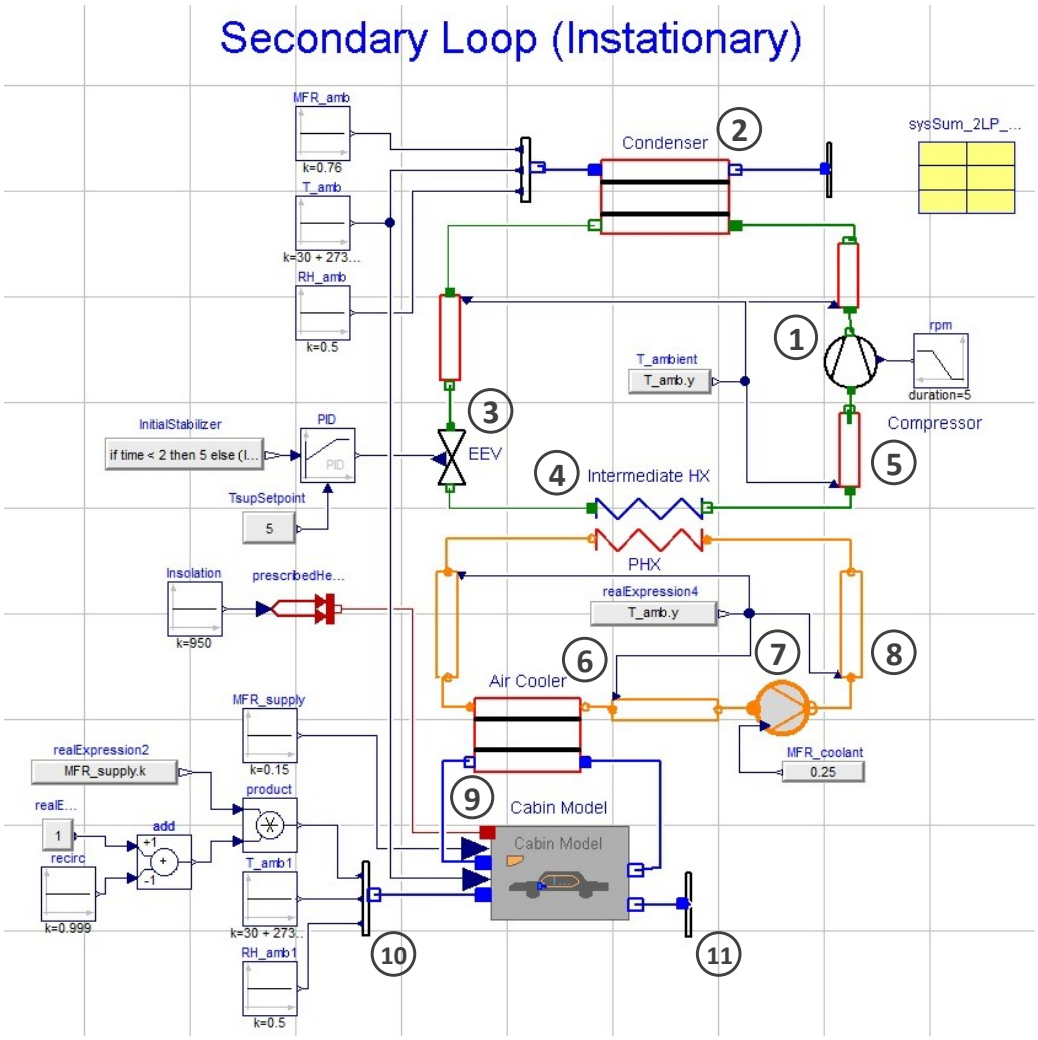

#	Component
1	Compressor, fixed displacement
2	Condenser, microchannel
3	Expansion Valve, PID controlled
4	Intermediate Heat Exchanger, plate type
5	Refrigerant Piping
6	Air Cooler, microchannel
7	Coolant Pump
8	Coolant Tubing
9	Cabin Model
10	Air Sink
11	Air Boundary
12	Heat Flow Boundary

Figure 11.8: Secondary Loop Transient System Model

11.3.2 R290 Secondary Loop Model Validation

The operation of the secondary loop system model was validated for steady-state, as well as transient operation. Table 11.6 shows the validation results for steady-state operation at different ambient temperature and idling, as well as highway driving conditions. As for the direct expansion system model, the secondary loop components were tuned, since the interior geometry of the intermediate heat exchanger and the air cooler were unknown. Across different ambient conditions, as well as driving conditions, high side pressure in the vapor compression cycle is very well predicted. However, low side pressure is overpredicted at highway driving conditions, while it is slightly underpredicted at idling conditions. Discharge pressure is within 2 K of the experimentally measured value during highway driving conditions, while it is underpredicted by about 5.66 K at idling conditions. Cooling capacity is underpredicted by less than 6% for highway driving, while it is overpredicted by about 6% for idling conditions. Simulated results for compressor power consumption are within 2% of the experimentally measured values for the examined operating conditions. Air-side COP was captured within deviations of 0.2 absolute, which corresponds to a 7.5% relative deviation at 25°C highway driving. Air-side cooler outlet temperature matches with measured results within less than 2 K. Following steady-state validation, the secondary loop model was used in conjunction with the cabin model to simulate transient pull-down and drive cycle operation.

Table 11.6: Secondary Loop Stationary System Validation Results

Parameter	Experiment	Simulation	Deviation [abs]
25°C / 50% ; highway			
High Side Pressure [kPa]	1326.8	1334.7	7.9
Low Side Pressure [kPa]	412.2	449.1	36.9
Discharge Temperature [°C]	58.8	57.4	-1.4
Cooling Capacity [W]	4425.7	4181	-244.7
Compressor Power [W]	2161.1	2143	-18.1
System COP [-]	1.98	1.83	-0.2
Cooler Outlet Temp. (col) [°C]	7.5	4.6	-2.9
Cooler Outlet Temp. (air) [°C]	7.7	7.7	0.0
30°C / 40% ; idle			
High Side Pressure [kPa]	1571.9	1572.6	0.7
Low Side Pressure [kPa]	720.2	700.2	-20.0
Discharge Temperature [°C]	66.3	60.8	-5.6
Cooling Capacity [W]	2390.6	2541.5	150.9
Compressor Power [W]	1032.5	1019.9	-12.6
System COP [-]	2.17	2.29	0.1
Cooler Outlet Temp. (col) [°C]	20.1	21.3	1.2
Cooler Outlet Temp. (air) [°C]	20.0	18.5	-1.5
30°C / 40% ; highway			
High Side Pressure [kPa]	1732.5	1744.7	12.2
Low Side Pressure [kPa]	506.7	574.0	67.3
Discharge Temperature [°C]	71.5	69.8	-1.7
Cooling Capacity [W]	5022.8	4889.2	-133.6
Compressor Power [W]	2809.4	2766.0	-43.4
System COP [-]	1.7	1.7	0.0
Cooler Outlet Temp. (col) [°C]	14.3	13.2	-1.1
Cooler Outlet Temp. (air) [°C]	14.9	15.2	0.3

Figure 11.9 shows a comparison of NEDC performance between the R290 2LP Modelica model and experimental results. Figure 11.9 a) shows the validation of the cabin temperature profile over time. The model underpredicts cabin temperature by about 1 K throughout the NEDC cycle, but captures the general trends very well. The validation results for cooling capacity, shown in Figure 11.9 b) present a similar conclusion as the R134a DX validation results. While the initial transients within the first minute were not captured well, the simulated results stay fairly true to experimentally measure results throughout the

latter stages of the cycle. Towards the middle of the NEDC, a slight overprediction of cooling capacity was observed, since the model cannot capture the re-evaporation of condensate during idling periods. Compressor power consumption, shown in Figure 11.9 c), followed the trend of the experimental data. However, power consumption was slightly overpredicted throughout the cycle, which was especially prominent during the idling periods.

A comparison of the total energy available for air-side cooling, the total input to the system, and the transient performance factor during the NEDC is shown in Table 11.7. Deviations of accumulated capacity and accumulated compressor power are within 6%. Due to an overprediction of capacity, as well as compressor power, the simulated TPF shows only a very small deviation (-0.7%) from experimental TPF.

Table 11.7: Secondary Loop NEDC Acc. Performance Validation

Parameter	Experiment	Simulation	Deviation [%]
NEDC, 35°C/50%, 5.6 K soak			
Accumulated Capacity (air) [kWh]	0.946	0.989	*4.5*
Accumulated Compr. Power [kWh]	0.689	0.727	*5.5*
Transient Performance Factor [-]	1.37	1.36	*-0.7*

Figure 11.10 shows a comparison of performance parameters during a pull-down test at 30°C/50% ambient condition and an initial degree of soak of 12 K. The cabin temperature profiles during pull-down are compared in Figure 11.10 a). During the initial minutes, the Modelica model predicts a cabin temperature, which is decreased by about 1 K from the experimentally measured value.

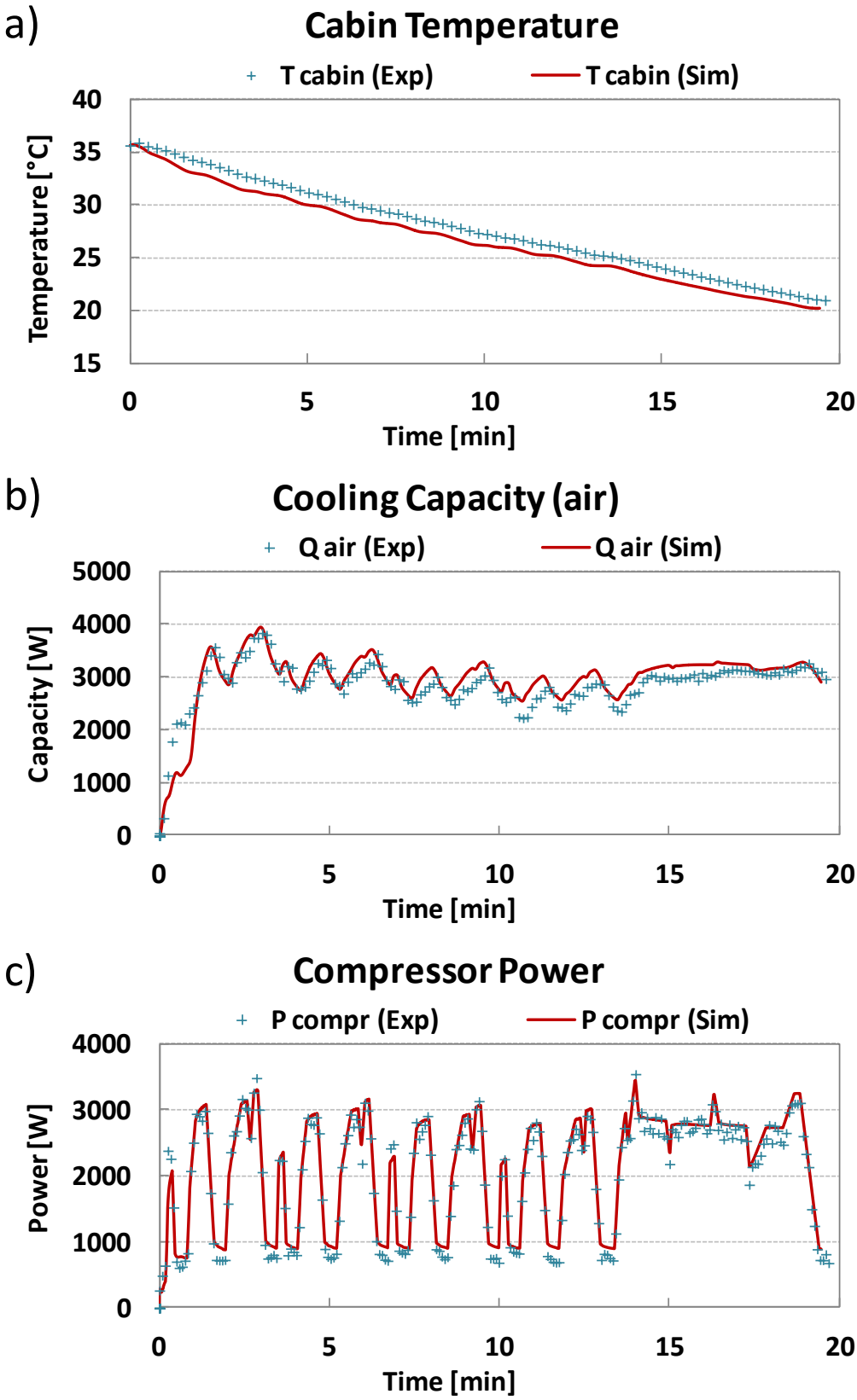

Figure 11.9: Secondary Loop NEDC Validation Results

This can be attributed to the thermal storage associated with the windtunnel in the experimental measurements. During the later part of the pull-down, simulated cabin temperature follows experimental cabin temperature very closely. A comparison of air-side cooling capacity is shown in Figure 11.10 b). As observed in the direct expansion system results, capturing the initial transients due to the electronic expansion valve adjustments is challenging for the model. However, the general trends throughout the pull-down tests are observed, with a slight overprediction of cooling capacity by the model. Figure 11.10 c) compares power consumption profiles for experimental and simulated compressor data. Much similar to the cooling capacity results, initial transients during the first minute of the pull-down test are not captured precisely. However, power consumption during the remainder of the test follows experimentally measured power consumption closely.

Table 11.8 shows the a comparison of accumulated pull-down performance. Total energy available for cooling cabin supply air was predicted with a deviation of 1.8% by the model. Energy consumed by the compressor over the duration of the test was captured by the model with a deviation of 2.4%. Simulated TPF decreased by 0.6% compared to experimental TPF.

Table 11.8: Secondary Loop Pull-down Acc. Performance Validation

Parameter	Experiment	Simulation	Deviation [%]
PIldn, 30°C/50%, 12 K soak, 1550rpm			
Accumulated Capacity (air) [kWh]	0.892	0.876	*1.8*
Accumulated Compr. Power [kWh]	0.631	0.616	*2.4*
Transient Performance Factor [-]	1.41	1.42	*-0.6*

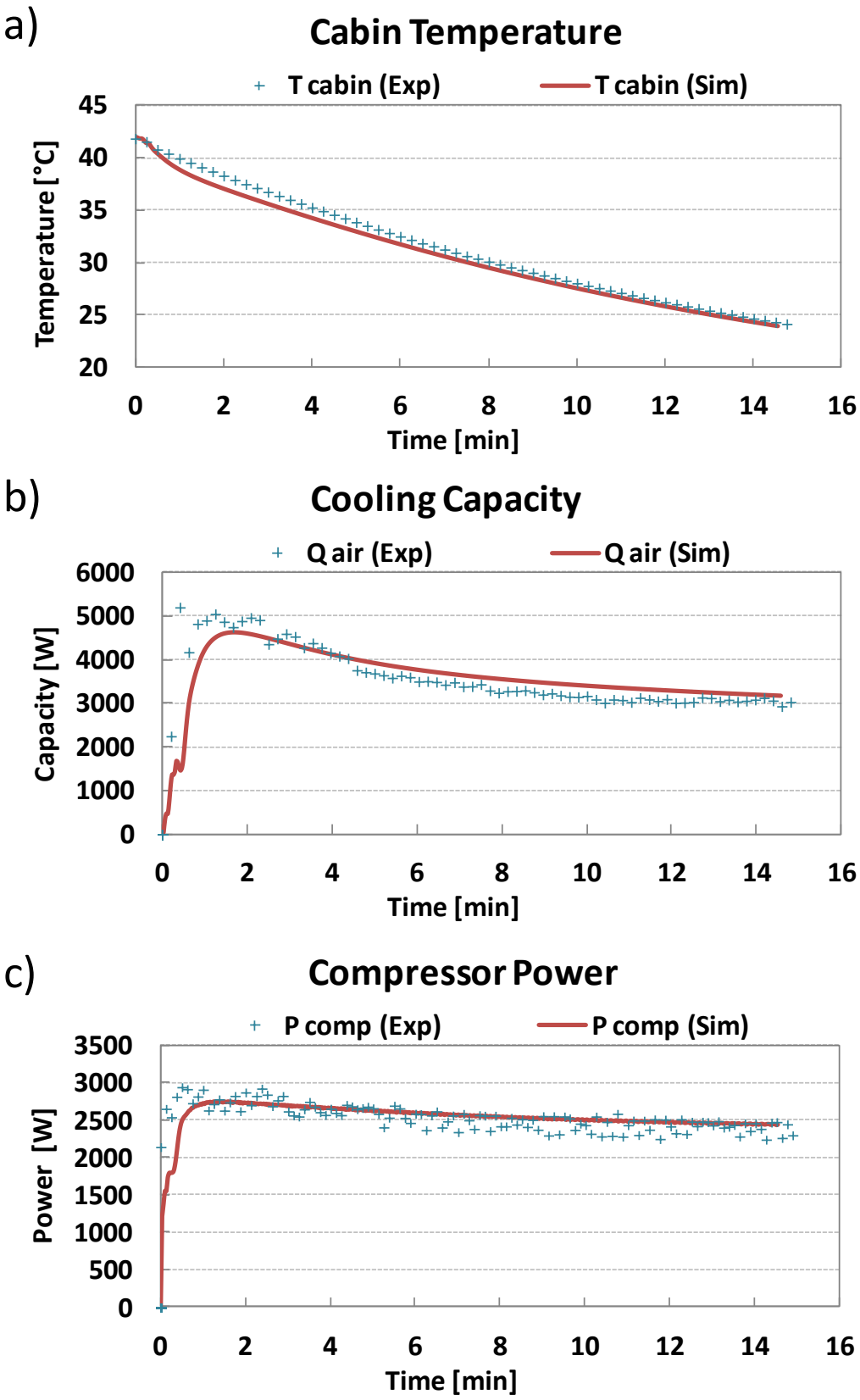

Figure 11.10: Secondary Loop Pull-down Validation Results

11.4 Influence of Coolant Volume on Transient Performance

The current experimental system had a coolant charge of about 5 liters. The coolant charge was heavily dependent on the facility layout and the components and space available. It is to be expected that a smaller charge may result in faster cool down of the cabin and a better system efficiency. On the other hand, a larger coolant charge may be beneficial for thermal comfort during off-cycle periods. The R290 2LP Modelica® model, introduced in Chapter 11.3, was used to perform a parametric study investigating the influence of coolant volume in the secondary loop on cabin pull-down and cabin warm-up performance. To this end, the length of coolant tubing in the model was varied. This approach was chosen, due to the possibility of secondary loop systems being used for electronics and battery cooling, as well as seat cooling/heating or radiative surfaces. A water-ethylene glycol mixture of 32wt% ethylene glycol was used, which equals the coolant used in the experimental study. The pull-down test was simulated using an ambient condition of 30°C and 50% relative humidity. At the start of the simulation the cabin was soaked to 42°C. The R290 2LP highway compressor speed of 1,550 rpm was chosen, as well as the R209 2LP coolant mass flow rate of 250 g/s. After reaching comfort temperature (24°C), the compressor was turned off and the cabin was allowed to warm up, while the coolant pump was still running to employ the thermal storage of the secondary loop for cooling during the off-cycle period.

Figure 11.11 shows the influence of coolant volume on cabin pull-down performance. Figure 11.11 a) shows supply temperature profiles for different

coolant charges. As expected, increasing coolant charge added thermal mass and increased supply temperature. Consequently, time to comfort increased with increasing coolant volume. Throughout most of the pull-down period, an increase in one liter of coolant resulted in roughly a 0.6 K increase in cabin supply temperature. Cooling capacity profiles are compared in Figure 11.11 b). It was observed that the influence of coolant volume on capacity is largest during the initial minutes of the pull-down test. At the point of largest divergence, every additional liter of coolant decreases capacity by roughly 150 W. However, the significance of coolant charge diminishes after the initial minutes. Figure 11.11 c) shows the system power (compressor + pump). Pump power consumption is dependent on coolant density and viscosity. Despite the increase in pipe length, it was found that pump power slightly decreased with increasing coolant charge, since the coolant stayed at a higher temperature and viscosity was reduced. The effects were negligible when compared to the overall system power consumption. From Figure 11.11 c) it was observed that changes in system power consumption resulting from variation of coolant charge were small.

Figure 11.12 shows the influence of coolant volume on cabin warm-up behavior during off-cycle periods. During the initial minutes, the addition of one liter of coolant may decrease the cabin supply temperature by about 0.7 K. The influence of coolant volume decreases with increasing warm-up time. After 15 minutes, the effect of an additional liter of coolant volume on the supply temperature became negligible. Figure 11.12 b) shows a comparison of cooling capacity, which is preserved by the thermal mass of the secondary loop system.

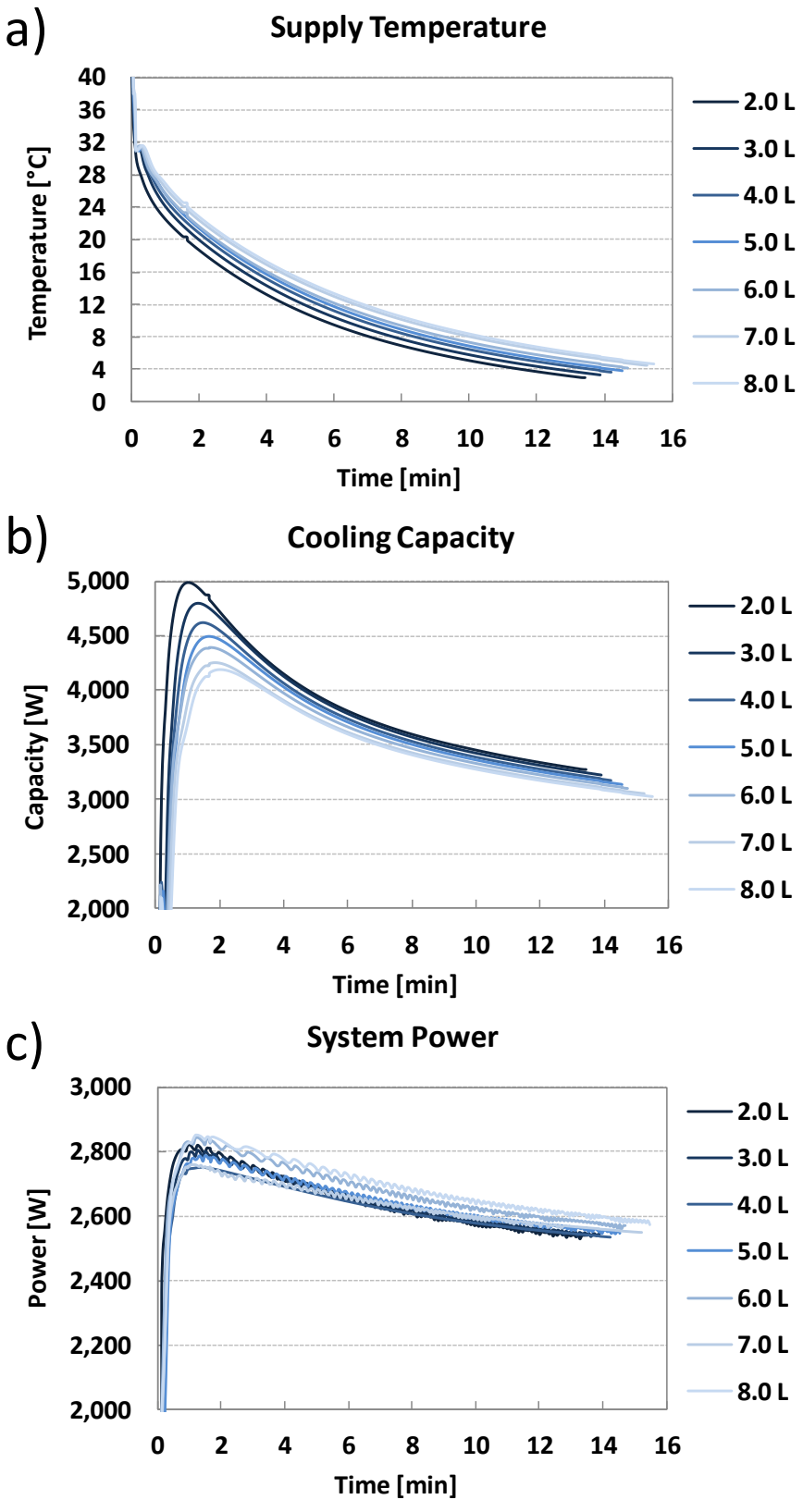

Figure 11.11: Influence of Coolant Volume on Cabin Pull-down (R290 2LP, T30/RH50, 12 K soak, 1550 rpm, 250 g/s)

The influence of coolant volume on the system power during cabin warm-up is presented in Figure 11.12 c). Since the compressor is turned off, only the coolant pump is contributing to power consumption. A larger coolant volume results in longer tubing, as well as a lower coolant temperature during cabin warm-up. Consequently, power consumption during off-cycle periods increases with increasing coolant volume. The relative increase can be as much as 3%-4% per additional liter of coolant, but the absolute increase is small.

Figure 11.13 shows the influence of coolant charge on typical pull-down performance metrics, such as time to comfort, energy consumption during the course of the cabin pull-down, and transient performance factor. It can be observed that time to comfort increases by about 22 seconds per additional liter of coolant. At the same time, energy consumption increases by about 17 Wh per additional liter of coolant, as observed in Figure 11.13 b). Figure 11.13 c) shows the influence of coolant volume on transient performance factor. It was found that each additional liter of coolant decreases TPF by about 0.03.

While some of the above mentioned results may vary based on system configuration and operating conditions, this parametric study provided a qualitative answer to the question of influence of coolant volume on transient system performance. In summary, it can be stated that small variations in coolant charge below 1 to 2 liters may not result in significant changes of thermal performance and passenger comfort.

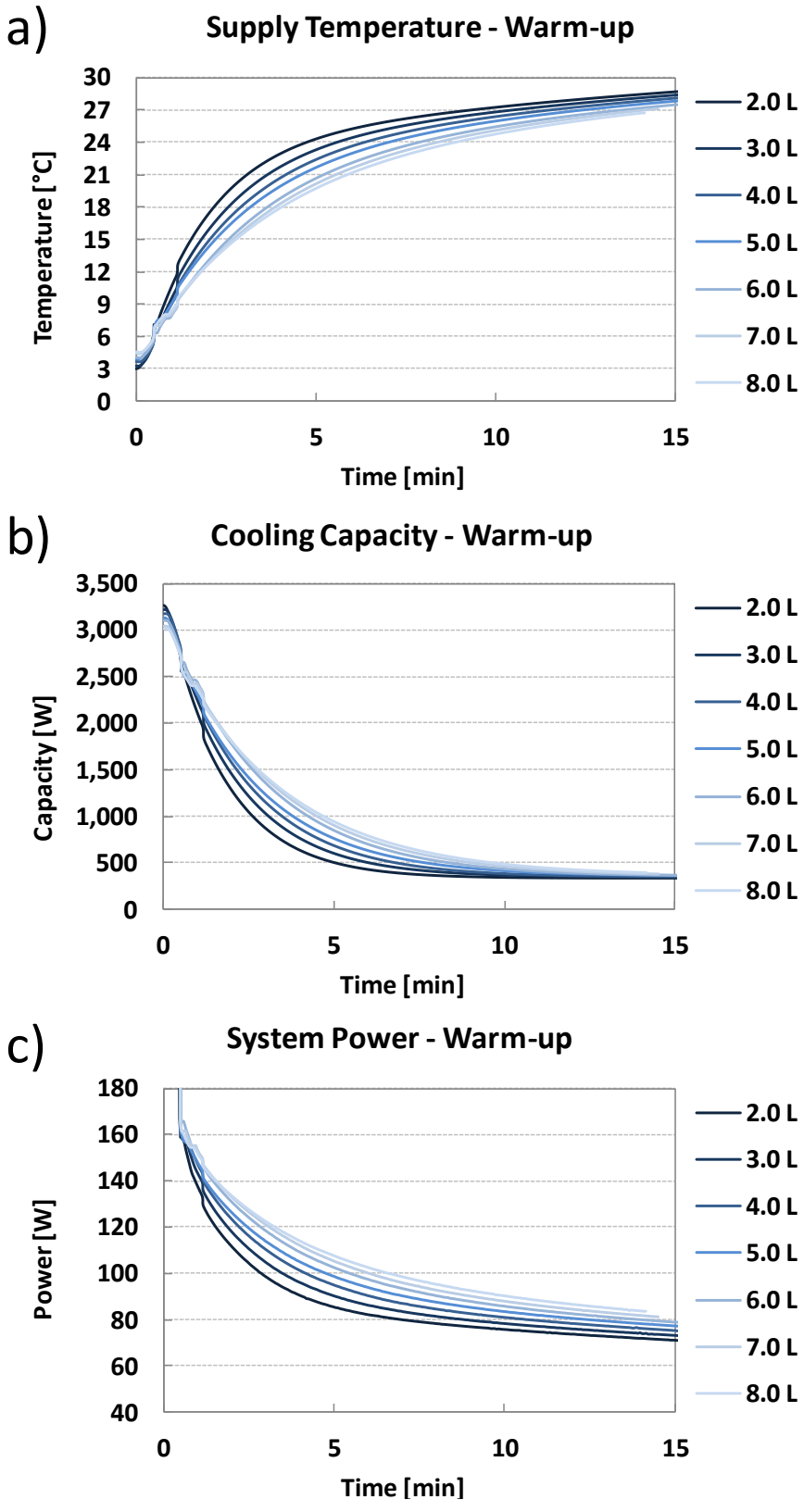

Figure 11.12: Influence of Coolant Volume on Cabin Warm-up (R290 2LP, T30RH50, 12 K soak, 1550 rpm, 250 g/s)

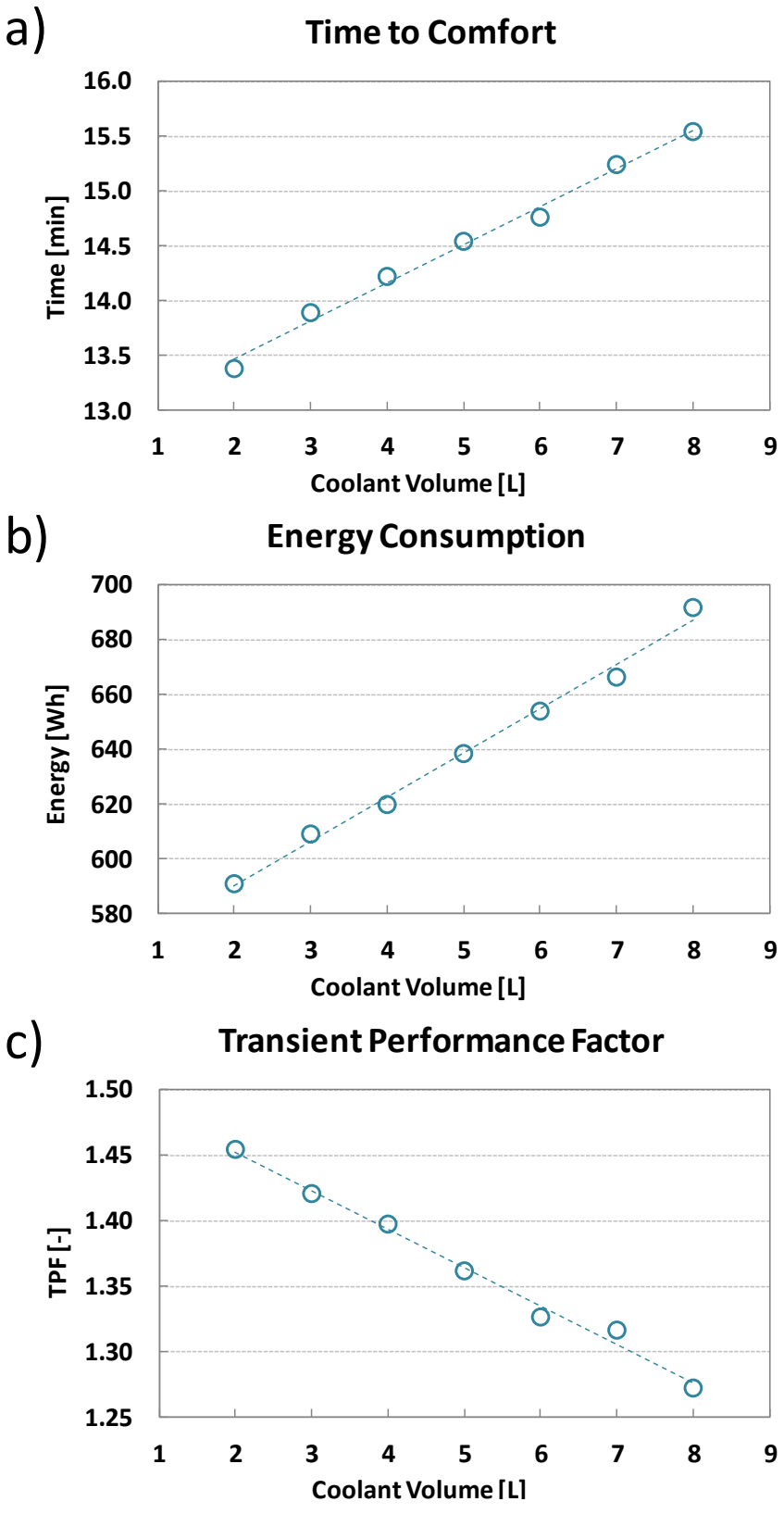

Figure 11.13: Influence of Coolant Volume on Performance Metrics (R290 2LP, T35RH50, 12 K soak, 1550 rpm, 250 g/s)

11.5 Influence of Coolant Concentration on Transient Performance

Previous research on secondary loop systems by Ghodbane [104] used a coolant mass fraction of 32wt% ethylene glycol in water. It was accepted that the mixture could freeze in harsh winter conditions, but the pressure would stay below the burst pressure of the tubing. The research was performed under the assumption that the secondary loop system would be used for cabin cooling in the summer only. However, recent developments (Eilemann [132], Battista [133], Di Sciullo [134], Petitjean [135], Seccardini [136], etc.) show that secondary loop systems (also called indirect systems) may be used for general thermal management in future vehicles. Possibly, engine thermal management, thermal management of batteries and auxiliary systems, as well as passenger cabin thermal management could be combined into one compact, smart thermal management system. Since this system would need to be operated in low ambient winter conditions as well, a coolant mass fraction of 32wt% ethylene glycol may not be permissible. Based on the freezing temperature of water-ethylene glycol mixtures with varying concentration, shown in Figure 11.14, a 32wt% mixture will freeze at roughly -15°C. For countries with a strong winter, coolant concentration may need to be increased to 50wt% or above. In countries with a yearlong hot climate, it may be beneficial to reduce coolant concentration to 20wt% or below to take advantage of the better heat transfer properties of pure water. The R290 2LP Modelica® model was used to investigate the influence of coolant concentration on the transient performance of a secondary loop system during cabin pull-down and cabin warm-up.

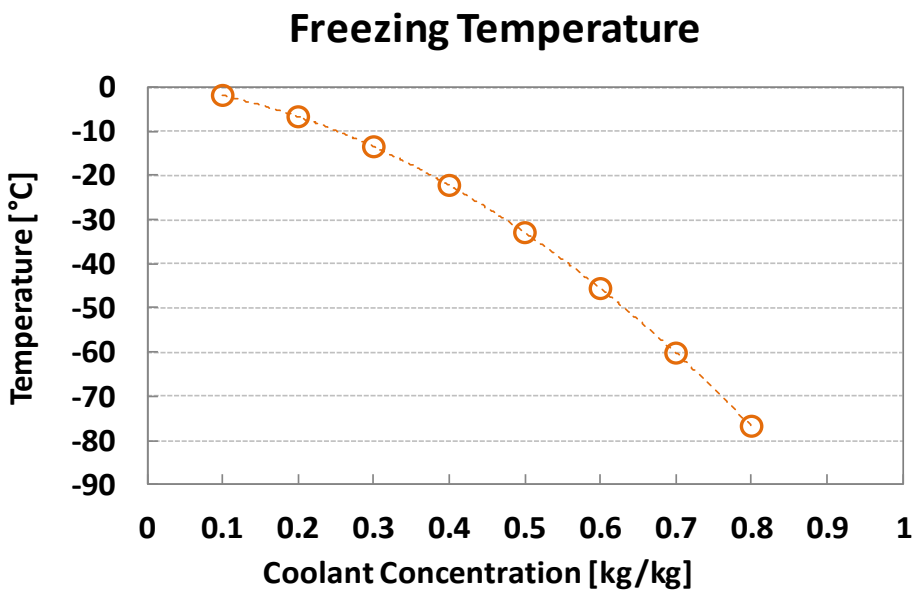

Figure 11.14: Change of Freezing Temperature of an Aqueous Ethylene Glycol Mixture based on Mass Fraction

The simulation was performed under an ambient temperature of 30°C, ambient relative humidity of 50%, and an initial soak of 12 K. A compressor rpmof 1,550, as well as a coolant mass flow rate of 250 g/s were assumed. After the cabin reached a comfort temperature of 24°C, the compressor was turned off and the cabin was allowed to warm up. The following paragraphs discuss the results of the pull-down portion, as well as the cabin warm-up portion of the simulation.

Figure 11.15 shows the influence of water-ethylene glycol concentration on the cabin pull-down process. It can be observed that at 10% difference in mass fraction may result in a 0.8 K difference during the initial minutes of the pull-down process. At the end of the pull-down (after ~15 min) the difference in supply temperature per 10% change in mass fraction decreases to 0.25 K.

Cooling capacity, shown in Figure 11.15 b), is not significantly affected by coolant mass fraction past the first two minutes into the pull-down process. However, system power consumption, shown in Figure 11.15 c), changes significantly due to the change in coolant pump power consumption. As the glycol mass fraction increases, viscosity and density increase, resulting in an increase in pressure drop and pressure head. At the end of the pull-down process, instantaneous system power consumption may be increased by as much as 2.4% per 10% increase in coolant mass fraction.

Figure 11.16 presents the influence of coolant mass fraction on the warm-up process of the cabin during an off-cycle period. As can be observed in Figure 11.16 a), the influence of coolant mass fraction on supply temperature during cabin warm-up is nearly constant throughout the first 15 minutes of the off-cycle period. Supply temperature increases by about 0.4 K for every 10% increase of glycol mass fraction. This is due to the additional capacity available for low mass fraction coolants, as observed in Figure 11.16 b). While the change in mass fraction represents a significant change in cooling capacity during the later stages of the off-cycle period, when cooling capacity is low, the influence on power consumption is significant. Due to the increased pump power at high glycol mass fractions, instantaneous off-cycle period power consumption may increase -on average- by about 15 W per 10% increase in glycol mass fraction.

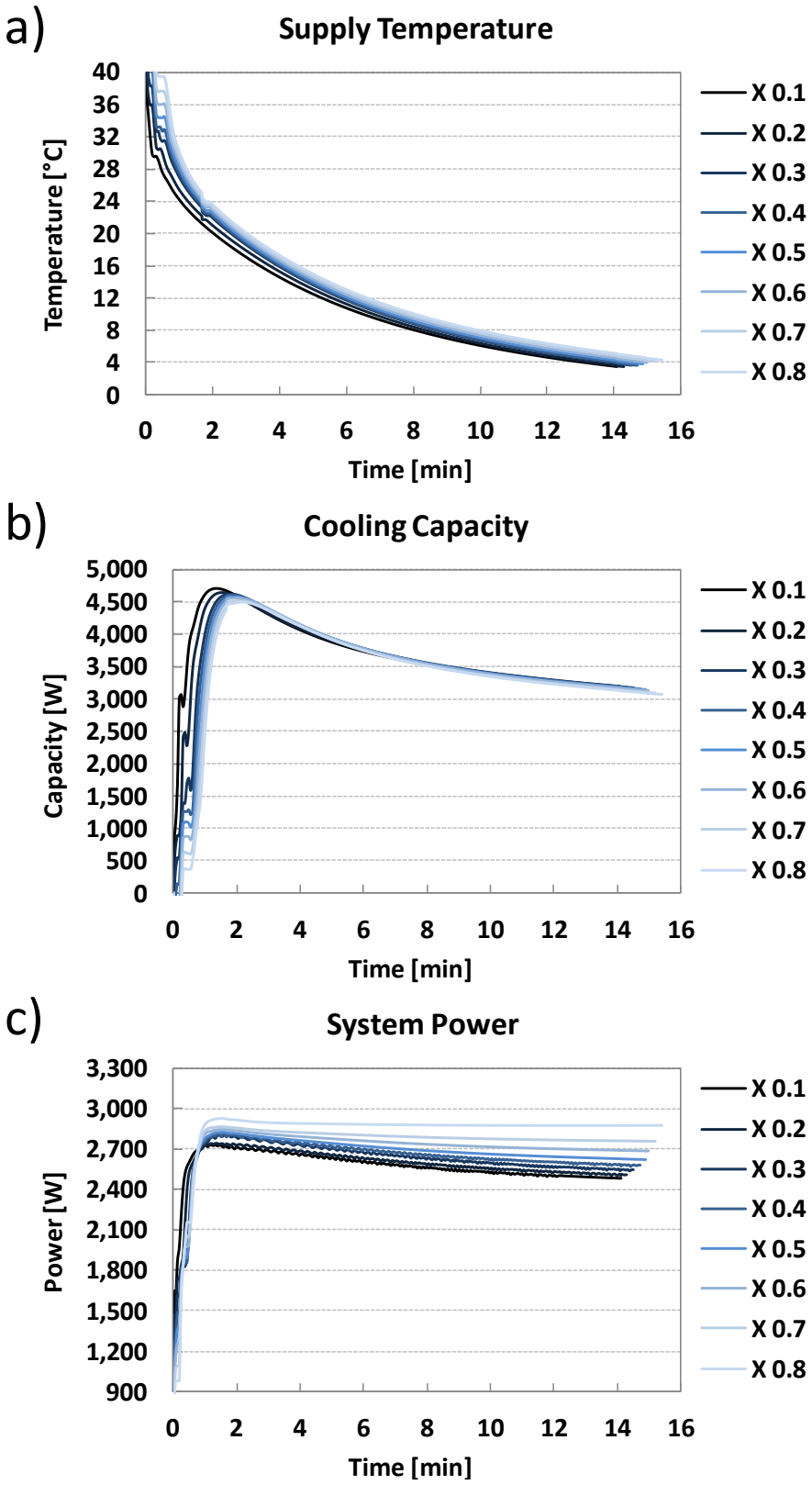

Figure 11.15: Influence of Coolant Concentration on Cabin Pull-down (R290 2LP, T30RH50, 12 K soak, 1550 rpm, 250 g/s)

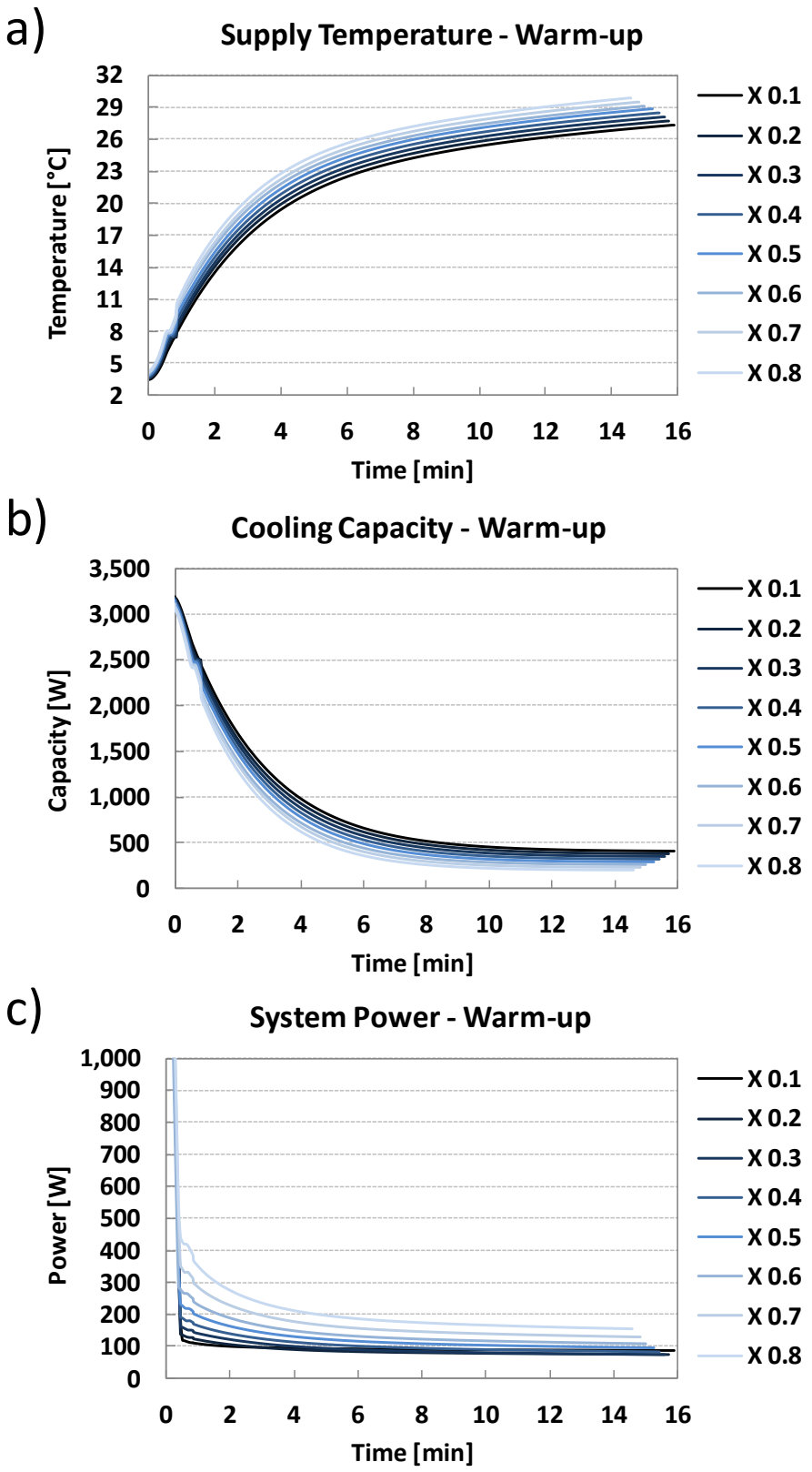

Figure 11.16: Influence of Coolant Concentration on Cabin Warm-up (R290 2LP, T30RH50, 12 K soak, 1550 rpm, 250 g/s)

Figure 11.17 shows the effect of coolant concentration on typical performance metrics for a pull-down process. Time to comfort is nearly linearly dependent on the glycol mass fraction and increases by roughly 12 seconds per 10% increase in mass fraction. As shown in Figure 11.17 b), a 10% increase in coolant mass fraction result in a 18 Wh increase of energy consumption (~2.8% relative increase). TPF decreases by about 0.035 for a 10% increase in coolant concentration.

The mass fraction range of interest is marked by a shaded area in Figure 11.17 a) through c). It was found that when changing from a 30% glycol mass fraction to a 60% mass fraction time to comfort is expected to increase by about half a minute. Energy consumption during a pull-down would be increased by about 7.8%, while TPF is expected to decrease by about 0.1.

It can be concluded that glycol mass fraction has only little influence on time to comfort, while it has a more significant influence on thermal comfort during off-cycle periods. To save energy and reduce pull-down-time, it would be advantageous to reduce glycol mass fraction, possibly below 30%. However, increasing mass fraction to 50% or 60% may result in an increase of energy consumption of about 8% or less and a small increase in time to comfort.

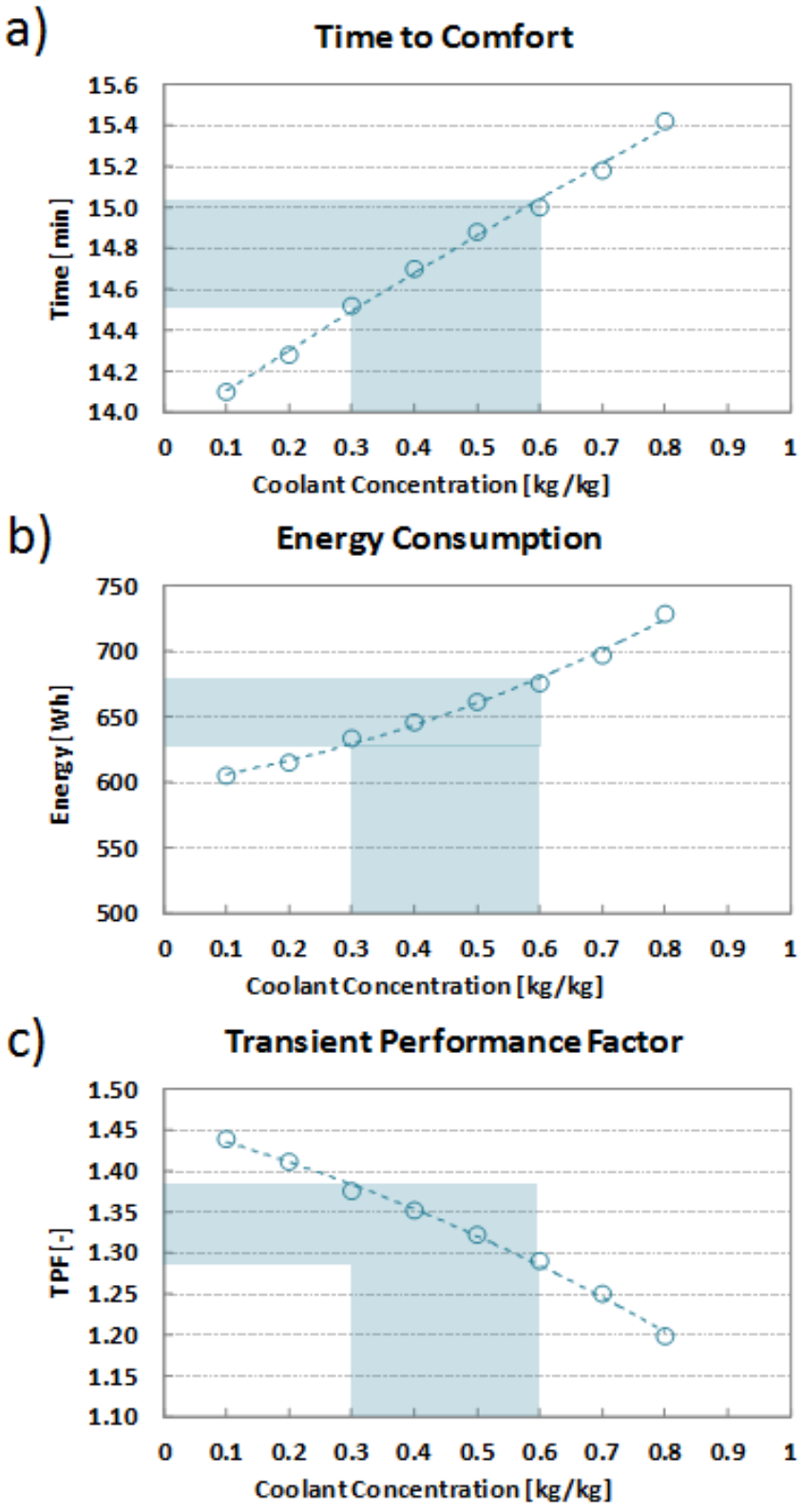

Figure 11.17: Influence of Coolant Concentration on Performance Metrics (R290 2LP, T30RH50, 12 K soak, 1550 rpm, 250 g/s)

12 Summary and Future Work

The present research focused on the performance evaluation of secondary loop systems for automotive air-conditioning. The use of efficient and inexpensive refrigerants, as well as the potential to reduce A/C energy consumption by applying thermal storage alternatives were investigated.

12.1 Research Contributions

The present research resulted in the following contributions:

- Development and operation of a dynamic laboratory-scale test bench, which allows for testing of drive cycles in changing climates and enables the testing of A/C control algorithms
- Conclusive characterization of transient performance of secondary loop systems during pull-down and drive cycle tests
- Experimental evaluation of Propane in automotive secondary loop air-conditioning systems with respect to energy consumption and transient performance
- Quantification of benefits from secondary loop thermal storage during short off-cycle periods in drive cycles and prolonged off-cycle cabin warm-up
- Experimental characterization of the benefits of ice storage in secondary loop systems
- Evaluation of alternative control strategies and cabin pre-conditioning in electric vehicles with regard to reducing A/C energy consumption for secondary loop systems with thermal storage

- Development of a validated model to perform transient simulation of secondary loop systems in Modelica

12.2 Summary of Research Outcomes

A summary of outcomes for the present research is given as follows:

- A test facility was built to test direct expansion, as well as secondary loop systems. Controls were implemented to allow for drive cycle testing and investigation of A/C control strategies. A passenger cabin model, first developed in previous research, was modified to include typical A/C controls, as well as the ability to use ambient drive cycles (temperature, relative humidity, and solar insolation)

- A secondary loop system using R152a as primary refrigerant was tested in steady-state, as well as transient operation. Using the same components as a baseline R134a direct expansion system, the R152a 2LP system showed a reduced power consumption at about the same capacity. Steady-state COP was increased by up to 10%. During transient pull-down tests, the secondary loop system showed some thermal lag, as well as increased power consumption. Although time to comfort was increased, the transient performance factor was within 5% of R134a DX results. Due to increased thermal mass, the energy available to cool the air during an NEDC test decreased by about 10%. Due to a slight increase in power consumption (5%), TPF decreased by 10%.

- R290 was investigated as possible refrigerant in the VCC of secondary loop systems. Regular R134a components were used in the VCC. Compressor speed was adjusted to simulate a smaller compressor and reduce high cooling capacity and compressor power consumption. The R290 2LP system was found to perform well with an increase in COP

of 8% in comparison to R134a DX during highway driving operation. When idling, COP decreased by 15% from R134a DX. The decrease in efficiency was attributed to low compressor isentropic and volumetric efficiencies at idling conditions. Due to the adjustment of compressor rpm, the comparison of transient accumulated capacity and power consumption was somewhat ambiguous. However, TPF for pull-down at highway driving conditions was similar or better than R134a DX TPF. For NEDC testing, R290 2LP TPF was decreased by 5% with respect to R134a DX, showing a better performance than R152a 2LP. It was concluded that if the cycle, primarily the compressor, would be optimized for R290, the R290 2LP system could achieve a performance significantly better than an R134a direct expansion system.

- The thermal storage potential of secondary loop systems and it's benefits for thermal comfort and energy consumption were investigated. New test procedures were defined for this research. During Start/Stop operation R290 2LP TPF was equal to R134a DX TPF. When tripling the off-cycle periods in the cycle (traffic light stops), R290 2LP TPF increased by roughly 10% over R134a DX TPF. While preserving thermal comfort, the secondary loop system also achieved a better thermal performance with increasing length of off-cycle periods. For cabin warm-up during extended off-cycle periods, the secondary loop system was able to keep the cabin 3 K lower, while cabin humidification due to re-evaporation was reduced.

- The possibility of using ice storage for added thermal comfort and reduced power consumption during commutes was evaluated. The present research used a custom made heat exchanger in a 15 L ice storage tank, which was charged by the R290 vapor compression cycle. It was observed that ice storage could reduce time to comfort by more than 15%, while reducing the power consumption of the

compressor. However, for long periods a bypass should be used once evaporating temperature decreased to the point where ice storage prevents a faster pull-down. During off-cycle periods after a pull-down to comfort temperature, the present ice storage box was able to sustain thermal comfort and prevent excessive cabin humidification for more than 20 minutes.

- The benefits of alternative compressor controls and cabin pre-conditioning with regards to reducing power consumption in electric vehicles were investigated. It was found that total energy consumption, including re-heating, can be reduced by as much as 60% when controlling cabin supply humidity with either compressor speed or by cycling. Using ice storage together with alternative control strategies showed the most benefits for cyclic operation, rather than continuous operation. Cabin pre-conditioning was found to be detrimental for the traditional concept of compressor cycling for frost prevention and re-heating for temperature control. In contrast, when employing alternative control strategies where the compressor cycles to control cabin supply humidity while cabin temperature is close to the comfort setpoint, energy savings of up to 30% were observed by pre-conditioning the cabin.

- Models of the passenger cabin and the secondary loop system were developed in the Modelica language. Models of an automotive direct expansion system, the secondary loop system, and the passenger cabin were validated with experimental data for steady-state operation, as well as transient pull-down and drive cycle operation. The models were further used to evaluate the influence of coolant volume and coolant concentration on transient system performance.

12.3 Recommendations for Future Work

Based on experience from the present research, current developments in the area of automotive air-conditioning, and insights from reviewed literature, the following recommendations are given for possible future work:

- The automotive air-conditioning industry is moving towards an integrative approach, in which the thermal management system of the front end is partially integrated with the climate system and auxiliary thermal management tasks, such as battery or electronics cooling. It is recommended to focus future research on completely indirect systems, where both, the A/C condenser, as well as the cabin air cooler are cooled by a secondary (indirect) coolant loop.

- With the alternative cooling strategies discussed in the present research, it was possible to reduce total power consumption in electric vehicles considerably. Another big step in reducing power consumption could be achieved by removing the need of some kind of heater power for re-heating. To this end, the indirect loop which cools the A/C condenser could be used for re-heating the cabin air. Re-heating for summer cooling operation is typically only needed 10+ minutes after the air-conditioning is turned on and enough heating capacity is available at the condenser. Energy savings and implications of this solution should be quantified by experiment.

- In addition to cooling, heating for winter operation is a challenging task for electric vehicles. The use of secondary loop systems for heat pumping needs to be investigated. Thermal storage, possibly ice storage, could be used to provide a relatively high fixed temperature for the heat pump when operating in sub zero ambient conditions. Transient simulations, as well as experiments should be performed to quantify benefits and challenges

- Thermal storage may be a key technology in electric vehicles, both for summer time cooling, as well as winter time heating. In the present research, the use of ice storage was investigated, using a custom made heat exchanger. A second generation heat exchanger, optimized for the task at hand could improve the performance of such a system. While ice as a phase change material is conveniently available, well understood and ready to use, the present research should be extended to include other phase change materials, which can be integrated more seamlessly into the existing thermal management system.

- The present cabin passenger model is a lumped model, working with energy and mass balances. A more sophisticated, multi-dimensional model of the passenger cabin would open the door to thermal comfort research. The use of indirect cooling loops in the summer, as well as in the winter would lend itself to the operation of radiant heat exchangers in the cabin, as well as seat cooling and heating. Numerous studies in the residential and commercial air-conditioning area show that the use of radiant hydronic systems increases energy efficiency and reduces the need for extremely low (or high) cabin air temperatures. A multi-dimensional model of the cabin in Dymola, as well as a thermal comfort model will be needed for this research.

Appendix A Specification of Test Facility Components

Appendix A provides the specifications of the main components, used in the experimental test facility. Parameters and dimensions are given to the best knowledge of the author. Heat exchanger outer dimensions were measured where possible, and inner dimensions were estimated based on outer dimensions. Specifications of compressor, pump, and valve are given based on manufacturer's data.

Table A.1 provides specifications for the automotive evaporator used only in the direct expansion baseline system. The evaporator was a plate and fin heat exchanger with louver fins and unknown inner geometry.

Table A.1: Evaporator Specifications

Parameter	Magnitude	Unit
Number of passes	2	[-]
Number of tubes per pass	20	[-]
Number of ports per tube*	8	[-]
Tube pitch	0.01358	[m]
Tube length	0.2125	[m]
Tube depth	0.035	[m]
Tube height	0.00333	[m]
Fin depth	0.035	[m]
Fin density	12.9	[1/in]
Fin thickness	0.00008	[m]
Port hydraulic diameter*	0.001814	[m]
Inner Volume	0.000711	[m^3]

*values estimated based on outer dimensions

Table A.2 provides specifications for the automotive condenser used in all system configurations throughout this study. The condenser was a micro channel

heat exchanger with louver fins and unknown port geometry. It did not feature an integrated receiver-dryer, as some other models do.

Table A.2: Condenser Specifications

Parameter	Magnitude	Unit
Number of passes	1	[-]
Number of tubes per pass	35	[-]
Number of ports per tube*	12	[-]
Tube pitch	0.01095	[m]
Tube length	0.66	[m]
Tube depth	0.0185	[m]
Tube height	0.002	[m]
Fin depth	0.0185	[m]
Fin density	17	[1/in]
Fin thickness	0.00008	[m]
Port hydraulic diameter*	0.00075	[m]
Inner Volume	0.000292	[m^3]

*values estimated based on outside dimensions

Table A.3 provides specifications for the intermediate heat exchanger used in the secondary loop system. The intermediate heat exchanger was a commercially available plate type heat exchanger with unknown inner geometry.

Table A.3: Intermediate Heat Exchanger Specifications

Parameter	Magnitude	Unit
Rated capacity (R134a)	6.1	[kW]
Rated pressure drop	7.6/3.7	[kPa]
Number of channels	11/12	[-]
Refrigerant-side volume	0.000935	[m^3]
Refrigerant-side volume	0.00102	[m^3]

Table A.4 provides specifications for the cooler used in the secondary loop system. The cooler was a micro channel heat exchanger with louver fins and unknown port geometry.

Table A.4: Cooler Specifications

Parameter	Magnitude	Unit
Number of passes	2	[-]
Number of tubes per pass	36	[-]
Number of ports per tube*	12	[-]
Tube pitch	0.00675	[m]
Tube length	0.216	[m]
Tube depth	0.028	[m]
Tube height	0.0015	[m]
Fin depth	0.028	[m]
Fin density	18	[1/in]
Fin thickness	0.00009	[m]
Port hydraulic diameter*	0.00123	[m]
Inner Volume	0.000877	[m^3]

*values estimated based on outside dimensions

Table A.5 provides specifications for the compressor used in all system configurations throughout this study. The compressor is a variable speed, fixed displacement compressor. The efficiency information given in the table was back calculated from experimentally measured data and is a rounded average over a several ambient conditions and compressor speeds.

Table A.5: Compressor Specifications

Parameter	Magnitude	Unit
Displacement	75	[cm^3]
Maximum speed	6500	[rpm]
Volumetric efficiency*	0.9	[-]
Isentropic efficiency*	0.8	[-]

*average values, determined from experimental measurement

Table A.6 provides the specifications for the electronic expansion valve used in all system configurations throughout this study.

Table A.6: Expansion Valve Specifications

Parameter	Magnitude	Unit
Rated evaporating temperature	4.44	[°C]
Rated differential pressure	650	[kPa]
Rated Capacity (R134a)	7.53	[kW]
Number of steps	500	[-]

Table A.7 provides specifications for the coolant pump used in the secondary loop system. The coolant pump is a gear pump.

Table A.7: Coolant Pump Specifications

Parameter	Magnitude	Unit
Maximum differential pressure	690	[kPa]
Motor rated power	0.33	[hp]
Motor rated rpm	1725	[rpm]

Appendix B Control Flow Charts

Appendix B provides flow charts for the controls of the facility and facility components.

Figure B.1 shows the flow chart of the Cabin Model. The flow chart describes the various controls embedded in the Cabin Model, including the option to use pre-defined ambient drive cycles, the option to use a virtual heater core to artificially raise supply temperature, and the option to either turn off or enable the continuous measurement of evaporator/cooler air flow rate after the compressor is turned off (used during off-cycle testing). The Cabin Model is turned on and off by a switch, embedded in the LabVIEW GUI of the Main DAQ Ctrl.

A more detailed description of the virtual heater core is given in the thermostat control flow chart, Figure B.2. The flow chart describes the operation of the virtual heater core, once thermostat control was activated. The heater is typically only used when the compressor is running, otherwise the original supply temperature is not altered. If heating functionality is needed to preserve comfort temperature, an artificially heightened supply temperature signal, controlled by a software PID control, is fed to the Cabin Model equations.

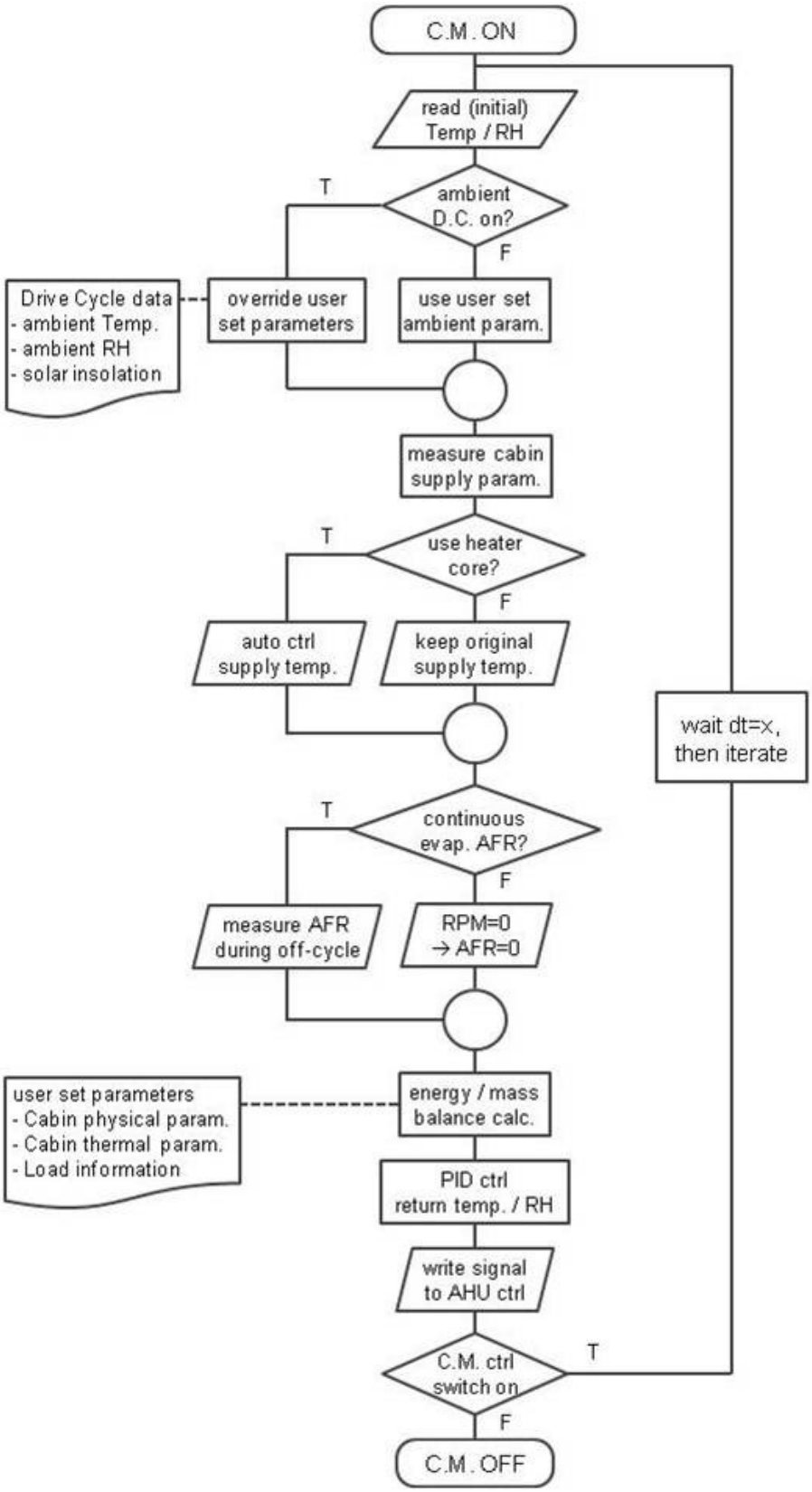

Figure B.1: Cabin Model Flow Chart

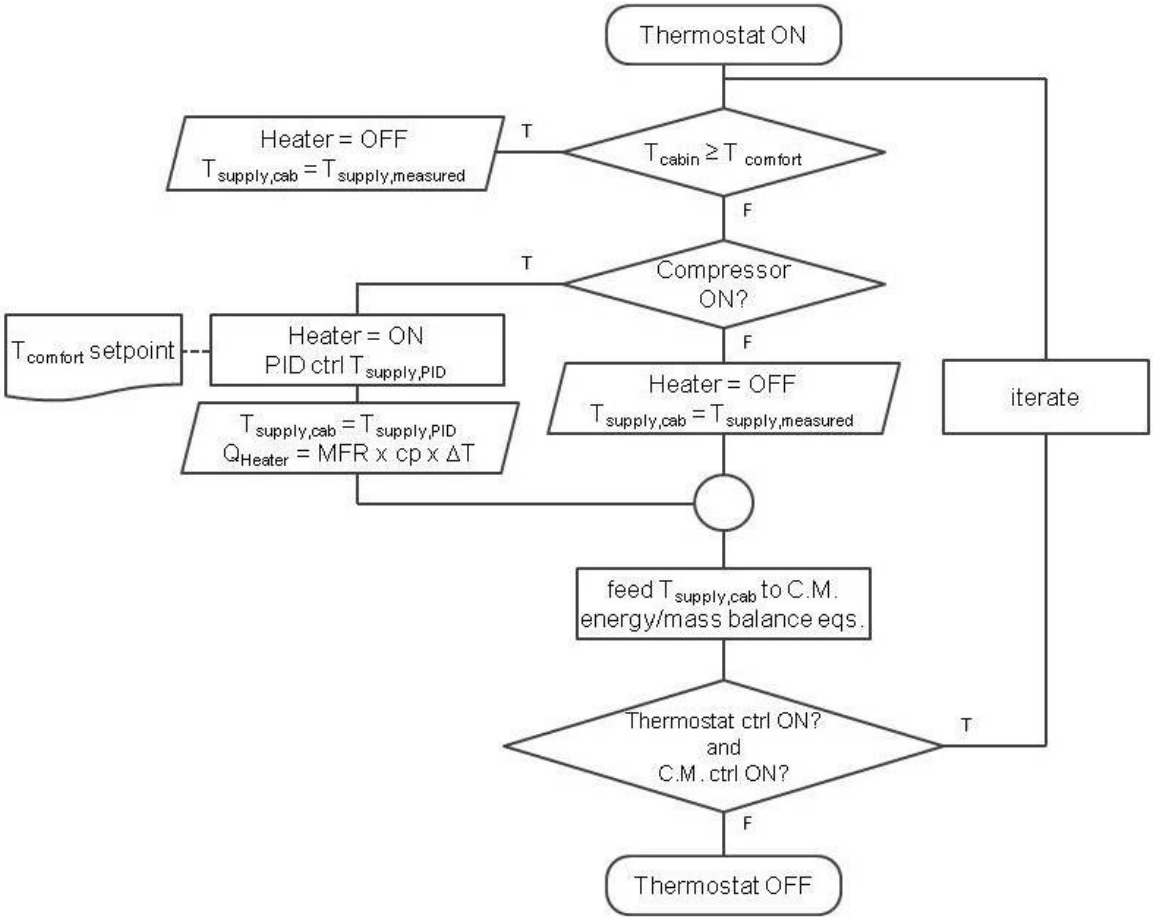

Figure B.2: Thermostat Control Flow Chart

The drive cycle module, shown in Figure B.3, uses PID control to operate components of the test facility. Since the setpoint profile is known, setpoints of future time steps can be used to control components more accurately (feed forward control). The output signal can be confined to a minimum and maximum magnitude to stay within safe operating conditions (e.g.: to prevent a full closing of the EXV). The drive cycle module moves forward to the next entry in the respective drive cycle file, until the last entry of the profile.

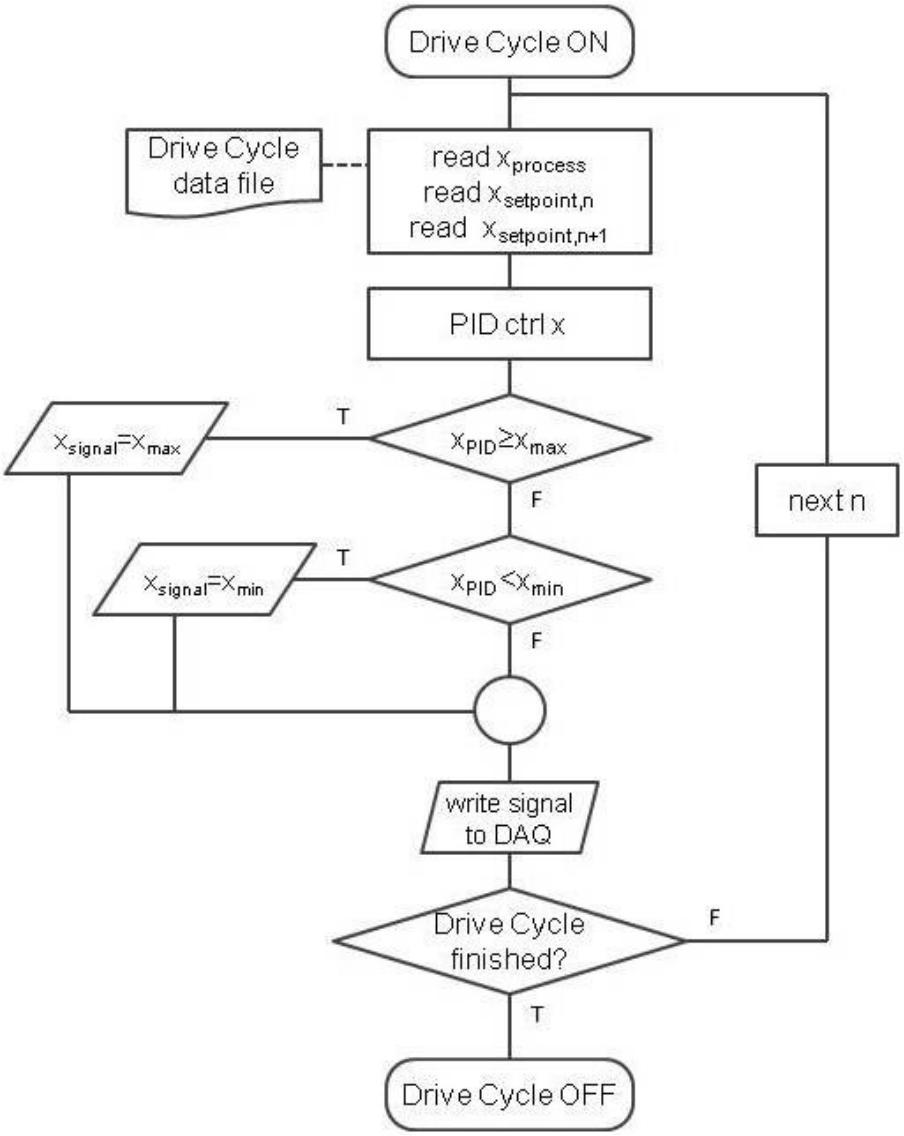

Figure B.3: Drive Cycle Control Flow Chart

Two electronic expansion valves were used in the test facility to control superheat. The EXV flow chart, shown in Figure B.4, provides information about control on the top level (one valve used vs. both valves used), and on the valve level. Valves can be controlled either manually, by emergency override, or by PID control, which is the usual operation mode. Manual control, as well as the

emergency override function are used mainly during tuning of the PID control to prevent erratic behavior, which could damage the compressor. To prevent loss of superheat for an extended time, a sub function, which reduces EXV opening in pre-defined increments, was added.

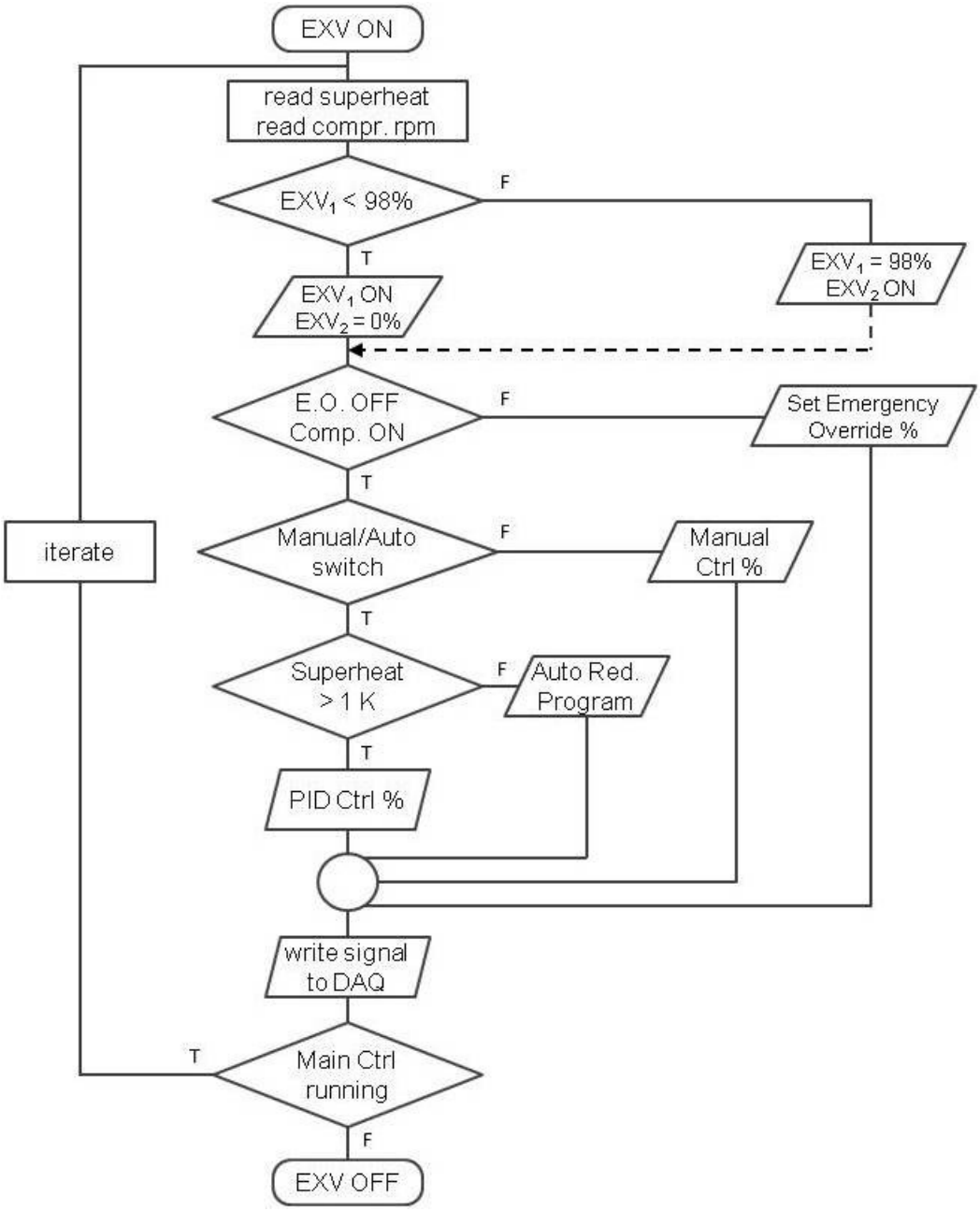

Figure B.4: Electronic Expansion Valve Flow Chart

Figure B.5 shows the flow chart of the coolant pump control. The pump can either be controlled manually, or by PID control. In the latter case, the control variable can be either MFR, or cabin temperature. During temperature control mode, the pump can be cycled on and off to keep cabin temperature close to the comfort setting. Similarly, pump speed can be reduced using PID control to reduce power consumption as much as possible, while cabin temperature is close to or lower than comfort setpoint.

Figure B.6 shows the flow chart for the control of compressor clutch and compressor rpm. The compressor can be controlled in seven ways, six of which are shown in Figure B.6. The seventh is drive cycle control, with a pre-determined compressor speed and clutch actuation profile. The first operation mode is manual operation, in which the compressor rpm and the clutch actuation can be chosen from the GUI of the Main DAQ Ctrl. The pump temperature control mode turns off the compressor clutch, precluding the VCC from cooling the cabin. Pull-down off-cycle mode turns off the compressor clutch, once a pre-defined comfort temperature is reached in the passenger cabin. The temperature in the cabin will subsequently rise, without the compressor turning back on. Compressor defrost cycling, relative humidity cycling, and continuous compressor control are modes used for air-conditioning controls research. All three modes of operation are used to keep the cabin at a stable temperature, once comfort conditions have been achieved. In relative humidity cycling and continuous mode, relative humidity is controlled in addition to cabin temperature.

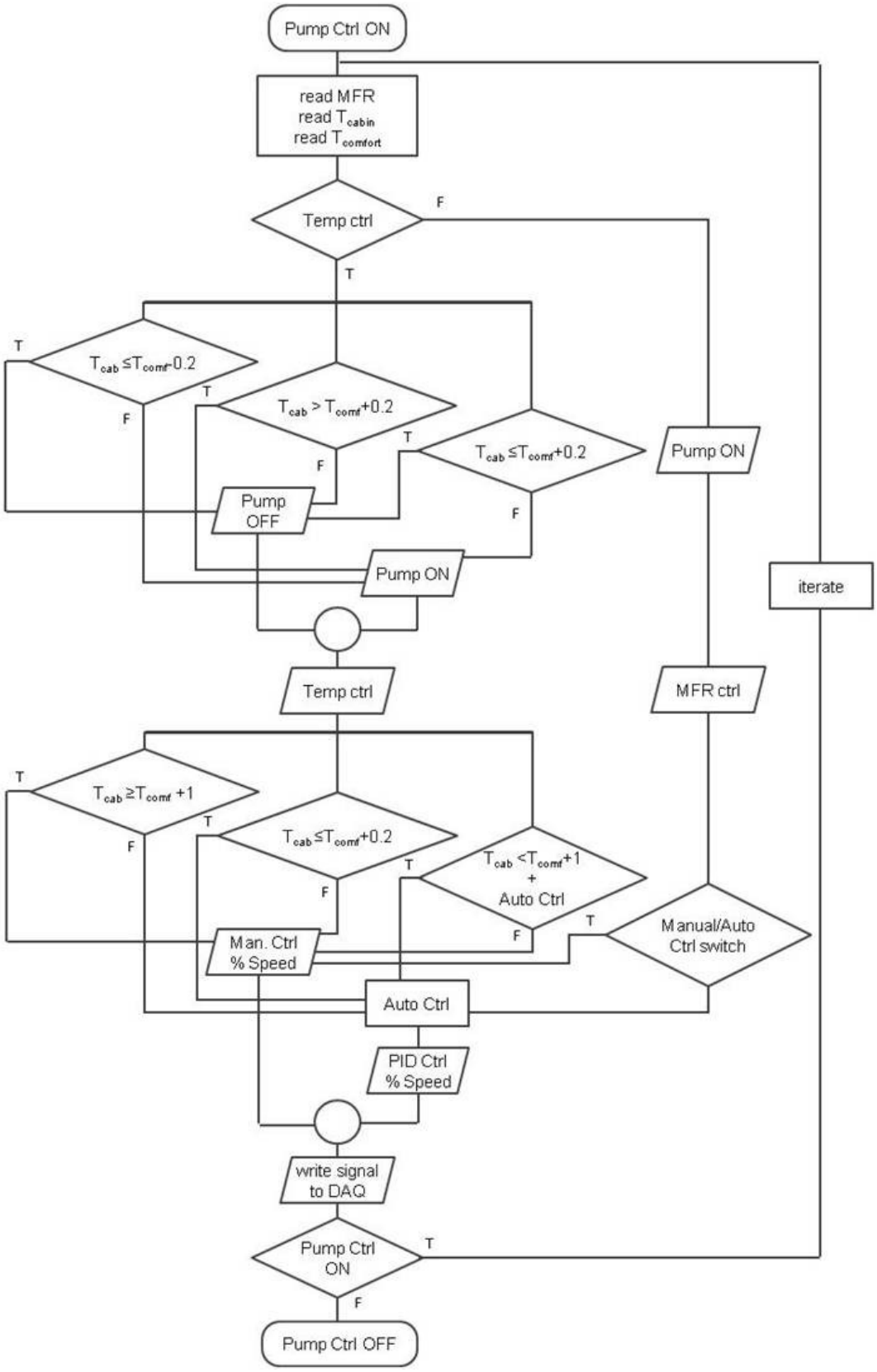

Figure B.5: Coolant Pump Control Flow Chart

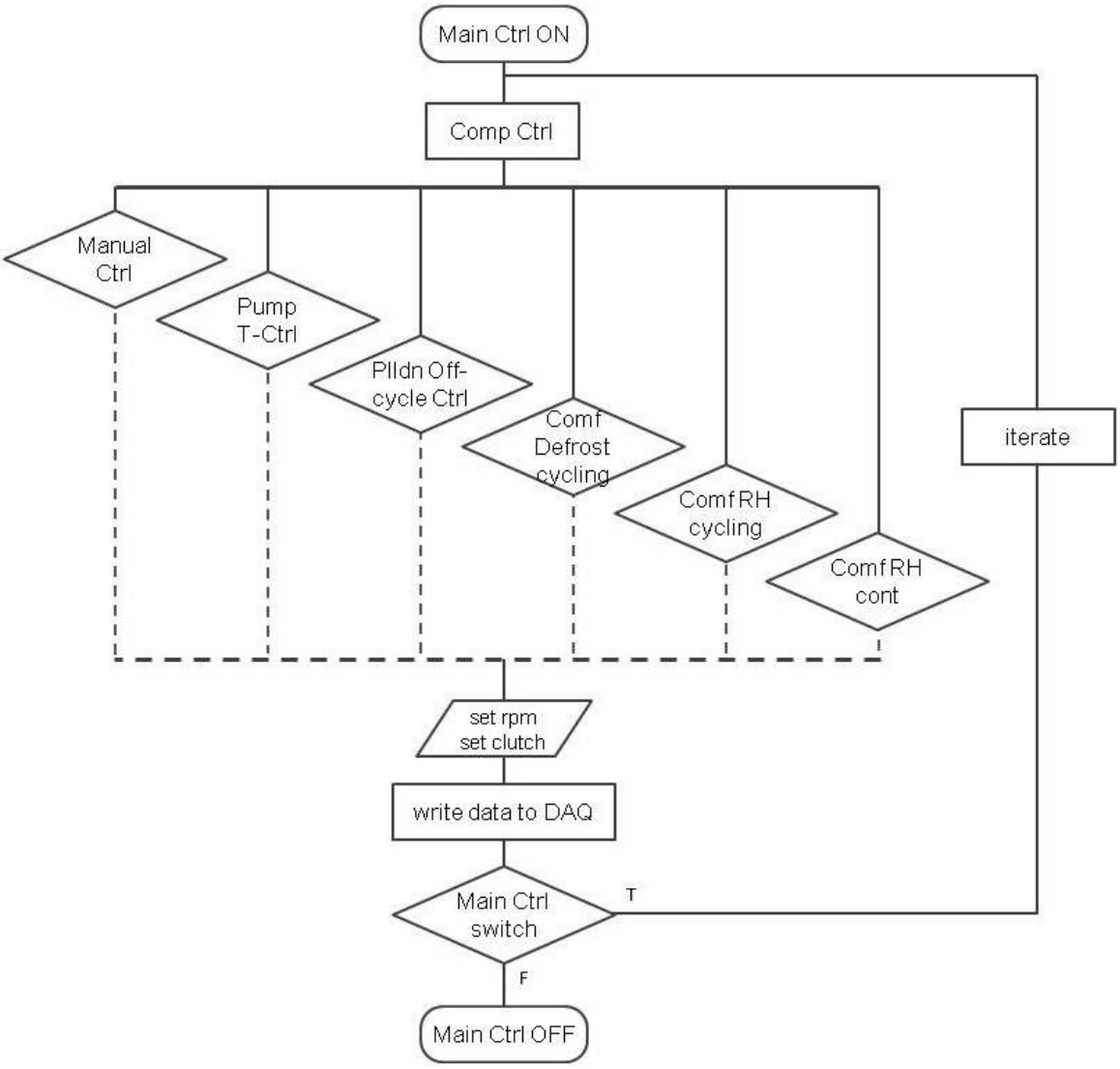

Figure B.6: Compressor Control Flow Chart

The controls outlined in Figure B.6 are shown in detail in the following flow charts.

Figure B.7 shows the manual control flow chart. In the Main Ctrl DAQ GUI, the user can set the desired rpm, as well as turn on and off the compressor clutch.

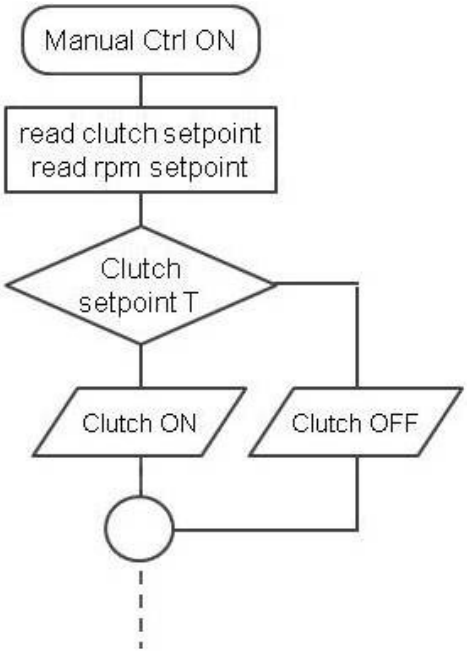

Figure B.7: Manual Compressor Control Flow Chart

Figure B.8 shows the control chart for temperature control mode of the pump. This control mode is used when only ice storage is used to cool the cabin. Consequently, the compressor clutch remains turned off while in this mode and the thermostat function remains disabled.

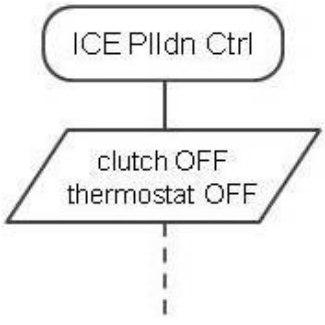

Figure B.8: Pump Temperature Control Flow Chart

The pull down control, shown in Figure B.9, enables the recording of off-cycle pull down data. The control turns off the compressor clutch, once comfort temperatures are achieved during a pull down test. A flag is set to prevent the compressor from turning on once the cabin temperature starts increasing during the off cycle.

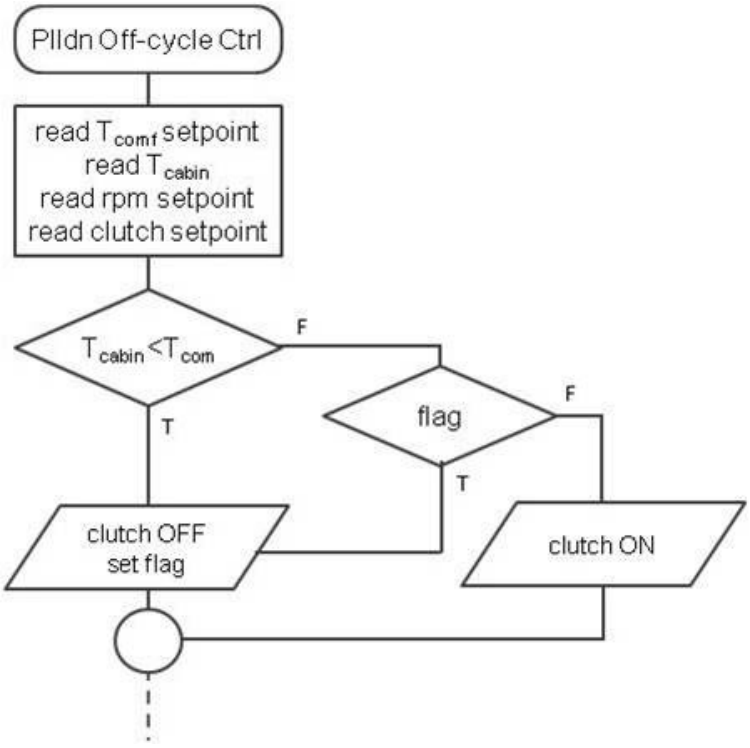

Figure B.9: Compressor Pulldown Control Flow Chart

Figure B.10 shows the defrost cycling control chart. Once air-side evaporator outlet temperature decreases below a certain set point, the compressor shuts odd to prevent frosting.

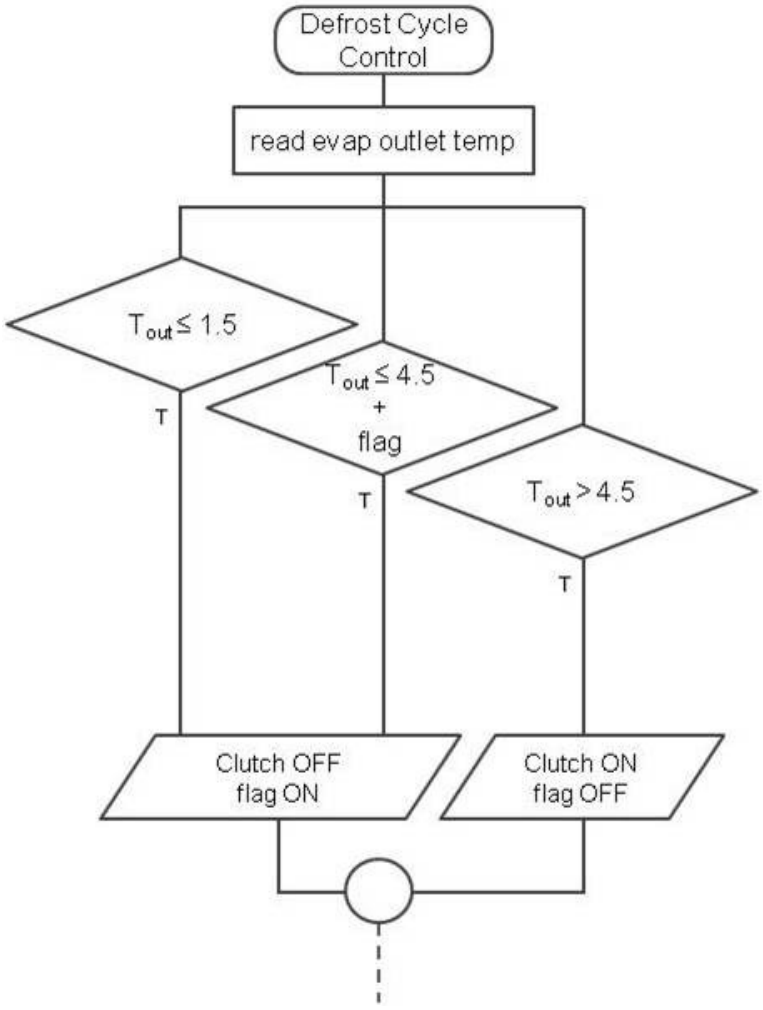

Figure B.10: Defrost Cycling Control Flow Chart

Figure B.11 shows the flow chart for relative humidity cycling control. If cabin temperature gets close to comfort temperature, the compressor starts controlling relative humidity of the cabin supply air stream, rather than prioritizing to pull the cabin temperature down further. The thermostat control is used to prevent cabin temperature from dropping below comfort setpoint. If the cabin temperature is close to comfort conditions and the relative humidity of the supply air is low enough, the compressor is turned off to save energy.

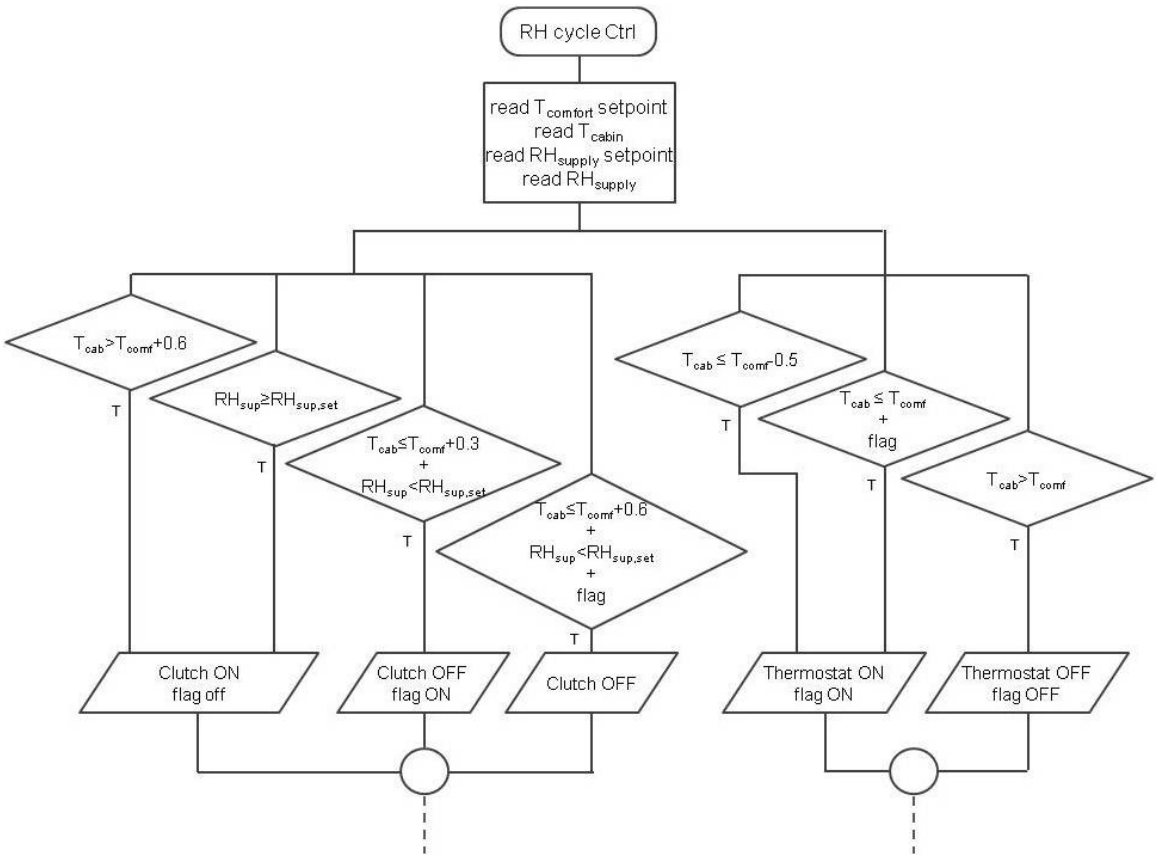

Figure B.11: Relative Humidity Cycling Control Flow Chart

The continuous relative humidity control, shown in Figure B.12, controls the compressor speed and coolant pump speed, using a PID control, once cabin temperature is close to setpoint. Thermostat control is used to retain cabin temperature close to the comfort setting.

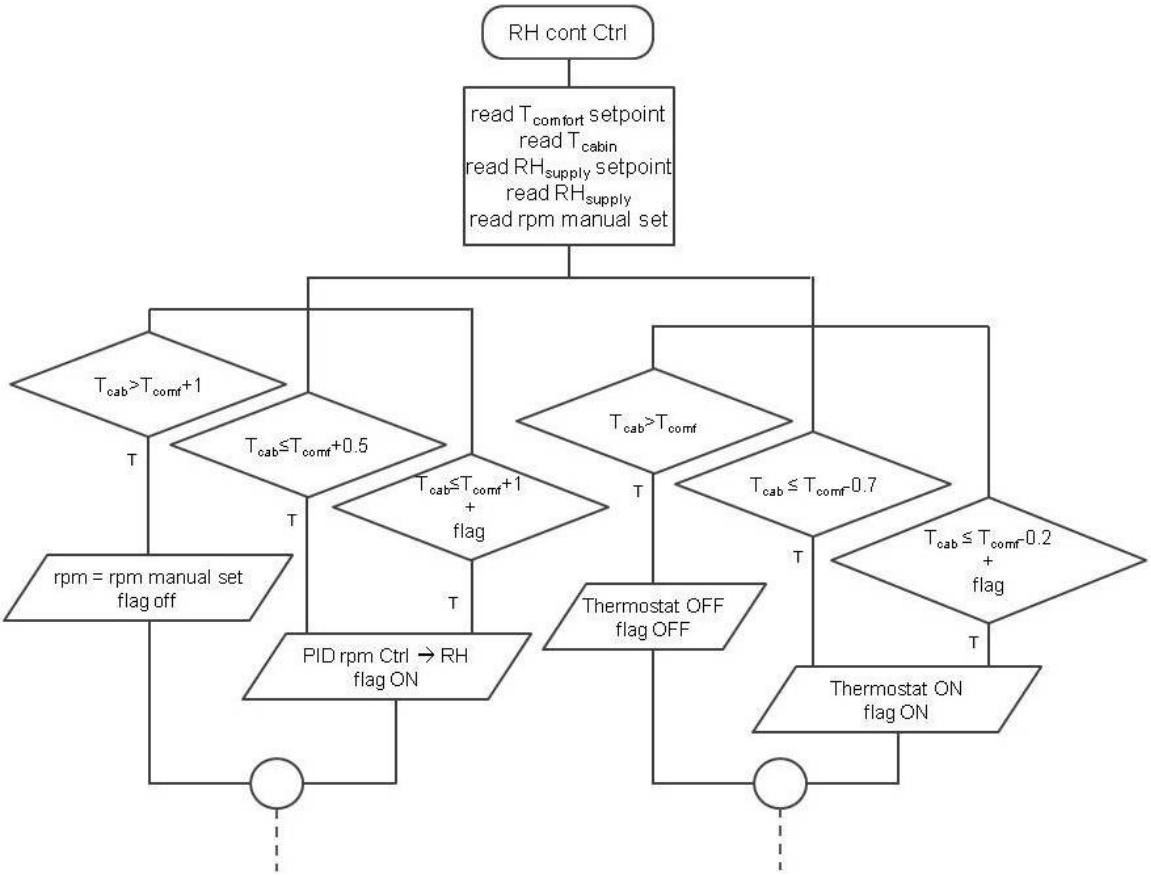

Figure B.12: Relative Humidity Continuous Control Flow Chart

Appendix C Drive Cycle Development

Appendix C provides more details how the conversion of the NEDC drive cycle (and similar drive cycles) from vehicle speed to compressor speed. In addition, the implementation of drive cycle into LabVIEW, and the development of a novel drive cycle to showcase the versatility of the test facility, are discussed. development of drive cycles and drive cycle control in the data acquisition system, which was performed to gain the ability to run drive cycle, such as the NEDC and the I-95 cycle.

The NEDC drive cycle, as well as other drive cycles, such as the USA urban or extra-urban cycle, are given by a vehicle speed versus time profile. In the current study MAC components are tested on a test bench, while the vehicle is replaced by a cabin model. This results in the need to convert the original drive cycle profiles to compressor rpm versus time profiles. Table C.1 shows specifications for a medium size, 2.2L engine 5-speed manual car. The shown parameters are used to convert vehicle speed to engine rpm, based on gear choice.

Table C.1: Automobile Parameters for Speed to RPM Conversion

Gear	Gear Ratio (5-speed manual)
1.	3.58
2.	2.02
3.	1.35
4.	0.98
5.	0.69
Final Drive Ratio	3.94
Pulley Ratio	0.786

Tire Specifications	
Tire Type	P195/70R14
Rolling Circumference [m]	1.9748

Figure C.1 shows the conversion results in form of graphs. For each gear, a linear relationship between vehicle speed and A/C compressor rpm was determined. The conversion equations, shown next to the respective gear curves, were used in the conversion fo the NEDC drive cycle and the I-95 cycle.

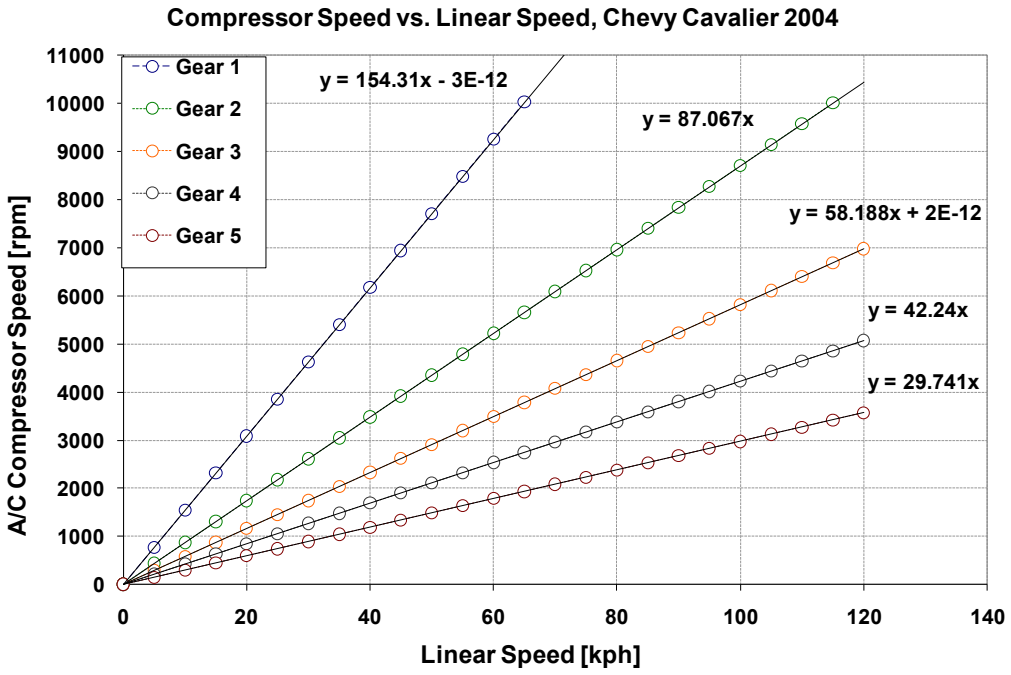

Figure C.1: Gear Equations for vehicle speed to compressor rpm conversion

To make above conversion equations useful, gear selection at every point during the drive cycle needs to be known. To this end, an urban drive cycle and an urban shift cycle, based on EPA data [110], were superimposed. Figure C.2 shows gear selection, based on superposition of the two cycles, which allows the correlation of speed and gear choice.

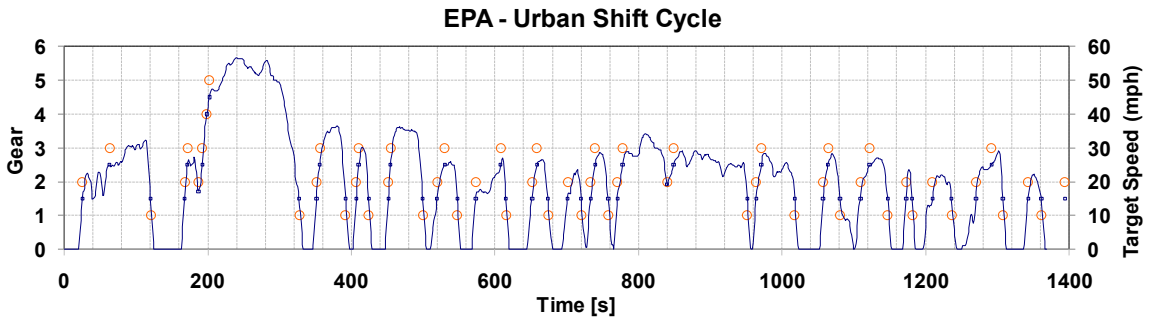

Figure C.2: Superimposed EPA FTP Drive Cycle and Shift Cycle

However, the superposition reveals only a gear selection at a specific speed along the drive cycle and not the exact speed at which gears are shifted. Since gear shifts in practice vary between acceleration and deceleration, shift points need to be chosen according to driving situation. During acceleration, the driver usually shifts up at higher rpm, while during deceleration the driver usually shifts down at lower rpm. This was taken in consideration in Table C.2.

Table C.2: Shift Point Table for Vehicle Acceleration and Deceleration

Gear	Gear Selection (EPA) [kph]	Accel.Shift Pt. [kph]	Decel. Shift Pt. [kph]
1.	24	22.5	16
2.	40	38.5	32
3.	64	62.5	54
4.	72	71	64
5.	-	-	-

The resulting compressor rpm profile for the NEDC drive cycle is shown in Figure C.3, along with the original vehicle speed profile for comparison. Idle compressor speed is 850 rpm, while maximum compressor speed increases up to 3600 rpm. At shift points, changes in compressor rpm can be abrupt and result in severe transients. To prevent excessive load on the electric motor, which drives the compressor, the rpm profile was smoothed to prevent excessive transients.

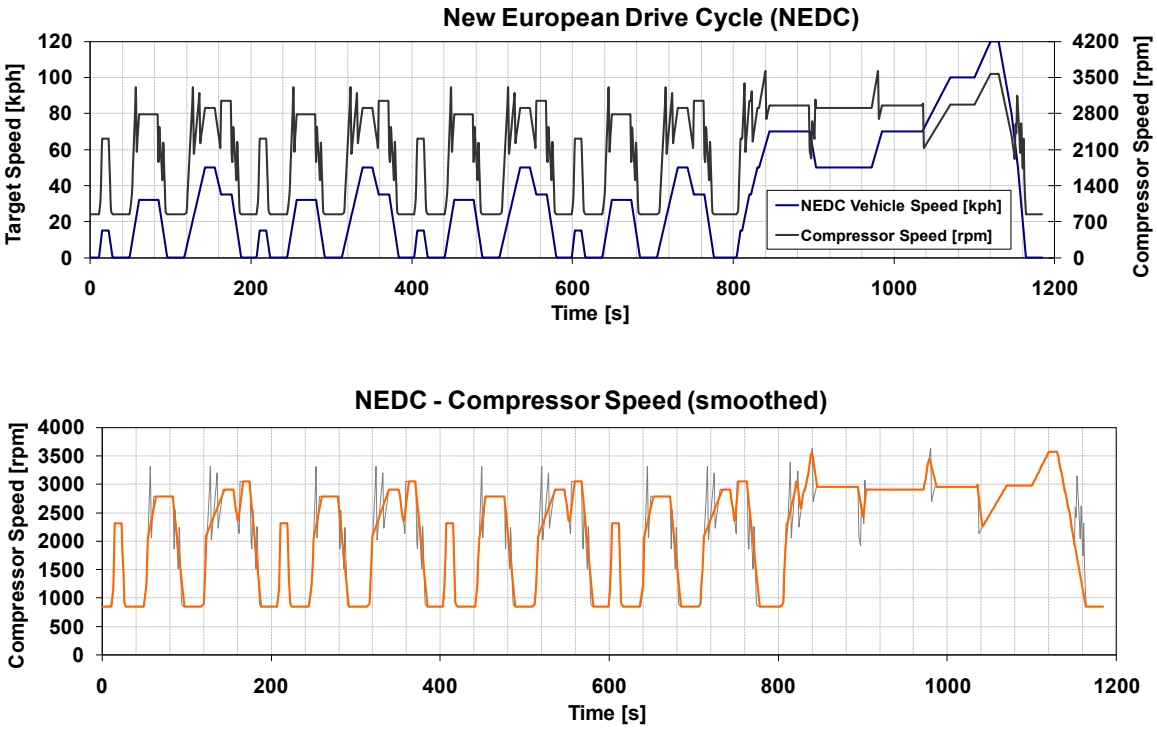

Figure C.3: NEDC Compressor Speed Profile

To showcase the abilities of the test facility control (and initially for truck anti-idling research), a new drive cycle, the I-95 drive cycle was developed. The goal was to assess air-conditioning performance in a more realistic, but highly

variable setting, which includes multiple climate zones. The I-95 cycle simulates a car driving down the I-95 corridor from Maine to Florida on the United States east coast. Climate data along the route was acquired in form of TMY2 data from the National Renewable Energy Laboratory (NREL) [111]. As TMY2 data was available only for a limited number of cities, the respective cities were used to pinpoint locations along the route. Google maps was used to determine distances between locations and travel time during regular traffic hours. Table C.3 provides the I-95 route locations, as well as distances and average speed in between locations.

Table C.3: I-95 Cycle - Route and Travel Information

#	City (State)	Travel time [s]	Distance [km]	Avg. Speed [km/h]
1	Caribou (ME)	18600	481.2	93.1
2	Portland (ME)	7800	172.2	79.5
3	Boston (MA)	3900	80.8	74.6
4	Providence (RI)	7800	196.3	90.6
5	Bridgeport (CT)	5400	97.2	64.8
6	New York City (NY)	1800	16.7	33.5
7	Newark (NJ)	6300	147.4	84.2
8	Philadelphia (PA)	2100	46.5	79.7
9	Wilmington (DE)	5400	112.3	74.9
10	Baltimore (MD)	20400	495.7	87.5
11	Raleigh (NC)	8100	210.8	93.7
12	Wilmington (NC)	13200	331.5	90.4
13	Columbia (SC)	10200	255.9	90.3
14	Savannah (GA)	9300	223.7	86.6
15	Jacksonville (FL)	6300	143.6	82.0
16	Daytona Beach (FL)	12300	318.6	93.3
17	West Palm Beach (FL)	4800	114.3	85.7
18	Miami (FL)	-	-	-

For simplicity, it was assumed that the driver would start at 8:00am every morning and drive until 12:00pm. There would be a rest time of one hour during which the engine would be turned off. Following the rest time, the driver would

drive from 1:00pm through 9:00pm. The driver would then stop for the night to take 11 hours rest. The average speed can vary in between cities, based on speed limits and traffic situation that is usually encountered in the respective locations.

Dry bulb temperature, relative humidity, and solar insolation profiles were determined using TMY2 weather data. TMY2 weather data is available as hourly data for one location. The data is available averaged over the last 30 years, for the chosen month at the specified day, hour, and location. As the data is available only for a limited number of locations along the route, the data needs to be interpolated in steps of one hour between locations. This creates transient profiles which change temporally and spatially. The developed profiles for dry bulb temperature, relative humidity, and solar insolation, are shown in Figure C.4 a) through c). The profiles were used as drive cycle input to the cabin model, and the controls of the environmental chamber.

During each start and stop of the car, the car was assumed to leave the I-95 to stop at a restaurant or inn. One set of the urban drive cycle portion of the NEDC was chosen to be performed during each start and stop operation. The compressor speed profile was developed with the method outlined above. The clutch profile follows the starts and stops for rest and night stops.

Operation of one complete I-95 cycle lasted about 88 h, which is the time a car would need to drive from Caribou, Maine, to Miami, Florida, under the

assumptions previously mentioned. The test facility was controlled in time steps of 2 seconds.

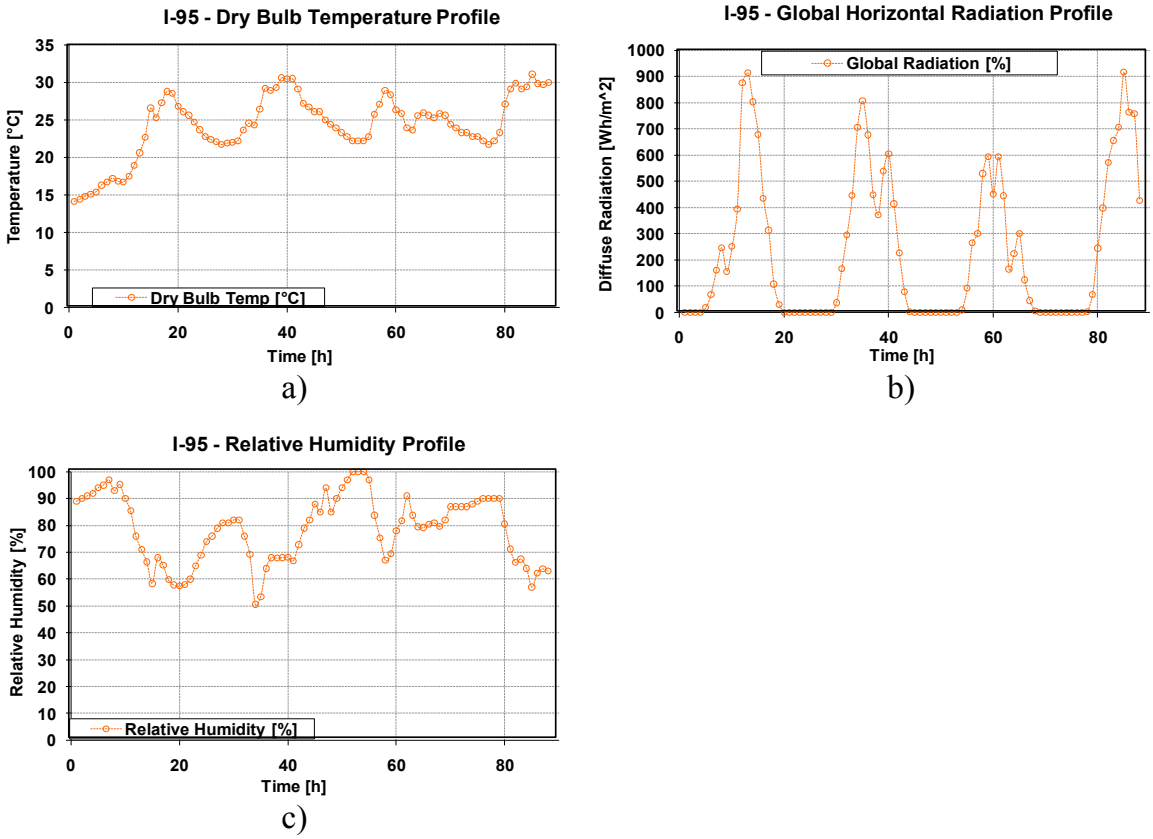

Figure C.4: I-95 Cycle TMY2 Interpolated Climate Data

Figure C.5 shows performance parameters which were measured during the I-95 cycle test, such as cooling capacity and compressor power. It can be observed that cooling capacity is smallest, around 1.65 kW in the colder climate of Maine, during the beginning of the first day. The capacity remains nearly constant at about 1.9 kW during the remaining days of the I-95 test. Compressor power increases with ambient temperature. At the same time, compressor power follows the compressor speed profile. Compressor power in Maine was on

average about 0.75 kW, while the average compressor power was about 1.25 kW in Florida.

Figure C.6 shows the profile of cabin temperature during the entire I-95 cycle. The ambient temperature, as well as the solar insolation, are shown for better explanation of the cabin temperature behavior. It can clearly be observed that the cabin model was able to control the cabin temperature at a comfort setting around 25°C for the entire on-cycle portion of the I-95 test. During afternoon stops and early evening stops, the cabin soaks due to solar insolation. This can most prominently be observed during the last afternoon stop in Florida, around 4,600 minutes into the test, where the strongest soaking was determined to be about 14 K. At night, when the A/C is turned off, the cabin temperature follows the outdoor temperature. This can be observed well at around 1,000 minutes or 2,500 minutes.

Cabin relative humidity is shown in Figure C.7. The relative humidity remains constant at about 32% after a short start-up period. At night the cabin relative humidity increases up to a relative humidity of 53%, due to the decrease in cabin temperature and the exchange with colder ambient air. During afternoon stops, the relative humidity decreases, due to the soaking of the cabin.

From above results it can be concluded that the existing test facility is capable of controlling all parameters relevant to capture transient performance of a MAC system for a driving vehicle, including varying climate conditions and day and night cycles.

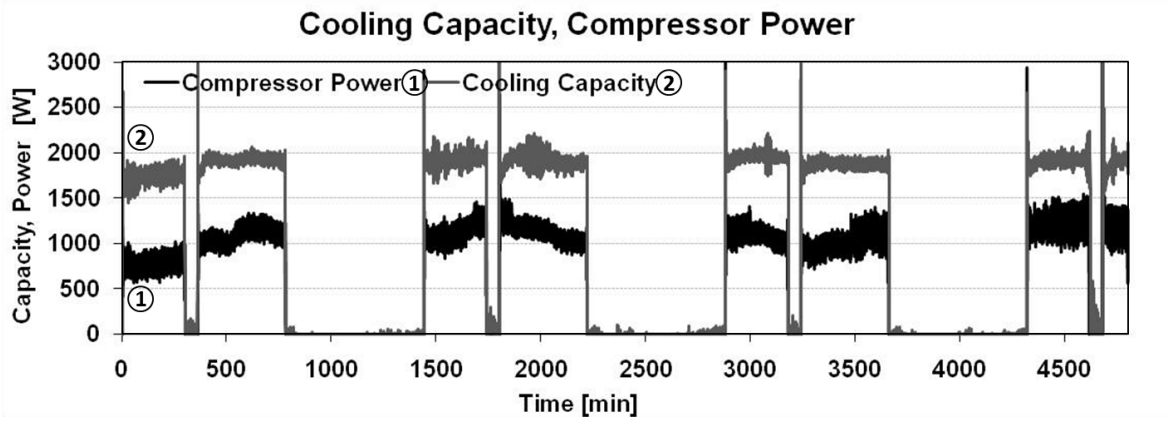

Figure C.5: I-95 Cycle - Cooling Capacity and Power Consumption

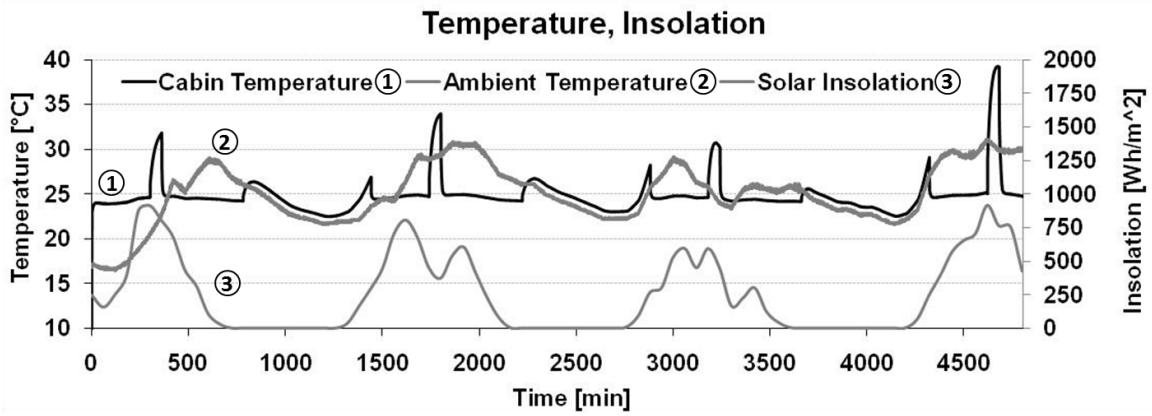

Figure C.6: I-95 Cycle - Cabin Temperature

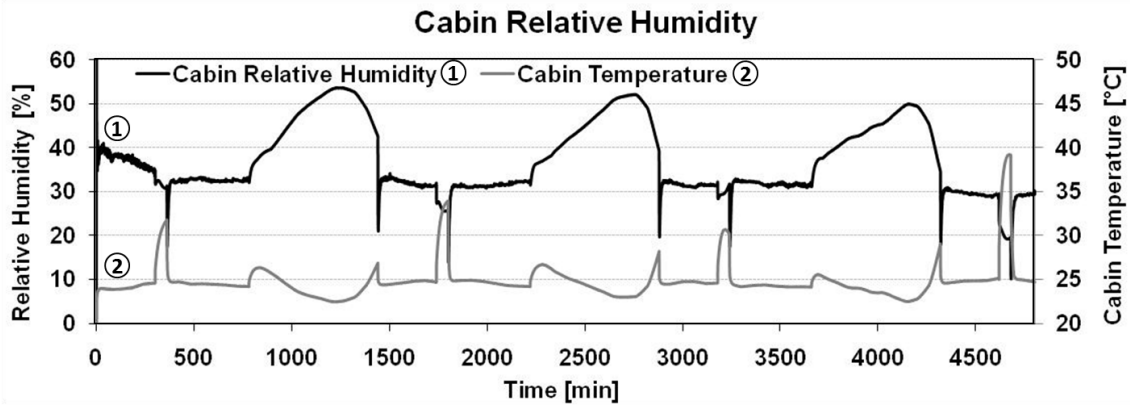

Figure C.7: I-95 Cycle - Cabin Relative Humidity

Appendix D Steady-state Results Summary: Secondary Loop Versus Direct Expansion

Appendix D provides a summary of steady-state experimental results for the comparison of secondary loop system to direct expansion system, using R152a as refrigerant.

Figure D.1 shows steady-state trends for relative magnitude of performance metrics over a range of ambient temperatures and relative humidities for idling and highway driving conditions, with respect to R134a DX magnitudes. The relative humidities which accompany respective ambient temperatures is shown in Table 7.1.

Figure D.1 a) shows variation of cooling capacity, while Figure D.1 b) shows variation of power consumption, and Figure D.1 c) shows variation of cycle COP. As a general trend, cooling capacity of both, R152a DX and R152a 2LP are similar to R134a DX at highway speed. During idling, cooling capacity decreases by about 5% to 10% for R152a 2LP systems. A comparison of power consumption shows that R152a DX consumes 10% to 15% less power compared to R134a DX at highway conditions. 2LP power consumption is increased, due to additional power consumption by the coolant pump. This is especially felt during idling at low temperatures, as the compressor consumes the least power in these conditions and pump power is a higher fraction of total power. However, power consumption does not rise above R134a DX power consumption even at low temperature idling. COP of R152a DX is generally higher than for R152a 2LP

systems. R152a 2LP COP is typically increased by 5% to 10% above R134a DX, except for idling at low ambient temperatures.

Figure D.2 provides a summary of sensible and latent performance for a range of ambient conditions. From Figure D.2 a) it can be observed that sensible cooling capacity of the R152a DX and 2LP systems are close to the capacity of the R134a DX system. At idling, sensible capacity of the R152a 2LP system seems to be slightly increased to the R152a DX system. In comparison to the R134a DX system, the secondary loop system seems to have a similar sensible capacity at moderate temperatures, while it is reduced by more than 10% at low and high ambient temperature. Latent capacity, shown in Figure D.2 b), is less conclusive, as high measurement uncertainties apply. However, at highway speeds, the latent capacity of R152a 2LP is similar to R134a DX capacity. At idling, trends seem to be unclear, except of at high ambient temperature of 45°C, where latent capacity is zero for all systems. A summary of sensible heating factor (SHF) values, not commonly reported in the automotive area, is shown in Figure D.2 b). Both for R152a DX, as well as for R152a 2LP, the SHF stays within 5% of its value for R134a DX, except of during idling at low ambient temperatures.

R152a compressor volumetric efficiencies, both for the DX and the 2LP system, shown in Figure D.3 a), are observed to be higher than R134a DX at highway speeds. At idling speeds, R152a DX volumetric efficiencies are the same as R134a DX efficiencies, while R152a 2LP efficiencies are up to 10% decreased at low ambient temperatures.

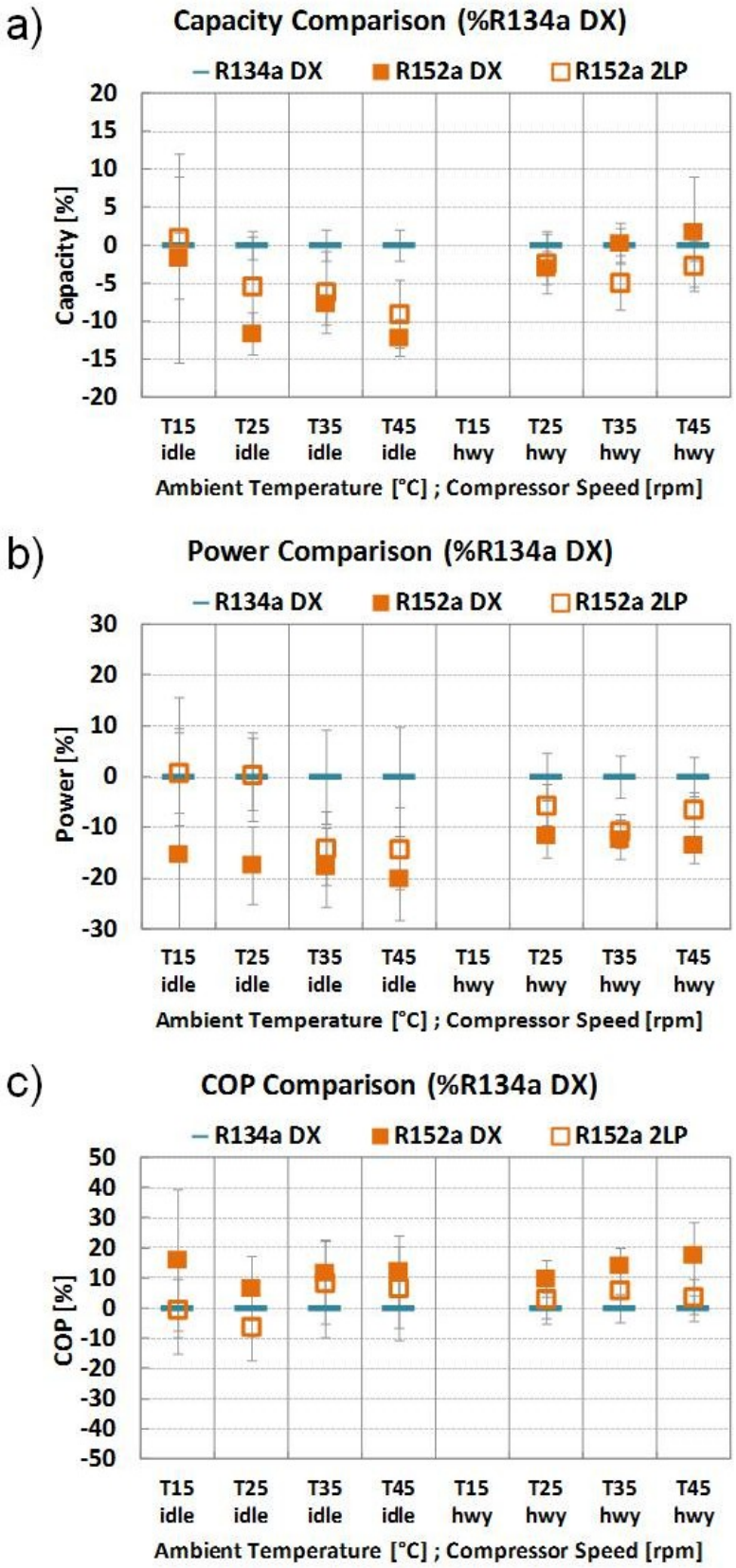

Figure D.1: Steady-state Performance Metrics Summary (2LP Versus DX)

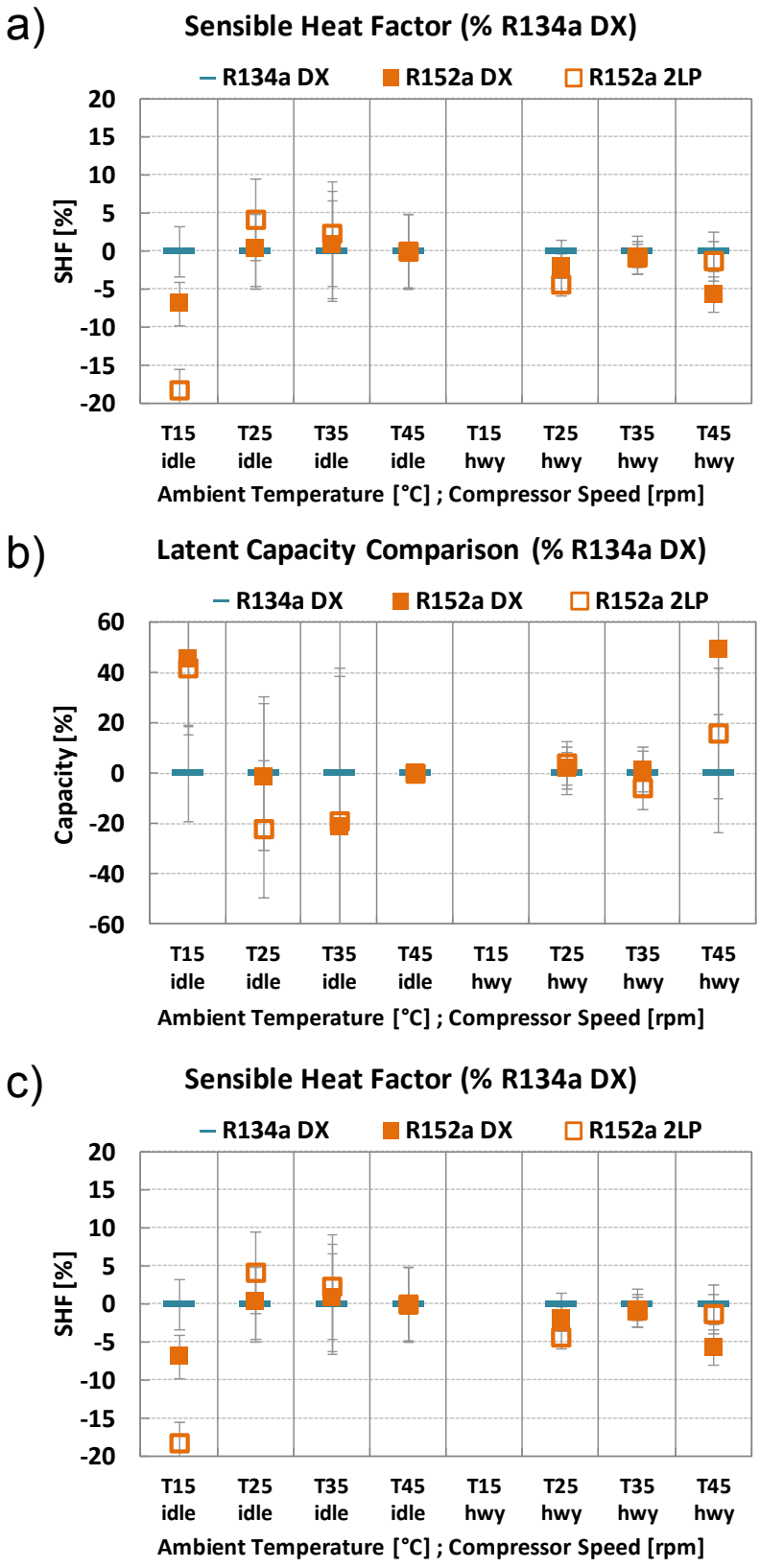

Figure D.2: Steady-state Sensible/Latent Performance Summary (2LP Versus DX)

Isentropic efficiencies, shown in Figure D.3, are increased by about 10% when using R152a as drop-in in the direct expansion system during highway driving. An increase of about 20% can be observed for the R152a secondary loop system. During idling, the R152a DX system shows an increase of up to 10% in isentropic efficiency, decreasing with ambient temperature. The R152a 2LP system showed isentropic efficiencies similar to R134a DX at low ambient temperature and increases of about 10% at higher ambient temperature.

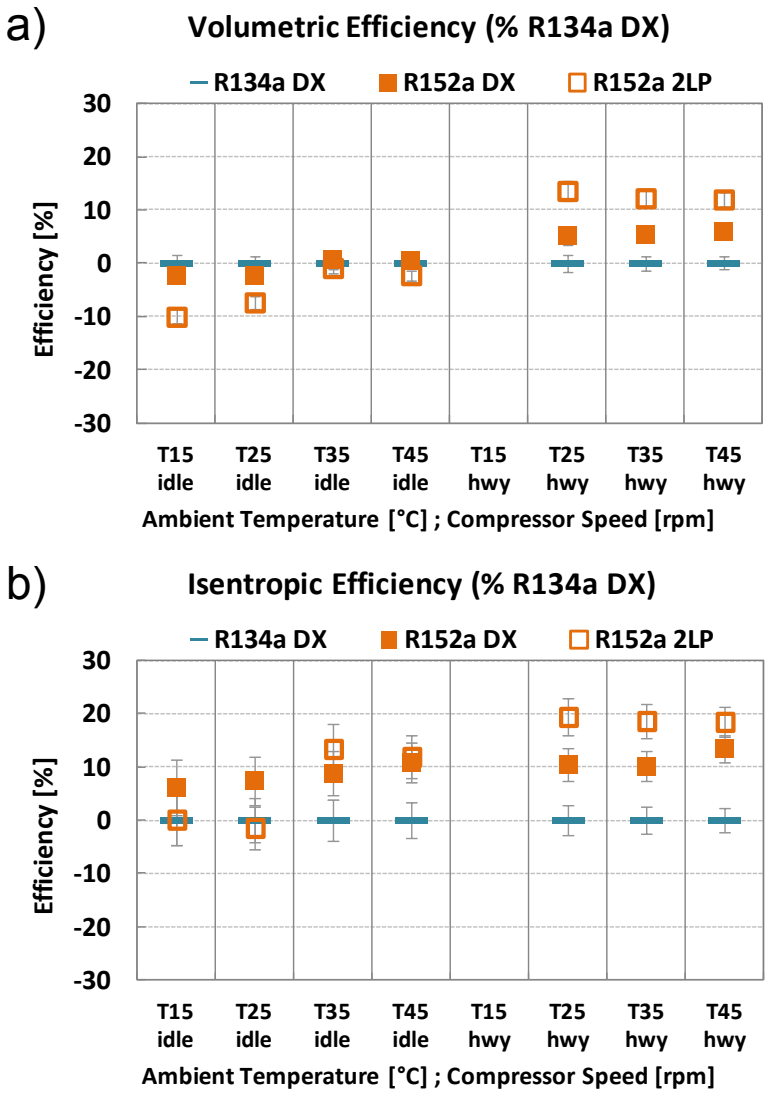

Figure D.3: Steady-state Compressor Efficiency Summary (2LP Versus DX)

Appendix E Transient Test Procedure Illustrations

Appendix E provides illustrations of all transient test procedures used in the present study. The illustrations show profiles of controlled parameters, such as compressor speed and heater core load, as well as their effect on cabin temperature and relative humidity. All illustrations show the progress of time over the length of a test on the x-axis. The magnitude of parameters is not identified at the axis, as the illustrations are meant to merely facilitate understanding of test procedures and resulting trends in cabin parameters.

Figure E.1 shows the test procedure for a pull-down test. Pull-down tests are performed at fixed compressor speeds and fixed condenser air flow rates, corresponding to an automobile driving at a steady speed. The compressor is turned on at time zero, providing cooling capacity to pull down the cabin to a pre-defined comfort temperature. Once the cabin has reached comfort temperature, the test is stopped.

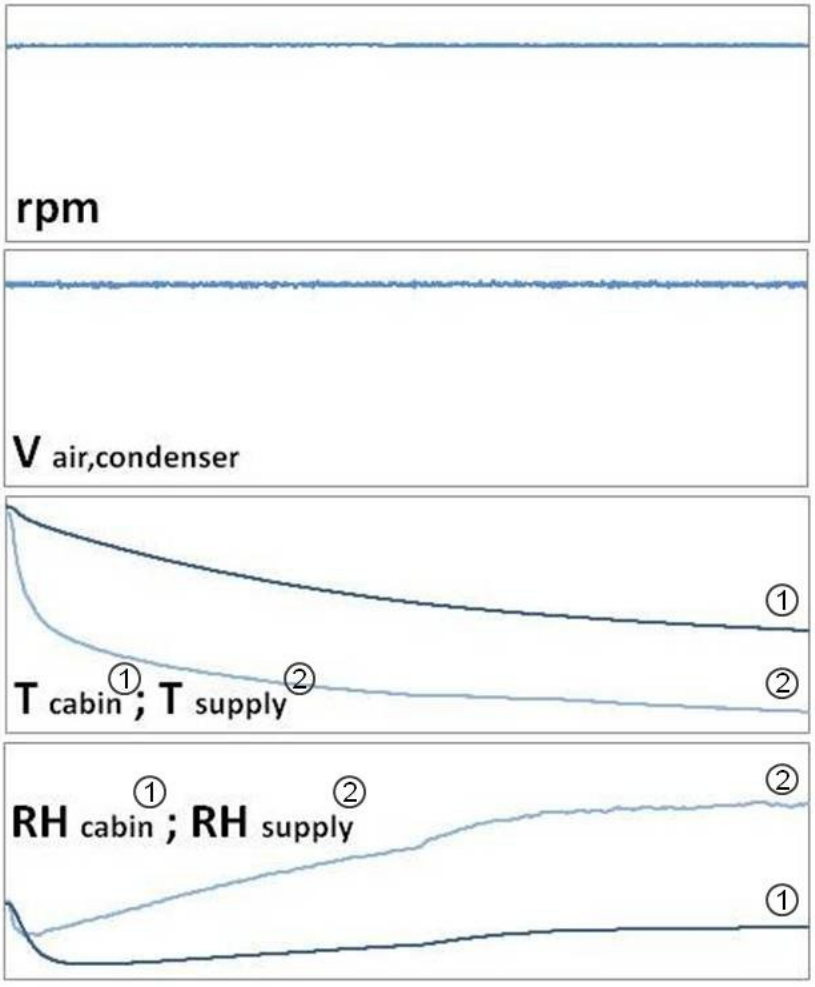

Figure E.1: Pull-down Test Procedure Illustration

Figure E.2 provides an illustration of the New European Drive Cycle (NEDC) test procedure. The NEDC is a fixed profile of vehicle speed over time. The vehicle speed profile was converted into the compressor speed profile (rpm), shown in the figure. The condenser air flow rate still follows the original outline of the vehicle speed profile, since it is directly correlated with vehicle speed. The general trends of supply and cabin temperature and their fluctuation with compressor speed are shown.

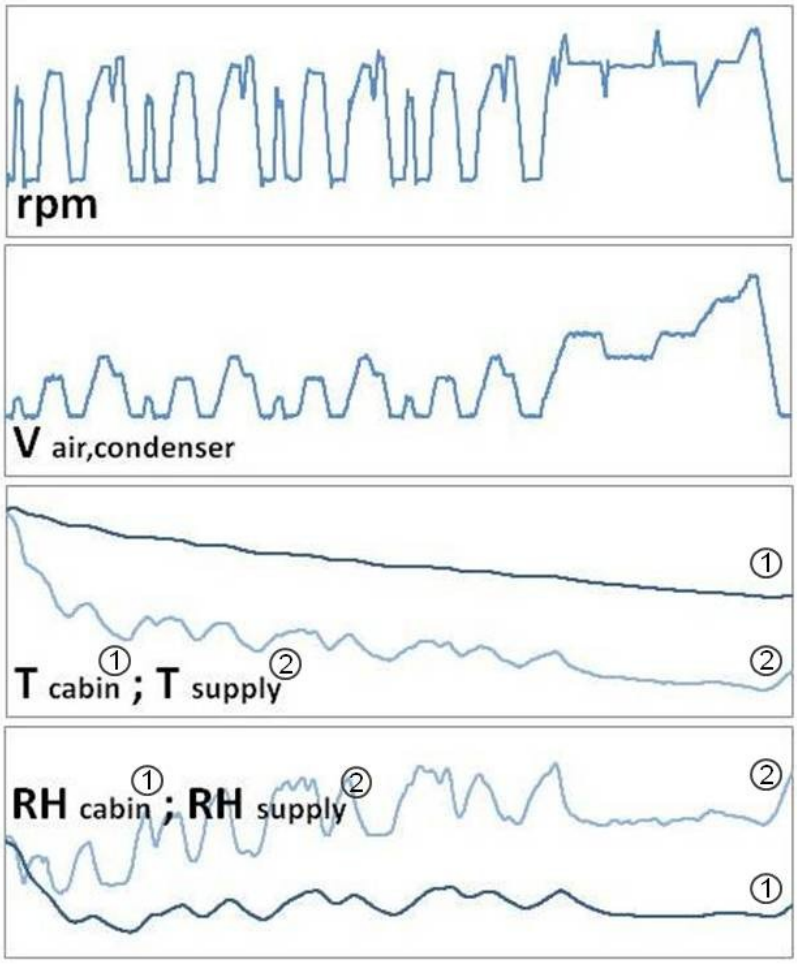

Figure E.2: NEDC Test Procedure Illustration

To test thermal storage characteristics of secondary loop systems, off-cycle test procedures were developed. The pull-down off-cycle test, shown in Figure E.3, is a variation of the original pull-down test. Once cabin temperature corresponds to the comfort setting, the compressor is turned off and the cabin is allowed to heat up again. Temperature and relative humidity trends are recorded to allow the comparison between secondary loop and direct expansion systems.

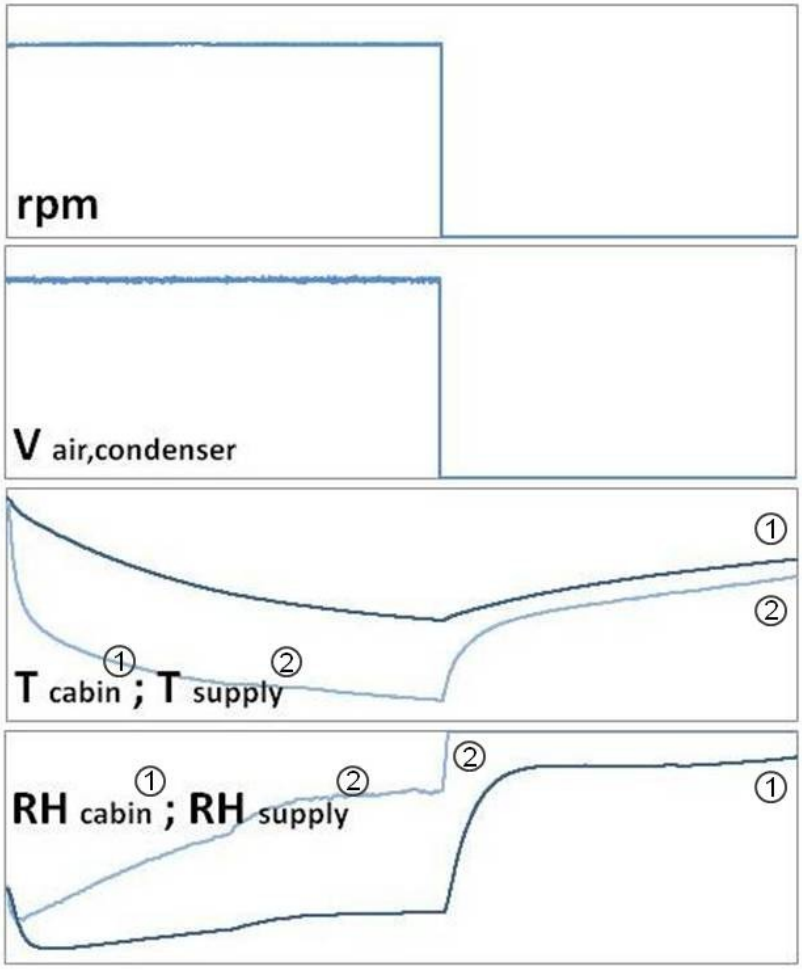

Figure E.3: Pull-down Off-cycle Test Procedure Illustration

A second test procedure for off-cycle testing, the Start/Stop cycle, is shown in Figure E.4. The Start/Stop cycle is an NEDC, modified to the extent that idling sections were replaced by compressor off sections. This simulates the start/stop automatic mechanism, used in modern cars, which turns off the engine instead of idling when waiting for a traffic light.

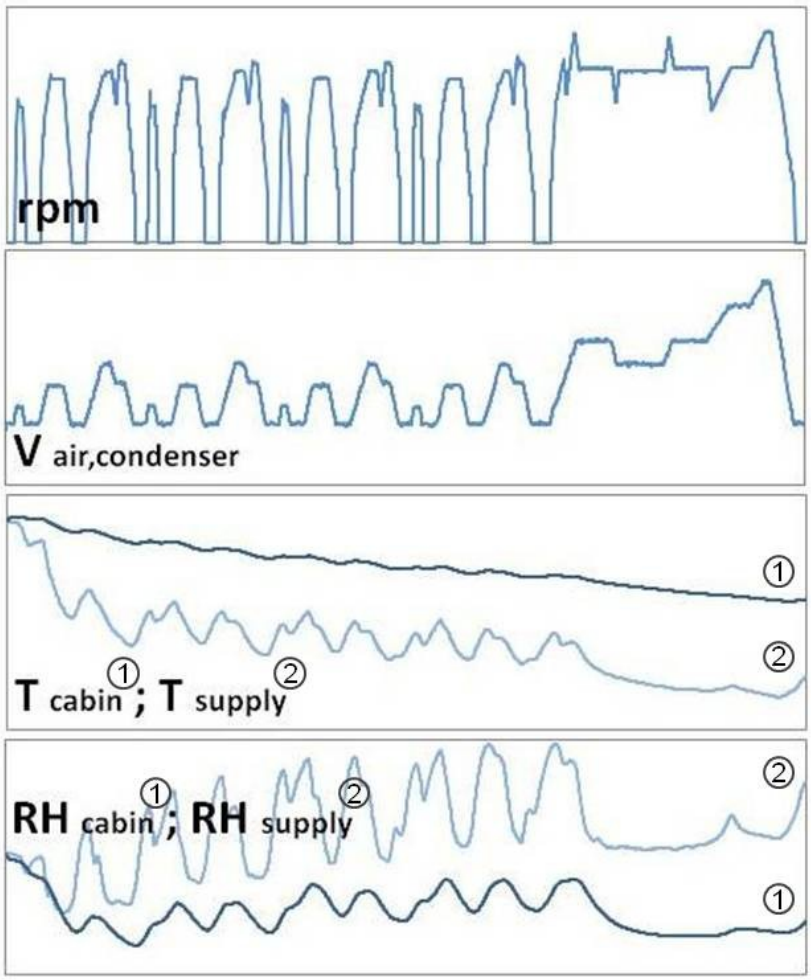

Figure E.4: Start/Stop Test Procedure Illustration

The start/stop cycle was further modified to increase engine-off time. Figure E.5 shows the Start/Stop three times idling (SS3xI) test procedure. The engine-off times were tripled with respect to the Start/Stop engine-off times (and NEDC idling sections), thereby introducing greater fluctuations in supply temperature and relative humidity. The thermal storage advantage of secondary loop systems can be observed better with increasing engine-off times.

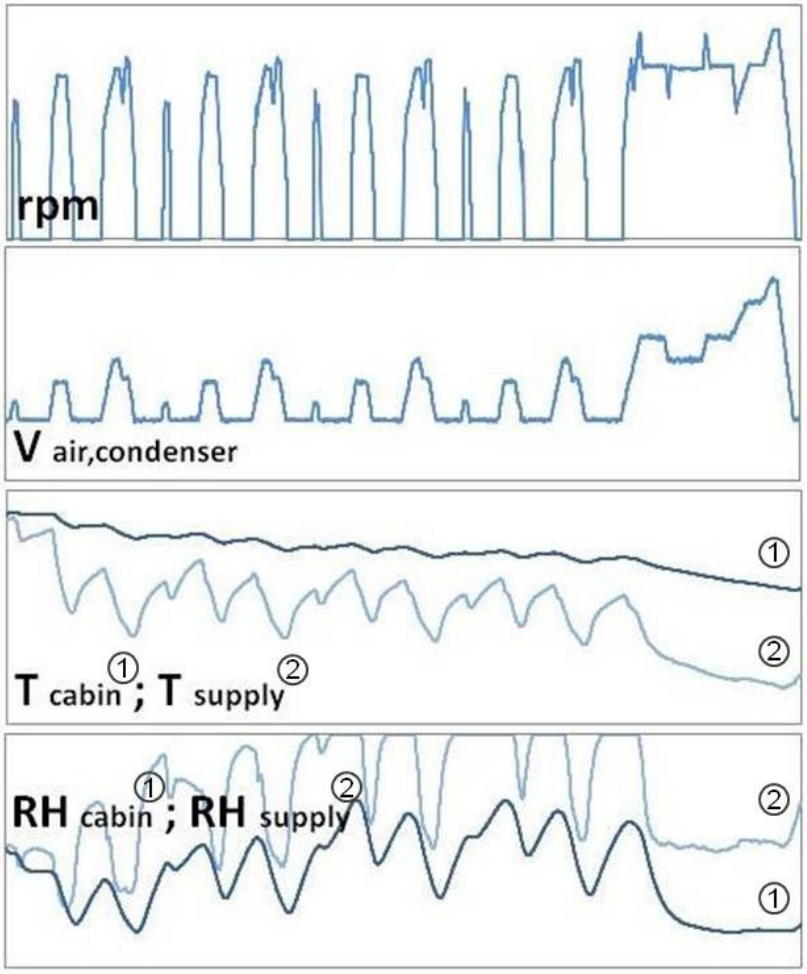

Figure E.5: Start/Stop 3x Idling Test Procedure Illustration

Figure E.6 through Figure E.8 introduces three test procedures for A/C controls research. Figure E.6 shows the procedure for frost cycling tests. A regular pull-down procedure decreases cabin temperature to comfort setting. After comfort temperature is achieved, the compressor continues to run, while a heater core is employed to keep the cabin at comfort temperature. Since the compressor is still running, supply temperature will eventually decrease until evaporator outlet temperature is close to frost condition. At this point the

compressor is cycled to prevent frosting. As a result, power consumption of compressor and heater are high, while supply relative humidity is low.

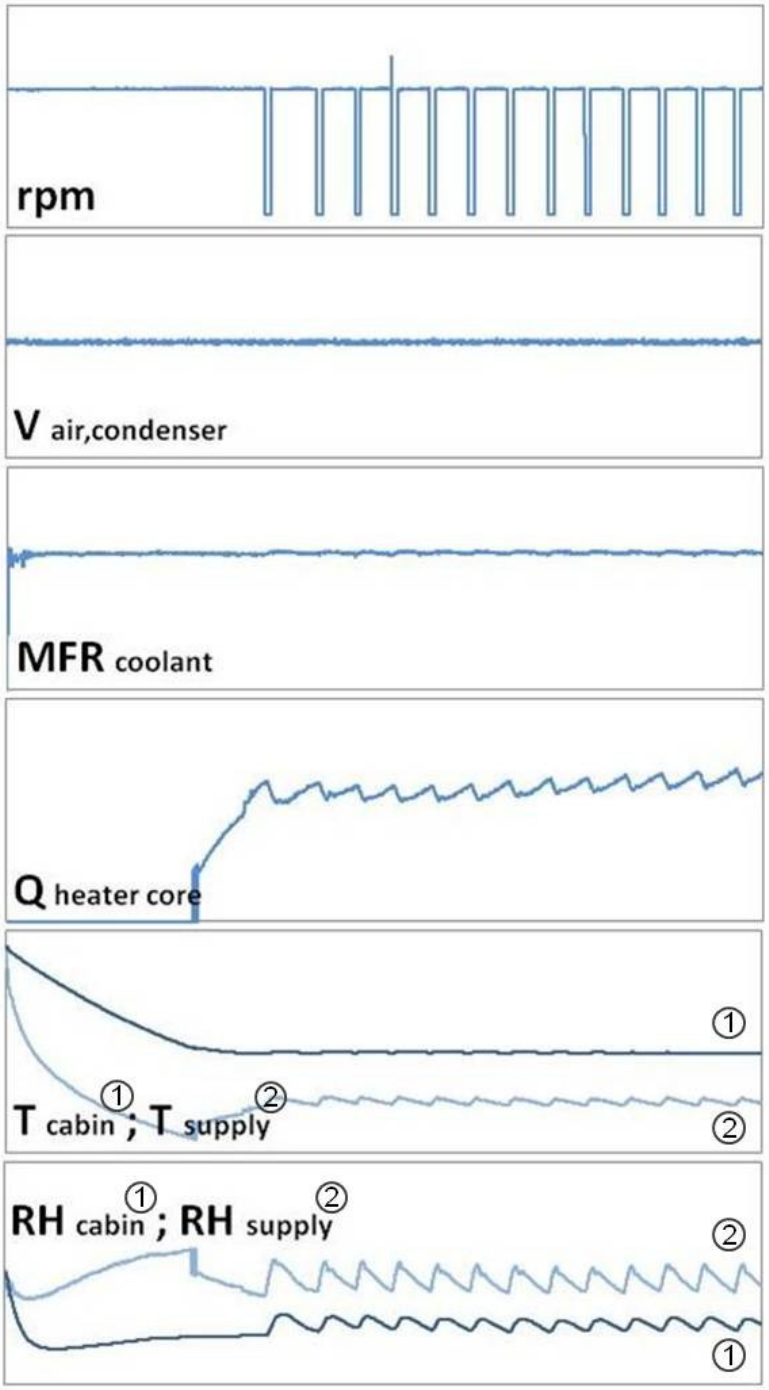

Figure E.6: A/C Ctrl - Frost Cycling Test Procedure Illustration

Figure E.7 shows the test procedure for relative humidity cycling control. The relative humidity cycling control procedure is similar to the frost cycling procedure, though the cycling trigger is changed. Instead of cycling at the onset of frost at the evaporator, the compressor is mainly turned off when the cabin temperature is close to comfort setting. As long as relative humidity of the supply air does not increase above a pre-defined setpoint, the compressor remains turned off. This allows to expend less heater power and reduces power compressor consumption, though fluctuations in supply temperature and relative humidity are increased.

Figure E.8 introduces the continuous relative humidity control procedure. Similar to the relative humidity cycling, the compressor is used to control relative humidity. However, instead of cycling, compressor speed is controlled by a PID controller to keep supply relative humidity at a pre-defined setpoint, as long as cabin temperature does not warrant higher compressor speeds to gain additional cooling capacity.

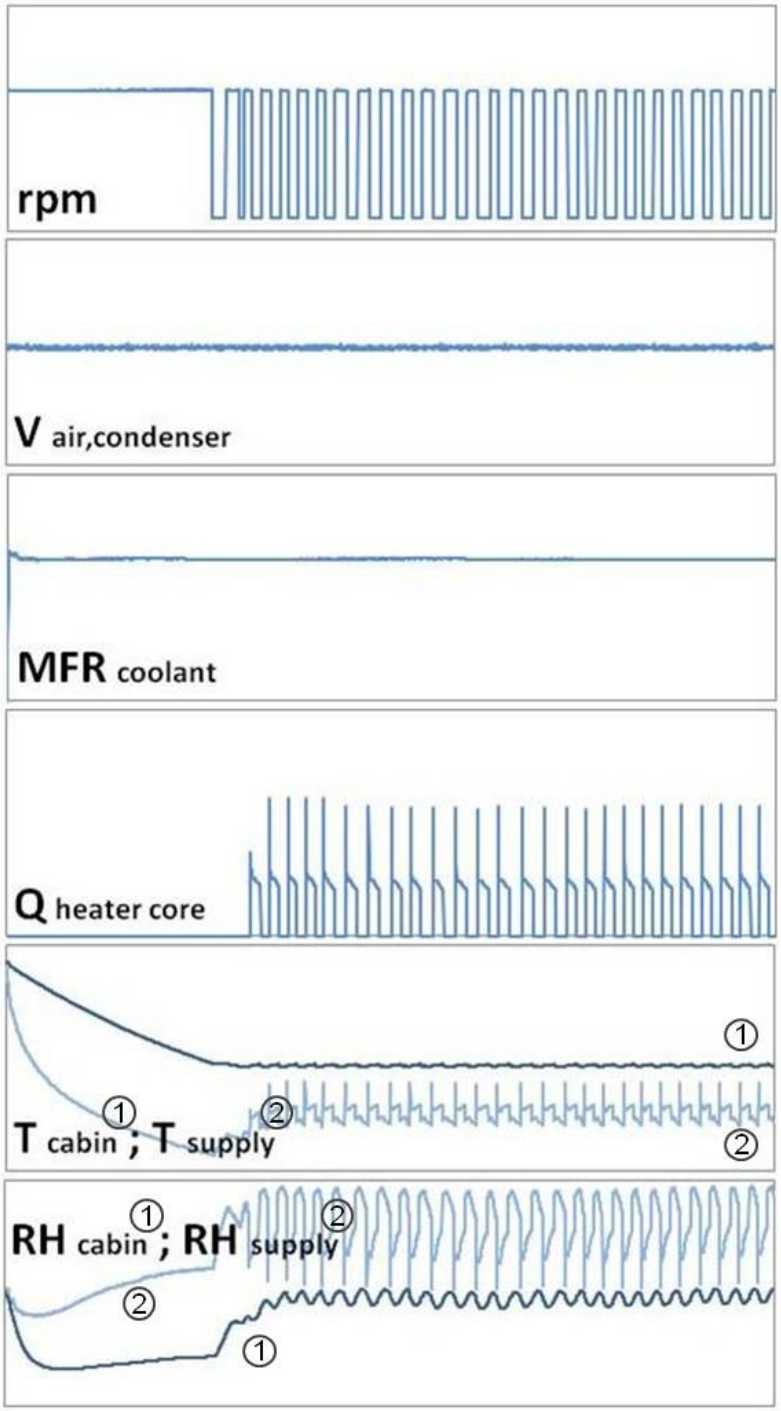

Figure E.7: A/C Ctrl - RH Cycling Test Procedure Illustration

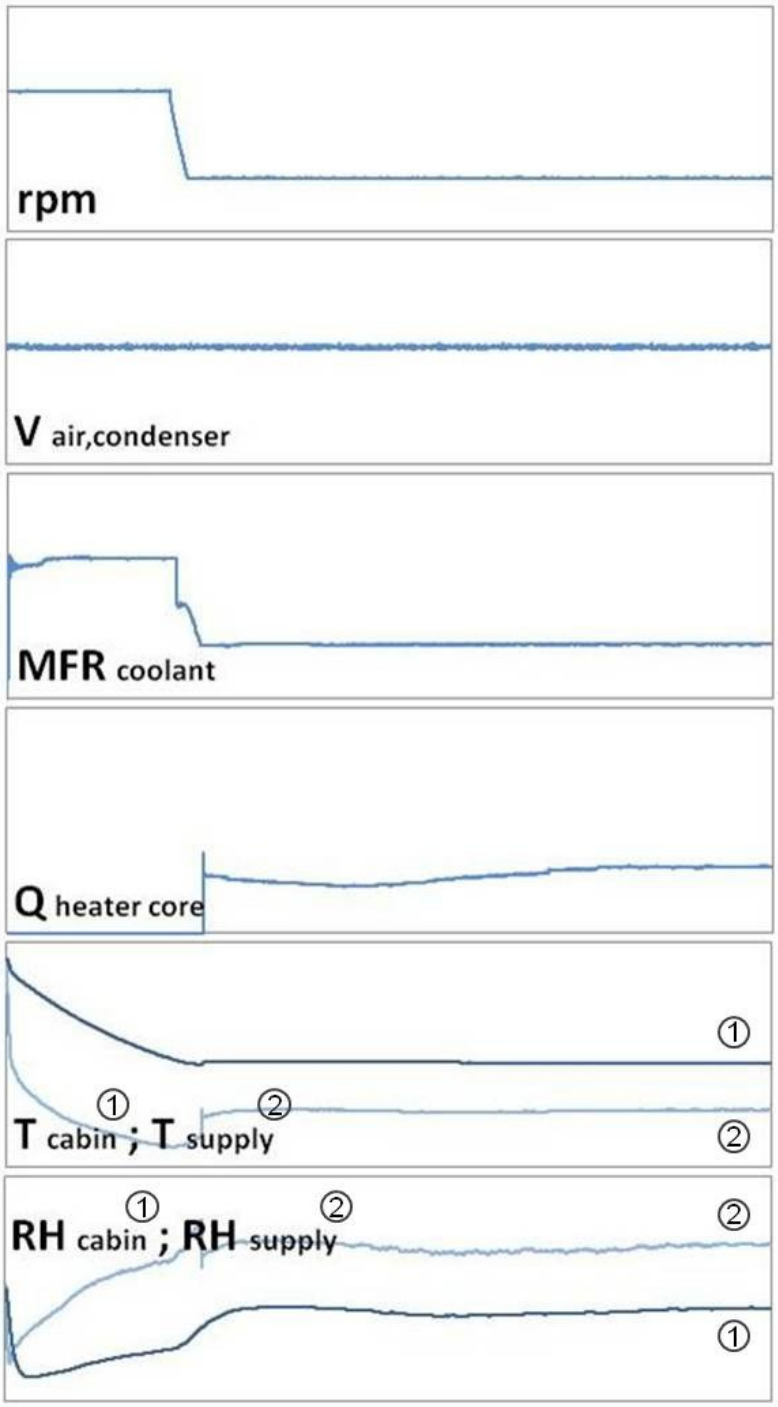

Figure E.8: A/C Ctrl - RH Continuous Test Procedure Illustration

Appendix F Steady-state Results Summary: Propane 2LP

Appendix F provides a summary of R290 2LP steady-state results over a range of ambient temperatures for idling, as well as highway driving conditions with respect to R134a DX. Figure F.1 shows am summary of cooling capacity, total power consumption, and transient performance factor (TPF), while Figure F.2 focuses on sensible versus latent performance, and Figure F.3 provides information on compressor efficiencies.

Figure F.1 a) shows the cooling capacity of R290 2LP with respect to R134a DX. When operating under highway driving conditions, the R290 2LP capacity was decreased by less than 10%. During idling, the capacity was about 20% decreased. As discussed in Chapter 8, R290 2LP compressor speed was reduced for both, idling and highway driving, which decreased cooling capacity. Therefore, cooling capacity results can be varied actively by adjusting compressor rpm. In an automobile, a compressor with a different displacement might be used. A comparison of power consumption, shown in Figure F.1 b), shows that power consumption was up to 16% reduced at high speed conditions. At idling conditions, power consumption was reduced up to 11%. COP of R290 2LP, shown in Figure F.1 c), was increased by up to 9% at highway driving and moderate ambient temperatures. At idling conditions, power consumption was reduced between 10% and 15%. Although uncertainty during idling is increased, it can be observed that R290 2LP COP is generally decreased as compared to R152a 2LP COP. During highway driving, COP of R290 2LP is similar or higher than COP of R152a 2LP.

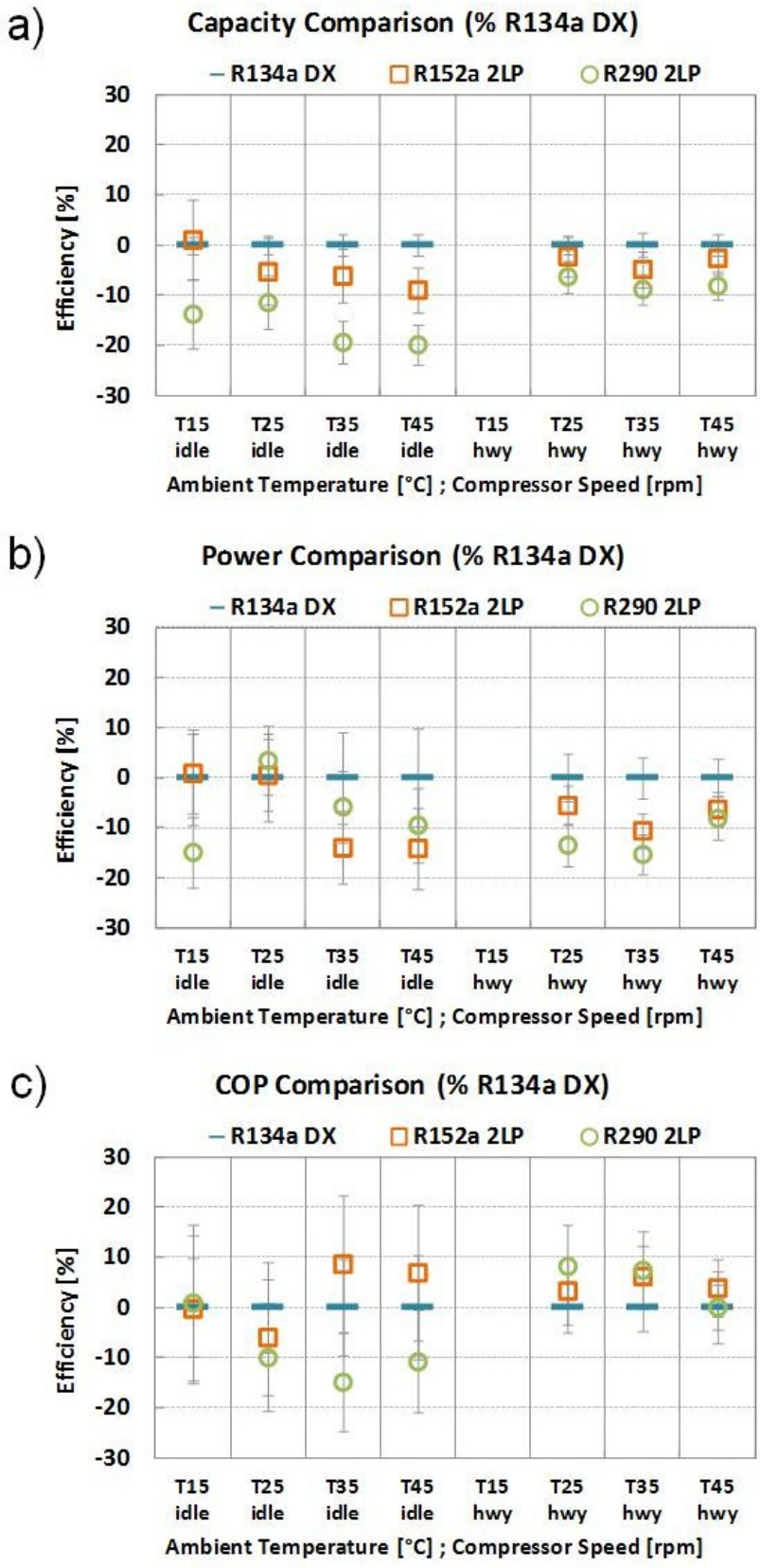

Figure F.1: Steady-state Performance Metrics Summary (Propane 2LP)

Figure F.2 shows a relative comparison of sensible and latent capacity, as well as the sensible heating factor (SHF). Figure F.2 a) shows a comparison of accumulated sensible capacity. It can be found that R290 2LP sensible capacity is similar to R152a sensible capacity. The impact factor for is the secondary loop and the need to sensibly cool the additional thermal mass. At low temperature idling conditions, sensible capacity is reduced by 25%, though measurement uncertainty prevents a clear cut conclusion. Figure F.2 b) shows a comparison of accumulated latent capacity. Latent capacity is associated with high measurement uncertainties, especially at idling conditions, since absolute latent capacity is very low. In general latent capacity at highway driving conditions is similar to latent capacity of R134a DX. A clear trend cannot be observed at idling conditions. Figure F.2 c) shows a comparison of SHF. At highway driving conditions, SHF of R134a DX, R152a 2LP and R290 2LP compare with each other within 5%. At idling speed, R290 2LP latent capacity is increased by 10% at moderate ambient temperatures, while it is slightly decreased at low ambient temperatures.

Figure F.3 shows a comparison of volumetric and isentropic compressor efficiencies at different ambient and driving conditions. In general, it can be observed that R290 2LP compressor efficiencies are increased by about 10% at highway driving conditions. At idling conditions, both volumetric and isentropic efficiencies, are decreased by about 20% at moderate to high ambient temperatures. At low ambient temperatures, compressor efficiency decreases significantly by more than 30%.

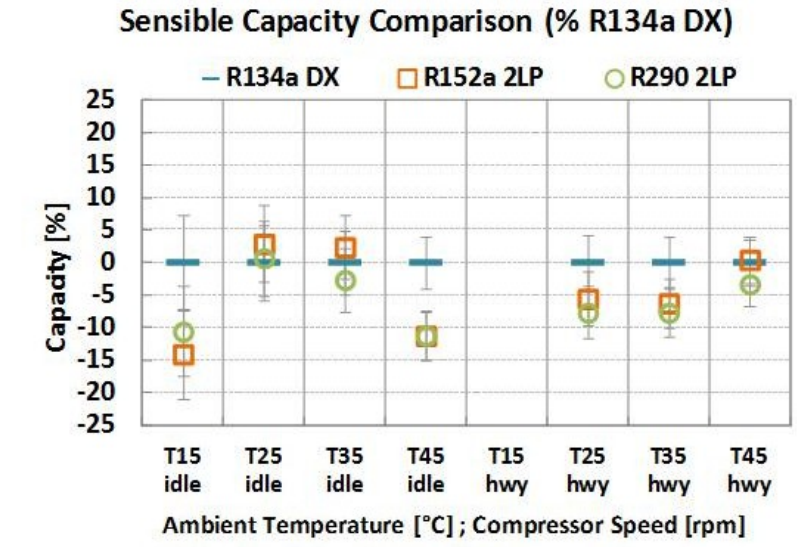

b)

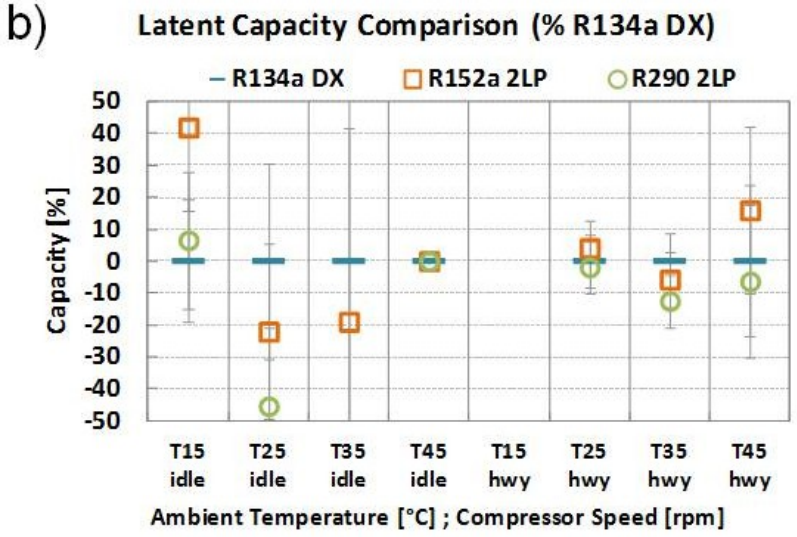

c)

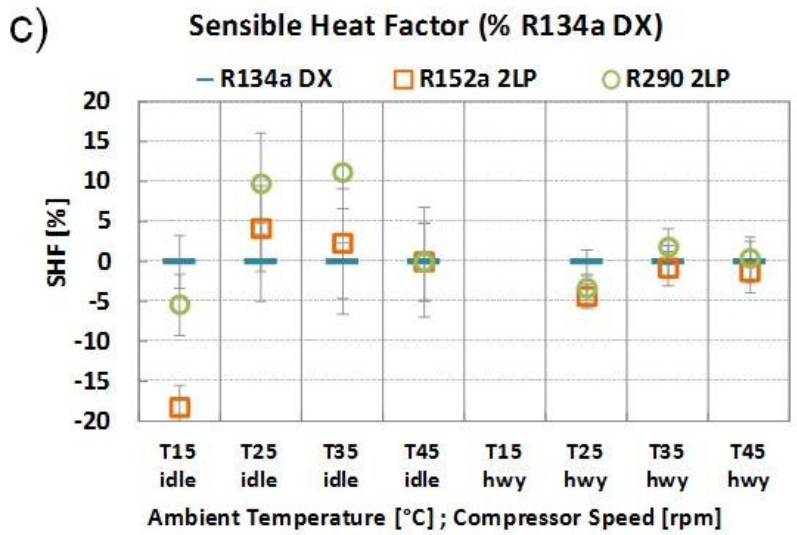

Figure F.2: Steady-state Sensible/Latent Performance Summary (Propane 2LP)

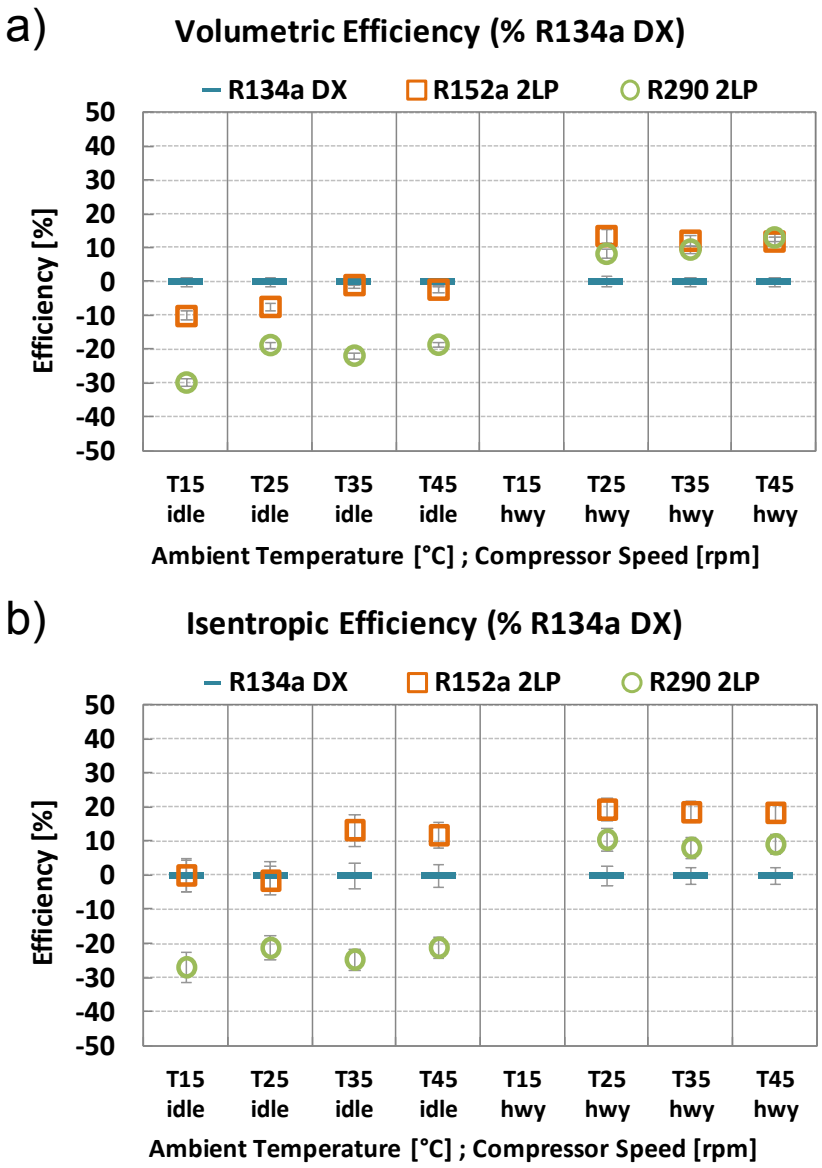

Figure F.3: Steady-state Compressor Efficiency Summary (Propane 2LP)

Appendix G Glycol Property Equations

The properties of the secondary working fluid, ethylene glycol, were calculated using property equations from M. Conde Engineering [109]. The respective equations were used in LabView, as well as in the Modelica glycol media package and are restated below for completeness.

The properties (P) density, thermal conductivity, and specific heat capacity can be determined for an aqueous ethylene glycol mixture by Equation (G1), while dynamic viscosity and Prandtl number can be calculated with the help of Equation (G2). T is the temperature in [°C] at which properties are evaluated, while x is the mass fraction of glycol in water. Coefficients used in the following equations are detailed in XXX.

$$P = A_1 + A_2 x + A_3 \frac{273.15}{\mathrm{T}} + A_4 x \frac{273.15}{T} + A_5 \left(\frac{273.15}{T}\right)^2 \quad \text{(G1)}$$

$$LN(P) = A_1 + A_2 x + A_3 \frac{273.15}{T} + A_4 x \frac{273.15}{T} + A_5 \left(\frac{273.15}{T}\right)^2 \quad \text{(G2)}$$

Table G.1: Ethylene Glycol Property Equation Coefficients

Parameter Order	ρ [kg/m^3]	Cp [kJ/kg K]	k [W/m K]	μ [Pa s]	Pr [-]
0					1.0
1	658.49825	5.36449	0.83818	-4.63024	-0.06982
2	-54.81501	0.78863	-1.37620	-2.14817	-0.35780
3	664.71643	-2.59001	-0.07629	-12.70106	
4	232.72605	-2.73187	1.07720	5.40536	
5	-322.61661	1.43759	-0.20174	10.98990	

Appendix H Modelica Direct Expansion System Equations

Appendix H provides information about the general equations used in the modeling of the direct expansion system components. The modeling work for the direct expansion components was done by Hongtao Qiao. The following equations can be found together with a more detailed discussion in Qiao [129].

The expansion cycle consists of four components, namely the compressor, expansion device, and the two heat exchangers.

The compressor was modeled as a quasi-steady state, efficiency-based component, where refrigerant mass flow rate was computed as a function of displacement, revolutions per minute, suction density and volumetric efficiency, given by Equation (H1). Discharge enthalpy as a function of isentropic efficiency was computed according to Equation (H2). The power due to adiabatic compression work was determined by Equation (H3).

$$\dot{m} = V_d N/60\eta_V \rho_s \quad \text{(H1)}$$

$$h_d = \frac{h_{is,d} - h_s}{\eta_{is}} \quad \text{(H2)}$$

$$W = \dot{m}(h_d - h_s) \quad \text{(H3)}$$

Similar to the compressor model, the expansion valve was modeled as a quasi-steady state isenthalpic throttling process. Mass flow rate through the valve was determined by flow coefficient, flow area, inlet density and pressure drop across the valve, as shown in Equation (H4).

$$\dot{m} = C_v A\sqrt{2g\rho_{in}\Delta p} \quad \text{(H4)}$$

Heat exchanger models are composed of three control volumes, which are connected by heat transfer mechanisms. The control volumes are the refrigerant control volume, the finned wall, and the air-side control volume. The following conservation laws apply to the control volumes:

Refrigerant-side

$$V\left[\left(\frac{\partial \rho_r}{\partial p_r}\right)_h \frac{dp_r}{dt} + \left(\frac{\partial \rho_r}{\partial h_r}\right)_p \frac{dh_r}{dt}\right] = \dot{m}_{r,i} - \dot{m}_{r,o} \quad \text{(H5)}$$

$$V\left[h_r\left(\frac{\partial \rho_r}{\partial p_r}\right)_h - 1\right]\frac{dp_r}{dt} + V\left[h_r\left(\frac{\partial \rho_r}{\partial h_r}\right)_p + \rho_r\right]\frac{dh_r}{dt} = \dot{m}_{r,i}h_i - \dot{m}_{r,o}h_o - Q_{rw} \quad \text{(H6)}$$

$$p_{r,i} - p_{r,o} = f(\dot{m}) \quad \text{(H7)}$$

Finned Wall

$$(MC_p)\frac{dT_w}{dt} = Q_{rw} - Q_{wa} \quad \text{(H8)}$$

Air-side

$$T_{a,o} = T_w - (T_w - T_{a,i})exp\left(-\frac{\eta_f \alpha_o A_T}{\dot{m}_a c_{p,a}}\right) \quad \text{(H9)}$$

Mass and energy balance are calculated in control volumes, whereas the momentum balance is calculated between control volumes (through connectors). For the microchannel heat exchanger models, air and refrigerant splitter models, as well as air and refrigerant mixer models were added before and after the respective control volumes.

Appendix I R134a DX Steady-state Reference Data

Chapters 7, 8, and 9 show experimental results of the secondary loop system using various primary refrigerants relative to the results of the R134a DX system. Appendix I provides absolute R134a DX data as a reference point for these comparisons.

Figure I.1 shows a summary of steady-state performance metrics data for a variety of ambient temperatures during idling and highway driving conditions. Cooling capacity, shown in Figure I.1 a), was lowest, about 2 kW, during idling at 15°C ambient temperature. The highest cooling capacities, 5.5 kW, were measured at highway driving (high compressor rpm) and high ambient temperatures of 35°C and 45°C. Figure I.1 b) shows compressor power consumption over a range of ambient temperatures for idle, as well as highway driving conditions. Power consumption varied from as low as 0.6 kW during idling at 15°C ambient temperature to 4.3 kW during highway driving at 45°C ambient temperature. R134a DX coefficient of performance, shown in Figure I.1 c) decreases with increasing compressor rpm, as well as with increasing ambient temperature.

A summary of sensible and latent performance data is shown in Figure I.2. Sensible capacity, shown in Figure I.2 a), increases with ambient temperature. The lowest sensible capacity, 1.5 kW, was measured at 15°C ambient temperature during idling. The highest sensible capacity was measured to be 4.6 kW at 45°C ambient temperature during highway driving.

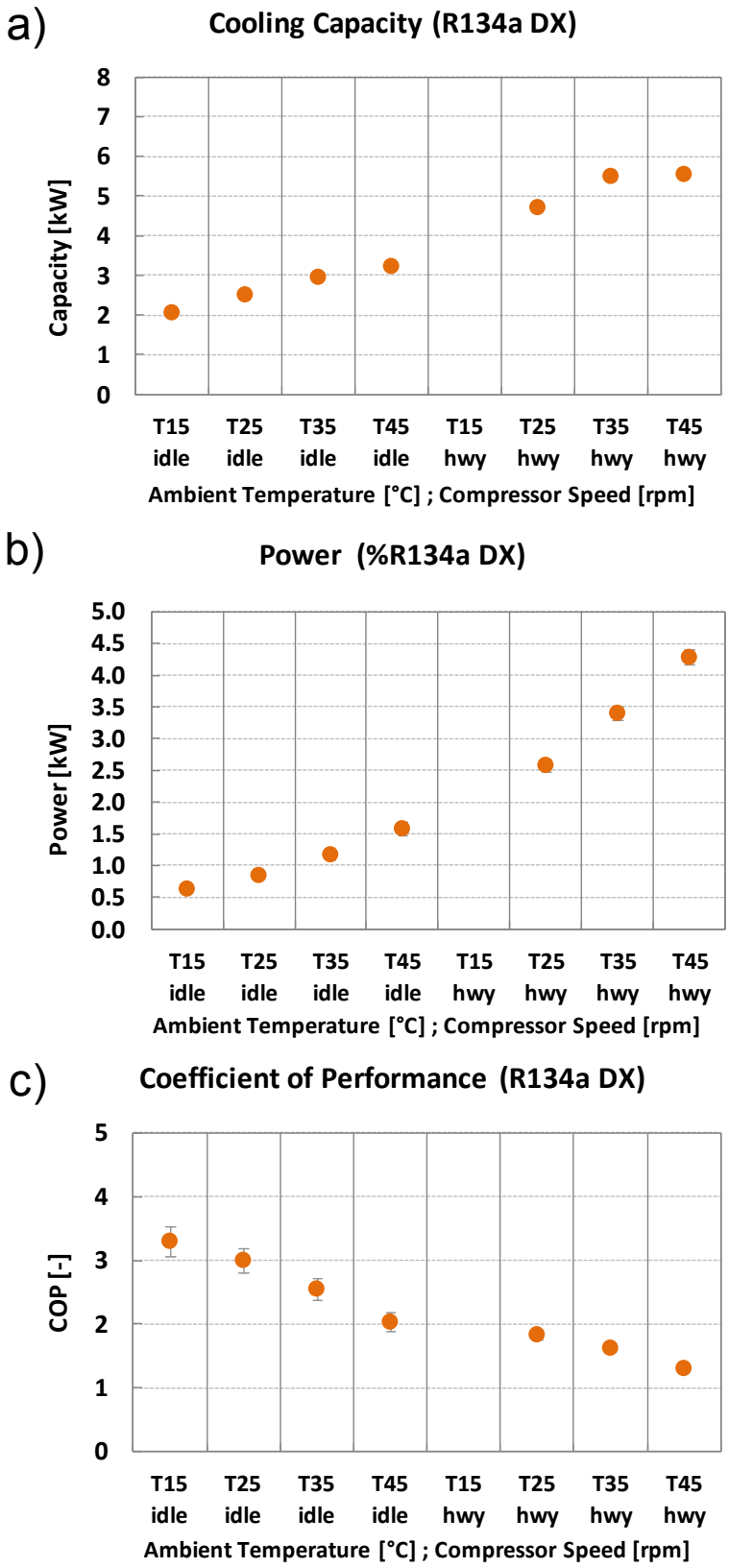

Figure I.1: Steady-state Performance Metrics Summary (R134a DX)

Figure I.2 b) presents latent capacity results. In general, latent capacity was decreased compared to sensible capacity. During idling, latent capacity decreased with increasing ambient temperature from 0.5 kW (15°C) to 0 kW (45°C). Latent capacity increased significantly during highway driving with the highest latent capacity measured to be 2.0 kW at 35°C. Figure I.2 c) presents the variation of sensible heat factor (SHF) with ambient temperature under idling and highway driving condition. During idling the sensible heat factor is continuously increasing from 0.73 at 15°C ambient temperature to 1.0 at 45°C. During highway driving, the lowest SHF was measured at 35°C with 0.64, while the highest SHF was measured at 45°C with 0.88.

Figure I.3 shows a summary of steady-state compressor efficiencies for the R134a DX system. Volumetric efficiency, shown in Figure I.3 a), decreases with increasing ambient temperature. On average, idling volumetric efficiency was calculated to be 0.91, while volumetric efficiency during highway driving conditions was calculated to be 0.84. Figure I.3 b) presents isentropic efficiency results. Isentropic efficiency decreased with increasing ambient temperature. During idling conditions, isentropic efficiency decreased from 0.85 (15°C) to 0.77 (45°C). During highway driving conditions, isentropic efficiency decreases from 0.69 (25°C) to 0.66 (45°C).

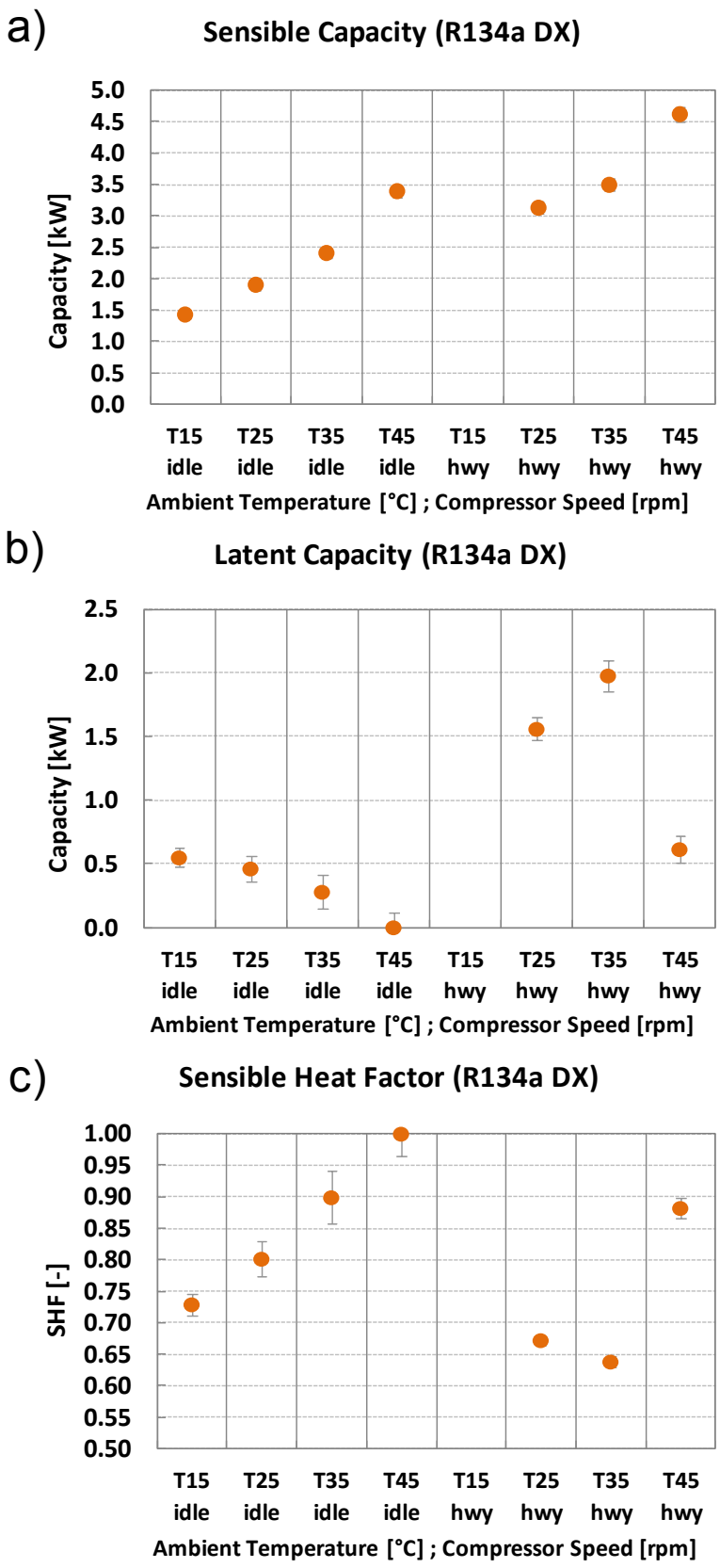

Figure I.2: Steady-state Sensible/Latent Performance Summary (R134a DX)

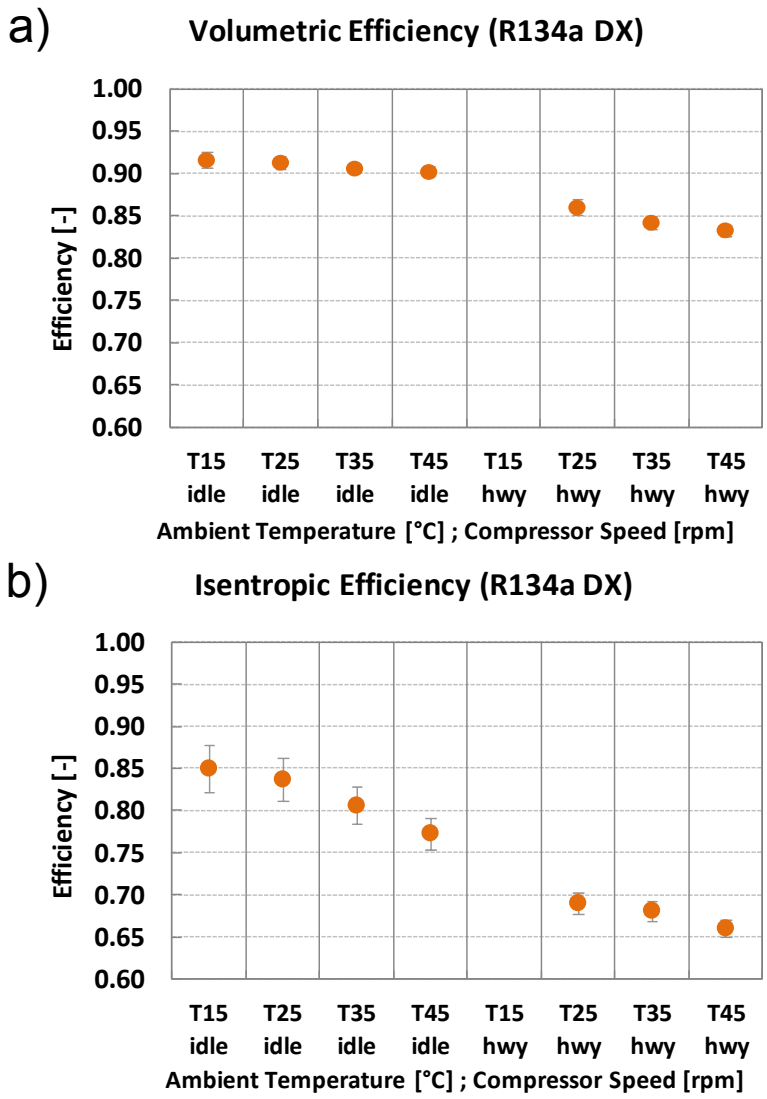

Figure I.3: Steady-state Compressor Efficiency Summary (R134a DX)

References

[1] J. E. Rubio-Quero, W. E. Dunn, and N. R. Miller, “A Facility for Transient Testing of Mobile Air Conditioning Systems,” 1995.

[2] C. D. Collins and N. R. Miller, “Experimental Study of Mobile Air Conditioning System Transient Behavior,” 1996.

[3] P. G. Weston, W. E. Dunn, and N. R. Miller, “Design and Construction of a Mobile Air Conditioning Test Facility for Transient Studies,” 1996.

[4] P. Hrnjak, “Some Lessons Learned from SAE AR CRP,” in *SAE Phoenix*, 2002.

[5] P. Hrnjak and B. Hill, “OVERVIEW OF THE SAE ALTERNATE REFRIGERANT COOPERATIVE RESEARCH PROGRAM.” 2003.

[6] P. Hrnjak, “Challenges and Results of MAC Cooling and Energy Efficiency Performance Exploration Project at the University of Illinois,” in *MAC Summit*, 2004.

[7] B. Hill, “Overview of Systems under Evaluation in SAE Alternate Refrigerant Cooperative Research Program,” in *SAE Phoenix*, 2002.

[8] J. Wertenbach, “SAE Alternate Refrigerant Cooperative Research Project Presentation - Energy Analysis of Refrigerant Cycles,” *SAE Phoenix*, p. 37, 2003.

[9] W. Atkinson, “SAE Alternate Refrigerant Cooperative Research Project - Project Overview,” in *SAE Phoenix*, 2003.

[10] W. Atkinson, “SAE Alternate Refrigerant Cooperative Research Program And Industry Impact,” *MAC Summit*, pp. 1–19, 2006.

[11] J. Baker, M. Ghodbane, J. Rush, and W. Hill, “Alternative Refrigerant Demonstration Vehicles,” 2007.

[12] A. E.-S. Gado, “Development of a Dynamic Test Facility For Environmental Control Systems,” *Thesis, University of Maryland*, 2006.

[13] A. Gado, Y. Hwang, and Reinhard R, “Dynamic Behavior of Mobile Air-Conditioning Systems,” *HVAC&R Research*, vol. 14, no. 2, p. 16, 2008.

[14] M. B. Yahia and C. Petitjean, “Transient phenomena effect on energy consumption Environmental background,” in *SAE Phoenix*, 2002.

[15] C.-C. D. Huang, “A Dynamic Simulation Model For Automobile Passenger Compartment Climate Control And Evaluation,” 1998.

[16] M. Wang, D. L. Farley, and L. L. Leitzel, “Air Conditioning System Head Pressure Spike During Vehicle Acceleration,” in *SAE*, 2000, no. 724.

[17] T. J. Hendricks, “Optimization of Vehicle Air Conditioning Systems Using Transient Air Conditioning Performance Analysis,” in *SAE VTMS*, 2001.

[18] R. Marzy, J. Hager, and C. Doppelbauer, “Optimization of Warm Up Using Simulation Tools,” *SAE VTMS*, 2001.

[19] C. Tian and X. Li, “Transient behavior evaluation of an automotive air conditioning system with a variable displacement compressor,” *Applied Thermal Engineering*, vol. 25, no. 13, pp. 1922–1948, Sep. 2005.

[20] H. Tummelscheit and D. Limperich, “The AirConditioning library for simulation of advanced vehicle A/C systems,” in *SAE VTMS*, 2007, pp. 23–32.

[21] I. Bayraktar, “TIME DEPENDENT SIMULATION METHODS FOR VEHICLE THERMAL MANAGEMENT,” *GVSETS Proceedings*, pp. 1–4, 2009.

[22] B. Li and A. G. Alleyne, “A Full Model of a HVAC Vapor Compression Cycle Interacting with a Dynamic Environment,” in *American Control Conference*, 2009, pp. 3662–3668.

[23] K. Sandhu, C. Chatham, A. Milosevic, D. Adekeye, and M. Warner, “Method of Evaluating the Effect of Air Conditioning on Vehicle Energy Management,” p. 20.

[24] ASHRAE, “ANSI/ ASHRAE Standard 34, Designation and Safety Classifications of Refrigerants, American Society of Heating, Refrigerating, and Air-Conditioning Engineers.” Atlanta, GA, 2004.

[25] ISO, “ISO Standard 817: Refrigerants Designation System, International Organization for Standardization.” Geneva, Switzerland, 2005.

[26] K. Wang, M. Eisele, Y. Hwang, and R. Radermacher, “Review of secondary loop refrigeration systems,” *International Journal of Refrigeration*, vol. 33, no. 2, pp. 212–234, Mar. 2010.

[27] E. Union, “Directive 2006/40/EC of the European parliament and of the Council of 17 May 2006, Official J. Eur. Union L 161 (12).” 2006.

[28] M. Spatz and B. Minor, “HFO-1234yf – a low GWP refrigerant for MAC,” in *VDA Alternative Refrigerant Winter Meeting*, 2008.

[29] E. Granryd, “Hydrocarbons as refrigerants,” *International Journal of Refrigeration*, no. 24, pp. 15–24, 2001.

[30] J. M. Corberan, J. Segurado, D. Colabourne, and J. Gonzalvez, “Review of standards for the use of hydrocarbon refrigerants in a/c, heatpump and refrigeration equipment,” *International Journal of Refrigeration*, no. 31, pp. 748–756, 2008.

[31] CEN, “prEN 378-2, Refrigerating Systems and Heat Pumps – Safety and Environmental Requirements, European Committee for Standardization.” Brussels, Belgium, 2006.

[32] BSI, “BS EN 378-1: Refrigerating Systems and Heat Pumps, Safety and Environmental Requirements, Basic Requirements, Definitions, Classification and Selection Criteria, British Standard Institute, Bristol, U.K.” Bridtol, U.K., 2008.

[33] DIN, “DIN 8975-12: Refrigerating Plants –Safety Principles for Design, Equipment and Installation; Test Certificate and Identification Plate - Part 12. Recovery Systems, Deutsches Institut fuer Normung e.V., Berlin, Germany.” Berlin, Germany, 2004.

[34] D. Colbourne, “An overview of hydrocarbons as replacement refrigerants in commercial refrigeration and air-conditioning, Refrigeration Northern Ireland Centre for Energy Research and Technology.” 2000.

[35] D. Colbourne and K. O. Suen, “Assessment of performance of hydrocarbon refrigerants,” *Science et technique du froid*, pp. 149–156, 2000.

[36] D. Colbourne and T. J. Ritter, “Compatibility of non-metallic materials with hydrocarbon refrigerant and lubricant mixtures,” *Science et technique du froid*, pp. 413–418, 2000.

[37] I. L. Maclaine-Cross and E. Leonardi, “Comparative performance of hydrocarbon refrigerants,” *I.I.F. – I.I.R. –Commissions E2, E1, B1, B2, Melbourne, Australia*, 1996.

[38] K. A. Joudi, A. S. K. Mohammed, and M. K. Aljanabi, “Experimental and computer performance study of an automotive air-conditioning system with alternative refrigerants,” *Energy Conversion and Management*, no. 44, pp. 2959–2976, 2003.

[39] M. Ghodbane, “An Investigation of R152a and Hydrocarbon Refrigerants in Mobile Air Conditioning,” in *SAE*, 1999, no. 724.

[40] I. L. Maclaine-cross and E. Leonardi, “Hydrocarbon refrigerant risk in car air-conditioners,” in *International CFC and Halon Alternatives Conference*, 1995.

[41] V. Razmovski, “Safety of hydrocarbon refrigerants for car air- conditioning systems, School of Mechanical Engineergin, UNSW, Sydney,” UNSW, Sydney, 1994.

[42] “Arthur D. Little Ltd., Risk Assessment of Flammable Refrigerants, Part 3: Car Air-Conditioning. Final Report to Calor Gas Ltd., Cambridge UK,” 1995.

[43] D. J.T., J. Bentley, and A. Varone, “Non-Inert Refrigerant Study for Automotive Applications.” 1991.

[44] S. J. Elbers and M. Verwoerd, “Quantitative risk assessment of a heat pump system with propane refrigerant, Final Report of TNO (for Lodam Energi A/S), Apeldoorn, Netherland,” Apeldoorn, Netherland, 1997.

[45] T. J. Ritter and D. Colbourne, “Quantitative risk assessment: hydrocarbon refrigerants, IIF - IIR –Sections B and E, Oslo, Norway,” 1998.

[46] J. Jetter, F. Reynaldo, and R. Rubenstein, “Fault tree analysis for exposure to refrigerants used for automotive air-conditioning in the United States,” *Risk Analysis*, no. 21, pp. 157–171, 2001.

[47] D. Colbourne and K. O. Suen, “Appraising the flammability hazards of hydrocarbon refrigerants using quantitative risk assessment model, partII, model evaluation and analysis,” *International Journal of Refrigeration*, 2004.

[48] B. Palm, “Hydrocarbons as refrigerants in small heat pump and refrigeration systems – a review,” *Internal Journal of Refrigeration*, no. 31, pp. 552–563, 2008.

[49] Danfoss, “Practical Application of Refrigerant R290 Propane in Small Hermetic Systems.” 2000.

[50] J. M. Corberan, J. F. Urchueguia, I. Navarro, J. Gronzalvez, and A. Gala, “Performance of a reciprocating hermetic refrigerant compressor using propane as working fluid,” in *IIR - Gustav Lorentzen Conference of Natural Working Fluids*, 2000, pp. 225–232.

[51] C. L. Pellec, C. Marvillet, and D. Clodic, “Experimental study of flat heat exchangers in ammonia refrigeration unit,” *IIR - Gustav Lorentzen Conference of Natural Working Fluids*, pp. 785–794, 1996.

[52] T. Setaro, G. Boccardi, J. M. Corberan, J. Urchueguia, and J. Gonzalvez, “Comparative study of evaporation and condensation of propane and R22 in a brazed plate heat exchanger and a tube and fins coil,” in *IIR - Gustav Lorentzen Conference of Natural Working FluidsGustav Lorentzen*, 2000.

[53] P. S. Hrnjak and M. R. Hoehne, “Charge minimization in systems and components using hydrocarbons as a refrigerant, ACRC TR-224.” 2004.

[54] P. Fernando, B. Palm, T. Ameel, P. Lundqvist, and E. Granryd, “Propane heat pump with low refrigerant charge: design and laboratory tests,” *International Journal of Refrigeration*, no. 27, pp. 761–773, 2004.

[55] P. Fernando, B. Palm, T. Ameel, P. Lundqvist, and E. Granryd, “A minichannel aluminum tube heat exchanger – part I: evaluation of single-phase heat transfer coefficients by the Wilson plot method,” *International Journal of Refrigeration*, no. 31, pp. 669–680, 2008.

[56] P. Fernando, B. Palm, T. Ameel, P. Lundqvist, and E. Granryd, “A minichannel aluminum tube heat exchanger – part II: evaporator performance with propane,” *International Journal of Refrigeration*, no. 31, pp. 681–695, 2008.

[57] P. Fernando, B. Palm, T. Ameel, P. Lundqvist, and E. Granryd, “A minichannel aluminum tube heat exchanger – part III: condenser performance with propane,” *International Journal of Refrigeration*, no. 31, pp. 696–708, 2008.

[58] P. Likes, “Secondary refrigerant systems for supermarket equipment,” in *Conference on Ozone Protection Technologies*, 1996, pp. 158–164.

[59] L. Rolfsman, “CO2 and NH3 in the supermarket ICA-focus,” in *IIR - Conference of on Applications for Natural Refrigerants*, 1996, pp. 219–225.

[60] K. Evenmo, “A new secondary fluid,” in *IIR - Gustav Lorentzen Conference on Natural Working Fluids*, 1998, pp. 679–688.

[61] W. T. Horton, E. A. Groll, and E. Sharp, “Testing of a drop-in secondary loop refrigeration system for medium temperature supermarket application,” in *IIR - Gustav Lorentzen Conference on Natural Working Fluids*, 1998, pp. 690–700.

[62] J. Nyvad and S. Lund, “Indirect cooling with ammonia in supermarkets,” in *IIR - Gustav Lorentzen Conference on Natural Working Fluids*, 1998, pp. 725–734.

[63] “Tyforop Chemie Gmbh, SecondaryRefrigerants(OrganicSalts), http://www.tyfo.de/index_english.html.” 2009.

[64] J. Arias and P. Lundqvist, “Field experiences in three supermarkets in Sweden,” in *IEA Annex 26 Workshop, IEA Heat Pump Centre*, 2000.

[65] R. T. Faramarzi and D. H. Walker, “Investigation of Secondary Loop Supermarket Refrigeration Systems, Consultant Report, Foster-Miller, Inc. CaliforniaEnergy Commission 500-04-0132004,” 2004.

[66] V. Minea, “Supermarket refrigeration system with completely secondary loops,” *ASHRAE Transactions*, no. 49, p. 40, 2007.

[67] V. Minea, “Low charge and low emission supermarket refrigeration systems,” in *IIR - Gustav Lorentzen Conference on Natural Working Fluids*, 2008, pp. 901–908.

[68] N. Rivers, “Unconventional secondary refrigeration in a UK supermarket,” in *IEA Heat Pump Centre Newsletter 18*, 2000, pp. 18–19.

[69] V. D. Baxter, “Advances in Supermarket Refrigeration Systems,” in *IEA Annex 26 Summary*, 2006.

[70] D. K. Choi, P. A. Domanski, and D. A. Didion, “Evaluation of flammable refrigerants for use in a water-to-water residential heat pump,” in *IIR - Conference on Applications for Natural Refrigerants*, 1996, pp. 467–476.

[71] Y. S. Chang, M. S. Kim, and S. T. Ro, “Performance and heat transfer of hydrocarbon refrigerants and their mixtures in a heat pump system,” in *IIR - Conference on Applications for Natural Refrigerants*, 1996, pp. 477–486.

[72] O. Pelletier and B. Palm, “Performance of plate heat exchangers and compressor in a domestic heat pump using propane,” *IIR - Conference on Applications for Natural Refrigerants*, pp. 497–506, 1996.

[73] W. V. Payne, P. A. Domanski, and J. Muller, “A study of a water-to-water heat pump using flammable refrigerants,” in *IIR - Gustav Lorentzen Conference on Natural Working Fluids*, 1998, pp. 658–667.

[74] J. Stene, “Investigation of a residential brine-water CO2 heat pump for combined low-temperature space heating and hot water preparation,” in *IIR*

- *Conference on Applications on Natural Working Fluids*, 2002, pp. 268–275.

[75] T. Yanagisawa, M. Fukuta, N. Ogura, and H. Kaneo, “Operating characteristics of natural circulating CO2 secondary loop refrigeration system working with NH3 primary loop,” in *IIR - Gustav Lorentzen Conference on Natural Working Fluids*, 2004.

[76] P. A. Domanski and D. Yashar, “Comparable performance evaluation of HC and HFC refrigerants in an optimized system,” in *IIR - Gustav Lorentzen Conference on Natural Working Fluids*, 2006.

[77] K. Mani and V. Selladurai, “Experimental analysis of a new refrigerant mixture as drop-in replacement for CFC12 and HFC134a,” *International Journal of Thermal Sciences*, no. 47, pp. 1490–1495, 2008.

[78] W. Hill, “Risk assessment and performance evaluation of HFO-1234yf,” in *VDA Alternative Refrigerant Winter Meeting*, 2008.

[79] EPA, “USA Environmental Protection Agency, Legal Status of HC-12a ®, DURACOOL 12a ®, and OZ-12 ®,” 2010. [Online]. Available: http://www.epa.gov/ozone/snap/refrigerants/hc-12a.html.

[80] “USA Environmental Protection Agency, Unacceptable Substitute Refrigerants,” 2010. [Online]. Available: http://www.epa.gov/ozone/snap/refrigerants/lists/unaccept.html.

[81] Z. Ure, “Secondary Refrigeration - European Experiences,” *ASHRAE Transactions*, vol. 109, pp. 1–6, 2003.

[82] R. Delventura, C. L. Evans, and I. Richter, “Magazine: Secondary loop SyStemS for the Supermarket induStry White Paper,” *White Paper*, no. September, 2007.

[83] A. Melinder, “Thermophysical properties of aqueous solutions used as secondary working fluids,” Royal Institute of Technology, 2007.

[84] P. W. Egolf and M. Kauffeld, “From physical properties of ice slurries to industrial ice slurry applications,” *International Journal of Refrigeration*, no. 28, pp. 4–12, 2005.

[85] Z. Ure and M. Mashrae, “Slurry ice based cooling systems,” in *20th International Congress of Refrigeration*, 1999.

[86] J. W. Meewise and C. A. I. Ferreira, “Optimal properties of ice slurries in secondary cooling systems,” in *IIR - Gustav Lorentzen Conference of Natural Working Fluids*, 2000, pp. 513–520.

[87] M. J. Wang and V. Goldstein, “A novel ice slurry generation system and its application,” in *IIR - Conference on Applications for Natural Refrigerants*, 1996, pp. 543–551.

[88] K. G. Christensen and M. Kauffeld, “Ice slurry accumulation,” in *IIR - Gustav Lorentzen Conference on Natural Working Fluids*, 1998, pp. 701–711.

[89] M. Wang, J. Y. Inoue, and V. Goldstein, “Ice thermal storage in modern building,” in *20th International Congress of Refrigeration*, 1999, pp. 19–24.

[90] S. Fukusako, Y. Kozawa, M. Yamada, and M. Tanino, “Research and development activities on ice slurries in Japan,” in *First Workshop on Ice Slurries of the International Institute of Refrigeration: Proceedings of the International Meeting in Yverdon-les-Bains, Switzerland*, 1999, pp. 83–105.

[91] A. Saito, “Recent advances in research on cold thermal energy storage,” *International Journal of Refrigeration*, no. 25, pp. 177–189, 2002.

[92] D. Hinde, S. Zha, and L. Lan, “CO2 experiences in North American supermarkets,” in *IIR - Gustav Lorentzen Conference on Natural Working Fluids*, 2008, pp. 1098–1104.

[93] A. Melinder, “Secondary Fluids for Low Operating Temperatures,” in *IIR - Gustav Lorentzen Conference on Natural Working Fluids*, 2004.

[94] A. C. Pachai, “Experience with CO2 as refrigerant in supermarkets,” in *IIR - Gustav Lorentzen Conference on Natural Working Fluids*, 2004.

[95] A. Pearson, “Carbon dioxide - new uses for an old refrigerant,” *Internal Journal of Refrigeration*, no. 28, pp. 1140–1148, 2005.

[96] S. F. Pearson, “Cooling Method and Apparatus, British Patent Number 2258298,” 1995.

[97] K. G. Christensen, “Use of CO2 as primary and secondary refrigerant in supermarket application,” in *20th International Congress of Refrigeration*, 1999, pp. 1936–1942.

[98] P. O. Nilsson, J. Rogstam, S. Sawalha, and K. Shahzad, “Ice rink refrigeration system with carbon dioxide as secondary fluid in copper

tubes," in *IIR - Gustav Lorentzen Conference on Natural Working Fluids*, 2006.

[99] K. Jahn, "Natural refrigerants in dairy processing, supermarket refrigeration and airconditioning," *GTZ Proklima: Natural Refrigerants - Sustainable Ozone - and Climate - Friendly Alternatives to HCFCs Eschborn Germany, Deutsche Gesellschaft fuer Technische Zusammenarbeit (GTZ) GmbH, German Technical Cooperation – Programme Proklima*, 2008.

[100] L. Dentis, A. Mannoni, and M. Parrino, "HC refrigerants: an ecological solution for automotive a/c systems," in *Vehicle Thermal Management of Systems Conference*, 1999, pp. 133–147.

[101] M. Ghodbane, "On Vehicle Performance of a Secondary Loop A/C System," *SAE Technical Paper*, no. 724, p. 7, 2000.

[102] M. Ghodbane and J. A. Baker, "Secondary loop system for passenger compartment heating and cooling, Unites States Patent Number 6405793," 2002.

[103] P. S. Kadle and M. Ghodbane, "Heat pump with secondary loop air-conditioning system, United States Patent Number 7063137," 2006.

[104] M. Ghodbane, T. D. Craig, and J. A. Baker, "Demonstration of an Energy-Efficient Secondary Loop HFC-152a Mobile Air Conditioning System," 2007.

[105] "ANSI/ASHRAE 41.2-1987 (RA92) - Standard Methods for Laboratory Airflow Measurement," *Order A Journal On The Theory Of Ordered Sets And Its Applications*. American Society Of Heating Refrigerating And Air-Conditioning Engineers, Atlanta, GA, 1992.

[106] "http://www.ni.com/dataacquisition/." .

[107] "http://www.optimizedthermalsystems.com/." .

[108] E. W. Lemmon, M. L. Huber, and M. O. McLinden, "NIST Standard Reference Database 23: Reference Fluid Thermodynamic and Transport Properties-REFPROP, Version 9.0, National Institute of Standards and Technology, Standard Reference Data Program." Gaithersburg, 2010.

[109] M. Conde Engineering, "Properties of Working Fluids, THERMOPHYSICAL PROPERTIES OF BRINES." Zurich, 2011.

[110] "USA Environmental Protection Agency, Dynamometer Drive Schedules," 2012. [Online]. Available: http://www.epa.gov/nvfel/testing/dynamometer.htm.

[111] “National Renewable Energy Laboratory, U.S. Department Of Energy, Typical Meteorological Year, Version 2,” 2005. [Online]. Available: http://rredc.nrel.gov/solar/old_data/nsrdb/1961-1990/tmy2/State.html.

[112] M. Ghodbane, “On vehicle performance of a secondary loop system,” in *SAE Phoenix*, 1999.

[113] D. A. Didion, “The Influence of the Thermophysical Fluid Properties of the New Ozone-Safe Refrigerants on Performance,” *International Journal of Applied Thermodynamics*, vol. 2, no. 1, pp. 19–35, 1999.

[114] M. O. McLinden and D. A. Didion, “Quest for Alternatives,” *ASHRAE Journal*, vol. 29, pp. 32–42, 1987.

[115] G. Alefeld, “Efficiency of compressor heat pumps and refrigerators derived from the 2nd Law,” *International Journal of Refrigeration*, vol. 10, no. 6, pp. 331–341, 1987.

[116] F. Ayad, L. Leitzel, and F. D. Sciullo, “Numerical and experimental study of a secondary cooling loop including a liquid cooled charge air cooler and a liquid cooled condenser,” in *4th European Workshop: Mobile Air Conditioning and Vehicle Thermal Systems*, 2011.

[117] SAE, “Surface Vehicle Standard, SAE J2765 OCT2008, Procedure for Measuring System COP (Coefficient of Performance) of a Mobile Air Conditioning System on a Test Bench.” 2008.

[118] S. K. Fischer, “Comparison of Global Warming Impacts of Automobile Air-Conditioning Concepts,” in *International CFC and Halons Alternative Conference*, 1995.

[119] S. Papasavva, W. R. Hill, and R. O. Brown, “Green-MAC-LCCP: A Tool for Assessing Life Cycle Greenhouse Emissions of Alternative Refrigerants,” *SAE International Journal of Passenger Cars - Mechanical Systems*, vol. 1, no. 1, pp. 746–756, 2008.

[120] U.S. Department of Commerce and U.S. Census Bureau, “Commuting in the United States : 2009,” Washington, DC, 2011.

[121] D. Clodic, E. Zgheib, and S. Mortada, “Impacts of Heating and Cooling on Electrified vehicles,” in *4th European Workshop: Mobile Air Conditioning and Vehicle Thermal Systems*, 2011.

[122] C. Reynolds and M. Kandlikar, “How hybrid-electric vehicles are different from conventional vehicles: the effect of weight and power on fuel

consumption," *Environmental Research Letters*, vol. 2, no. 1, p. 014003, Jan. 2007.

[123] V. H. Johnson, "Fuel Used for Vehicle Air Conditioning : A State-by-State Thermal Comfort-Based Approach," *Society of Automotive Engineers*, 2002.

[124] R. Farrington and J. Rugh, "Impact of Vehicle Air- Conditioning on Fuel Economy , Tailpipe Emissions , and Electric Vehicle Range - Preprint," in *Earth Technologies Forum*, 2000, no. September.

[125] K. Umezu and H. Noyama, "Air-Conditioning system For Electric Vehicles (i-MiEV)," in *SAE Automotive Refrigerant & System Efficiency Symposium*, 2010.

[126] W. O. Forrest and M. S. Bhatti, "Energy Efficient Automotive Air Conditioning System," *SAE 2002 World Congress*, no. 724, 2002.

[127] D. Roy, P. P. Jean, D. Clodic, and K. E. Khoury, "Influence of thermal preconditioning technologies on A/C system power and passengers' thermal comfort," *IMechE*, pp. 205–214, 2003.

[128] D. Roy, P. Petitjean, D. Clodic, and K. E. Khoury, "Experimental Investigation of a Thermal Preconditioning of a Car Cabin," *SAE Technical Paper Series*, vol. 01, no. 2057, 2005.

[129] H. Qiao, V. Aute, and R. Radermacher, "Comparison of Equation-Based and Non-Equations-Based Approaches for Transient Modeling of a Vapor Compression Cycle," in *International Refrigeration and Air Conditioning Conference at Purdue*, 2012, p. 2190.

[130] F. W. Dittus and L. M. K. Boelter, "Heat Transfer in Automobile Radiators of the Tubular Type," *International Communications in Heat and Mass Transfer (originally published in University of California Publications in Engineering)*, vol. 12, no. 1, pp. 3–22.

[131] F. P. Incropera and D. P. DeWitt, *Introduction to heat transfer (3rd ed.)*. New York: John Wiley & Sons, 1996.

[132] A. A. Eilemann, J. Diem, H. Hofmann, B. Gmbh, and C. Kg, "From indirect Charge Air Cooling to a 2-layer Cooling Module : Assumptions , Preconditions and Perspectives," in *4th European Workshop: Mobile Air Conditioning and Vehicle Thermal Systems*, 2011.

[133] R. Cipollone, D. D. Battista, and A. Gualtieri, "INTEGRATION OF COOLING VEHICLE THERMAL NEEDS ON ENGINE COOLING

SYSTEM," in *4th European Workshop: Mobile Air Conditioning and Vehicle Thermal Systems*, 2011.

[134] F. D. Sciullo, W. Ferraris, C. Malvicino, C. Ricerche, S. C. Fiat, F. Vestrelli, and F. Beltramelli, "Two Levels Cooling (Smart Cooling) Application to B-segment vehicle Sc," in *4th European Workshop: Mobile Air Conditioning and Vehicle Thermal Systems*, 2011.

[135] J. Benouali, R. Beauvis, and C. Petitjean, "R-1234yf A/C system improvements & further link to engine cooling loop," in *4th European Workshop: Mobile Air Conditioning and Vehicle Thermal Systems*, 2011.

[136] R. Seccardini, F. Mattiello, and C. Malvicino, "TIFFE thermal system Light commercial vehicle application," in *4th European Workshop: Mobile Air Conditioning and Vehicle Thermal Systems*, 2011.